The incidence of extreme climatic rainfall in Thailand

Emma Louise Gale

A dissertation submitted in partial fulfillment

of the requirements for the degree of

Doctor of Philosophy

of

University College London.

Department of Space and Climate Physics

University College London

January 29, 2017

I, Emma Louise Gale confirm that the work presented in this thesis is my own. Where information has been derived from other sources, I confirm that this has been indicated in the thesis.

Abstract

Extreme climatic rainfall, defined as extreme rainfall over monthly to annual timescales with a return period of 10 years or more, is common in Thailand due to its location and climate. Flooding from persistent heavy rainfall causes much of the insured and economic losses from natural hazards in the country. Despite this, there is little detailed historical information regarding the incidence of extreme climatic rainfall in Thailand. In this study I aimed to quantify the incidence of extreme climatic rainfall in Thailand, primarily through return period analysis. I used gridded (1901–2012) rainfall data to produce distribution-fitted return period curves with uncertainties, and then derived a catalogue of return period maps for Thailand. Extreme climatic precipitation events were identified for further study, including the 2011 flood, which caused the highest ever insured loss (US$12 billion) from a freshwater flood disaster worldwide. For each event, I examined the nature, impacts, rainfall totals and anomalies, and climate causes. Return period analysis assessed the likelihood of re-occurrence of each event. The extreme climatic rainfall return periods varied depending on length of dataset and the fitted distribution used. Various estimates suggest a precipitation return period of 79 (August), 385 (June–August) and 164 years (annual) for 1942, 1995 and 2011 respectively. Analysis found that the El Niño Southern Oscillation (ENSO) was the primary driver of interannual rainfall variability in Thailand. Rainfall during a La Niña phase was, on average, 8.7 % higher than during an El Niño phase. This difference increased when the ENSO event persisted in the same phase for multiple years; rainfall was 14.4 % higher during multi-year La Niña events than during multi-year El Niño events. These findings are of particular importance to the insurance and risk management industry, and the methodology is easily transferable for use in other Southeast Asian countries.

Contents

List of Figures

List of Tables

Chapter 1

Introductory Material

1.1 Introduction

Extreme weather is a worldwide phenomenon that affects millions of people and causes large-scale devastation. Extreme climatic rainfall, defined here as extreme rainfall over monthly, seasonal or annual timescales with a return period of 10 years or more, is common in Thailand due to its tropical location and monsoonal climate. Flooding caused by persistent heavy rainfall occurs regularly in Thailand (Table 1.1) and causes much of the insured and economic losses from natural hazards in the country (Guha-Sapir et al., 2016). During 2011, Thailand experienced its wettest year in the country's precipitation record (Thai Meteorological Department, 2011), resulting in extensive flooding throughout much of the country. The flooding caused considerable damage to homes, sites of historical interest, and industrial estates run by large multi-national companies (including Sony, Honda and Toyota; Aon Benfield, 2012a; Haraguchi and Lall, 2014). The insured loss of US$12 billion ranks as the highest ever from a freshwater flood disaster worldwide (Swiss Re, 2012).

Despite the substantial impacts from extreme climatic rainfall events in Thailand, there is little detailed historical information regarding the incidence of such events. The insurance industry was unprepared for the widespread damage experienced in Thailand in 2011; re-insurers suffered substantial losses from the flooding (Aon Benfield, 2012a). However, post-2011, general interest for business in Thailand continues among re-insurers. For this reason, there is significant interest from the industry for quantitative information regarding extreme climatic rainfall in Thailand. This information can be used to improve catastrophe modelling for Thailand, which will in turn help to improve the accuracy of insurance pricing and reduce the impact on the insurance industry from events such as the

Table 1.1: Notable flood events in Thailand 1994–2012. The data are taken from the Dartmouth Flood Observatory Global Active Archive of Large Flood Events (Brakenridge, 2012).

Date	Magnitude	Duration (days)	Area affected (km^2)	Main cause(s)
3 Sept–18 Dec 1994	7.1	107	65 000	Heavy rain
1 Aug–9 Nov 1995	7.9	101	444 000	Heavy rain
18 Jul–21 Aug 1996	7.0	35	314 000	Tropical storms
3 Oct–28 Oct 1996	6.5	26	116 000	Monsoonal rain
11 Jul–10 Aug 2000	6.6	31	120 000	Monsoonal rain
17 Aug–20 Sep 2002	6.3	35	52 000	Heavy rain
18 Aug–26 Nov 2002	7.9	101	372 000	Monsoonal rain
17 Sep–2 Dec 2002	7.0	77	140 000	Monsoonal rain
12 Sep–12 Oct 2003	7.0	31	315 000	Monsoonal rain
3 Oct–25 Oct 2003	6.0	23	22 000	Heavy rain
6 Aug–3 Oct 2004	7.6	59	378 000	Monsoonal rain
13 Aug–26 Sep 2005	7.1	45	134 000	Monsoonal rain
23 Nov 2005–12 Jan 2006	6.9	51	71 000	Monsoonal rain
22 May–11 Jun 2006	6.5	21	78 000	Monsoonal rain
20 Aug–13 Dec 2006	7.7	116	213 000	Monsoonal rain
10 Oct–4 Nov 2006	6.7	26	213 000	Monsoonal rain
5 Sep–10 Nov 2007	7.3	67	300 000	Monsoonal rain
11 Sep–4 Oct 2008	6.8	23	166 000	Monsoonal rain
20 Nov–10 Dec 2008	6.4	21	58 000	Heavy rain
10 Oct–15 Nov 2010	5.5	37	4000	Heavy rain
5 Aug 2011–9 Jan 2012	7.5	158	97 000	Tropical storms & monsoonal rain

Flood magnitude $=$ log(Duration $\times$ Severity $\times$ Area affected)

Severity depends on the estimated recurrence interval of floods in the region affected and is defined on a scale between 1 and 2.

2011 flood.

The aim of this thesis is to quantify the incidence of extreme climatic rainfall in Thailand, and to clarify the causes and impacts of this rainfall.

This chapter presents the introductory material for this work. Section 1.2 describes the climate of Thailand and Southeast Asia. Section 1.3 discusses the main causes of extreme rainfall in Thailand: the summer monsoon and tropical storms. Lastly, Section 1.4 details the causes of interannual variability in Thailand

climatic rainfall: the El Niño Southern Oscillation (ENSO) and the Indian Ocean Dipole (IOD).

Chapter 2 describes the data that underpin this thesis; precipitation is the primary data type used, although other data types are also presented. Chapter 3 first defines extreme climatic rainfall, and then details the method developed to calculate extreme climatic rainfall return periods and their uncertainties for Thailand. This methodology is subsequently applied to analyse the 2011 Thailand flood (Chapter 4) and five other notable historic climatic floods in Thailand (Chapter 5). These chapters describe, for each flood event, the underlying causes and impacts, analyse the climatic rainfall anomalies and calculate the climatic rainfall return period(s). Chapter 6 examines the observational relationship between ENSO and climatic rainfall in Thailand. The chapter describes the new and physically sound method developed to identify ENSO events before examining the strength, significance and stationarity of the link between Thai rainfall and ENSO. Finally, Chapter 7 concludes this work and discusses future research directions.

1.2 Climate in Thailand

Thailand, located in the centre of mainland Southeast Asia, lies within the tropics between the Indian and Pacific Oceans. Figure 1.1 shows the topography and major rivers of Thailand. The country can be divided into two main regions: continental and peninsular Thailand.

The geography of continental Thailand is dominated by two major river systems: the Chao Phraya River basin (CPRB) in the west, and the Mekong River basin (MRB) in the east. The first of these basins is situated between the northern and western mountain ranges and is the heartland of Thailand (Encyclopedia Britannica, 2016). The Chao Phraya River proper begins at the confluence of the Ping and Nan Rivers, just south of 16°N, and flows through the central plains and Thailand's capital city, Bangkok, before discharging into the Gulf of Thailand. The Mekong River forms Thailand's eastern and north-eastern border with Laos; its basin spans much of eastern Thailand.

Peninsular Thailand has a mountainous spine along the west separating

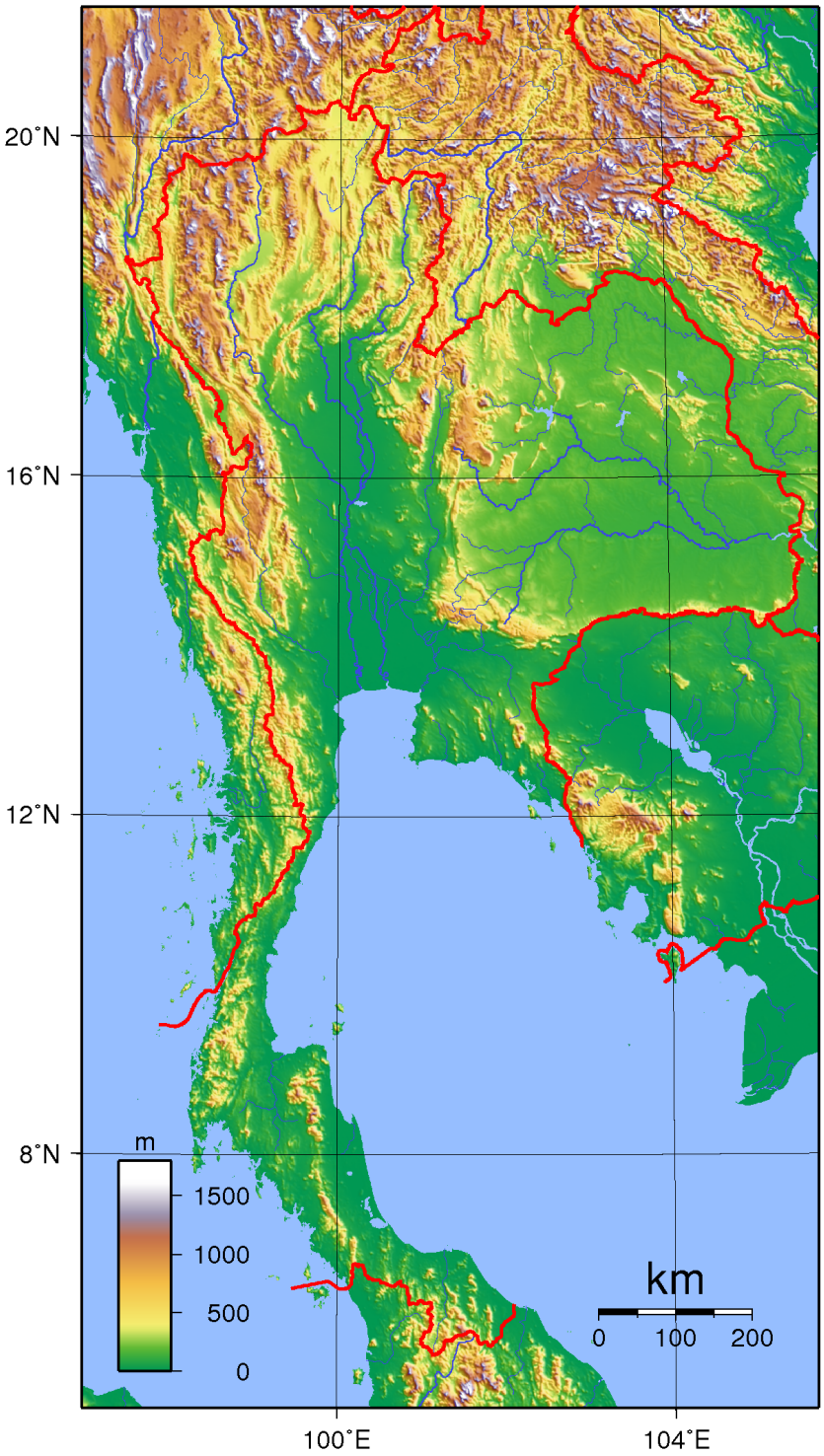

Figure 1.1: The topography and major rivers of Thailand. The height above sea level (m) is shown. The major rivers are represented by blue lines. The red lines denote land borders (Wikimedia, 2016).

Thailand and Myanmar, and a gently sloping coastline to the east. The peninsula is bordered by Malaysia in the south. Off the rugged west coast lie numerous islands popular with tourists (e.g. Phuket; Encyclopedia Britannica, 2016).

Thailand's climate is predominantly monsoonal; the changing seasons are associated with rainfall rather than temperature variations. Temperatures at or near sea level remain fairly constant throughout the year. Increasing elevation causes a decrease in average temperature, and an increase in latitude causes an increase in variability in monthly averages. In contrast, precipitation varies throughout the year; the pattern of variability changes depending on location within the country. There are two rainfall seasons: the winter (or dry/north-east) monsoon and the summer (or wet/south-west) monsoon. The first of these seasons occurs during November–March (NDJFM), bringing dry, cool air and little precipitation to the mainland, and heavy rain to parts of the south. The prevailing wind reverses during the summer monsoon (May–October (MJJASO)), which results in heavy rainfall over the mainland. A detailed physical explanation of the monsoon system is given in Section 1.3.1.

Parts of Thailand are also affected by tropical cyclones. The Northwestern Pacific basin is the most active in the world for tropical storm formation; an average of 26 storms per year are classed as a tropical storm or greater (sustained winds $> 17\,\mathrm{m\,s^{-1}}$), and 16.5 storms per year are classed as a typhoon (sustained winds $> 33\,\mathrm{m\,s^{-1}}$; NOAA Hurricane Research Division, 2013). Figure 1.2 shows the tracks and landfall location points of typhoons that made landfall in the Southeast Asian region of the Northwestern Pacific basin (1950–2010)—note this figure does not show the many additional storms in the region that were weaker than the typhoon classification. Thailand is predominantly affected by the remnants of storms that weaken overland to the east, although the peninsula is occasionally directly hit by storms. Tropical cyclones bring heavy rainfall to the areas over which they pass, typically affecting a smaller area than that of the monsoon system. However, later chapters will show that tropical storm rainfall can cause flooding on a large-scale, and can enhance summer monsoonal precipitation resulting in major flood disasters.

Thailand is a developing country. Many of the large Thai cities are

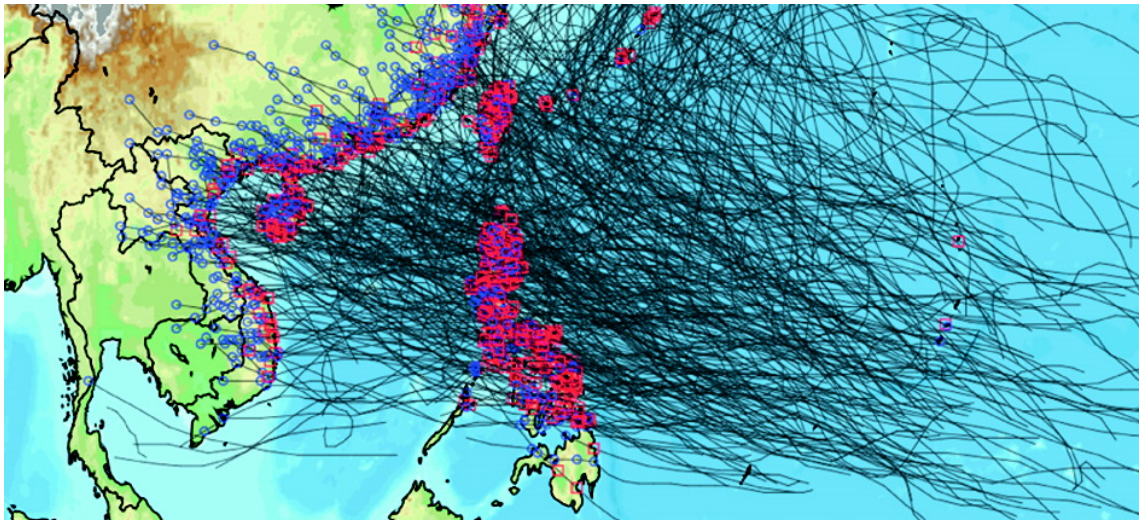

Figure 1.2: Map showing the tracks and landfall location points of storms that made landfall at typhoon intensity in the Southeast Asian region of the Northwestern Pacific basin (1950–2010). The black lines connect the 6-hourly best-track positions, the red squares indicate a typhoon-force landfall location point and blue circles indicate overland observations of tropical storm strength (Weinkle et al., 2012).

growing industrial centres with increasing investment from large multi-national corporations. Despite this, 1.2 % of the Thai population live in poverty (living on less than US$3.10 per day at 2011 international prices; The World Bank, 2016). Those living on lower incomes often rely on agriculture to survive, so are likely to suffer greatly when crops fail due to high flood waters. In areas where there are high levels of urbanisation—such as Thailand's capital, Bangkok—flooding is likely to cause extensive damage to buildings, industry and infrastructure. Insured and economic losses from flooding in the more developed areas are likely to be higher than those in the poorer areas.

Thailand was chosen as the primary country for this study, but many of the methods applied throughout this work are applicable to other countries in Southeast Asia. The large-scale flood of 2011 was devastating to much of the population, and insured losses of US$12 billion ranks as the highest ever from a freshwater flood disaster worldwide (Swiss Re, 2012). The insurance and re-insurance industry was unprepared for the widespread damage experienced in Thailand in 2011; the country has undergone rapid industrial development in recent years, and many multi-national corporations now have industrial bases in the country's largest cities (including Sony, Honda and Toyota; Aon Benfield,

2012a). For this reason, there is significant interest from the insurance and re-insurance industry for more information regarding extreme climatic rainfall in Thailand. This information can be used to improve catastrophe modelling for Thailand, which will in turn help improve the accuracy of insurance pricing and reduce the impact on the insurance industry from events such as the 2011 flood.

Precipitation in Thailand is dominated by the summer monsoon, with additional influence from tropical storm activity. The mean annual precipitation for the country is 1657 mm (1901–2012; data taken from the CRU TS3.21 dataset; Harris et al., 2014). This is much higher than the annual average precipitation for the UK (1154 mm; 1981–2010; Met Office, 2015b). Annual precipitation varies across the country (Figure 1.3); peninsular Thailand is the wettest region and the north-western region is the driest. A combination of orographic enhancement—where convection is enhanced by high ground—and the prevailing westerly wind during the summer monsoon means rainfall in peninsular Thailand is higher in the

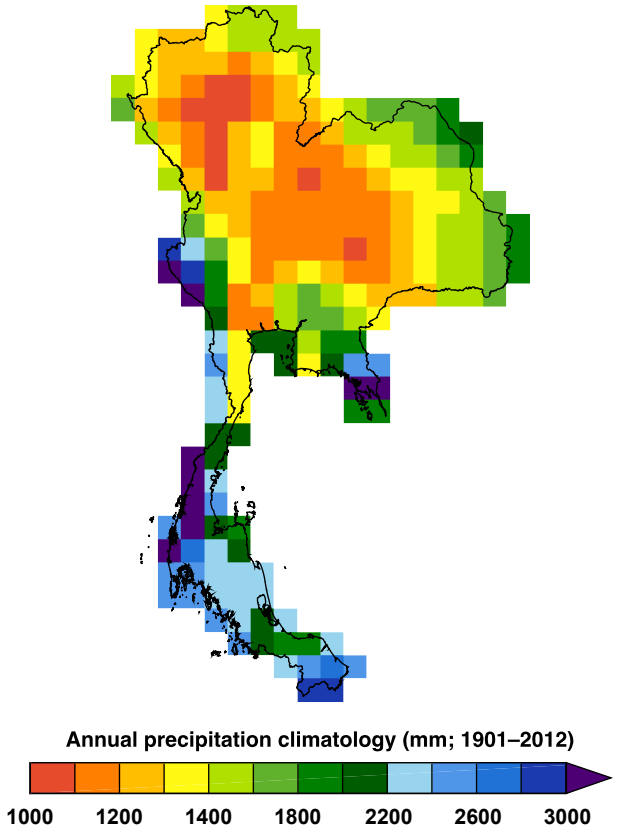

Figure 1.3: Map showing the variation of annual average precipitation across Thailand (1901–2012; data taken from the Climatic Research Unit (CRU) TS3.21 dataset; Harris et al., 2014).

west than in the east.

The summer monsoon is responsible for the inter-seasonal variability of precipitation in Thailand. The majority of annual rainfall occurs during MJJASO, when the summer monsoon is dominant. Figure 1.4 provides a spatial and graphical representation of precipitation variation by month across Thailand. Annual rainfall distribution graphs are shown for four major cities in Thailand: Chiang Mai (northern region), Udon Thani (north-eastern region), Bangkok (central region), and Hat Yai (south-eastern region). The three stations in continental Thailand show a clear increase in precipitation between April and May, and a decrease at the end of the summer monsoon season in October. Rainfall in the southern city of Hat Yai is not influenced by the summer monsoon. Here the precipitation is highest between October and December, with very little rainfall variation throughout the rest of the year. Overall, Hat Yai is much wetter than the other three stations.

1.3 Causes of extreme climatic rainfall in Thailand

1.3.1 Summer monsoon

The monsoon system can be defined simply as a seasonal reversal of the prevailing wind direction (Figure 1.5). Monsoon systems are fundamentally driven by solar heating of the land during the spring, creating a land-sea temperature difference. This triggers a low-level flow of moisture from the surrounding oceans to the warmer land nearby. Convection occurs over the land, resulting in the transported moisture being rained out over the monsoonal regions. The additional latent heat released by convection higher in the atmosphere draws in additional moisture, which maintains the wet season over a period of approximately six months. The change in seasons results in a shift of the peak solar heating equator-ward and into the southern hemisphere. This reverses the prevailing wind direction (as the ocean is now heated more than the land) and the monsoon rainfall moves to the opposite hemisphere (e.g. Figure 1.5; World Climate Research Programme, 2011).

Figure 1.6 shows the eight monsoon regions of the world. Thailand

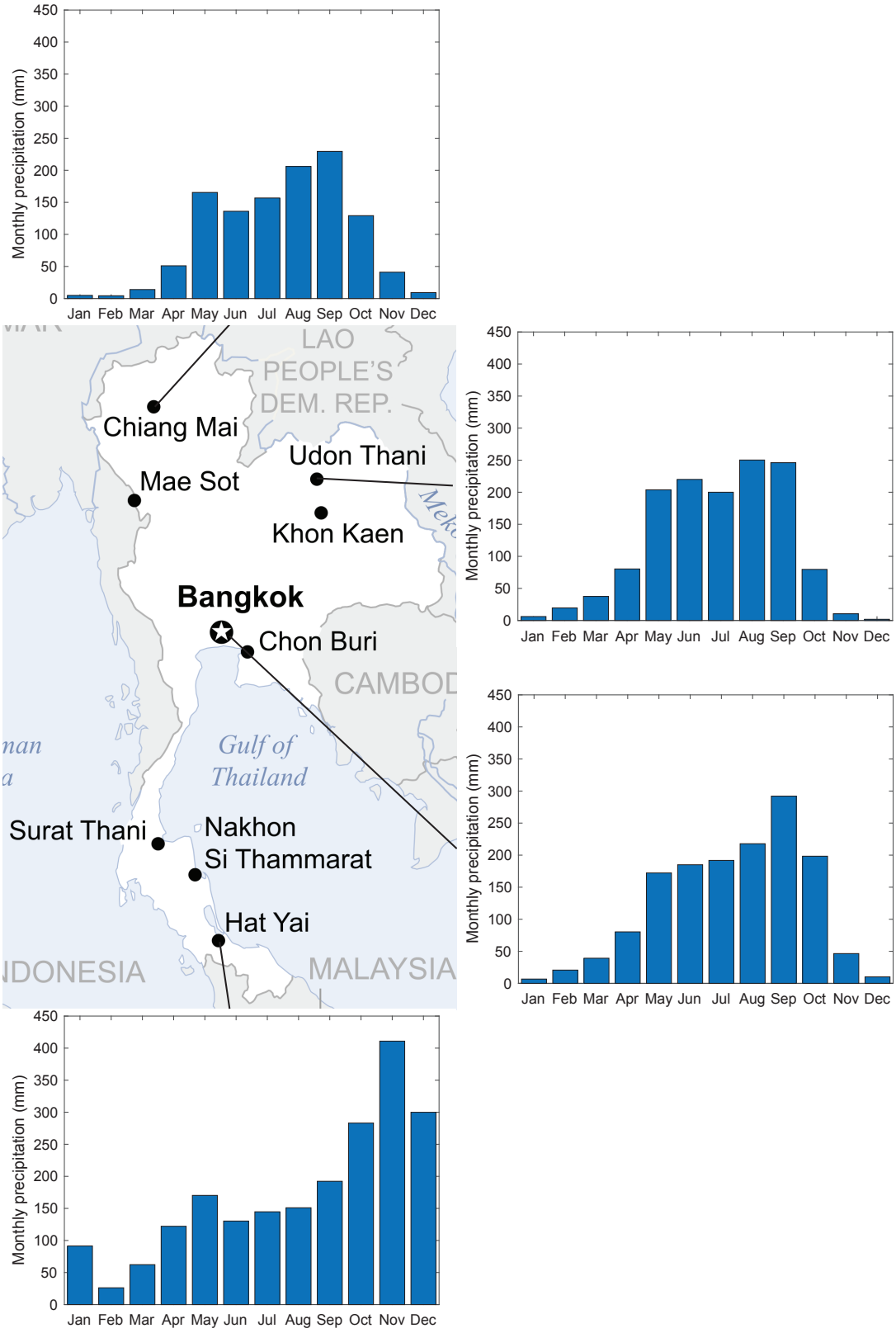

Figure 1.4: Annual precipitation distribution graphs for four cities located throughout Thailand (1901–2012; data taken from the Climatic Research Unit (CRU) TS3.21 dataset; data are for the grid square containing the given city; Harris et al., 2014). From the top left in a clockwise direction: Chiang Mai in the north, Udon Thani in the north-east, Bangkok in the central region, and Hat Yai in the south-east.

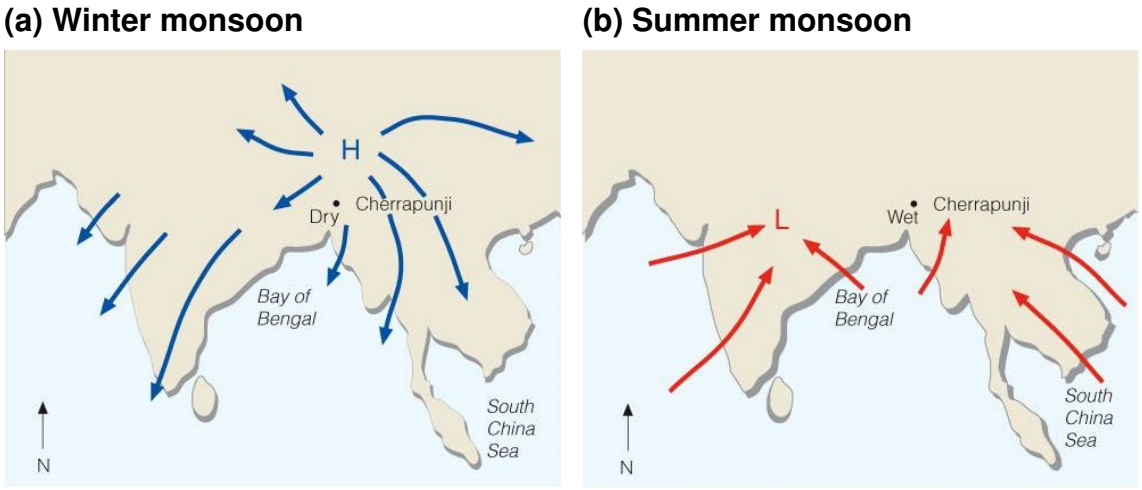

Figure 1.5: The changing prevailing wind patterns associated with the Indian (a) winter (November–March (NDJFM)) and (b) summer (May–October (MJJASO)) monsoon (Ahrens, 2008).

is predominantly affected by the Indian monsoon (IND), but the Western North Pacific monsoon (WNP) may also influence precipitation in the country, particularly in the east.

The Indian monsoon is the strongest monsoon globally. But why is that the case? Unique to the Asian continent, the expansive land mass of the Tibetan

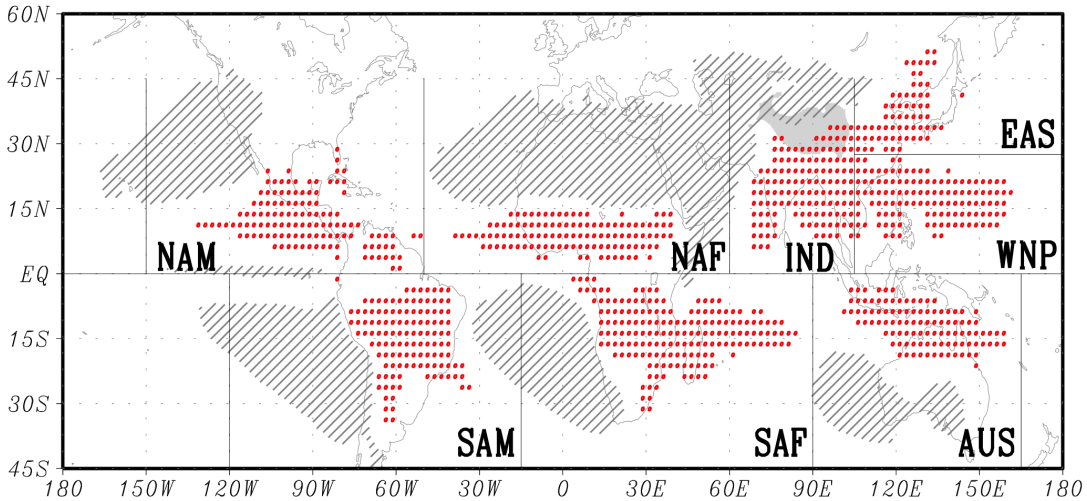

Figure 1.6: The approximate global monsoon precipitation domain. The red dots depict areas where the local summer-minus-winter precipitation rate is $> 2.5\,\mathrm{mm\,day^{-1}}$ and the local summer precipitation is $> 55\,\%$ of the annual total. Here summer is defined as May–September and November–March (NDJFM) for the northern and southern hemisphere respectively. Dry regions (summer precipitation $< 1\,\mathrm{mm\,day^{-1}}$) are shown by the grey hatchings, and the 3000 m height contour surrounding the Tibetan Plateau is shaded in grey (World Climate Research Programme, 2011).

Plateau acts as a massive heat source during the summer, and a heat sink in winter (Wang, 2006). The excessive heating of the plateau creates a large differential of temperature between the land and ocean, which strengthens the monsoon system over India and Southeast Asia. The plateau also acts as a huge air pump; strong ascent (descent) of the air column over the Tibetan Plateau in summer (winter) works to regulate the annual cycle of global circulation and the monsoon climate over Asia, Africa and Australia (Wang, 2006).

1.3.2 Tropical storms

Tropical storms form in the Intertropical Convergence Zone, the area surrounding the equator where convergence of the trade winds results in rising air and formation of low pressure systems. Various trigger mechanisms are required to strengthen the depression into a tropical storm (Met Office, 2015a). The most influential factors are:

1. A source of warm, moist air derived from tropical oceans with sea surface temperatures of $\geq 27\,^{\circ}\mathrm{C}$.

2. Ocean surface wind convergence, which causes air to rise and storm clouds to form.

3. Low wind shear, which allows the storm clouds to rise vertically to high levels.

4. Sufficient distance from the equator, which allows for rotation of the depression.

The conditions in the Northwestern Pacific Ocean are particularly favourable for the formation of many large tropical storms, which affect a large portion of Southeast Asia.

Due to Thailand's location, many of the storms that impact the county are remnants of storms that have weakened post-landfall in Vietnam. Occasionally, tropical storms track further south and make landfall over the southern peninsular region of Thailand. Figure 1.7 shows the number of tropical storms per month to impact Thailand during 1992–2011, based on best-track data from the Joint

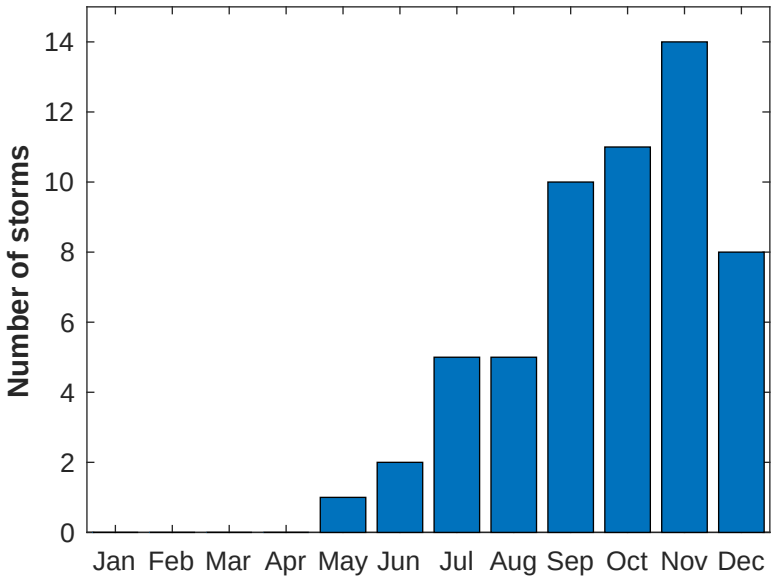

Figure 1.7: The number of tropical storms per month to affect Thailand over the period of 1992–2011 (based on best-track data from the Joint Typhoon Warning Center (JTWC); Chu et al., 2002).

Typhoon Warning Center (JTWC) (Chu et al., 2002). The peak of storm activity occurs late in the summer monsoon season. Storms can therefore exacerbate existing flooding from anomalously high precipitation from the summer monsoon.

1.4 Causes of interannual variability in Thailand climatic rainfall

As shown in Section 1.2, Thailand has a monsoonal climate where the majority of annual rainfall occurs during the summer months. Anomalously high summer monsoonal rainfall can cause large scale flooding in Thailand (Chapter 4); therefore, it is important to understand the causes of variability in summer monsoon strength, and therefore variability in Thai rainfall. This section describes two possible causes of this variability: ENSO and the IOD.

1.4.1 El Niño Southern Oscillation (ENSO)

ENSO refers to a broad scale phenomenon related to the anomalously warm or cold water that occasionally forms across the tropical eastern and central Pacific, and the interaction this has with the atmosphere. The phenomenon has two phases (Figure 1.8): the warm phase, El Niño, where SSTs are anomalously

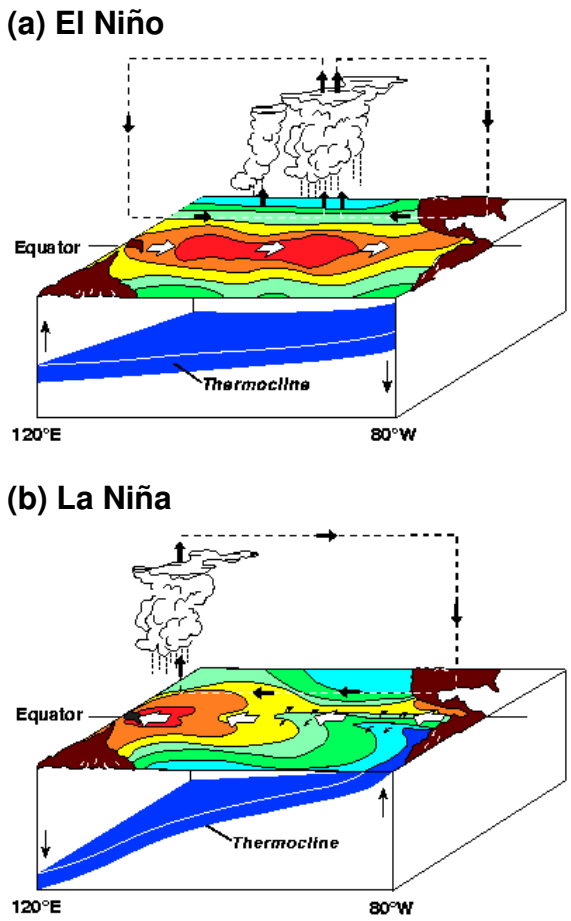

Figure 1.8: The El Niño Southern Oscillation (ENSO) and its associated ocean and atmosphere conditions (NOAA Tropical Atmosphere Ocean Project, 2016). Warm sea surface temperatures (SSTs) are shown in red, orange and yellow. Cool sea surface temperatures (SSTs) are shown in green and blue. The white arrows represent the flow of warm water. The dashed lines with black arrows represent the atmospheric circulation pattern. The black arrows below the ocean surface represent the movement of the thermocline, the layer of the ocean that divides the mixed upper layer from the calm deep water below.

warm in the tropical eastern and central Pacific, and the cold phase, La Niña, where SSTs are cooler than normal.

Various studies have examined the link between ENSO and rainfall in Thailand (e.g. Singhrattna et al., 2005a,b; Smith et al., 2012; Bridhikitti, 2013). It is generally thought that La Niña conditions cause anomalously high rainfall in Thailand. This is due to increased mean sea level pressure (MSLP) in the western Pacific subtropics during La Niña events, which enhances the easterlies and increases moisture transport to Thailand (as shown in Figure 1.8(b)). However, there is no clear consensus within the current literature as to the strength,

significance and seasonality of this correlation.

Singhrattna et al. (2005b) examined the link between summer monsoonal rainfall in Thailand and the Southern Oscillation Index (SOI) (a sea level pressure-based ENSO index; Section 2.3.1). The 21-year moving window correlations between August–October (ASO) Thailand rainfall and ASO SOI are shown in Figure 1.9 (solid line). Significant correlations between rainfall and ENSO were not seen until 1980 (in turn the correlation between SOI and the Indian monsoon weakened (dashed line)). Similarly, Cook and Buckley (2009) observed a shift in the correlation between summer monsoon indices (onset, withdrawal and length) and SSTs in the ENSO region between 1951–1979 and 1980–2005. Using the Multivariate ENSO Index (MEI) (Wolter and Timlin, 1998) and daily precipitation observations from stations in Thailand, Cook and Buckley (2009) observed a weak correlation between the MEI and the summer monsoon indices during the first period examined. In the latter period, summer monsoon onset and length both correlated strongly with the MEI (Spearman's rank correlations of +0.72 and –0.70 respectively), hence La Niña (El Niño) events caused an earlier (later) summer monsoon onset and a longer (shorter) overall summer monsoon season.

On a seasonal scale, Bridhikitti (2013) examined the connection between ENSO, the IOD and Thai rainfall anomalies. While no significant association

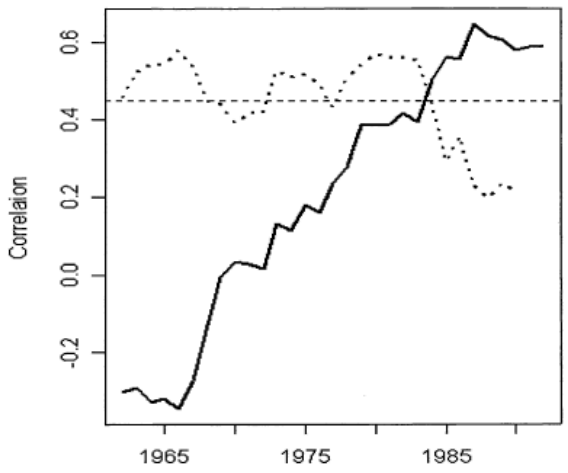

Figure 1.9: The 21-year moving window correlation between the Thailand summer monsoonal (August–October (ASO)) rainfall and the ASO Southern Oscillation Index (SOI) (solid line); and between the Indian summer monsoonal rainfall (June–September (JJAS)) and the JJAS SOI. The dashed horizontal line represents the 95 % significance level (Singhrattna et al., 2005b).

between ENSO signals and June–August (JJA) rainfall was seen, the study found that ENSO significantly affected Thai rainfall in the prior and subsequent months. High La Niña signals in January–March (JFM) correlated strongly with high precipitation anomalies in the following spring (March–May (MAM); correlation with the SOI of +0.78). Bridhikitti (2013) also observed a significant positive correlation (+0.56) between the SOI in spring and rainfall anomalies in the following autumn (September–November (SON)). Mason and Goddard (2001) also observed this link between ENSO and MAM precipitation anomalies.

On a longer timescale, Räsänen and Kummu (2013) observed strong links between large scale annual precipitation variations in the MRB (encompassing parts of eastern Thailand) and the decay of an ENSO phase. During La Niña events, MRB-averaged precipitation anomalies increased from 0 % in the onset year to +6.6 % during the decay year(s). A similar change was seen during El Niño events (–0.5 % to –5.3 %). The correlation between precipitation anomalies and La Niña was more significant in the Thailand area of the basin; the correlation with El Niño was more significant further north.

Chapter 6 examines the relationship between ENSO and climatic rainfall in Thailand in more detail.

1.4.2 Indian Ocean Dipole (IOD)

The IOD is a coupled ocean-atmosphere system with fluctuations in SST anomalies across the Indian Ocean (Saji et al., 1999; Webster et al., 1999). The Dipole Mode Index (DMI) (Saji et al., 1999)—used to measure the IOD—describes the zonal gradient in SST anomalies across the Indian Ocean between the west (50°E–70°E, 10°S–10°N) and the east (90°E–110°E, 10°S–Equator). The SST anomalies, which appear in June and peak in October, force changes in atmospheric circulations and rainfall patterns across the Indian and western Pacific Ocean regions (shown in Figure 1.10).

During the negative mode of the IOD (Figure 1.10(b)), cool SSTs in the western Indian Ocean and warm SSTs in the east cause a westerly low-level wind and increase convection over parts of Southeast Asia and Australia. This increased convective activity causes increased rainfall over the region, which

(a) Positive dipole mode

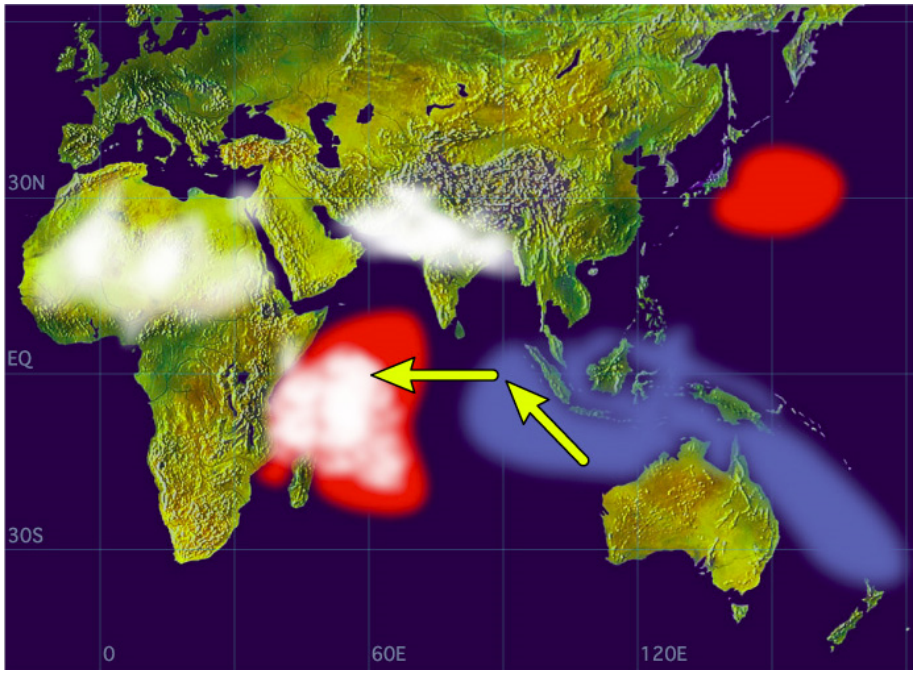

(b) Negative dipole mode

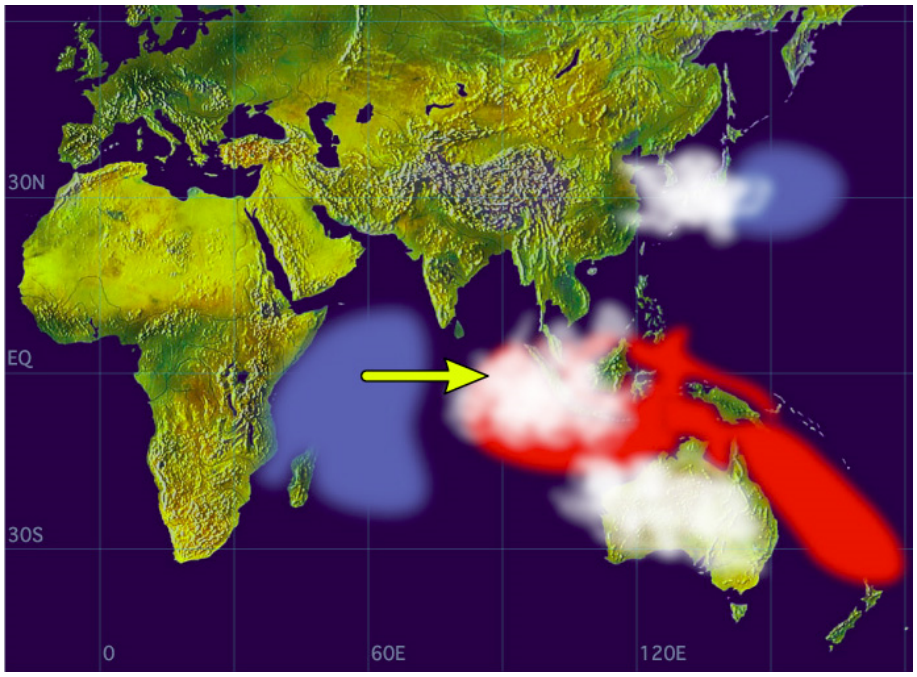

Figure 1.10: The Indian Ocean Dipole (IOD) and its associated negative (blue) and positive (red) sea surface temperature (SST) anomalies. Areas of increased convective activity are shown in white. The yellow arrows represent the low-level wind direction (Saji et al., 1999).

coincides with the summer monsoon season in Southeast Asia. These conditions reverse during the positive mode (Figure 1.10(a)). With respect to Thailand, various studies have assessed the link between the IOD and summer rainfall. Chansaengkrachang et al. (2011) found that strong negative phases of the IOD may cause higher rainfall in corresponding months. However, results from Saji and Yamagata (2003) and Bridhikitti (2013) suggest a weak association between the JJA IOD and Thai rainfall in the corresponding season. On a longer timescale, Bridhikitti (2013) observed a strong positive correlation (+0.752) between the JJA DMI and the JJA Thailand rainfall in the subsequent year. Singhrattna et al. (2005a) found a statistically significant negative correlation (–0.70) between the DMI in MAM and the ASO precipitation in Thailand.

IOD events also have the potential to modulate the relationship between ENSO and the Asian monsoon (Ummenhofer et al., 2013). Bridhikitti (2013) observed an increase (decrease) in December–February (DJF) rainfall on the south-east coast of Thailand when negative (positive) IOD events coincided with La Niña (El Niño) events during October–December (OND). Ummenhofer et al. (2013) found that combined El Niño and positive IOD events caused severe drought in Southeast Asia. During these combined events, the climatological southeasterly flow during JJA was opposed by strong westerly circulation anomalies across the eastern Indonesian Archipelago, which caused a divergent flow over the area. Southeast Asia was dominated by strong northerly circulation anomalies, consistent with a weakening of the South Asian monsoon, resulting in severe drought conditions.

Chapter 2

Data

2.1 Introduction

Chapter 2 describes the data that underpin this thesis. Precipitation is the primary data type used (Section 2.2), with both gridded and station datasets employed. The other data types used are climate index data (Section 2.3), storm track data (Section 2.4), climate reanalysis data (Section 2.5) and river discharge data (Section 2.6).

2.2 Precipitation

Precipitation data underpin almost all the work in this thesis. Station daily precipitation data are used to estimate the 2011 rainfall return periods and to examine the influence of tropical storms on precipitation in 2011 (Chapter 4). Gridded monthly long precipitation data are used to calculate the incidence of climatic precipitation in Thailand (Chapter 3), to calculate the return period of major flood events in Thailand (Chapters 4 and 5), and to examine the effects of ENSO on Thai precipitation (Chapter 6). To select the most appropriate station and gridded precipitation datasets for my research, I compared and analysed six sources of precipitation data. These sources are summarised in Table 2.1 and are described in more detail in Sections 2.2.1 and 2.2.2. They were selected based on their temporal length and spatial coverage over Thailand. The selection of the station daily precipitation dataset and the gridded monthly long precipitation dataset used in this thesis is justified in Section 2.2.3.

As I began this work in 2012, the precipitation datasets examined and analysed are those that were available in mid/late 2012. These datasets primarily cover the period through to the end of 2011. New versions of certain gridded datasets were released in 2014 and 2015. Additionally, certain daily station

Table 2.1: A summary of the precipitation datasets used in this work. The temporal coverage given is for the dataset availability at the time of this research (2012, or 2013 for the Climatic Research Unit (CRU) dataset listed).

Dataset	Spatial coverage	Spatial resolution (°)	Temporal coverage	Temporal resolution	Data format
APHRODITE	Asia	0.25, 0.5	1951–2007	Daily	Gridded
CRU	Global	0.5	1901–2012	Monthly	Gridded & station
GPCC	Global	0.5, 1, 2.5	1901–2010	Monthly	Gridded
MIDAS	Global	-	1852–2011	Daily	Station
NCDC	Global	-	1929–2011	Daily	Station
TMD	Thailand	-	1992–2011	Daily	Station

datasets are updated on a daily/monthly basis. Thus more extended and arguably better precipitation datasets are available at the time of writing than was the case in 2012.

The requirements of the station daily precipitation data for my study are threefold:

1. The number of stations in the dataset should be as high and uniform as possible to increase confidence in the interpolated results across Thailand as a whole.

2. The amount of missing data should be low within the time period covered.

3. The dataset must include 2011 so that the major Thailand flood in this year can be analysed.

The requirements of the gridded monthly precipitation data for my study are fourfold:

1. The dataset must be extended (ideally at least 100 years) so that long return periods can be produced based on observations. The insurance industry requires return periods out to 100- and 200-years to estimate risk, and prefer such values to be underpinned by observations.

2. The dataset must include 2011 so that the major Thailand flood in this year can be analysed.

3. The number of underlying stations in the dataset should be as high and uniform as possible to increase confidence in the gridded results across Thailand as a whole.

4. The spatial resolution of the gridded data should be as high as possible over Thailand to offer results with the greatest spatial detail.

2.2.1 Station data

Three sources of station data are examined in this study. These are described in alphabetical order below.

Met Office Integrated Data Archive System (MIDAS)

The UK **M**et **O**ffice **I**ntegrated **D**ata **A**rchive **S**ystem (MIDAS) Land and Marine Surface Stations Dataset (Met Office, 2012) stores land and marine surface observations from the UK Met Office station network and stations from around the world. The dataset covers the period 1853 to present, although global weather data are only available from 1974 onwards. The global weather parameters stored in MIDAS are observed at 3-hourly intervals and include wind, precipitation, temperature and weather observations. The Thai precipitation data are reported in millimetres typically at 6-hourly intervals (at 0, 6, 12 and 18 UTC). Some stations report less often (e.g. every 12 or 24 hours), and the majority of stations have some missing data. This work only uses the data through to the end of 2011.

National Climatic Data Center (NCDC)

The Global Summary of the Day dataset from the USA National Climatic Data Center (NCDC) (part of the National Oceanic and Atmospheric Administration (NOAA); NCDC, 2012) is comprised of daily averaged data computed from global hourly station data. The 18 parameters stored in the dataset include temperature, pressure, wind speed and precipitation amount. Historical data are available from 1929 to present, although the data are most complete from 1973 onwards. Precipitation is recorded in inches, the US standard measurement for rainfall. Again, this work only uses the data through to the end of 2011.

Thai Meteorological Department (TMD)

The Thai Meteorological Department (TMD) kindly provided the final station dataset, which contains rain gauge data for stations across Thailand. Here precipitation is recorded daily and is measured in millimetres. These data cover the 20-year period from 1992 to 2011; unfortunately the Thai Meteorological Department (TMD) were unwilling to provide additional rainfall data, hence the short data period.

Station details

Appendix A.1 shows the details of the Thai stations within each dataset, including the station name, latitude and longitude, time period covered and the percentage of missing data within that time period. It is important to note that data may not be continuous throughout the given time period, and data may not be available from the beginning of the first year or to the end of the last year given.

There are 103 stations in total across the MIDAS, National Climatic Data Center (NCDC) and TMD datasets, although not all of the stations appear in each dataset (MIDAS: 61; NCDC: 64; TMD: 99). Figure 2.1 shows the location of each station in these datasets. The figure also displays the locations of the stations included in the CRU gridded precipitation dataset described in Section 2.2.2. The spatial coverage across Thailand afforded by the stations is reasonably good with only a few areas having sparse coverage (e.g. the western central area). The additional stations in the TMD dataset improve the spatial coverage in some areas (particularly in the south of Thailand), although many of them are clustered around other stations.

Figure 2.2 shows, per dataset, the 131-year time series (1882–2012) of the total number of stations with at least one precipitation measurement per year and the number of stations with no missing data per year. This display also includes the number of underlying stations for the gridded 0.25° APHRODITE and 0.5° GPCC datasets (described in Section 2.2.2). The majority of the MIDAS stations have records that extend from the mid to late 1980s to the present day; however, only data through the end of 2011 are used in this study. Although the time period covered by the NCDC stations is typically much longer than the MIDAS and TMD

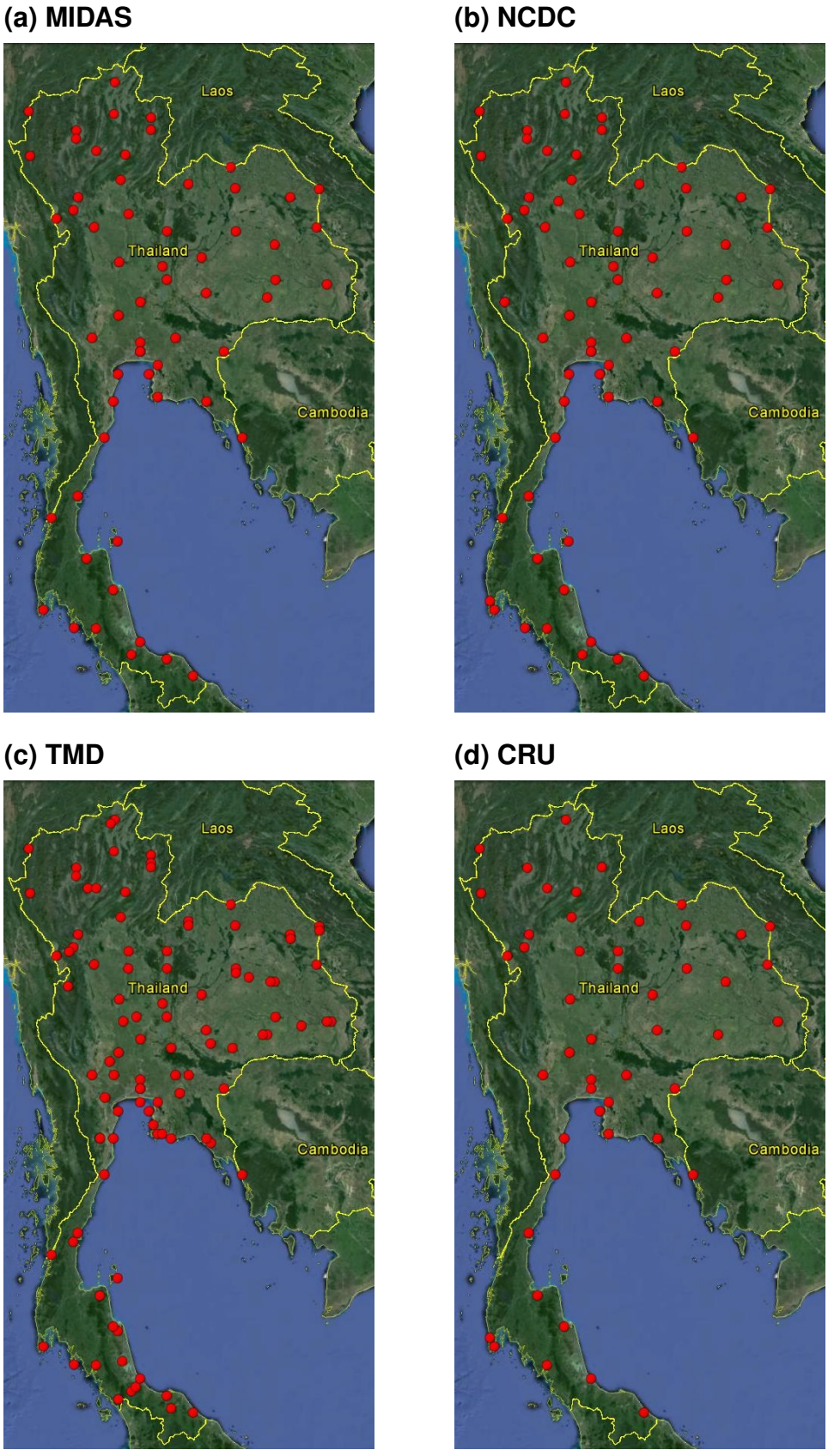

Figure 2.1: Maps showing the location of each Thai station in the (a) Met Office Integrated Data Archive System (MIDAS), (b) National Climatic Data Center (NCDC), (c) Thai Meteorological Department (TMD) and (d) Climatic Research Unit (CRU) datasets.

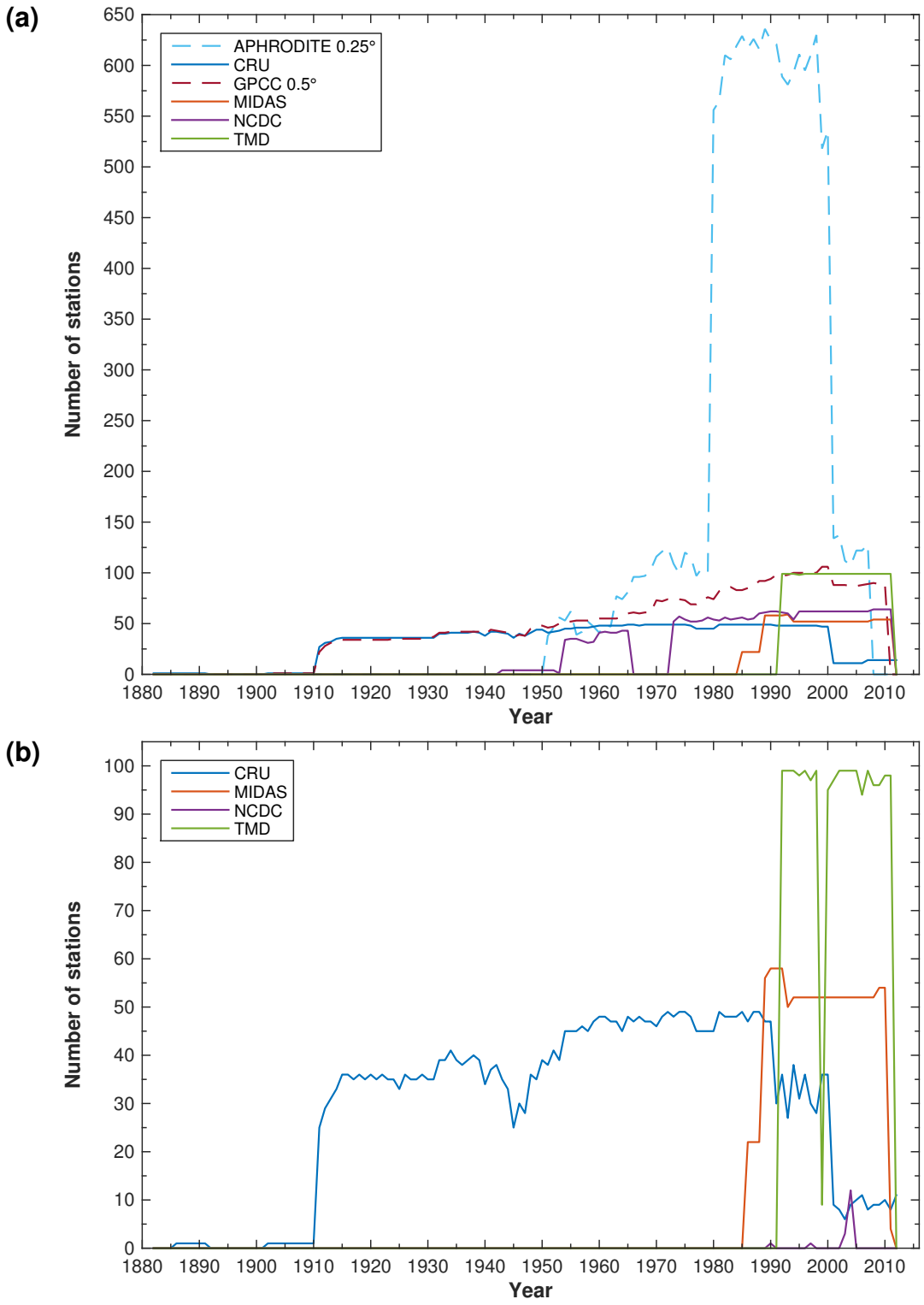

Figure 2.2: Time series (1882–2012) showing, per dataset and year, the (a) total number of stations (with at least one precipitation measurement recorded within a given year), and (b) the number of stations with no missing data. The dashed lines in (a) show the number of underlying stations in the APHRODITE (0.25°) and Global Precipitation Climatology Center (GPCC) gridded datasets. The station data for these gridded datasets are not available to download.

stations (many stations have records from the mid 1950s to present, although there is a 7-year gap from 1966 to 1972), the amount of missing data is high. On average across the 64 NCDC stations, 44.2 % of the data are missing within the time period covered. Only four years in the NCDC data period have stations with no missing data; 2004 is the best year with 12 stations with no missing data.

2.2.2 Gridded data

Three sources of gridded precipitation data are examined in this study. These are described in alphabetical order below. A summary of the strengths and weaknesses of these three precipitation data sources is given in Table 2.2.

APHRODITE

The APHRODITE project (**A**sian **P**recipitation—**H**ighly-**R**esolved **O**bservational **D**ata **I**ntegration **T**owards **E**valuation of Water Resources) developed state-of-the-art daily precipitation datasets for Asia. The data have a high spatial resolution (0.25° and 0.5° grids) and are available from 1951 to 2007 (Yatagai et al., 2012; APHRODITE, 2013). The project used data from the national hydrological and meteorological services of the countries covered (the west-east extent ranges from Turkey to Japan), other pre-compiled datasets (such as the Global Historical

Table 2.2: A summary of the strengths and weaknesses of the three gridded precipitation datasets described in Section 2.2.2. These points refer to the versions available at the time of this research (named in Section 2.2.2).

Dataset	Strengths	Weaknesses
APHRODITE	Daily data available	Only 57 years of data
	High spatial resolution (0.25°)	The data do not cover 2011
	Large underlying station network	Underlying station data unavailable
		Possibly inhomogeneous
CRU	112 years of data	Possibly inhomogeneous
	The data cover 2011	Comparatively smaller underlying station network
	Underlying station data available	
GPCC	110 years of data	The data do not cover 2011
	Large underlying station network	Underlying station data unavailable
		Possibly inhomogeneous

Climatology Network (GHCN) dataset) and data transmitted over the Global Telecommunication System (GTS).

Figure 2.2(a) shows the number of stations in the underlying station dataset over time. On average there are 276 stations per year over Thailand, but this number is skewed by a peak in station numbers between 1980 and 2000 (there are more than 515 stations per year during this period). The majority of these additional stations are around Bangkok. The APHRODITE project only provides the number of stations per grid square; the station data are not available.

Yatagai et al. (2012) performed quality control on the station data prior to interpolation; the data were checked for invalid dates, shifted columns and incorrect station locations. Discrepancies were often found between two or more databases containing the same measurements, so duplicated data were checked for consistency. In many cases, they were not able to judge which of these data were correct. They also identified unit conversion errors (e.g. errors with factors of 10 (cm to mm) or 25.4 (in to mm)).

Once the underlying data were sufficiently cleaned, Yatagai et al. (2012) calculated station climatologies for those stations with more than 5 years of recorded data. The ratio of the station climatology to the world climatology (WorldClim; Hijmans et al., 2005) was then taken for each month, and interpolated at a resolution of 0.05° using the robust empirical interpolation method called Spheremap (Willmott et al., 1985). This method uses angular distance weighting (Shepard, 1968), which takes into account the distances of the stations to the grid point, and the directional distribution of stations in relation to the grid point (to reduce the influence of clustered stations). A gridded monthly dataset was produced by multiplying these ratios by the world climatology, and Fourier transforms were then used to produce the final daily product.

This Climate Anomaly Method (Peterson et al., 1998a), where interpolation uses anomalies or ratios rather than raw precipitation amounts, improves the quantitative estimation of monthly rain gauge-based precipitation products (Chen et al., 2002; Schaake et al., 2004; Matsuura and Willmott, 2009). The use of Spheremap also improves the accuracy of gridded data; interpolation on the surface of a sphere (as in Spheremap)—rather than a Cartesian surface—

reduces the errors in gridded data fields.

For the purposes of this research, the APHRODITE data were summed to produce monthly, seasonal, summer monsoonal (MJJASO) and annual precipitation amounts.

Climatic Research Unit (CRU)

The CRU at the University of East Anglia, UK, produces a series of high-resolution (0.5°) global gridded datasets from monthly observations at meteorological stations across the world's land areas (TS1.0 (1901–1996), New et al. (1999, 2000); TS2.1 (1901–2002), Mitchell and Jones (2005); TS3.00 (1901–2005) to TS3.22 (1901–2013), Harris et al. (2014)).

Unlike the APHRODITE and GPCC datasets, the CRU provide the underlying station data used. These stations are plotted in Figure 2.1(d) and their details are given in Appendix A. Figure 2.2 shows the number of stations and the number of stations with no missing data over the period 1882–2012. In total, there are 49 stations in the CRU dataset, although this number is reduced in the first 29 years (1882–1910) and last 12 years (2001–2012). The time period covered by the CRU stations is longer than any of the other datasets; many of the stations have over 80 years of data. Of these stations, Bangkok has the longest extent, with 129 years of data from 1882 to 2012. The amount of missing data is low across all CRU stations; the highest is 11.2 % (Chaiyaphum). On inspection, many of the missing data are from the most recent years, particularly for those stations with data spanning through 2012. In 2001, the number of CRU stations reduces from 43 to 11. Personal communication (2015) with David Lister from the CRU revealed the majority of the Thai data used in the CRU dataset are taken from the World Weather Records dataset (World Meteorological Organization, 2015). The current version of this dataset (9th series) includes data through the end of 2000 only, hence the reduction in Thai station numbers post-2000.

Prior to interpolation, the CRU check the underlying station data for inhomogeneities. This is done using an automated method (essential for the large quantity of station data) that is only able to detect abrupt or widespread gradual changes, so the datasets are not truly homogeneous. The gridded

data are then constructed using the Climate Anomaly Method (described above), although percentage anomalies rather than ratios are used here. Station data are excluded from the gridding process if there are insufficient data (over 25 % missing values) over the base period (1961–1990), or if data are identified as outliers (for precipitation, values that fall more than 4.0 standard deviations from the normal). For some continents (including Asia), almost half of the station data were not used as it was impossible to calculate climate normals. Less than 1 % of the data were excluded as outliers (Harris et al., 2014). For any given grid square, gridded data are interpolated using data only from stations within the correlation decay distance (450 km for precipitation; Mitchell and Jones, 2005).

This work uses the TS3.21 (1901–2012) CRU dataset. Data were downloaded from the British Atmospheric Data Centre (Climatic Research Unit, 2013a,b). Although the datasets begin in 1901, there is only one station in the underlying dataset prior to 1911. The data in this period must be used with caution as the accuracy may be poor. Similarly, the data from 2001 to present are produced using far fewer stations than in the previous 90 years, so again, the accuracy of the data in this period may be reduced.

Global Precipitation Climatology Center (GPCC)

The GPCC, operated by Deutscher Wetterdienst, Germany, produce global gridded monthly precipitation datasets at 0.5°, 1° and 2.5° resolutions. At the time of writing, data are available for 1901–2013 (version 7; Schneider et al., 2015a,b,c), although I use version 6 (1901–2010; Schneider et al., 2011a,b,c) in this work (version 7 was not released until 2015).

Figure 2.2(a) shows the number of stations in the GPCC station dataset over time. The number of GPCC stations averages 76 per year for the period 1951–2007, which is higher than the CRU average but less than the APHRODITE average. Again, as with the APHRODITE dataset, the GPCC only provide the number of stations per grid square, not the actual station data.

The GPCC products use data obtained via the GTS combined with data contributions from national hydrological and meteorological services, international regional projects (e.g. APHRODITE, 2013), and global data

collections held by other institutions (such as the CRU and the GHCN; Becker et al., 2013). The GPCC use a semi-automatic quality control system described in detail by Schneider et al. (2014). An automatic system identifies possible outliers that are then checked visually so extreme values are not erroneously removed. After undergoing quality control, the station data are interpolated onto a 0.5° grid using a modified version of Spheremap (Willmott et al., 1985) that is described in detail by Becker et al. (2013). The GPCC interpolation method uses the closest 16 stations to each grid square, so the correlation decay distance varies. The coarser resolution grids (1° and 2.5°) are produced by area-weighted averaging the 0.5° grid boxes.

2.2.3 Comparison and selection of datasets

Before selecting the station daily precipitation data and gridded monthly precipitation data used in this thesis, it is instructive to highlight that differences exist between datasets and thus results can vary between datasets. This is demonstrated in Figure 2.3, which compares monthly and annual average rainfall (1992–2007) from the CRU station, TMD station and four gridded datasets (APHRODITE: 0.25° and 0.5°; CRU: 0.5°; GPCC: 0.5°) for three major cities, and Figure 2.4, which compares monthly rainfall time series (1992–2011) across two datasets (CRU gridded (0.5°) and TMD station). The grid squares selected all contain the corresponding station, and all 0.5° grid squares are identical in location. The MIDAS and NCDC station data were excluded as they contained a large amount of missing data during the period covered. Figure 2.3 shows that monthly and annual precipitation amounts vary between datasets. For monthly amounts the differences reach 88 mm, and for annual amounts the differences can be over 400 mm. The CRU station data differed from the TMD data for all three cities, particularly for annual average rainfall, although the CRU data contained some missing values during the period examined (which may affect the average rainfall amounts). As expected, the gridded and station data differed; the gridded data represent the entire grid box rather than the city itself. The precipitation averages also varied between the gridded datasets. These differences likely arise from differences in the underlying station datasets and

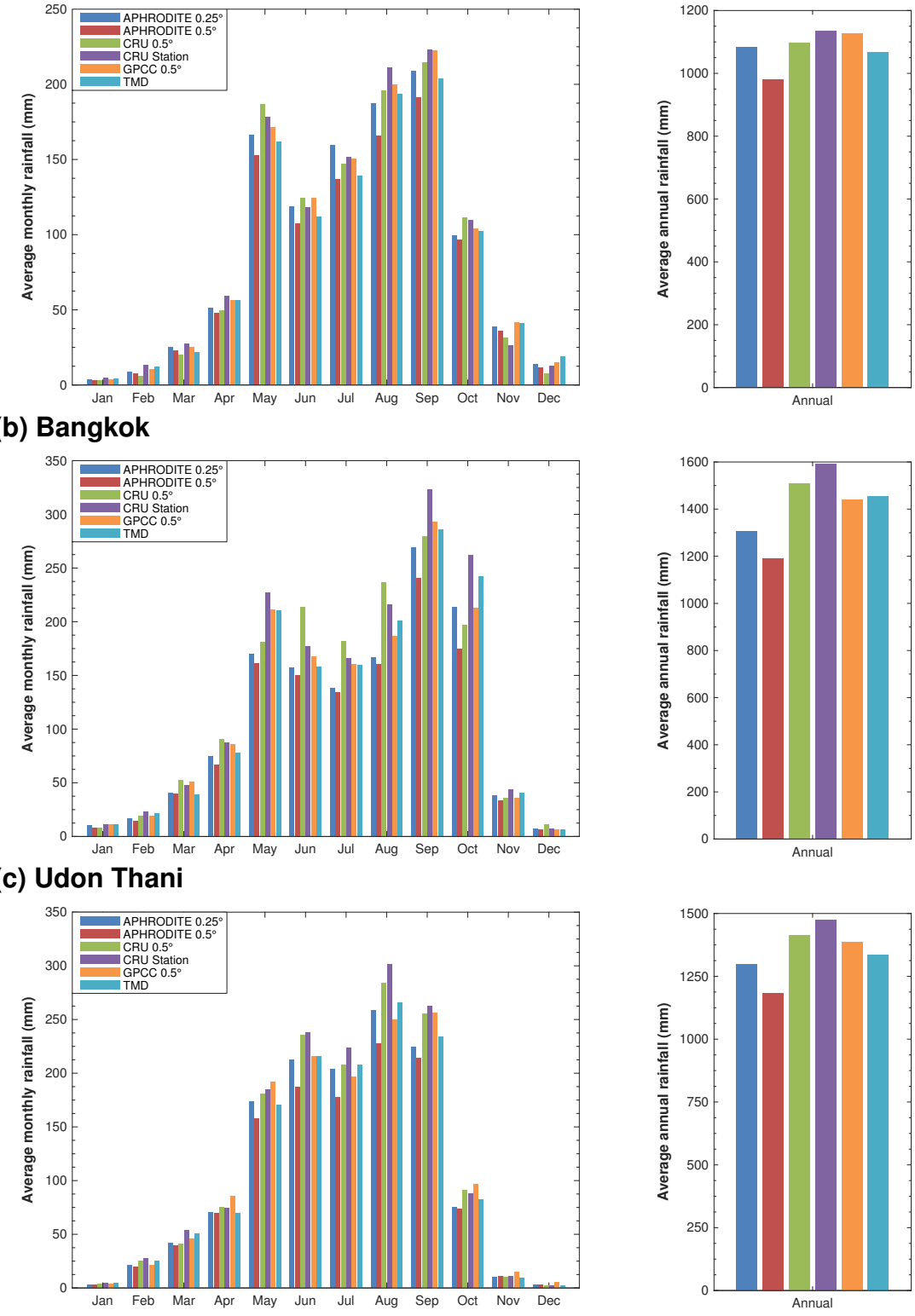

Figure 2.3: A comparison of average monthly (left) and annual (right) rainfall (mm; 1992–2007) across six datasets and three cities. The station data were compared to the data from the grid square containing that station. The Climatic Research Unit (CRU) station data contain some missing values during 1992–2007 (Chiang Mai: Feb, Nov and Dec; Bangkok: May and Jun; Udon Thani: Jan, Nov and Dec).

(a) Chiang Mai

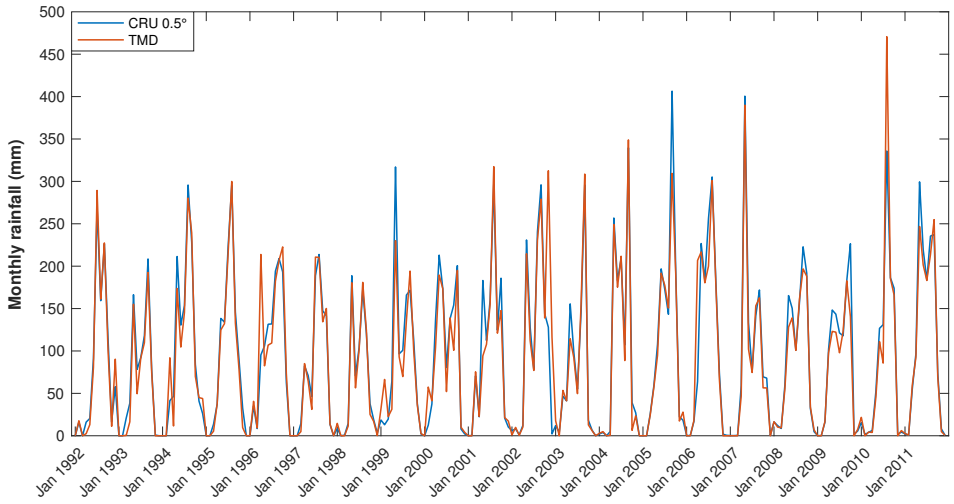

(b) Bangkok

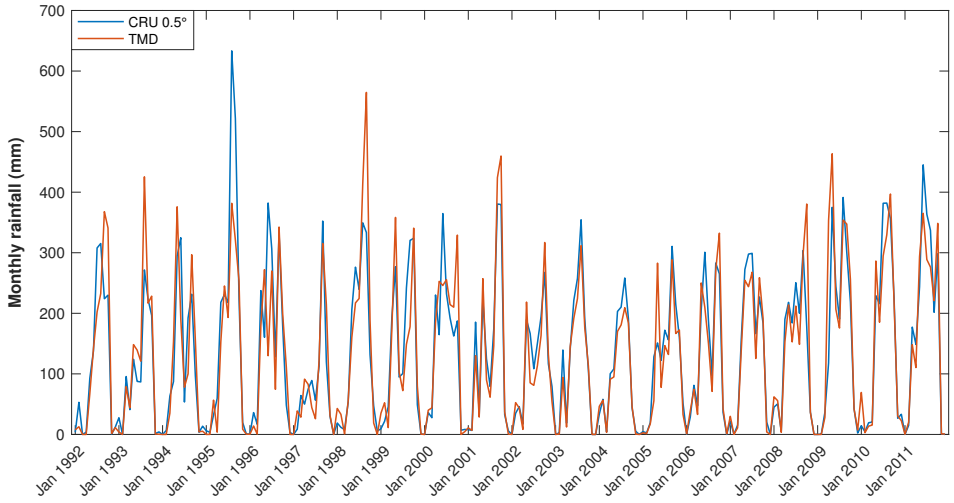

(c) Udon Thani

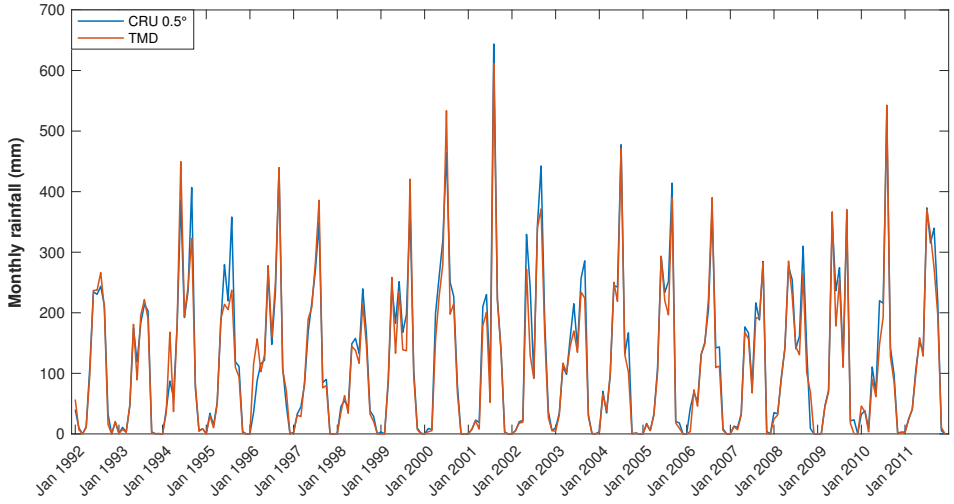

Figure 2.4: A comparison of monthly rainfall time series (mm; 1992–2011) across two datasets and three cities. The TMD station data were compared to the CRU data from the grid square containing that station.

in the interpolation methods. However, they may also reflect other sources of precipitation error as described in the next subsection. Figure 2.4 shows the differences between datasets are not consistent over time. The two datasets compared follow the same general pattern, but with some variances throughout the time series. Hence the source of the data differences is not a systematic error.

Sources of error in precipitation data

New et al. (2001) thoroughly reviewed different types of precipitation data, and described various errors that may appear within. Station data may include the following errors:

- Observer error, caused by taking inaccurate readings or by transcribing these readings inaccurately to paper or digital records.
- Measurement bias, caused by turbulence around the gauge deflecting precipitation, or by other factors such as evaporation or raindrops splashing out of the gauge (particularly common during heavy rainfall).
- Inhomogeneities in a station precipitation series, caused by changes in gauge type, site location, site conditions, or observing practices (Peterson et al., 1998b).

Detection of observer error is particularly difficult for daily rainfall data; all but the most extreme suspect measurements could potentially be correct. Identification of such errors is easier when comparing stations that appear in multiple datasets, although the process is extremely time consuming. Gauge biases can be corrected using generalised formulae (e.g. Legates and Willmott, 1990) although they are often acknowledged as a source of error and ignored (e.g. New et al., 2000). Inhomogeneities in the data record can sometimes be detected and corrected (Peterson et al., 1998b); changes in gauge type or site location often show a step in the record, but gradual changes in the site conditions result in gradual hard-to-detect changes in the data.

Interpolation, used to produce gridded data from point station records, introduces additional inaccuracies. Gridded rainfall is estimated using data from surrounding stations, therefore accuracy is lower where data are sparse.

The stations used during interpolation vary through time as the underlying station network changes, so some periods may use more stations than others. Few interpolation methods account for topography; this influences precipitation amounts, particularly near mountain ranges, so gridded rainfall in these areas may be over or underestimated. These additional errors found in gridded data must be acknowledged as a flaw but are commonly ignored.

Selection of station daily precipitation data

A simple comparison was done to identify any differences between matching stations in the three daily station datasets (MIDAS, NCDC and TMD). This yielded an unexpectedly high proportion of days where the data differed. This comparison was extended to calculate the percentage of data that could be considered incorrect using six different thresholds. For this purpose, the TMD data were considered correct. The MIDAS and NCDC data were compared to the TMD dataset using the criteria in the first two columns of Table 2.3. So for the first of these criteria, if the daily precipitation reported was ≥ 5 mm in both datasets and the difference between them was ≥ 1 mm, this reported precipitation amount was classed as incorrect.

The results in Table 2.3 are an average across all the stations compared; the number of differences varied across the stations. Many of the MIDAS stations had no incorrect reports (using these criteria), but two of the stations (Surat Thani and Lamphun) had a large amount of incorrect data (33.8 % and 77.8 % respectively, averaged across the six different criteria).

On average, 97.4 % of the NCDC data were incorrect. I examined the data in more depth to identify possible causes of these differences. Many of the NCDC data were one day out of sync with the TMD data, so shifting the NCDC data back by one day reduced the number of errors. Unfortunately, this error occurred in too few instances to justify shifting the values back by one day throughout the dataset.

I discovered a second timing issue when comparing US data from the NCDC with precipitation values from Hurricanes Ike and Irene (kindly provided by Dr. David Roth from NOAA). The hurricane rainfall data are recorded daily, but for

Table 2.3: Table showing the criteria used in, and the results of, the data validation process.

Precipitation in datasets $\geq$ (mm)	Difference between datasets $\geq$ (mm)	Incorrect reports (%)	
		MIDAS $\rightarrow$ TMD	NCDC $\rightarrow$ TMD
5	1	4.73	99.60
	5	3.69	98.29
	10	2.59	91.80
10	1	4.21	99.68
	5	3.29	98.38
	10	2.59	96.74

12Z–12Z rather than 0Z–0Z (as recorded in the NCDC dataset). However, the comparison showed 92 % and 88 % of the values matched for Ike and Irene respectively. This suggests the NCDC data are often 12Z–12Z totals rather than 0Z–0Z totals. This may account for some of the incorrect data found in the Thai NCDC stations but, without obtaining hourly station data, it was impossible to know for certain.

Yatagai et al. (2009) produced the APHRODITE dataset using a variety of data sources, including NCDC data. After their quality control process, they found a relatively low reporting rate in the NCDC data (compared to other sources), and a relatively high number of errors (including incorrect measurement units and missing data reported as 0 mm). Therefore, they only used the NCDC data in a grid box alongside another data source. For this reason, I decided the NCDC data quality was too poor to use the dataset in the remainder of this thesis.

To help identify the best station dataset, I ranked the three datasets against the three station data criteria given earlier (Section 2.2). The results of this ranking are shown in Table 2.4. The number of stations and the amount of missing data were ranked using the average over the 1992–2011 period covered by all three datasets. As expected, the TMD dataset ranks the highest for all three criteria. The NCDC dataset has more stations than MIDAS so ranks higher for that criterion, but there are more missing data in the NCDC dataset. Given these rankings and the other points discussed above, I decided to use the TMD dataset where daily data were required. However, the MIDAS data were used in the

Table 2.4: Ranking of three station datasets using the data criteria given earlier in Section 2.2. The ranks are given from 1 (worst) to 3 (best). The rank sum is a sum of the three criteria ranks, so the highest value indicates the best overall dataset. The number of stations and amount of missing data were ranked using the average values over the period 1992–2011 (the period covered by all three datasets). The dataset with the highest amount of missing data is ranked lowest.

	Rank			
Dataset	No. of stations	Missing data	2011 coverage	**Rank sum**
MIDAS	1	2	3	**6**
NCDC	2	1	3	**6**
TMD	3	3	3	**9**

quality control process, as described below.

I used a basic method to remove missing values from the TMD data and ensured each station had 100 % data coverage for the 20-year period. These are the steps taken to replace missing values:

1. If the station appeared in both datasets (MIDAS and TMD), I used the corresponding MIDAS value.

2. If MIDAS data were not available (no corresponding station or the MIDAS value required was also missing), I averaged the values from neighbouring stations (within a 50 km radius).

3. If there were no stations within a 50 km radius, I averaged the precipitation from the preceding and following days.

4. If the precipitation values from the preceding and following days were also missing, I used the average TMD value for that station and month.

Initially there were 122 stations in the TMD dataset; I excluded those with many missing data from further analysis and Table A.1 (e.g. Sukhothai, where data were only available from 2004 onwards). No quality control measures were applied to the gridded data.

Selection of gridded monthly precipitation dataset

To calculate the incidence of extreme climatic rainfall in Thailand, a long data record was vital but daily data were not required. Although the TMD data were considered the most accurate, the short data record (only 20 years) was insufficient. I ranked the three best gridded datasets across the four gridded data criteria (given earlier in Section 2.2) to help identify the best dataset to use in the remainder of this research (Table 2.5). The 0.5° APHRODITE dataset was omitted as the 0.25° dataset has a higher spatial resolution. The number of stations was ranked using the average number of stations in the underlying dataset over the period 1951–2007 (the period covered by all three datasets); interpolation tends to be more accurate when more stations are used (although this depends on whether the additional stations are clustered around others or dispersed more evenly; Webster and Oliver, 2007).

The CRU dataset ranked best in terms of length, although the quality may be poor prior to 1911 and post 2000 (as the number of stations is low in these periods). This dataset was also the only one to cover 2011. The APHRODITE dataset has the largest underlying station network (hence the quality is likely to be higher), but the length is the shortest of the three. The APHRODITE dataset also has the highest spatial resolution. Overall, the CRU dataset ranked the highest, primarily because of its length and coverage of 2011. Therefore, I chose to use

Table 2.5: Ranking of three gridded datasets using the data criteria given earlier in Section 2.2. The ranks are given from 1 (worst) to 3 (best). The rank sum is a sum of the four criteria ranks, so the highest value indicates the best overall dataset. The number of stations was ranked using the average values over the period 1951–2007 (the period covered by all three datasets). A dash is given where it is not possible to rank the dataset for a given criterion.

	Rank				
Dataset	Length	2011 coverage	No. of stations	Spatial resolution	**Rank sum**
APHRODITE 0.25°	1	-	3	3	**7**
CRU 0.5°	3	3	1	2	**9**
GPCC 0.5°	2	-	2	2	**6**

the gridded CRU dataset for the remainder of this thesis. As stated earlier in this section, I also use the TMD dataset where daily data improve the analysis (e.g. Chapter 4).

It is important to note that the analysis above is based on the dataset availability at the time of this research. If this work was repeated using the current versions of the datasets (as of 2015), I would use version 7 of the GPCC dataset (1901–2013) as there are more underlying stations than in the current CRU dataset (TS3.22, 1901–2013) and the longer length also allows analysis of the 2011 flood.

2.2.4 Trend analysis

To ensure accuracy when estimating the incidence of extreme climatic rainfall, there must be no underlying trend in Thailand rainfall. I performed a simple linear regression on the country-average annual precipitation time series (Figure 2.5) to identify any trend in the CRU rainfall data over the period used in this study (1901–2012). The aim of simple linear regression is to find the particular straight line,

$$\hat{y} = a + bx, \tag{2.1}$$

that minimises the squared vertical distances between it and the data points (x, y) (Wilks, 2011). The accent signifies a predicted value of y. The values of the parameters a and b that minimise these vertical distances are

$$b = \frac{\overline{xy} - \bar{x}\bar{y}}{\overline{x^2} - \bar{x}^2} \tag{2.2}$$

and

$$a = \bar{y} - b\bar{x}, \tag{2.3}$$

where a horizontal bar over a quantity indicates the mean of that quantity. In this case, the regression indicated a trend of +0.71 mm per year (black dashed line in Figure 2.5).

To calculate the statistical significance of this trend, I used the Student's *t*-test, a parametric test that considers the linear regression of y (precipitation in

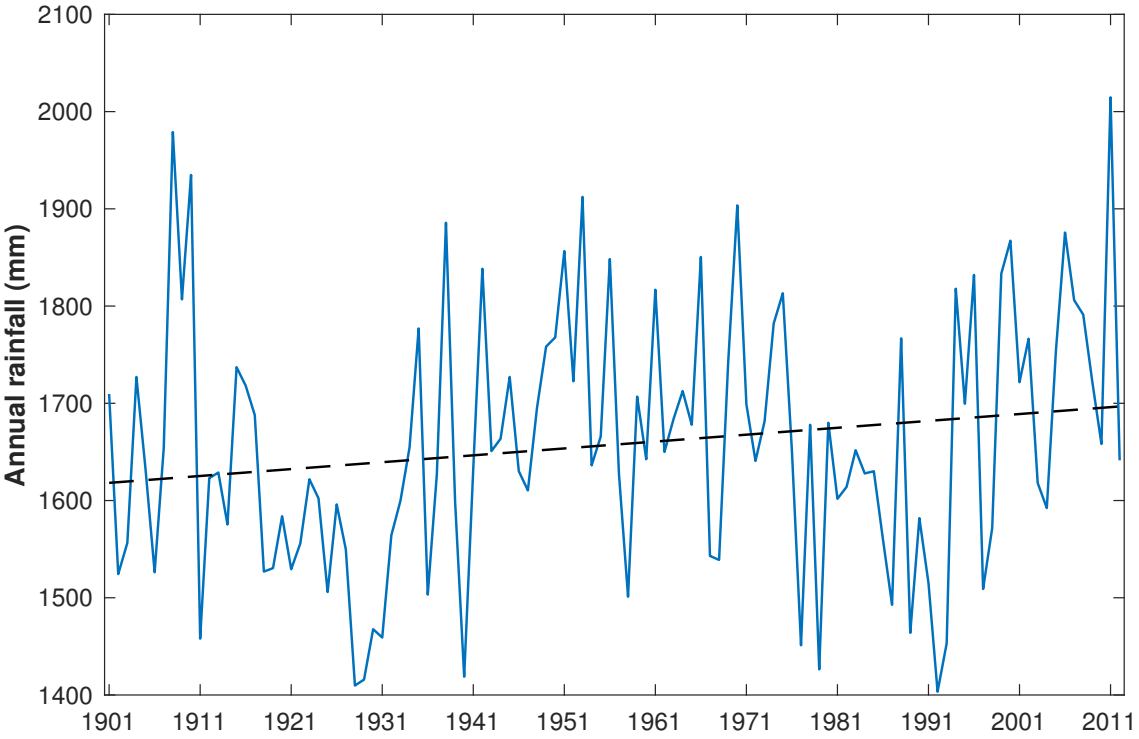

Figure 2.5: Time series (1901–2012) of Thailand-average annual precipitation (mm; blue) and corresponding regression line (black).

this case) on time x. The statistic

$$t = \frac{b(n-2)\sum (x_i - \overline{x})^2}{\sum (y_i - \hat{y}_i)^2} \tag{2.4}$$

follows the Student's *t* distribution with $n - 2$ degrees of freedom, where n is the sample size. The null hypothesis (that there is no trend) is rejected when the *t* statistic is greater in absolute value than the critical value $t_{\alpha/2}$, where α is the test level (Longobardi and Villani, 2009).

α is the probability of a type I error in statistical hypothesis testing: the incorrect rejection of a true null hypothesis (a 'false positive'). Ideally, this probability should be as small as possible, but as the probability of a type I error reduces, the probability of a type II error (the failure to reject a false null hypothesis (a 'false negative')) increases. In this work, I used a test level of 0.05 in all statistical analyses; this is the conventionally used value in statistics (Fisher, 1925a; Everitt, 2013).

In this case, $t = 1.843$ and $t_{0.05/2} = 1.982$; the *t* statistic is smaller than the critical value, so the null hypothesis (that there is no trend) cannot be rejected.

Hence the trend of +0.7 mm per year is not statistically significant and does not need to be considered in the remainder of this work.

2.3 Climate indices

2.3.1 Southern Oscillation Index (SOI)

The SOI (Troup, 1965) measures the strength and sign of ENSO (Chapter 1.4.1) and is calculated using the difference in MSLP between Tahiti, French Polynesia (east-central Pacific Ocean) and Darwin, Australia (west Pacific Ocean). To calculate the SOI, I employed the method used by the Australian Bureau of Meteorology (2015):

$$SOI = 10\frac{\left[P_{diff} - \overline{P_{diff}}\right]}{\sigma\left(P_{diff}\right)}, \tag{2.5}$$

where P_{diff} is the difference between the average Tahiti and Darwin MSLP for the month in question, $\overline{P_{diff}}$ is the long term average of P_{diff} for the month in question, and $\sigma\left(P_{diff}\right)$ is the long term standard deviation of P_{diff} for the month in question. In this thesis, I used the MSLP data available from the Australian Bureau of Meteorology (2014) and calculated the SOI using the 1901–2011 base climatology. The calculated SOI data are available for 1901–2011.

Prolonged below (above)-average east-central Pacific MSLP generally coincides with positive (negative) SST anomalies in the same region. Hence, sustained negative (positive) values of the SOI indicate an El Niño (La Niña) phase.

2.3.2 Oceanic Niño Index (ONI)

The second ENSO index used in this thesis, the Oceanic Niño Index (ONI), is the 3-month running mean of gridded SST anomalies (ERSST.v3b; Smith et al., 2008) in the Niño 3.4 region (5°N–5°S, 120°–170°W), based on centred moving 30-year base periods. These base periods are updated every 5 years so, for example, ONI values during 1961–1965 use the 1946–1975 base period, ONI values during 1966–1970 use the 1951–1980 based period, and so on. Recent ONI values (1996 to present) use the current 30-year base period (1981–2010). These moving base periods remove the effects of the significant warming trend

seen in the Niño 3.4 region SSTs since 1950 (Lindsey, 2013).

The ONI data are available from the NOAA Climate Prediction Center (2014) from 1950 to present, although I only use data from 1951 to 2011 in this work.

2.3.3 Dipole Mode Index (DMI)

The DMI, developed by Saji et al. (1999), measures the strength and sign of the IOD (Chapter 1.4.2). This index is simply the difference in SST anomaly across the tropical Indian Ocean from west (10°S–10°N, 50°–70°E) to south-east (10°S–Equator, 90°–110°E). The DMI data used here are derived using SST data from the Met Office Hadley Centre (HadISST; Rayner, 2003) and are available from JAMSTEC (2012) for 1958–2012. There are various other DMI datasets available derived from different sources of SST data (some of which date back to 1871) but this dataset was chosen as data are available for 2011.

2.4 Storm track data

Unisys (2015) provides an online catalogue of tropical storm track data, consisting of charts showing the track of storms in the various storm basins worldwide, and tables providing further details of each storm at 6-hour intervals (including position, maximum sustained winds, central pressure and storm category (using the Saffir-Simpson scale; Saffir, 1973; Simpson, 1974)). The storm tracks for the Western Pacific basin are compiled using data from the JTWC (Chu et al., 2002), and are available from 1945 to present.

Due to Thailand's location, many of the storms that affect the country (henceforth referred to as Thai storms) are remnants of stronger storms that dissipated over land to the east (Cambodia, Vietnam and Laos). The Unisys data only include track information when storms are classified as a Tropical Depression or greater, so the track data of Thai storms often terminate before crossing into Thailand. Therefore, I defined a Thai storm using two different criteria. Any storm whose track crossed Thailand's border was automatically classed as a Thai storm. For storms whose tracks terminated nearby (within 2.5° longitude to the east and 2.5° latitude to the north or south of Thailand's border), a spike in the TMD daily station precipitation data (in the approximate area and on the correct

date) was required for it to be classified as a Thai storm. As daily data were required to see these rainfall spikes, I only identified storms during the 1992–2011 period covered by the TMD station dataset. For the case studies in Chapter 5, I identified some additional storms that were possible causes of flooding, but their contribution to the excess rainfall was not quantified.

Figure 2.6 and Table 2.6 show the tracks and details of the 54 Thai storms during the 1992–2011 period. The dates given are those where a spike in the rainfall data was seen on the correct day in the approximate area of the country affected by the storm or its remnants.

2.5 Reanalysis data

The NCEP/NCAR reanalysis project uses a frozen state-of-the-art global data assimilation system with a long database of past data from multiple sources (Kalnay et al., 1996). Daily and monthly data for multiple variables are available from 1948 to present on a 2.5° resolution global grid. The long term monthly means also provided are derived using the 1981–2010 base climatology. In

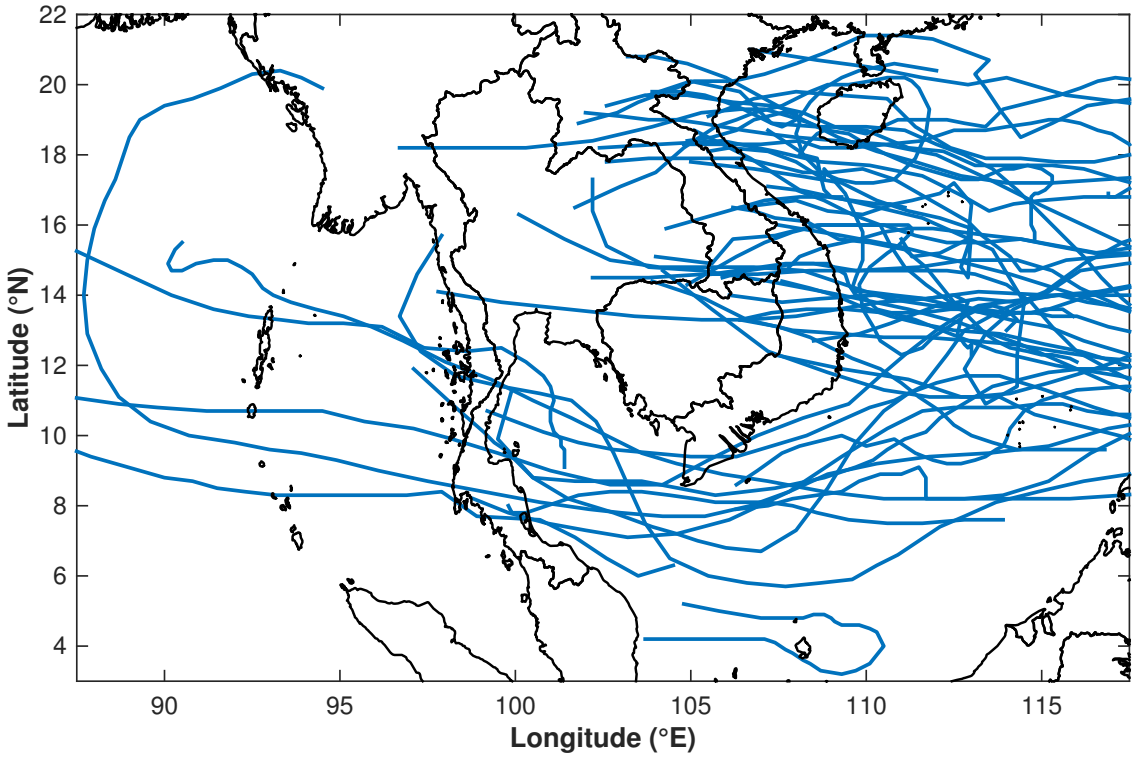

Figure 2.6: Map showing the tracks of the 54 tropical storms (or their remnants) that affected Thailand during 1992–2011. The data are taken from Unisys (2015).

Table 2.6: List of the 54 tropical storms (or their remnants) that affected Thailand during 1992–2011. The dates given are when the storm brought excess rainfall to the country. The storm names and classifications are those given by the Joint Typhoon Warning Center (JTWC), except Tropical Storm Jal, which was named by the Indian Meteorological Department. These classifications refer to the storm's maximum strength during its lifetime and not to its strength over Thailand. Tropical Storms are denoted by TS and Tropical Depressions are denoted by TD.

Year	Dates	Name	Year	Dates	Name
1992	28–29 Oct	Typhoon Angela	2001	10–12 Aug	TS Usagi
	15 Nov	TS Forrest		12 Nov	Typhoon Lingling
1993	12–13 Jul	Typhoon Lewis	2003	22–23 Jul	Typhoon Koni
	24–25 Nov	Typhoon Kyle		23–25 Oct	TS 23W
	9–10 Dec	Typhoon Lola	2004	13–15 Jun	Typhoon Chanthu
	15–16 Dec	Typhoon Manny		25–26 Nov	Typhoon Muifa
1994	27–28 May	TD 04W	2005	18–19 Sep	TS Vicente
	31 Jul	TS Amy		27–28 Sep	Typhoon Damrey
1995	29–31 Aug	Typhoon Lois		8–9 Oct	TD 20W
	11–12 Sep	TD 16W		21–22 Dec	TS 25W
	8 Oct	TD 23W	2006	25–26 Sep	TS 17W
	27 Oct	Typhoon Yvette		1–2 Oct	Typhoon Xangsane
	1–2 Nov	Typhoon Zack		6 Dec	Typhoon Durian
1996	23 Aug	Typhoon Niki	2007	7–9 Aug	TD 06W
	22–23 Sep	Typhoon Willie		3–5 Oct	Typhoon Lekima
	29 Oct–1 Nov	TD 34W	2008	30 Sep	TS Mekkhala
	3–4 Nov	TS 35W		15–18 Oct	TS 22W
	17–18 Nov	TS Ernie		19–20 Nov	TS Noul
	21–22 Dec	TD 41W	2009	13 Jul	TS Soudelor
1997	25–27 Sep	Typhoon Fritz		29 Sep–1 Oct	Typhoon Ketsana
	3–4 Nov	Typhoon Linda		3–5 Nov	Typhoon Mirinae
1998	20–21 Nov	TS Dawn	2010	1–2 Nov	TS Jal
	26 Nov	TS Elvis	2011	25–26 Jun	TS Haima
	12–13 Dec	Typhoon Faith		30–31 Jul	Typhoon Nock-ten
1999	3–5 Dec	TD 31W		27 Sep	TS Haitang
2000	22–23 Aug	TS Kaemi		5–7 Oct	Typhoon Nalgae
	10–12 Sep	Typhoon Wukong			
	9–10 Dec	TS Rumbia			

Chapter 4 I used MSLP data from this dataset to quantify the strength of the summer monsoon.

2.6 River discharge data

I obtained satellite-derived river flows for two locations (site (a): 16.0°N, 100.3°E; site (b): 15.5°N, 100.1°E) in the CPRB—the region most heavily flooded in 2011—from the Dartmouth Flood Observatory's online repository of global river discharge data (Brakenridge et al., 2012). The data used in Chapter 4 are from January 1992 to October 2012. The river flows are computed from passive satellite microwave observations and calibrated using global hydrological modelling (Robert Brakenridge et al., 2012). River flows obtained with this satellite-derived method agree well with flow estimates from ground-based discharge gauges.

Chapter 3

Thailand extreme climatic rainfall return periods

3.1 Introduction

In 2011, Thailand experienced its wettest year on record, resulting in widespread flooding that affected 65 out of 77 provinces and caused economic losses of US$30 billion (Chapter 4). A similar event in 1995 led to the worst Thai flood in the period 1985–2012 (when ranked by flood magnitude—a function of duration severity and area affected), as documented by the Dartmouth Flood Observatory (Brakenridge, 2012) (Chapter 5). Although flooding is a regular occurrence in Thailand (71 Thai flood events occurred in the 1985–2012 period; Brakenridge, 2012), events with magnitudes similar to the 1995 and 2011 floods are rare.

Flood management is increasingly shifting towards a risk based approach, where flood risk is the product of the probability of flooding and the potential consequences of such flooding (Few, 2003; Tunstall et al., 2004; Merz et al., 2010; Ward et al., 2011). The financial benefits of better flood risk modelling include improved flood defence policies, better government planning, and more accurate insurance pricing. The human benefits of improved flood risk modelling include greater protection to life and assets, and a positive impact on the well-being of those who are at risk (Clarke et al., 2015). These financial and human benefits have driven the growth of flood risk management across the UK and are now generating advances in flood risk management in developing countries such as Thailand (Aon Benfield, 2012b; JBA Consulting, 2014). This development shows the importance of understanding the incidence of extreme rainfall in Thailand, particularly on the climatic scale (the primary cause of the 2011 flood).

One measure of extreme rainfall incidence is the return period and the

associated return level (IPCC, 2012). The return period is the average length of time, in years, for an event of a given magnitude to be equalled or exceeded. Extreme value theory (EVT) is the most common method of modelling extreme rainfall and estimating the return periods for extreme rainfall events (e.g. Cowpertwait et al., 2002; Feng et al., 2007; Svensson and Jones, 2010). EVT provides two statistical models for the tail of a probability distribution: the Generalized Extreme Value (GEV) distribution and the Generalized Pareto distribution (GPD) (Coles, 2001). The GEV typically models maxima of finite-sized blocks (e.g. annual maximum daily rainfall; Chen and Knutson, 2008; Chu et al., 2009; Artlert et al., 2013), whereas the GPD models exceedances above a threshold (e.g. the highest 80 % of July–September (JAS) rainfall; van Oldenborgh et al., 2012). Rainfall is also modelled using other distributions, including the gamma (Pinkayad and Ertuna, 1970; Mooley, 1973; Ben-Gai et al., 1998; Husak et al., 2007), log-normal (Phien et al., 1980), and normal distributions (Berolo, 2013). Return periods can also be estimated simply using the number of exceedances of an event during the period examined (as in Ono and Kazama, 2011).

Various studies have estimated return periods for flood events or river flows in Thailand (Kidson et al., 2005; Supharatid, 2006; Prajamwong and Suppataratarn, 2009; Tingsanchali and Karim, 2010; DHI, 2011; Kure and Tebakari, 2012; Lim and Boochabun, 2012), but, at present, very little research has been done regarding rainfall return periods in the country. Previous work primarily focussed on the annual maximum of short-duration rainfall in Thailand (sub-hourly/hourly (Pinkayad and Ertuna, 1970) and daily (Ono and Kazama, 2011; Artlert et al., 2013)), although two studies examined Thai rainfall at longer timescales (monthly (Phien et al., 1980) and seasonal (van Oldenborgh et al., 2012)). These examples primarily used EVT to estimate return periods, although Ono and Kazama (2011) also used a basic method (the 5-year return period was equated to the fourth highest rainfall in the 20-year measurement period).

The aim of this chapter is to produce return periods for extreme rainfall for all grid squares across Thailand at multiple climatic timescales (monthly, seasonal, MJJASO and annual). As shown in Chapters 4 and 5, the floods in 2011 and

1995 were predominantly caused by persistent rainfall over many months, so it is important to quantify the incidence of extreme rainfall over these climatic timescales.

First I define extreme climatic rainfall (Section 3.2.1). I then describe the data (Section 3.2.2) and the two different methods (basic and distribution) used to calculate the return periods (Sections 3.2.3 and 3.2.4). Section 3.2.4 also details the selection of distributions for the latter method, and describes the method of calculating the uncertainty in these return periods. Finally I show the results of this distribution selection (Section 3.3.1) and examples of the three products produced in this chapter: return period curves (Section 3.3.2), return period maps (Section 3.3.3) and return level maps (Section 3.3.4).

3.2 Methodology

3.2.1 Definition of extreme climatic rainfall

As Stephenson (2008) states, extreme events are easy to recognise but difficult to define. There is no unique definition of 'extreme' used in the meteorology/climatology field, and 'extremeness' varies depending on context. Extreme rainfall in the UK, for example, differs greatly from extreme rainfall in Thailand.

NOAA's Climate Extremes Index (Karl et al., 1996), which quantifies observed changes in climate within the contiguous United States, defines extremes as occurrences that are outside the 90th/10th percentile over the data period (Gleason et al., 2008). Similarly, IPCC (2012) defines an 'extreme climate or weather event' or 'climate extreme' as 'the occurrence of a value of a weather or climate variable above (or below) a threshold value near the upper (or lower) ends of the range of observed values of the variable'. Quantitatively, IPCC (2012) define extremes in two ways: related to their probability of occurrence (i.e. percentiles of distribution functions, or specific return periods), or related to a specific threshold.

In this work, I define extreme climatic rainfall as monthly, seasonal, summer monsoonal (MJJASO) or annual rainfall with a return period of 10 years or

more (Figure 3.1). This is approximately equivalent to the 90th percentile of observations. The return level associated with a 10-year return period varies depending on the timescale and location.

3.2.2 Data

This chapter uses the gridded CRU data (Section 2.2.2) over Thailand for the period 1901–2012 (112 years). For each year and grid square, I summed the data to produce annual (Jan–Dec), summer monsoonal (MJJASO) and rolling three-month seasonal values (e.g. JFM, February–April (FMA)). Two seasons (November–January (NDJ) and DJF) span across multiple years so they have one fewer year of data. In this work, the NDJ and DJF values for a given year use the November and December values from the preceding year (e.g. NDJ 2011 spans from November 2010 to January 2011); therefore 1901 has no NDJ and DJF value.

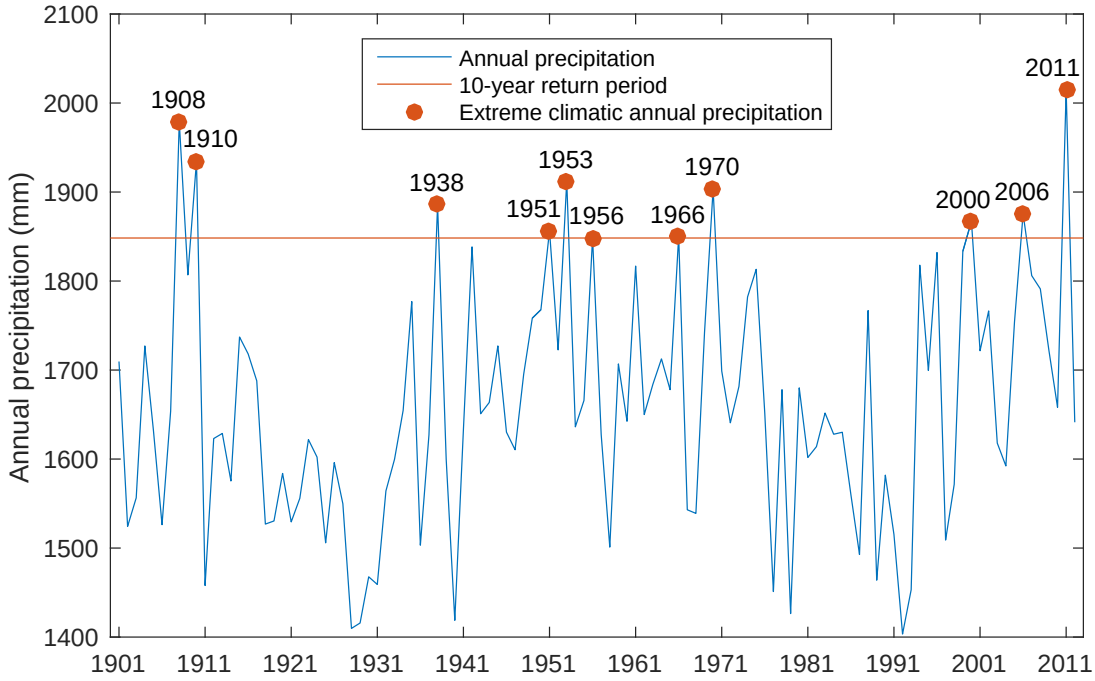

Figure 3.1: Time series (1901–2012) of Thailand annual precipitation (blue) depicting the definition of extreme climatic rainfall used in this work. The red line shows the 10-year return period calculated using the basic method (Section 3.2.3) and the red markers show the 11 years in the data period with extreme climatic annual rainfall.

3.2.3 Return period calculation: basic method

I used two different methods to calculate return periods: the basic method (Section 3.2.3) and the distribution method (Section 3.2.4).

The basic method uses the relationship between the return period (in years), R, and the probability of exceedance (per year), p_E, to estimate return periods. The probability of exceedance (of an event of specified magnitude) is the probability that an event of the specified magnitude will be equalled or exceeded during a one year period. These two variables are inversely related:

$$R = \frac{1}{p_E}, \quad p_E = \frac{1}{R}. \tag{3.1}$$

Firstly, I created various precipitation time series consisting of one value per year per timescale (e.g. annual mean, summer monsoon mean, JAS mean, July mean; e.g. Figure 3.1). The probability of exceedance per year was then estimated using basic probability principles:

$$p_E(x) = \frac{n_E(x)}{n}, \tag{3.2}$$

where $n_E(x)$ is the number of events in the time series where x, a given precipitation value (e.g. 1000 mm), is equalled or exceeded, and n is the total number of events in the time series (i.e. 112 years). Therefore the return period can be written as

$$R(x) = \frac{1}{p_E(x)} = \frac{n}{n_E(x)}. \tag{3.3}$$

This method is limited in two ways. Firstly, it is not possible to estimate return periods longer than n. So, with 112 years of data, the maximum possible return period is 112 years. Secondly, it is not possible to calculate uncertainty using this method. Therefore, the longer the dataset, the more accurate the return period estimate.

3.2.4 Return period calculation: distribution method

The distribution method utilises distribution fitting to estimate return periods longer than n. Here, the return period is estimated using

$$R(x) = \frac{1}{\omega[1 - F(x)]}, \tag{3.4}$$

where $F(x)$ is the probability of precipitation less than or equal to x taken from the fitted cumulative distribution function (CDF) and ω is the average sampling frequency, which is $1\,\mathrm{yr}^{-1}$ in this case (Wilks, 2011). Unlike the basic method, the use of distribution fitting allows the calculation of uncertainty.

Distribution selection

The most appropriate distribution depends on the timescale of the precipitation being modelled. Annual rainfall tends to follow a normal distribution (Bricquet et al., 2003), whereas monthly rainfall is highly non-symmetric (Berolo, 2013).

I used Easyfit (Mathwave, 2014) to fit 49 distributions to the data for four different grid squares across Thailand at four different timescales (from one month to one year). The program ranks the fit of each distribution using the Kolmogorov-Smirnov (KS) (Massey Jr., 1951), Anderson-Darling (Anderson and Darling, 1952) and Chi-Squared (Pearson, 1900) goodness-of-fit tests. I averaged the three rankings to identify the most appropriate distribution for each grid square and timescale tested. The gamma, GEV and normal distributions consistently performed well, so I chose to use these in the return period calculations. Here I describe the nature of these distributions and how I fitted the parameters of each distribution.

Gamma

The gamma distribution is commonly used to represent precipitation data as it is bounded on the left by zero and is positively skewed (Wilks, 2011). The gamma distribution is defined by the probability density function (PDF)

$$f(x) = \frac{(x/\beta)^{\alpha-1} \exp(-x/\beta)}{\beta\Gamma(\alpha)}, \quad x, \alpha, \beta > 0, \tag{3.5}$$

where α is the shape parameter and β is the scale parameter. The gamma function, $\Gamma(\alpha)$, is a standard mathematical function defined by the definite integral

$$\Gamma(\alpha) = \int_0^\infty t^{\alpha-1} \exp^{-t} dt. \tag{3.6}$$

Variation of the dimensionless shape parameter, α, affects the shape of the gamma distribution PDF (Figure 3.2(a)). For $\alpha < 1$, the distribution is strongly skewed to the right, with $f(x) \to \infty$ as $x \to 0$. The exponential distribution (a special case of the gamma distribution) occurs when $\alpha = 1$. In this case, the PDF intersects the vertical axis at $^1/_\beta$. For $\alpha > 1$, the PDF begins at the origin, $f(0) = 0$. Increasing α leads to less skewness and the PDF shifts to the right. Very large values of α (approximately > 50) result in a gamma distribution approaching the normal distribution in form.

Variation of the scale parameter, β, effectively stretches or squeezes the gamma PDF to the right or left depending on the overall magnitude of the data represented (Figure 3.2(b)). Larger values of β stretch the distribution to the right, which in turn means its height must drop to satisfy Equation 3.5. Conversely, as the PDF is squeezed to the left, its height must rise.

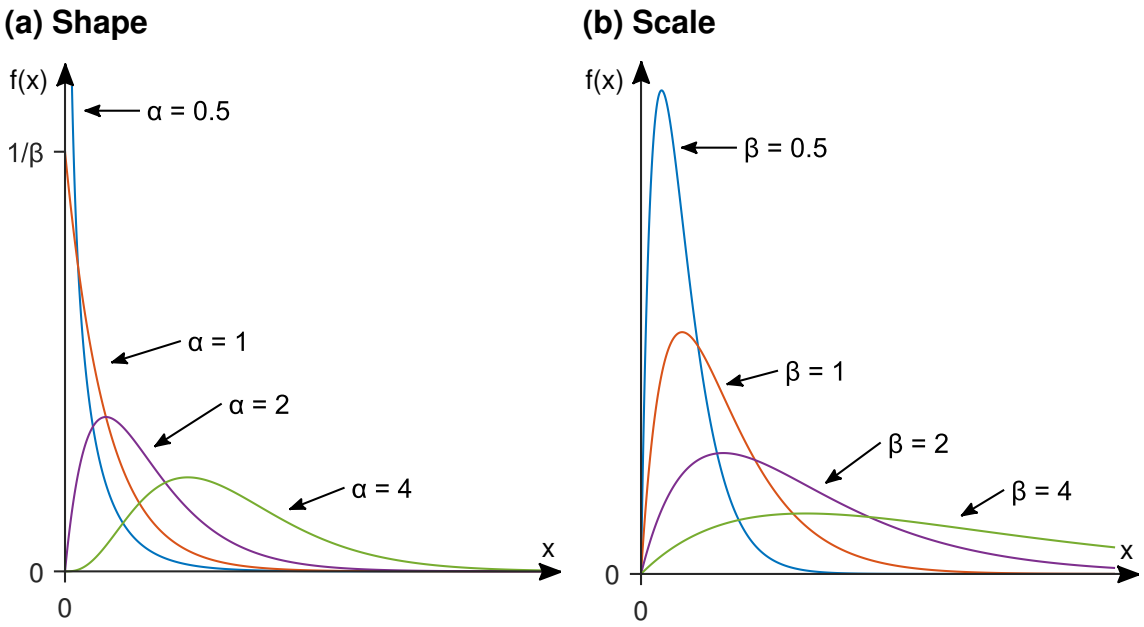

Figure 3.2: Gamma distribution probability density function (PDF) for four values of the (a) shape parameter, α, and (b) scale parameter, β (adapted from Wilks, 2011).

I used the method of maximum likelihood (Fisher, 1925b) to estimate the fitted gamma distribution parameters; this requires an iterative procedure that can completed using a built-in MATLAB function (`gamfit`; MATLAB, 2015a). However, this procedure is extremely time-consuming, so I instead used a computationally efficient approximation of the maximum-likelihood estimators. This approximation used the Thom (1958) estimators for the shape, $\hat{\alpha}$, and scale, $\hat{\beta}$, parameters:

$$\hat{\alpha} = \frac{1 + \sqrt{1 + {}^{4D}/_{3}}}{4D} \tag{3.7}$$

$$\hat{\beta} = \frac{\bar{x}}{\hat{\alpha}}, \tag{3.8}$$

where $\bar{x}$ is the data mean, D is the statistic

$$D = \ln(\bar{x}) - \frac{1}{n}\sum_{i=1}^{n} \ln(x_i), \tag{3.9}$$

and n is the length of the dataset (e.g. number of years). These Thom estimates for the shape and scale parameters match those estimated using the `gamfit` MATLAB function.

Generalized Extreme Value (GEV)

The GEV distribution, one of the two distributions from EVT, is described using the PDF

$$f(x) = \frac{1}{\beta}\left[1 + \frac{\alpha(x-\zeta)}{\beta}\right]^{1-\frac{1}{\alpha}} \exp\left\{-\left[1 + \frac{\alpha(x-\zeta)}{\beta}\right]^{-\frac{1}{\alpha}}\right\}, \tag{3.10}$$

$$1 + \frac{\alpha(x-\zeta)}{\beta} > 0, \quad \alpha, \zeta \in \mathbb{R}, \quad \beta > 0.$$

The three parameters are the location (or shift) parameter, ζ, the scale parameter, β, and the shape parameter, α. The location parameter, ζ, shifts the PDF along the x-axis (Figure 3.3(a)). The scale, β, and shape, α, parameters (Figures 3.3(b) and (c) respectively) behave like the gamma distribution equivalents.

I estimated the fitted GEV parameters using the method of maximum likelihood, again with a built-in MATLAB function (`gevfit`; MATLAB, 2015b). As

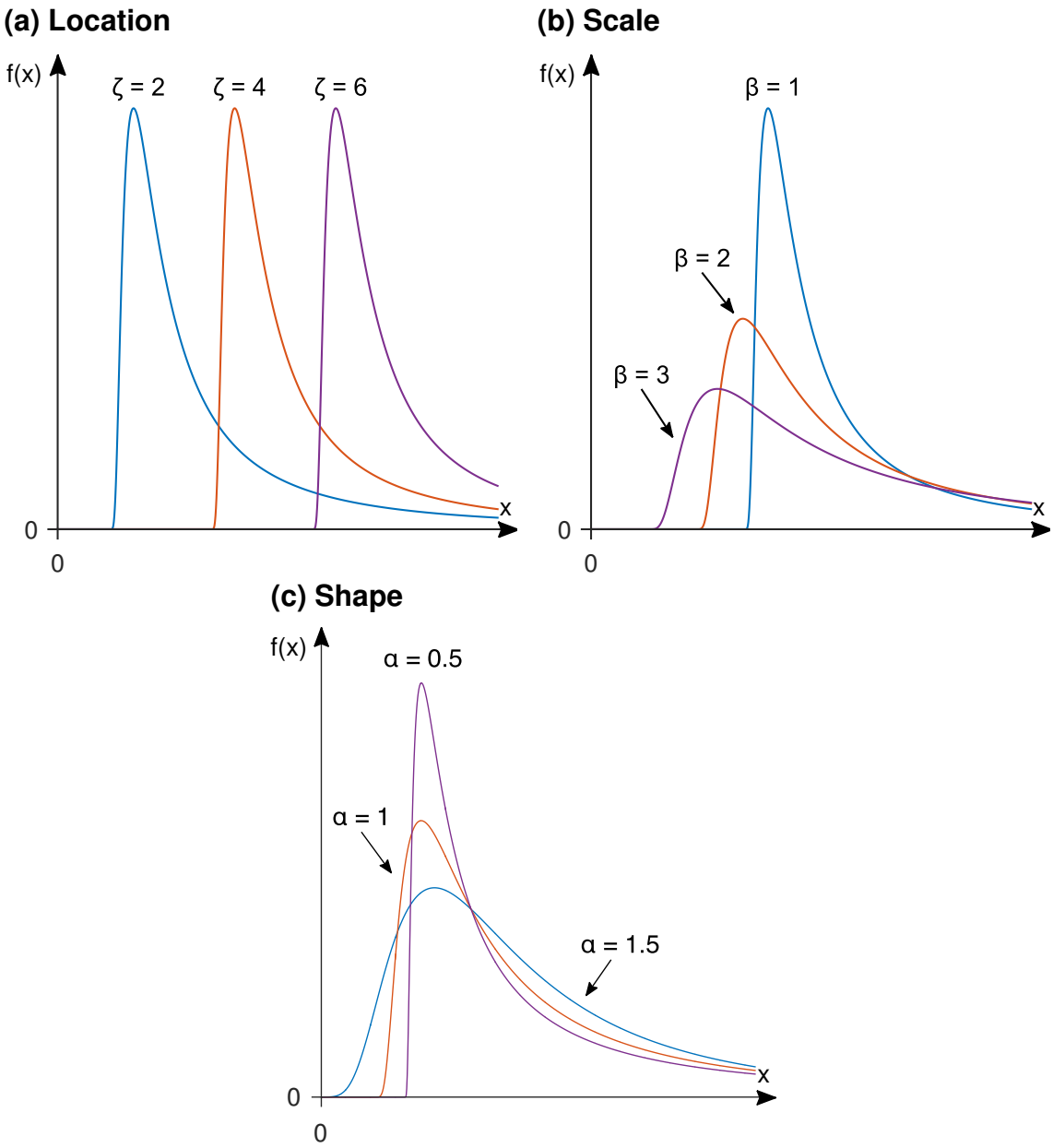

Figure 3.3: Generalized Extreme Value (GEV) distribution probability density function (PDF) for three values of the (a) location, ζ, (b) scale, β, and (c) shape, α, parameters.

with the gamma distribution, this method is very time-consuming, but a faster method is not available for the GEV distribution.

Normal

The normal distribution is perhaps the most well known of the continuous distributions, with its familiar bell-shaped PDF given by

$$f(x) = \frac{1}{\sigma\sqrt{2\pi}} \exp\left[-\frac{(x-\mu)^2}{2\sigma^2}\right], \quad \mu \in \mathbb{R}, \quad \sigma^2 > 0, \tag{3.11}$$

where μ is the mean, σ is the standard deviation, and π is the mathematical constant 3.14159.... The mean locates the centre of the symmetrical distribution (Figure 3.4(a)) and the standard deviation controls the spread (Figure 3.4(b)).

The fitted parameters for the normal distribution are simply the mean and standard deviation of the data.

Lilliefors Test

It is important to identify the most representative distribution for the data at each timescale (e.g. annual, seasonal). The KS test (Massey Jr., 1951) is a frequently-used goodness-of-fit test that simply compares the empirical and fitted CDFs. The null hypothesis (the observed data were drawn from the distribution being tested) is rejected if the discrepancy between the two CDFs is sufficiently large. This discrepancy is measured using the KS statistic

$$D_n = \max_x |F_n(x) - F(x)|, \tag{3.12}$$

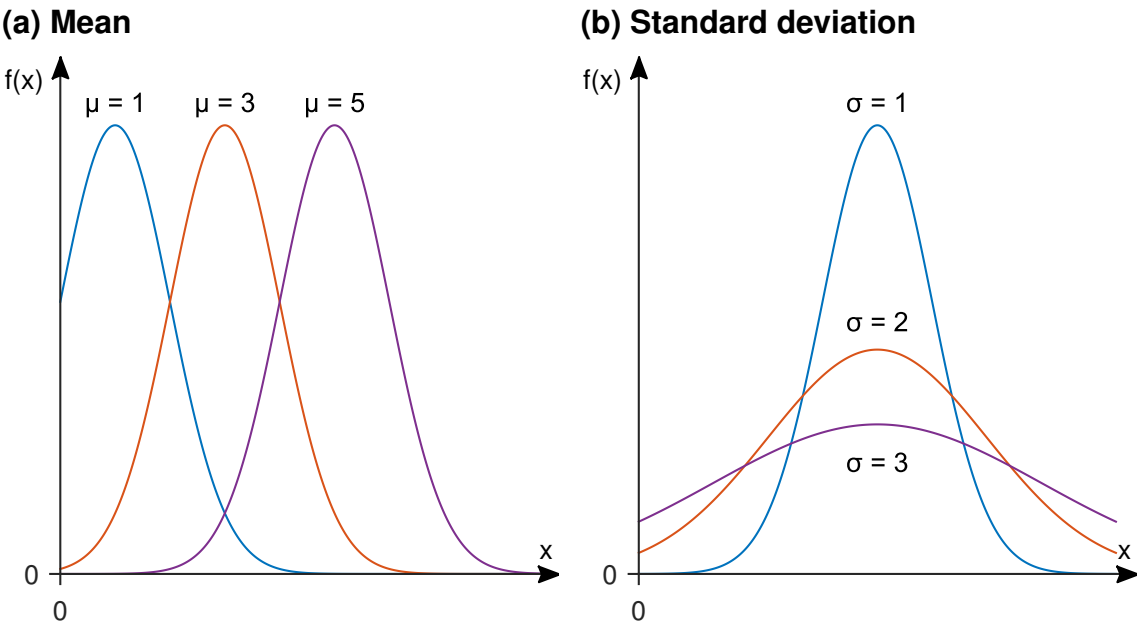

Figure 3.4: Normal distribution probability density function (PDF) for three values of the (a) mean, μ, and (b) standard deviation, σ.

where $F_n(x)$ is the empirical cumulative probability, estimated as $F_n(x_{(i)}) = i/n$ for the ith smallest data value; and $F(x)$ is the theoretical CDF denoted by

$$F(x) = \Pr\{X \leq x\} = \int_{X \leq x} f(x)dx. \tag{3.13}$$

The null hypothesis is rejected if $D_n \geq C_\alpha$, where C_α is the critical value obtained by approximation using

$$C_\alpha = \frac{K_\alpha}{\sqrt{n} + 0.12 + {}^{0.11}/_{\sqrt{n}}}, \tag{3.14}$$

where $K_\alpha = 1.358$ for test level $\alpha = 0.05$. This test is distribution-free, so Equation 3.14 is applicable to all distributions.

However, the KS test is only applicable when the distribution parameters have not been estimated from the data sample; erroneously using KS critical values that assume independence between test data and the estimated parameters often results in non-rejection of the null hypothesis when, in fact, it should be rejected. The Lilliefors test (Lilliefors, 1967) is a modified version of the KS test that is used when the distribution parameters are estimated using the same data used in the test. In this case, Equation 3.14 is insufficiently stringent; the critical values now depend on the fitted distribution and sample size, and are calculated using Monte Carlo simulations (Metropolis and Ulam, 1949).

Table 3.1, adapted from Crutcher (1975) using data from Lilliefors (1967, 1973), shows the difference between the KS test critical values (calculated using Equation 3.14) and those used for the Lilliefors test on the normal distribution. In all cases, the Lilliefors critical values are lower than those used in the KS test. Therefore the Lilliefors test is more stringent than the KS test (as a lower critical value requires a smaller difference between the empirical and theoretical CDF).

This work required the Lilliefors goodness-of-fit test as I estimated the distribution parameters using the precipitation data. I applied this test to:

- each timescale (annual, MJJASO, seasonal and monthly);
- each grid square;

Table 3.1: Table of example critical values, C_a, for the Kolmogorov-Smirnov and Lilliefors tests for various sample sizes, N, and test levels, a (adapted from Crutcher, 1975). The critical value must be multiplied by $N^{-1/2}$ when $N > 30$.

		Test level (a)				
	N	0.20	0.15	0.10	0.05	0.01
Kolmogorov-Smirnov test						
All distributions	25	0.208	0.220	0.238	0.264	0.317
	30	0.190	0.200	0.218	0.242	0.290
	>30	1.070	1.140	1.220	1.360	1.630
Lilliefors test						
Normal distribution	25	0.142	0.147	0.158	0.173	0.200
	30	0.131	0.136	0.144	0.161	0.187
	>30	0.736	0.768	0.805	0.886	1.031

- each distribution; and
- the whole time series, plus the wettest 25 % and 5 % of the data points in the time series (henceforth referred to as the upper 25 % and upper 5 %) only. This ensured extreme rainfall was adequately modelled by the distribution fits (essential for accurately estimating long return periods).

Hence for a given timescale and grid square, each distribution (gamma, GEV and normal) was fitted to the whole time series, and the Lilliefors test was then applied to the whole time series, the upper 25 % and the upper 5 % of the time series. For each timescale and distribution, I then discarded all grid squares that failed the test in any of the three data sections (all data, upper 25 %, upper 5 %).

To calculate the critical values required for the Lilliefors test, I:

1. took 112 randomly sampled precipitation values from the fitted distribution,
2. fitted the distribution to these sampled data, and
3. computed the KS statistic, D_n, using this fit.

I repeated these three steps 10 000 times. I approximated the 5 %-level critical value as the 95th quantile of the 10 000 D_n values (Wilks, 2011). The critical values for the upper 25 % and upper 5 % of the data were calculated using the

same method, although D_n was calculated using the upper 25 % and upper 5 % of the randomly sampled values only. These critical values were calculated for each distribution, timescale and grid square.

Figure 3.5 shows an example of the Lilliefors test on the gamma distribution for annual rainfall in a grid square in central Thailand (centre point located at 15.25°N, 100.25°E). The asterisks mark the point where the discrepancy between the empirical and theoretical CDFs is the greatest (i.e. D_n). In this example, the Lilliefors test failed in the full data series (Figure 3.5(a)) and the upper 5 % (Figure 3.5(c)) as $D_n \geq C_{5\%}$. Therefore, I discarded this grid square for all calculations using the gamma distribution and annual rainfall.

Uncertainty calculation

Calculating return periods using a limited number of data points understandably leads to some uncertainty in those estimates. This uncertainty has four causes:

1. Serial autocorrelation—successive data in the rainfall time series are not independent.

2. Length of dataset—the return period curves extend further than the length of the dataset.

3. Inaccuracy—the accuracy of station rainfall measurements is unknown and likely varies throughout the data period.

4. Temporal changes—the number of stations used in the CRU gridding process changes with time.

In this work, I have addressed the first and second of these causes. The third and fourth sources of uncertainty are difficult to quantify and are not addressed.

I corrected for serial autocorrelation by computing re-sampled 90 % confidence intervals using a parametric technique, which fits a distribution with randomly selected rainfall data corresponding to the number of degrees of freedom in the rainfall series. I describe this method in more detail below.

Serial autocorrelation refers to the correlation of a time series with its own past and future values. Precipitation measurements are not independent; the

likelihood of rain tomorrow is greater if rain occurs today than if today is dry. This relationship extends out to longer timescales due to multi-year-to-decadal

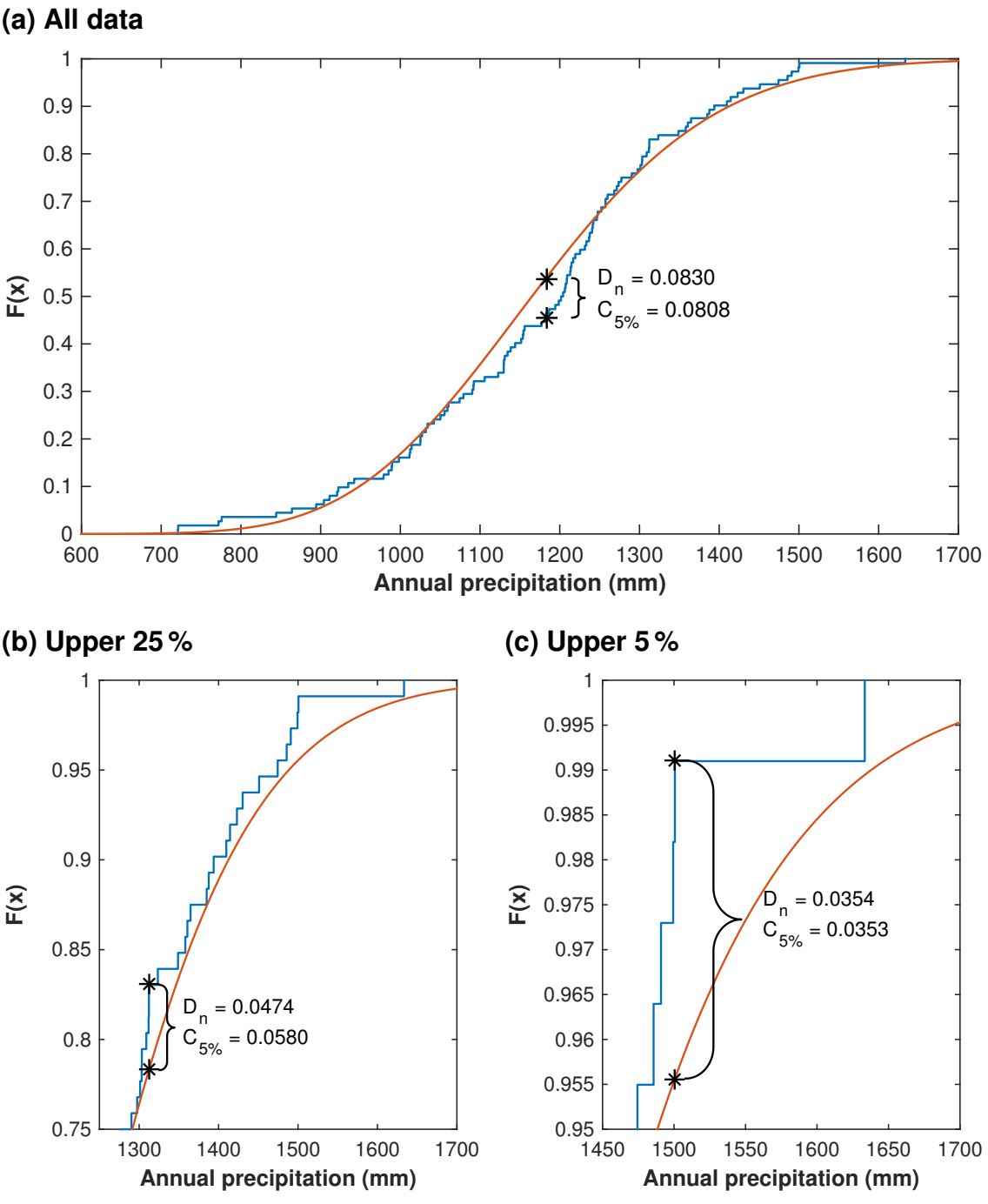

Figure 3.5: An example of the Lilliefors test on the gamma distribution for annual rainfall in a grid square in central Thailand (centre point located at 15.25°N, 100.25°E). The test was applied to (a) the full data series, (b) the upper 25 % and (c) the upper 5 % of the data. The blue line shows the empirical cumulative distribution function (CDF) and the red line shows the theoretical gamma CDF. D_n and $C_{0.05}$ denote the Kolmogorov-Smirnov (KS) statistic and the critical value for the 0.05 test level respectively. The black asterisks mark the points on the empirical and theoretical CDFs where D_n was calculated.

processes.

I corrected for this by computing the effective number of degrees of freedom, ν, in each rainfall time series (per grid square and timescale) (Saunders and Lea, 2005). I calculated this using

$$\nu = \frac{n}{1 + 2\sum A^2}, \tag{3.15}$$

where n is the number of years in the time series, and A is the sample autocorrelation function. The latter measures the correlation between x_t and x_{t+k} where $k = 0, \ldots, K$. The Box et al. (2008) formula for the autocorrelation for lag, k, is

$$A_k = \frac{c_k}{c_0}, \tag{3.16}$$

where

$$c_k = \frac{1}{T-1} \sum_{t=1}^{T-k} (x_t - \bar{x})(x_{t+k} - \bar{x}), \tag{3.17}$$

and c_0 is the sample variance of the time series. I used the built-in MATLAB `autocorr` function (MATLAB, 2015c) to calculate A out to a lag of $n/2$, where n is the number of years in the time series.

Once I calculated ν for each time series, I:

1. randomly sampled ν data points from the time series,
2. fitted each distribution to these data points, and
3. calculated the return period curve using the distribution method described above.

I repeated these steps 1000 times. For each distribution fitted return period curve, I then took the 95th and 5th percentile of these 1000 randomly sampled return period curves as the upper and lower confidence intervals respectively.

I chose this sample size as it is large enough to accurately estimate the confidence intervals but small enough to be computationally efficient when applied to a large number of grid squares. Figure 3.6 shows the effect of sample size on the confidence intervals; increasing the sample size by two or four times

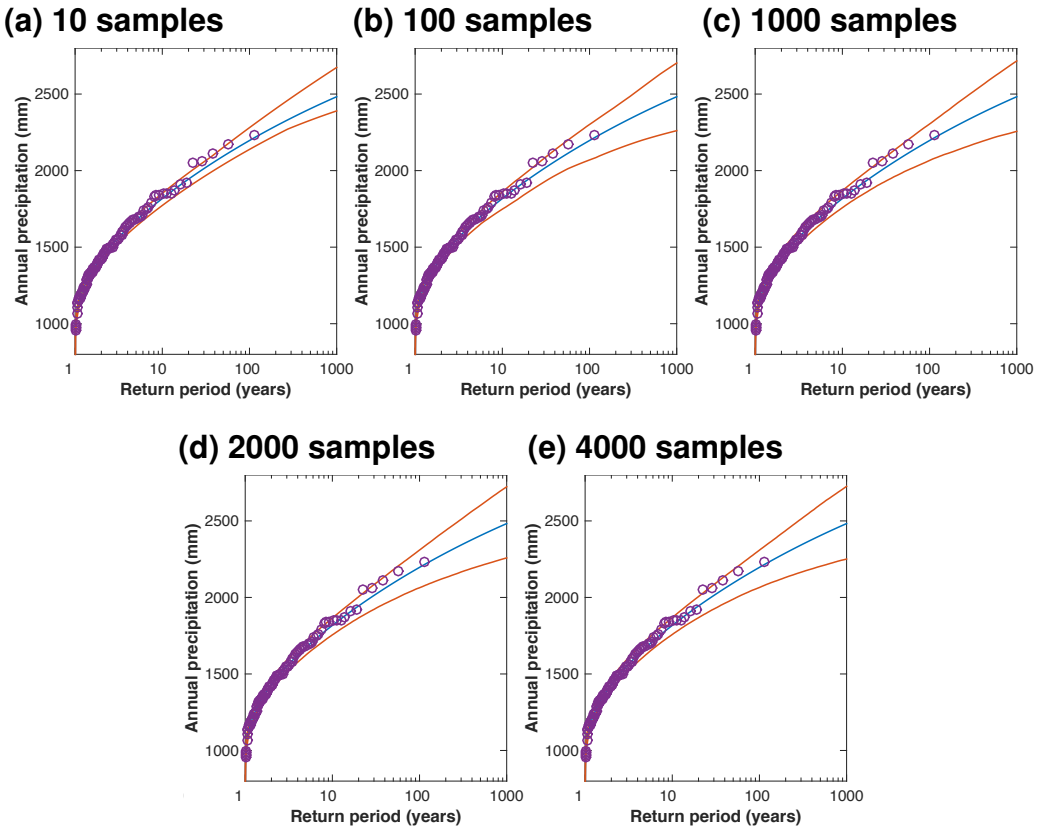

Figure 3.6: Return period curves showing the effect of sample size on the confidence intervals. The curves shown are for the GEV distribution fitted to annual rainfall in the grid square containing Bangkok (centre point: 13.75°N, 100.75°E).

has very little impact on the uncertainty, but decreasing the sample size falsely implies reduced confidence intervals.

To address the effect of dataset length on return period uncertainty, I repeated the random sampling process described above, replacing ν with three different dataset lengths: 20, 50 and 100 years. The resulting confidence intervals are shown in Figure 3.7. These curves do not correct for serial autocorrelation, so cannot be compared to those in other figures. As expected, as the length of the dataset increases, the return period uncertainty decreases. This further justifies the use of the longer CRU dataset rather than the shorter TMD dataset in this work.

3.3 Results

This section details the results of the Lilliefors test for each timescale and distribution (Section 3.3.1), and then provides examples of the outputs from this

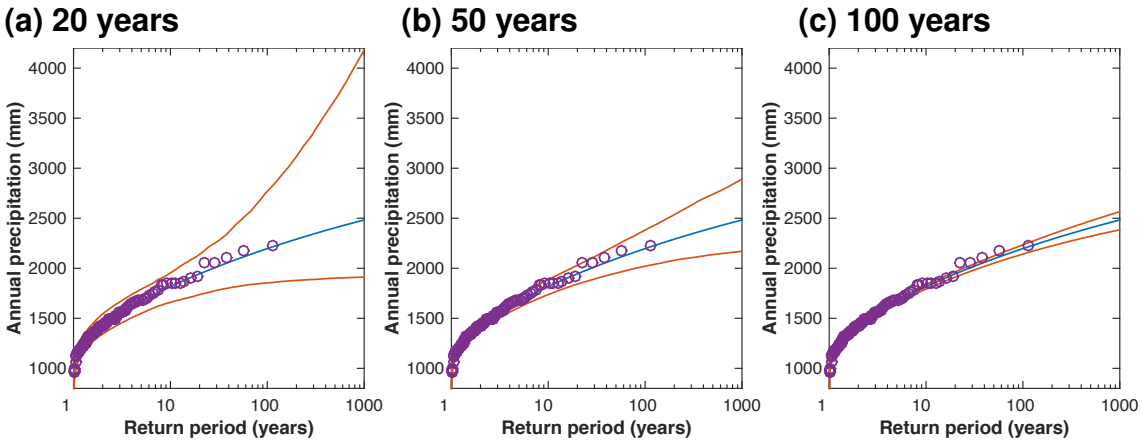

Figure 3.7: Return period curves showing the effect of dataset length on the confidence intervals. The curves shown are for the GEV distribution fitted to annual rainfall in the grid square containing Bangkok (centre point: 13.75°N, 100.75°E).

work in terms of return period curves (Section 3.3.2), return period maps (Section 3.3.3) and return level maps (Section 3.3.4).

3.3.1 Lilliefors test

Table 3.2 shows the percentage of grid squares in Thailand that were discarded as they failed the Lilliefors test at the 5 % significance level in at least one section of the data (all data, upper 25 %, upper 5 %). The normal distribution provided the best fit for annual and summer monsoonal rainfall (i.e. the lowest number of discarded grid squares); only 14.6 % and 16.3 % of grid squares were discarded respectively. The gamma and GEV were more suitable for seasonal and monthly rainfall (except for JAS rainfall, where the normal distribution resulted in the lowest number of discarded grid squares). The gamma distribution tended to provide the best fit for the drier months (NDJFM) and seasons (NDJ–JFM), whereas the GEV performed better for the wetter months (April–October). There was no consensus for the best fitting distribution in the wetter seasons.

The results of the Lilliefors test are divided further in Appendix B: Tables B.1, B.2 and B.3 show the percentage of grid squares that failed in each section of the data individually (all data, upper 25 % and upper 5 % respectively). Focussing on all 112 data points (111 for NDJ and DJF), the gamma distribution provided the best fit of annual and summer monsoonal precipitation, plus precipitation in the drier seasons and May–July (MJJ). The GEV distribution was best for all

Table 3.2: Table showing the percentage of grid squares that were discarded as they failed the Lilliefors test in at least one section of the data (all data, upper 25 %, upper 5 %). The results are shown for each distribution and timescale. The shading marks the most successful distribution(s) for each timescale.

		Discarded grid squares (%)		
Timescale		Gamma	GEV	Normal
Annual		18.5	24.5	14.6
Summer monsoonal		17.2	27.5	16.3
Seasonal	NDJ	39.5	51.5	84.1
	DJF	35.6	62.2	89.7
	JFM	25.8	27.0	82.4
	FMA	45.9	4.7	41.2
	MAM	33.0	22.7	42.9
	AMJ	21.5	15.5	32.6
	MJJ	14.2	18.5	30.5
	JJA	21.0	21.0	27.0
	JAS	25.3	27.5	19.3
	ASO	12.9	12.4	16.7
	SON	17.2	18.5	33.5
	OND	38.2	15.5	36.9
Monthly	Jan	80.3	82.8	98.7
	Feb	70.4	96.1	96.1
	Mar	39.9	56.2	97.0
	Apr	42.5	13.7	72.5
	May	32.6	22.7	42.5
	Jun	19.3	19.3	46.8
	Jul	21.9	15.5	53.6
	Aug	24.5	19.3	42.5
	Sep	18.5	12.4	38.2
	Oct	46.8	21.5	62.7
	Nov	50.6	65.7	92.7
	Dec	81.1	85.4	92.7

other seasons. The best distribution varied for monthly precipitation; the GEV performed best for the majority of the wetter months. For the upper 25 % of the data, the gamma distribution was the most suitable across the timescales. The GEV and normal distributions performed better for three seasons (JFM, FMA and

OND) and four months (Apr, July, Sep and Oct). The normal distribution was the most suitable for the upper 5 % of data at almost all timescales (all bar DJF, Jan, Feb, Mar, Nov and Dec).

Although a number of grid squares passed the Lilliefors test in the drier months and seasons, the GEV and normal distributions must be used with care. These distributions are not lower bounded by zero, so the distribution fits occasionally suggested the possibility of negative rainfall (as shown in Figure 3.8).

Figure 3.9 shows the locations of the discarded grid squares for annual precipitation. These discarded grid squares had no clear pattern. However, 40 % of these discarded grid squares (gamma and GEV distributions; 29 % for normal) had their centre point located outside of Thailand. This was likely caused by a lack of CRU stations in neighbouring countries (Laos, Vietnam and Cambodia to the east, and Myanmar to the west), which impacted the gridded rainfall data in grid squares on the Thailand border.

Fifteen grid squares (6 % of the total number) were discarded for all three distributions, and 25 (11 %) were discarded for at least two distributions. Of these grid squares, 6 (40 %; all three distributions) and 11 (44 %; at least two distributions) were grid squares with their centre point located outside Thailand.

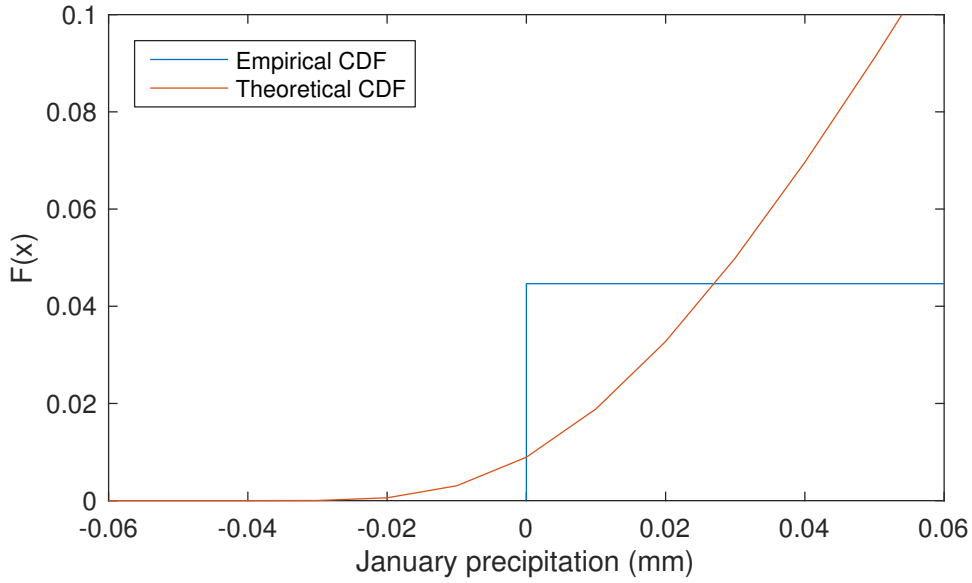

Figure 3.8: A section of the theoretical Generalized Extreme Value (GEV) cumulative distribution function (CDF) (red line) for January precipitation in a grid square in eastern Thailand (centre point: 14.75°N, 105.75°E). The empirical CDF is shown for comparison (blue line).

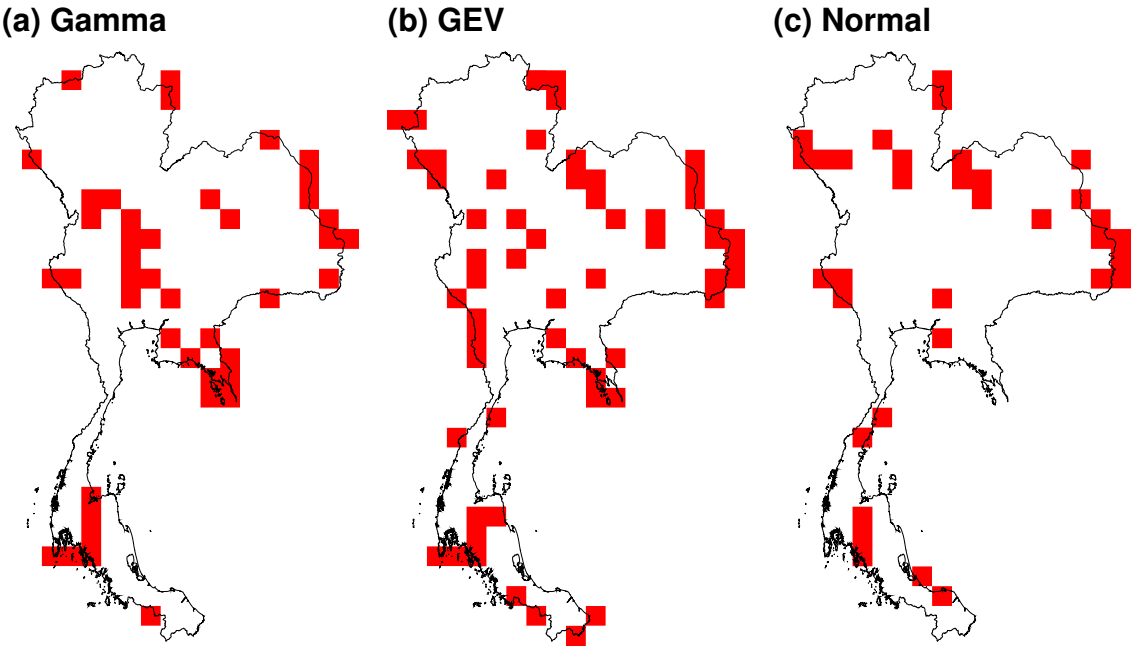

Figure 3.9: Lilliefors test results for annual precipitation data (1901–2012) using the (a) gamma, (b) Generalized Extreme Value (GEV), and (c) normal distributions. Red shading denotes the grid squares that were discarded as they failed the Lilliefors test at the 5 % significance level in at least one area of the distribution tested (all data, upper 25 %, upper 5 %).

Figure 3.10(a) shows the CDF for a grid square to the north-east of Bangkok (centre point: 14.25°N, 101.25°E) that was discarded for all three distributions. In this case, the three distribution fits passed the Lilliefors test on the upper 25 % and upper 5 % of the data but failed when using all the data. For all three distributions, the failure occurred in the centre of the CDF (1728.8 mm). This was caused by a large number of observations occurring within a small precipitation range (16 within 35.4 mm), resulting in a sharp jump in the empirical CDF. The fitted distributions were unable to model this. The histogram of this data (Figure 3.10(b)) fails to show this jump clearly as these 16 observations fall into two different histogram bins. However, it is clearly evident the three distributions were unable to capture the shape of the precipitation distribution between 1500 mm and 2000 mm.

As a comparison, Figure 3.11 shows the CDF and histogram for the grid square directly to the south. This grid square passed the Lilliefors test in all sections of the data for all three distributions. Here the largest discrepancies

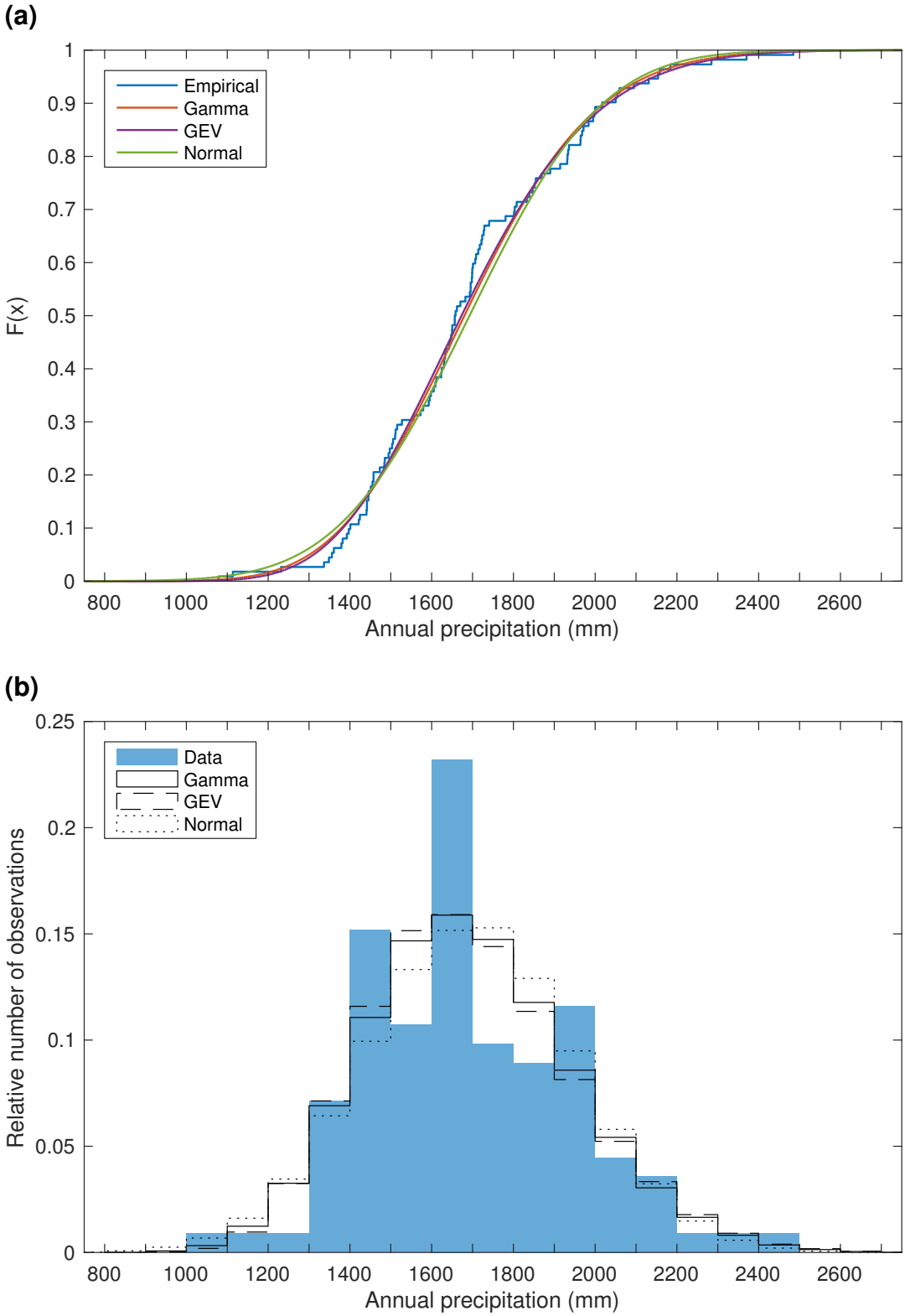

Figure 3.10: (a) Cumulative distribution function (CDF) for annual precipitation in a grid square in central Thailand (centre point: 14.25°N, 101.25°E). The empirical CDF (blue) is shown alongside the theoretical gamma (red), Generalized Extreme Value (GEV) (purple) and normal (green) CDFs. (b) Histogram of the same precipitation data (blue) and the theoretical distributions fitted to these data (gamma (solid line), GEV (dashed line), and normal (dotted line)).

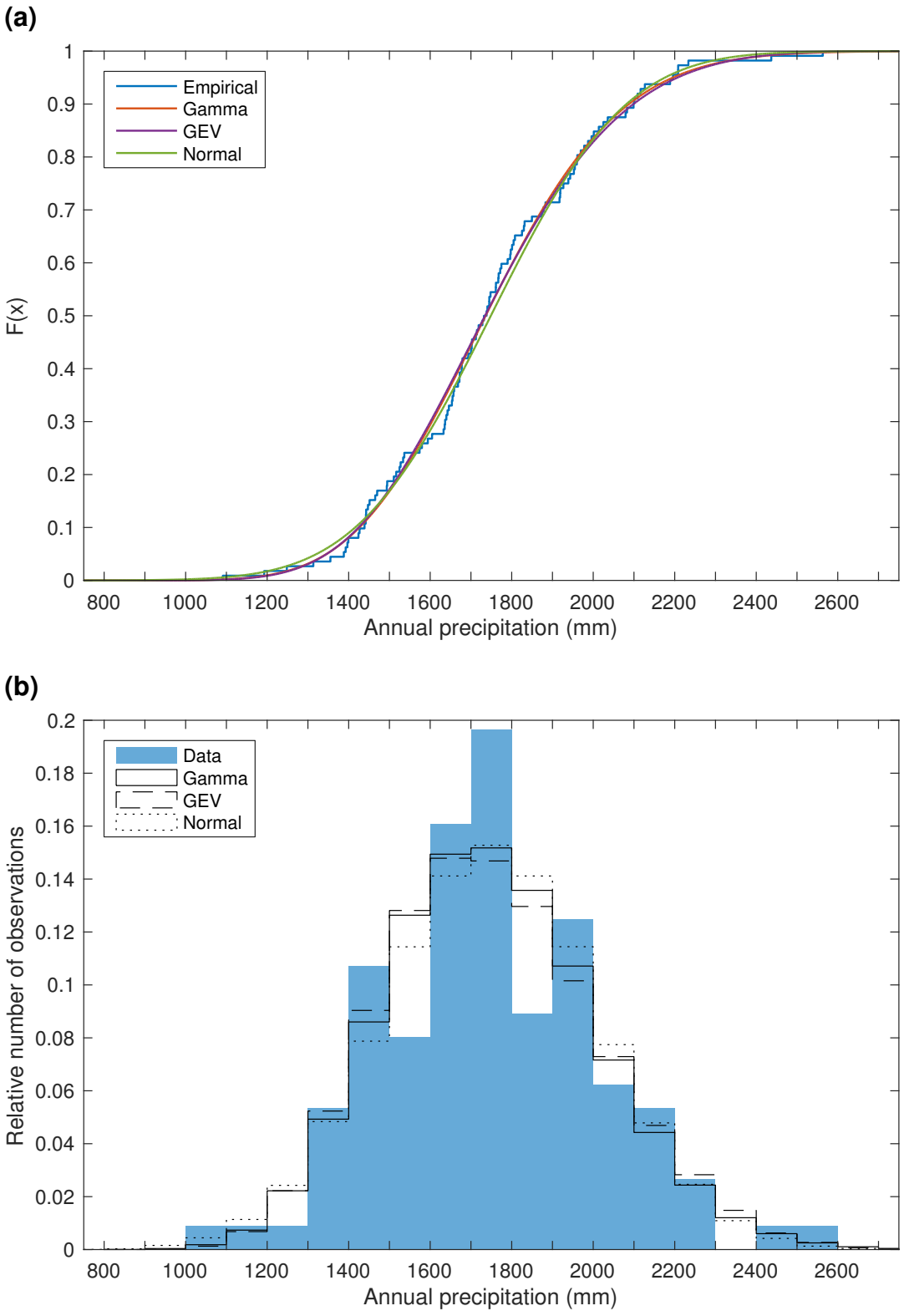

Figure 3.11: As Figure 3.10 but for the grid square directly to the south (centre point: 13.75°N, 101.25°E).

occurred in two locations: 1633 mm (gamma and GEV) and 1808 mm (normal). Although the gradient is steep at these locations, it is shallower than the gradient in Figure 3.10 that resulted in failure. In this example, the histogram shows dips in the measurements either side of the peak that were not modelled by the fitted distributions. The distributions also failed to model the peak between 1700 mm and 1800 mm. Despite this, overall the distribution fits were more successful than in the previous example.

Figure 3.12 shows a further example of the Lilliefors test result, in this instance for monthly precipitation using the GEV distribution only. Here there was a clear pattern to the failures. The GEV distribution was not suitable for much of continental Thailand from November through February, although it can be used to model rainfall in the south for the first three of these months. The distribution was unable to model rainfall in dry months, where the majority of the measurements were zero. In March, the majority of discarded grid squares were located in the west and east of the country. In April and May, the discarded grid squares were predominately confined to one area: the west and east respectively. There were no clear patterns to the discarded grid squares in the remaining months (June to October).

Appendix B includes the Lilliefors test results for the remaining timescales (e.g. seasonal) and distributions. There was no clear pattern to the discarded grid squares for MJJASO precipitation (Figure B.1). Most of the discarded grid squares in the dry months were in continental Thailand (Figures B.5 and B.6). This pattern also occurred for seasonal rainfall (Figures B.2, B.3 and B.4), but was less evident than for monthly.

3.3.2 Return period curves

The first output from this work is the return period curve. I produced these for each grid square, timescale and distribution. This subsection shows four example return period curves for various timescales and grid squares.

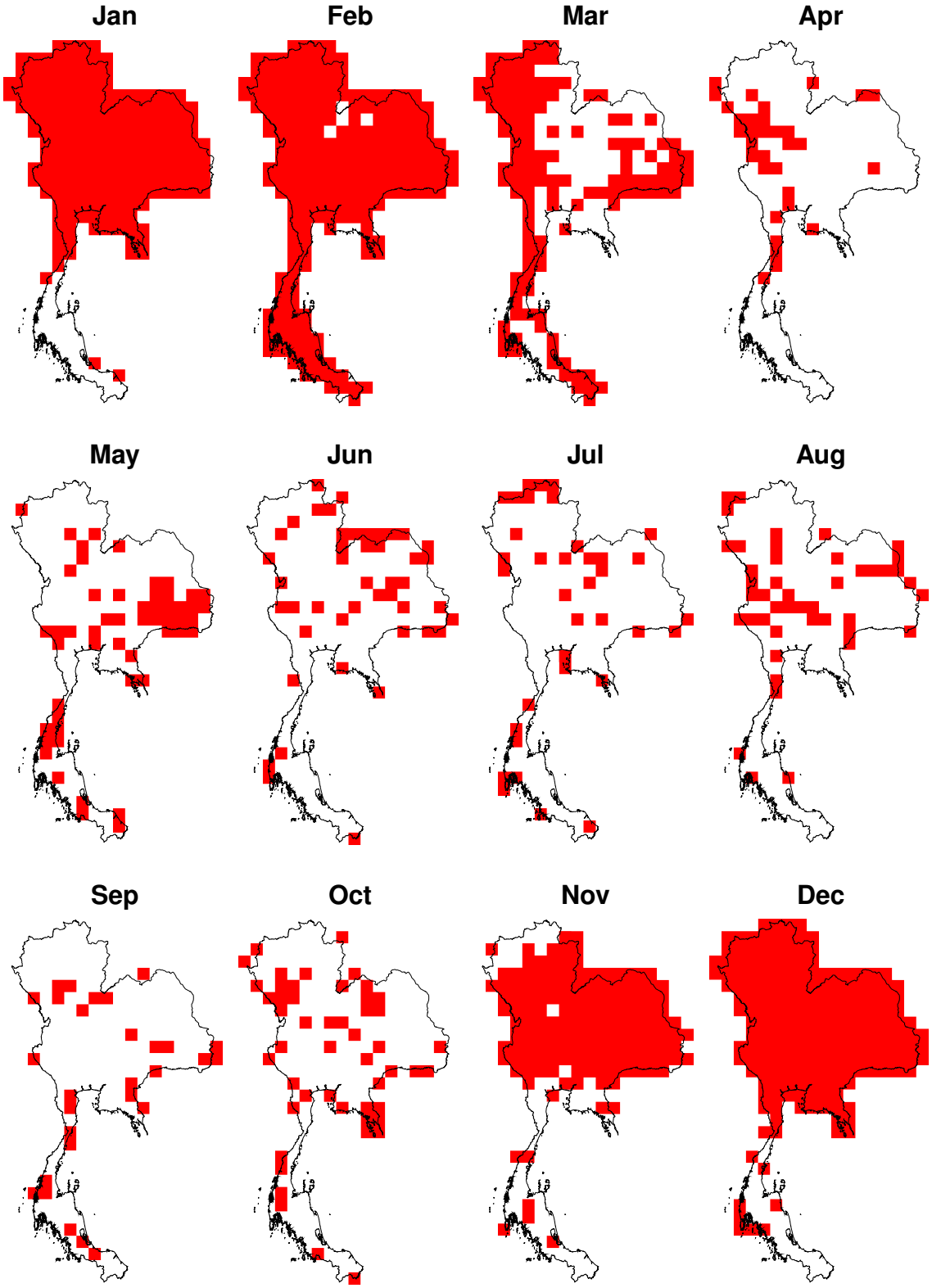

Figure 3.12: As Figure 3.9 but for monthly precipitation using the Generalized Extreme Value (GEV) distribution only.

Annual precipitation

The first of these examples (Figure 3.13) shows the return period curves ((a) gamma, (b) GEV, and (c) normal distributions) for annual precipitation in the grid square containing Bangkok (centre point: 13.75°N, 100.75°E). The KS statistics shown in each sub-figure identify the most suitable distribution in each section of the data. The lowest value for each section indicates the best fit. Here, the GEV distribution provided the best fit for all sections of the data.

Figure 3.13 also includes two tables showing (d) return level and (e) return period values extracted from the return period curves. The 90 % range of uncertainty is also given for each return level and return period estimate. In this example, the normal distribution return levels were the lowest for all return periods shown, and those using the GEV distribution were the highest. As stated previously, the GEV distribution provided the best fit for all three sections of the data. It also provided the most accurate estimates for return levels and return periods. The range of return level estimates across the three distributions varied by as little as 0.7 percentage points (10-year return period) and as much as 9.1 percentage points (200-year return period), although all estimates were within range of each other when considering the uncertainty surrounding them.

The second table (e) shows the return periods for the five most severe floods in Thailand (1985–2012) as taken from the Dartmouth Flood Observatory Global Active Archive of Large Flood Events (Brakenridge, 2012). The annual rainfall was classified as extreme during 1995 and 2011; the 'data' return periods for these events were 56 and 112 years respectively, which, as they were calculated using the basic method, shows they were the two highest rainfall observations in the 112 year data period. The distribution return periods for these two years exceeded the basic method estimates by at least 26 and 16 years for 1995 and 2011 respectively, although the uncertainty range meant these could be 9 and 46 years shorter than the basic method estimate. As the GEV distribution provided the best fit in this example, the return periods were 82.1 and 128.2 years for these two years respectively. These were the shortest of the three distribution estimates, and the closest to the basic method estimates.

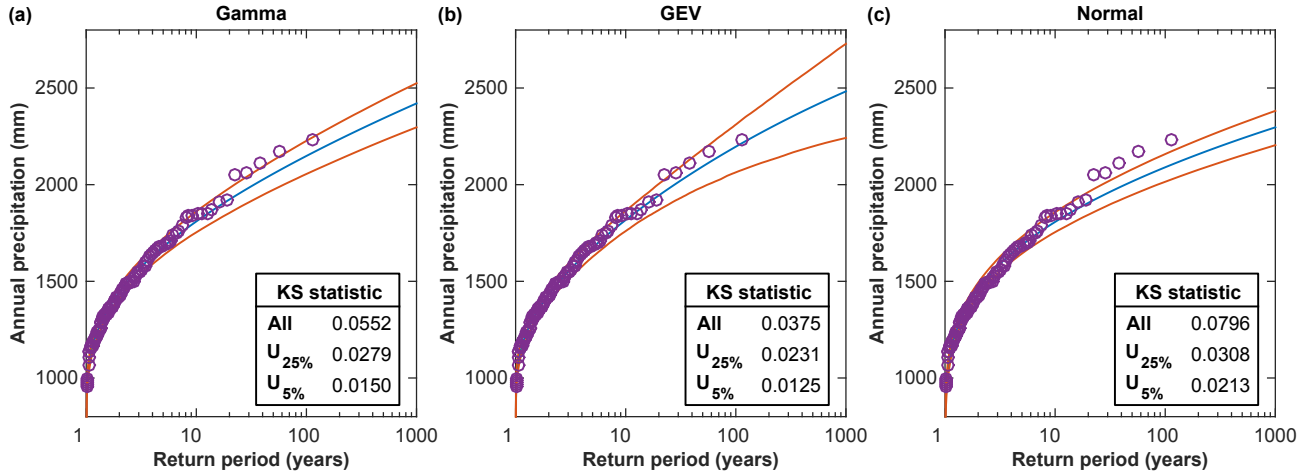

(d)

Return period (years)	Annual precipitation anomaly (%) Gamma	GEV	Normal
10	23.9 $^{+3.6}_{-3.9}$	24.4 $^{+3.3}_{-3.9}$	23.7 $^{+3.4}_{-3.6}$
25	34.0 $^{+4.2}_{-5.0}$	35.7 $^{+4.4}_{-5.6}$	32.4 $^{+3.9}_{-4.3}$
50	40.8 $^{+4.8}_{-5.7}$	43.4 $^{+6.0}_{-7.3}$	38.0 $^{+4.3}_{-4.7}$
100	47.1 $^{+5.4}_{-6.4}$	50.4 $^{+7.8}_{-9.1}$	43.1 $^{+4.7}_{-5.1}$
200	53.0 $^{+5.9}_{-7.1}$	56.8 $^{+10.1}_{-11.3}$	47.7 $^{+5.0}_{-5.5}$

(e)

Historical flood events	Return period (years) Data	Gamma	GEV	Normal
1995	56.0	116.8 $^{+164}_{-50.2}$	82.1 $^{+253}_{-35.5}$	224.9 $^{+397}_{-115}$
2002	1.7	1.6 $^{+0.1}_{-0.1}$	1.7 $^{+0.2}_{-0.1}$	1.6 $^{+0.1}_{-0.1}$
2004	1.2	1.2 $^{+0.1}_{-0.1}$	1.2 $^{+0.1}_{-0.1}$	1.2 $^{+0.1}_{-0.0}$
2006	2.9	2.7 $^{+0.4}_{-0.3}$	2.8 $^{+0.5}_{-0.4}$	2.5 $^{+0.4}_{-0.3}$
2011	112	193.7 $^{+321}_{-90.5}$	128.2 $^{+704}_{-62.9}$	455.0 $^{+989}_{-255}$

Figure 3.13: Return periods and return levels for annual precipitation in the grid square containing Bangkok (centre point: 13.75°N, 100.75°E). (a), (b) and (c): return period curves for annual precipitation (1901–2012). The return periods, calculated using the basic method, are plotted for each precipitation observation (purple markers). The return period curve (blue line) and confidence intervals (5 % and 95 %; red lines), calculated using the distribution method, are plotted for the gamma, Generalized Extreme Value (GEV) and normal distributions. Note the logarithmic scale on the x-axis. The Kolmogorov-Smirnov (KS) statistic is shown for each section of the data tested using the Lilliefors Test (all data, upper 25 % ($U_{25\,\%}$), and upper 5 % ($U_{5\,\%}$)). (d): annual precipitation return levels and uncertainties (given as a percentage above the annual rainfall climatology) for various return periods. These are shown for the gamma, GEV and normal distributions. (e): annual precipitation return periods and uncertainties for the five most severe Thai floods (1985–2012) as taken from the Dartmouth Flood Observatory Global Active Archive of Large Flood Events (Brakenridge, 2012). Those in the 'data' column were calculated using the basic method (Section 3.2.3).

As a comparison, Figure 3.14 shows the return period curves and tables for annual precipitation in the grid square containing Chiang Mai (centre point: 18.75°N, 98.75°E). In this grid square, the gamma distribution provided the best fit for the entire data series and the upper 25 %, but the normal distribution provided the best fit for the upper 5 %. The two highest rainfall observations (1942 and 1953) were much higher than the others (over 110 mm above the third highest observation), so the basic method grossly underestimated these return periods. The distribution method provided a more accurate estimate; the normal distribution (the best fit for the upper 5 % of observations) suggested return periods of 199 and 7491 years for 1942 and 1953 respectively, both of which were classed as extreme. The latter return period suggests the data for 1953 may be erroneous as it was much higher than any other measurement in the 112 year dataset.

Here the return levels for the five return periods were lower than those for the grid square containing Bangkok. In terms of annual precipitation anomaly given as a percentage of the annual climatology, the return levels were on average 5.5 percentage points lower in this grid square.

Unlike the previous example, the return periods for the five flood events were quite short; only the 2011 rainfall was classified as extreme in Chiang Mai, where the gamma estimate of 12.4 years was the most likely. Interestingly, aside from the 1995 event, the distribution return period estimates were shorter than those estimated using the basic method.

Seasonal precipitation

Figure 3.15 is an example of return period curves for seasonal precipitation. These curves are for ASO precipitation in the grid square containing Bangkok. In this example, the normal distribution fit failed the Lilliefors test in two sections of the data (all data and the upper 25 %), so the normal distribution was not used for this grid square. Hence, the results for this distribution are not shown. Here the GEV distribution performed best for all sections of the data.

Unlike the examples for annual precipitation, the ASO precipitation return levels were much higher than the climatology; they ranged from +33.0 % (10-year;

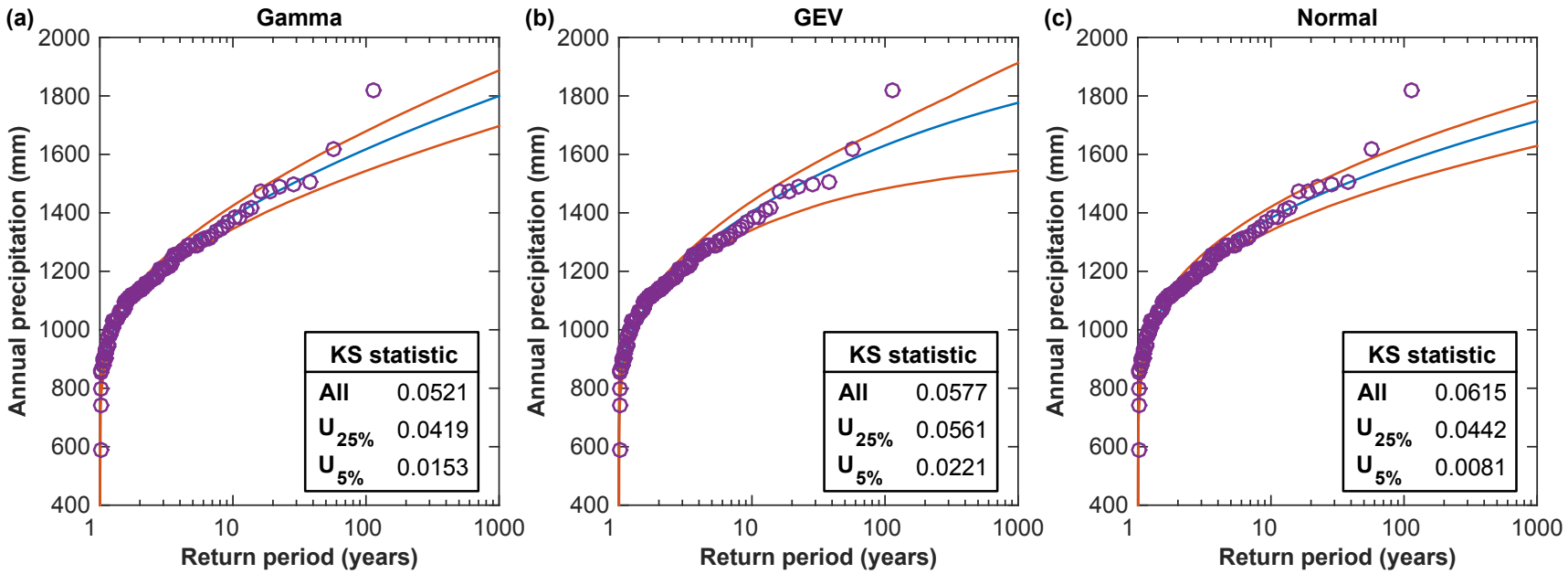

(d) Annual precipitation anomaly (%)

Return period (years)	Gamma	GEV	Normal
10	21.0 +3.1 -3.8	22.3 +3.1 -5.5	20.5 +3.3 -3.8
25	29.7 +4.0 -4.8	31.3 +3.8 -8.3	28.0 +4.0 -4.6
50	35.6 +4.8 -5.7	37.1 +4.4 -10.5	32.8 +4.5 -5.2
100	41.0 +5.4 -6.5	42.1 +5.2 -12.9	37.2 +5.0 -5.7
200	46.0 +6.1 -7.3	46.5 +6.7 -15.2	41.1 +5.4 -6.3

(e) Return period (years)

Historical flood events	Data	Gamma	GEV	Normal
1995	1.7	1.8 +0.2 -0.2	1.8 +0.2 -0.2	1.7 +0.2 -0.1
2002	4.3	4.2 +1.1 -0.7	4.0 +1.3 -0.6	4.1 +1.3 -0.7
2004	2.5	2.4 +0.3 -0.3	2.3 +0.3 -0.2	2.2 +0.3 -0.2
2006	6.6	5.6 +1.9 -1.0	5.2 +2.4 -0.9	5.5 +2.3 -1.1
2011	14.0	12.4 +7.6 -3.2	10.8 +14.9 -2.6	13.6 +10.6 -4.2

Figure 3.14: As Figure 3.13 but for the grid square containing Chiang Mai (centre point: 18.75°N, 98.75°E).

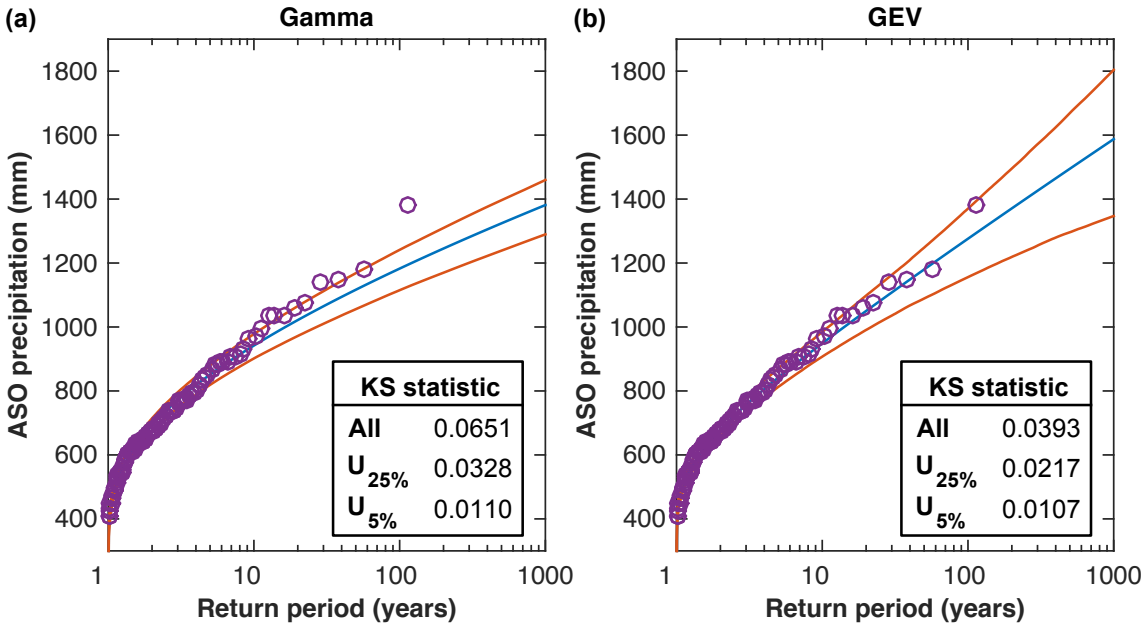

(d)

Return period (years)	ASO precipitation anomaly (%) Gamma	GEV	Normal
10	33.0 + 5.1 - 5.7	34.0 + 5.1 - 5.9	-
25	47.6 + 6.4 - 7.4	52.8 + 7.3 - 9.3	-
50	57.6 + 7.3 - 8.6	66.6 + 9.6 - 12.8	-
100	67.0 + 8.3 - 9.5	80.2 + 13.3 - 17.0	-
200	75.8 + 9.1 - 10.7	93.6 + 17.6 - 21.4	-

(e)

Historical flood events	Return period (years) Data	Gamma	GEV	Normal
1995	112	978.7 + Inf - 563	213.1 + Inf - 108	-
2002	1.5	1.5 + 0.1 - 0.1	1.5 + 0.1 - 0.1	-
2004	1.1	1.1 + 0.0 - 0.0	1.1 + 0.0 - 0.0	-
2006	1.7	1.6 + 0.1 - 0.1	1.7 + 0.2 - 0.1	-
2011	4.5	4.5 + 1.2 - 0.7	4.8 + 1.1 - 0.7	-

Figure 3.15: As Figure 3.13 but for August–October (ASO) precipitation. The results using the normal distribution are not shown here as the Lilliefors test failed for this distribution. 'Inf' in Table (e) means the upper bound is infinite.

gamma) to +93.6 % (200-year; GEV). This was primarily due to the increased skewness of the distribution fits. The skewness for annual precipitation was 0.34 and 0.56 for the gamma and GEV distributions respectively; this increased to 0.50 and 1.08 for ASO precipitation.

In this grid square, the rainfall in 1995 was the highest in the 1901–2012 period (as the 'data' return period was 112 years). As the GEV distribution provided the best fit here, the most likely return period for this event was 213 years (and therefore extreme), although the uncertainty was large. The ASO rainfall was not classified as extreme for the other four flood events.

Monthly precipitation

The final example shows the return period curves for September precipitation, again in the grid square containing Bangkok (Figure 3.16). The normal distribution provided the best fit for the entire data series and the upper 25 %, whereas the gamma distribution provided the best fit for the upper 5 %. Although the three distributions produced a fit sufficient enough to pass the Lilliefors test for all sections of the data, the highest 10 observations appeared to follow a different distribution to the remainder of the data series. This was also visible in the other examples, but to a lesser degree.

As with ASO precipitation, the September return levels were much higher than the climatology (ranging from +37.0 % to +89.9 %). Again, this was partially due to the highly skewed nature of the precipitation distribution. Similarly, the September rainfall in 1995 was also high (the second highest in the data period). As the rainfall for this year was in the upper 5 % of the data, the most likely return period for this event was 96 years (and therefore extreme), although this estimate could vary from 54 to 232 years due to the uncertainty range. Again, as with ASO precipitation, the other four flood events were not associated with extreme September rainfall in this grid square.

3.3.3 Return period maps

I produced return period maps for given years and timescales (e.g. annual rainfall in 2011). These were created using the curves to find the return period associated

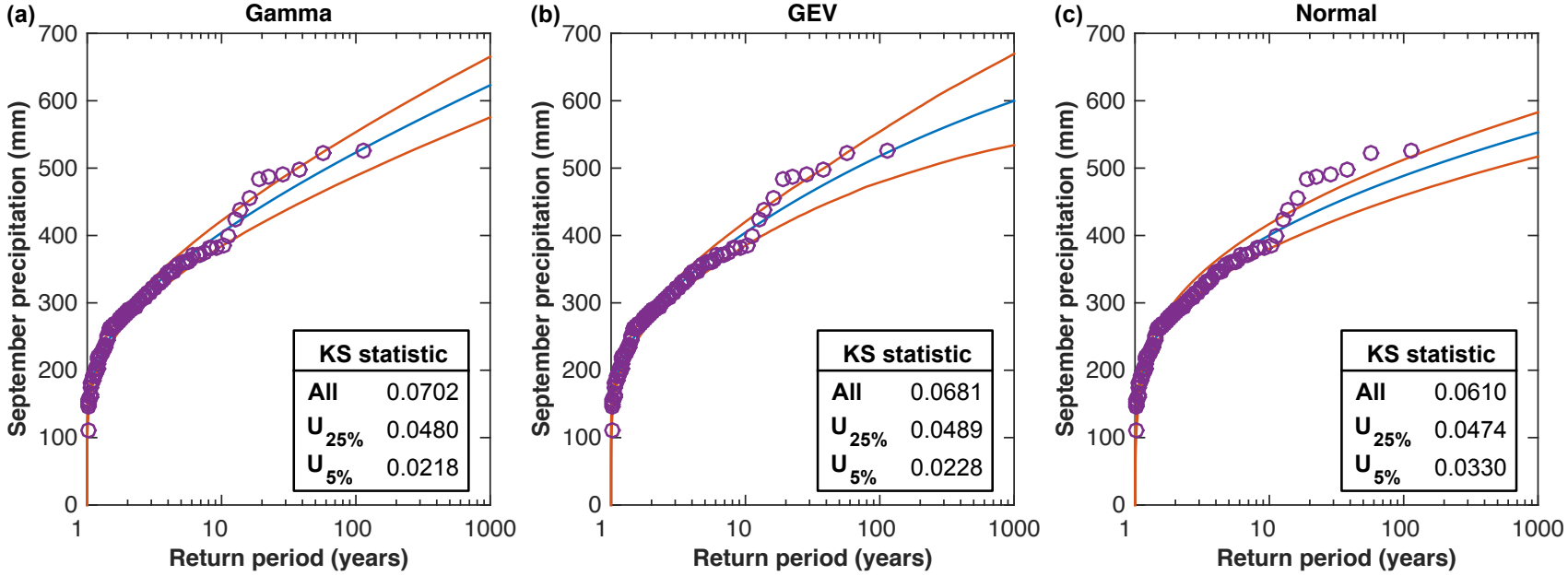

(d)

Return period (years)	September precipitation anomaly (%)		
	Gamma	GEV	Normal
10	38.3 +6.1 -6.8	38.4 +5.5 -6.6	37.0 +5.8 -6.8
25	55.8 +7.9 -8.9	55.6 +7.4 -8.9	50.6 +6.8 -8.5
50	67.8 +9.1 -10.4	67.0 +9.4 -11.1	59.4 +7.5 -9.3
100	79.1 +10.4 -11.9	77.3 +12.4 -13.4	67.3 +8.2 -10.0
200	89.9 +11.7 -13.3	86.6 +15.9 -16.1	74.5 +8.9 -10.8

(e)

Historical flood events	Return period (years)			
	Data	Gamma	GEV	Normal
1995	56.0	96.4 +136 -41.8	109.3 +412 -53.7	302.9 +913 -173
2002	1.1	1.1 +0.0 -0.0	1.1 +0.0 -0.0	1.1 +0.0 -0.0
2004	1.1	1.1 +0.0 -0.0	1.1 +0.0 -0.0	1.1 +0.0 -0.0
2006	1.9	2.0 +0.2 -0.2	2.0 +0.2 -0.2	1.8 +0.2 -0.2
2011	1.2	1.2 +0.0 -0.1	1.2 +0.0 -0.0	1.2 +0.0 -0.0

Figure 3.16: As Figure 3.13 but for September precipitation.

with rainfall in that year and timescale (as were the values shown in Table (e) of the return period curve figures). Chapters 4 and 5 show many examples of these maps, so an example is not included here.

The advantage of these maps is they provide a country-wide overview of the return periods for a given event. However, they do not convey the uncertainty associated with these return periods, nor do they show which distribution provides the best fit (and therefore the most accurate estimate). As this varies for each grid square, it is difficult to convey this information in a clear way in map form.

3.3.4 Return level maps

Return level maps show the precipitation amount required across the country for an n-year return period, where n is a given number of years. These can be computed for any value of n. Here I show four examples of return level maps for the 100-year return period rainfall at various timescales. For summer monsoonal rainfall, I also show the 10-year return level maps, and show uncertainty maps associated with the 100-year return level.

Annual precipitation

Figure 3.17 shows the annual precipitation return levels (given in (a) millimetres and (b) percentage above the annual precipitation climatology) for each of the three distributions used in this work. Averaging across the country, the 100-year return levels ranged from 2174 mm (GEV) to 2248 mm (gamma). Return levels were highest in the south and lowest in the centre of continental Thailand. Return levels in the south (average south of 12°N, the line of latitude located slightly south of Thailand's narrowest point) ranged from 3260 mm (normal) to 3357 mm (gamma). In comparison, the 100-year return levels in continental Thailand (average north of 12°N) were lower, ranging from 1942 mm (GEV) to 1988 mm (gamma). The return period pattern broadly follows the country's precipitation climatology (as shown by the reduced variation in Figure 3.17(b)), although annual return levels (in terms of percentage anomaly) tended to be lower in the east of the country. In terms of percentage anomaly, return levels across the country ranged from +21.7 % (GEV) to +58.1 % (gamma).

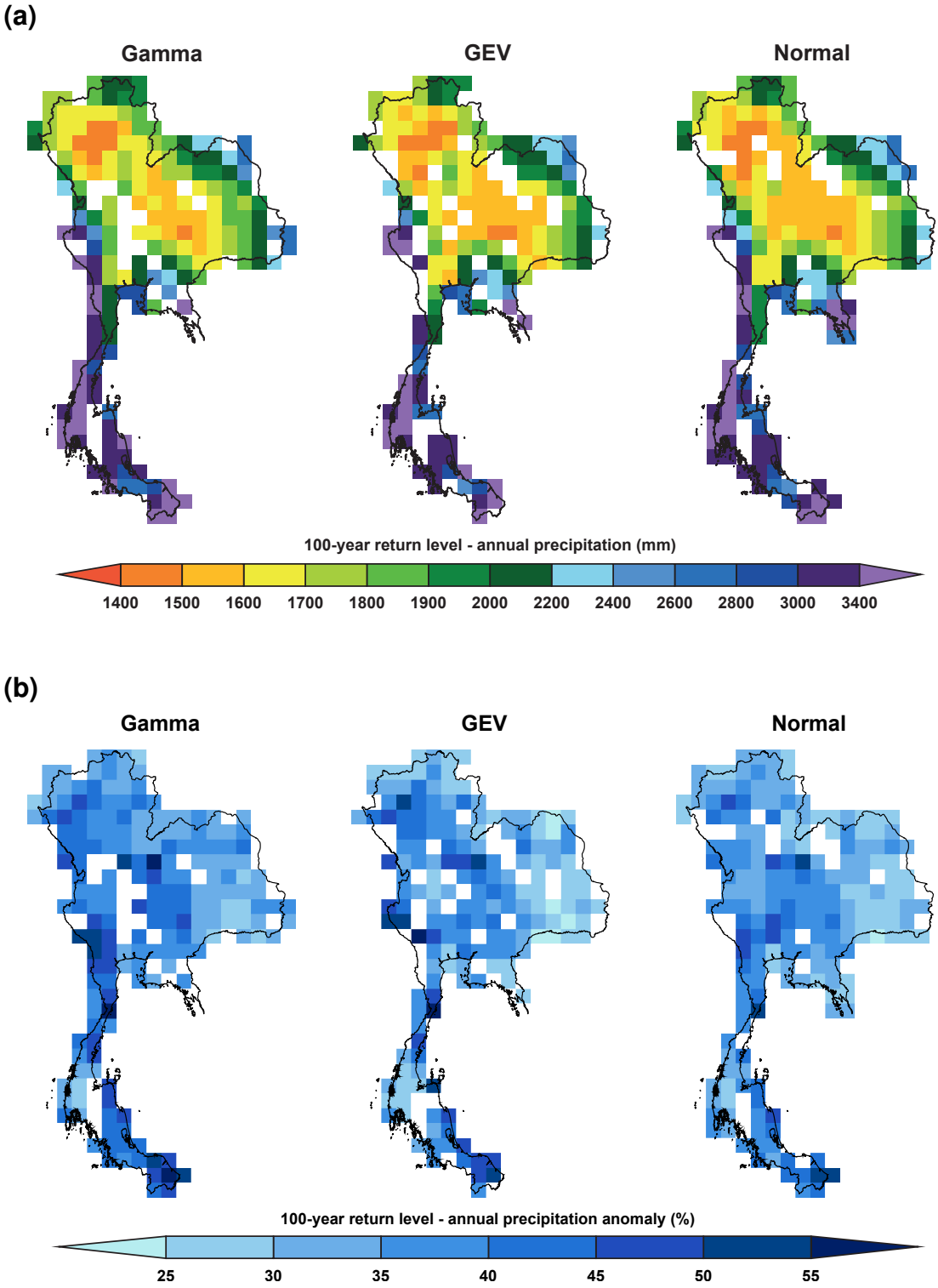

Figure 3.17: The annual precipitation return levels given in (a) millimetres and (b) percentage above the annual precipitation climatology for the 100-year return period shown for each of the three distributions (gamma, Generalized Extreme Value (GEV) and normal).

Summer monsoonal precipitation

The summer monsoonal precipitation return levels (in mm; Figure 3.18; note the change in colour scale between Figures 3.17(a) and 3.18(a)) varied more than those for annual precipitation, both across the country and across the three distributions. The country-wide average 100-year return level varied by over 1000 mm across the three distributions (gamma: 1857 mm; GEV: 1743 mm; normal: 1759 mm). Return levels varied by nearly 500 mm between continental and southern Thailand (continent: 1649 mm; south: 2146 mm (both GEV)). In the south of Thailand, return levels were higher in the west than the east. This pattern was likely caused by orographic enhancement, where the high ground in the west forces convection and increases the summer monsoonal rainfall in the west of this region. Figure 3.18(b) corroborates this theory; this east-west divide is not seen in the return levels given as a percentage anomaly. Like the annual return levels, the summer monsoonal precipitation return levels broadly follow the country's precipitation climatology. Again, return levels (percentage anomaly) tended to be lower in the east of the country.

Figure 3.19 shows the uncertainty range for the 100-year summer monsoonal precipitation return levels. Averaging across the country, the return level uncertainty range varied across the three distributions: 1779 mm–1923 mm (gamma), 1645 mm–1807 mm (GEV), 1696 mm–1815 mm (normal). The GEV distribution has the largest uncertainty and the normal distribution the smallest; this follows the uncertainty pattern seen in the return period curves shown in Section 3.3.2. The general pattern of the upper and lower bounds follows that of the return level maps.

For a comparison, I also include maps showing the summer monsoonal precipitation return levels for the 10-year return period (Figure 3.20). As expected, the return levels are much lower for the 10-year return period (both in terms of millimetres and percentage above the climatology), but the return level pattern remains much the same.

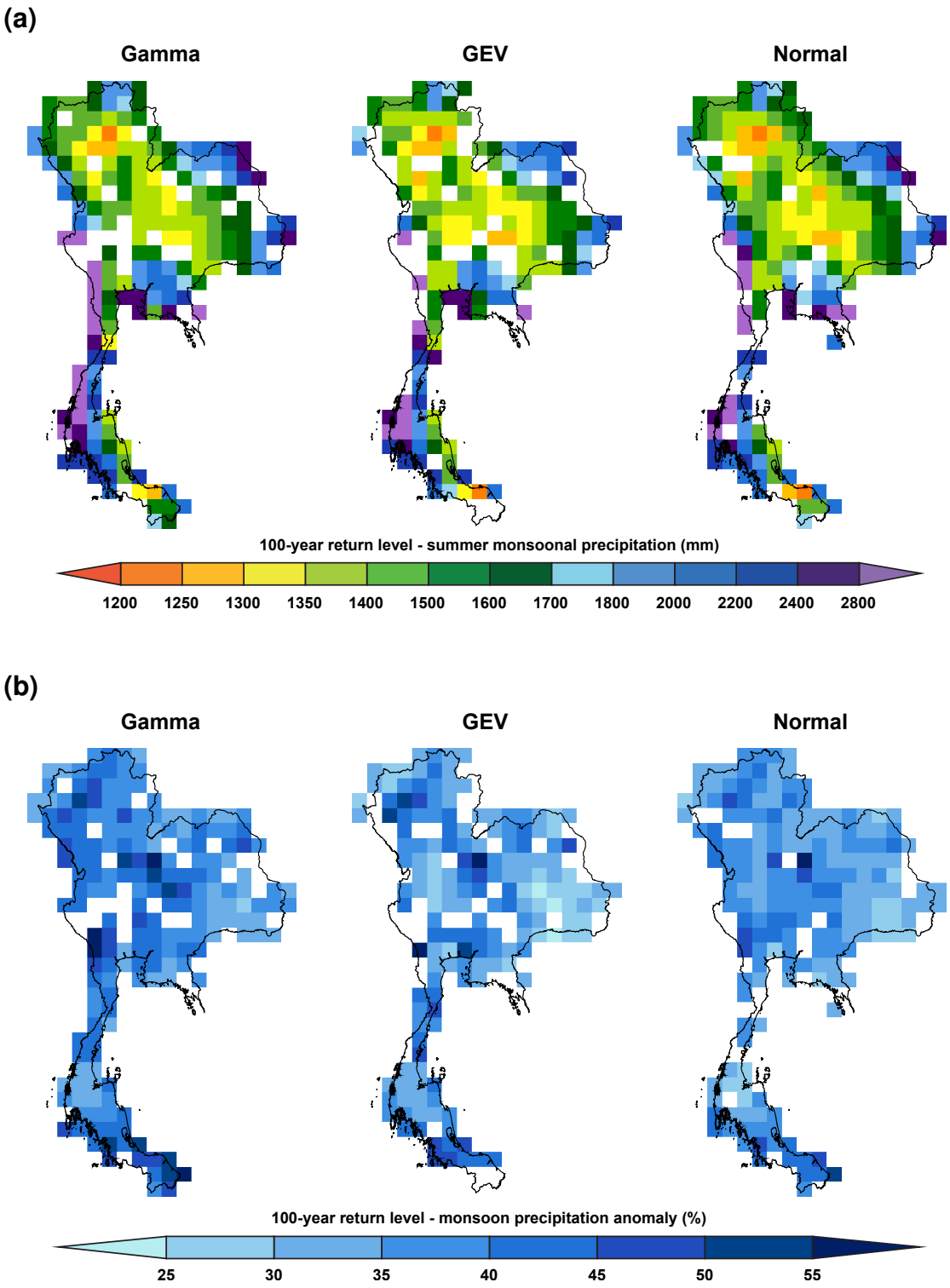

Figure 3.18: As Figure 3.17 but for summer monsoonal (May–October (MJJASO)) precipitation. Note the change in colour scale between Figures 3.17(a) and 3.18(a).

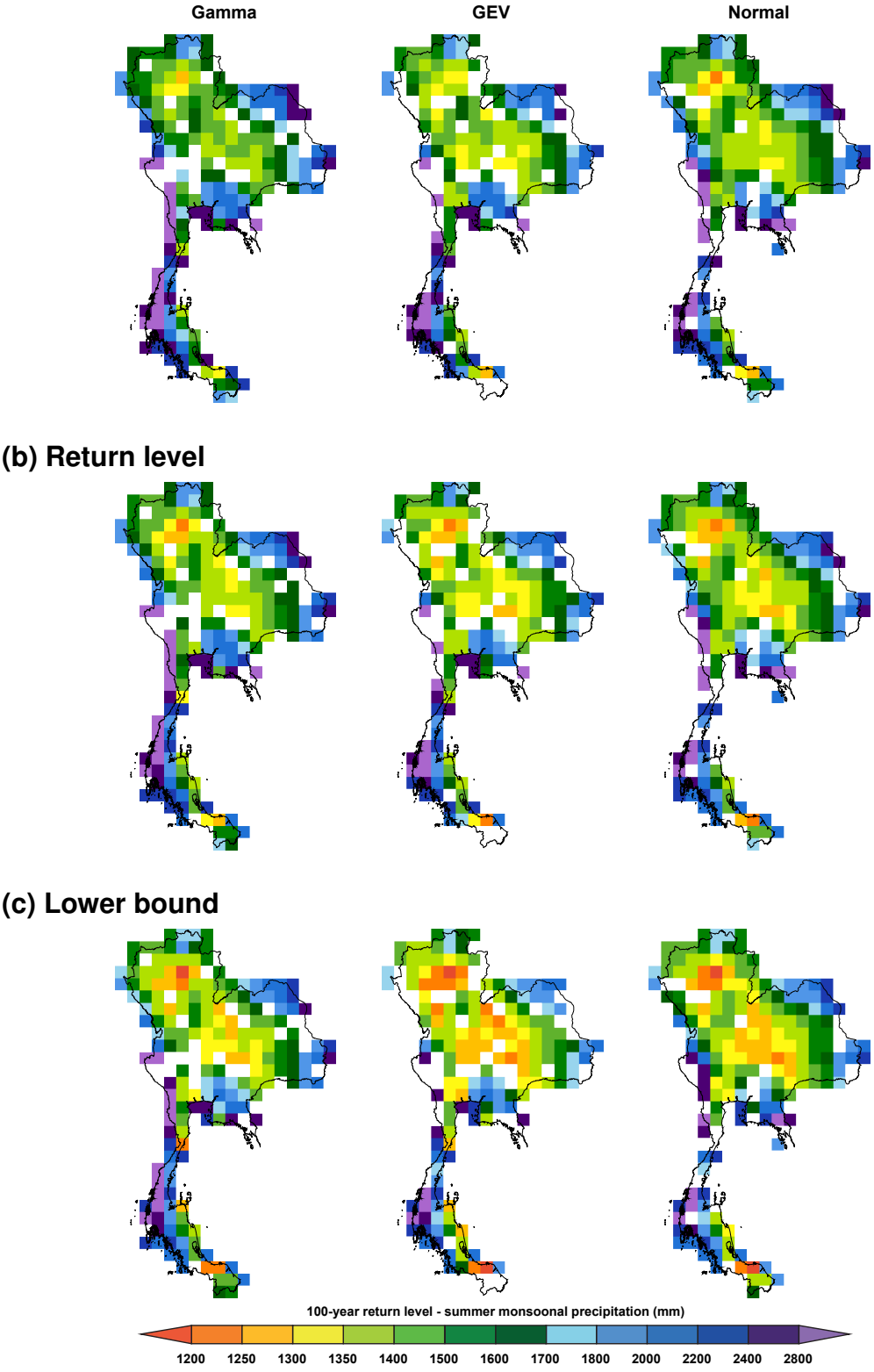

Figure 3.19: (b) The summer monsoonal precipitation return levels (in millimetres) with the associated (a) upper and (c) lower bound return levels for the 100-year return period shown for each of the three distributions (gamma, Generalized Extreme Value (GEV) and normal).

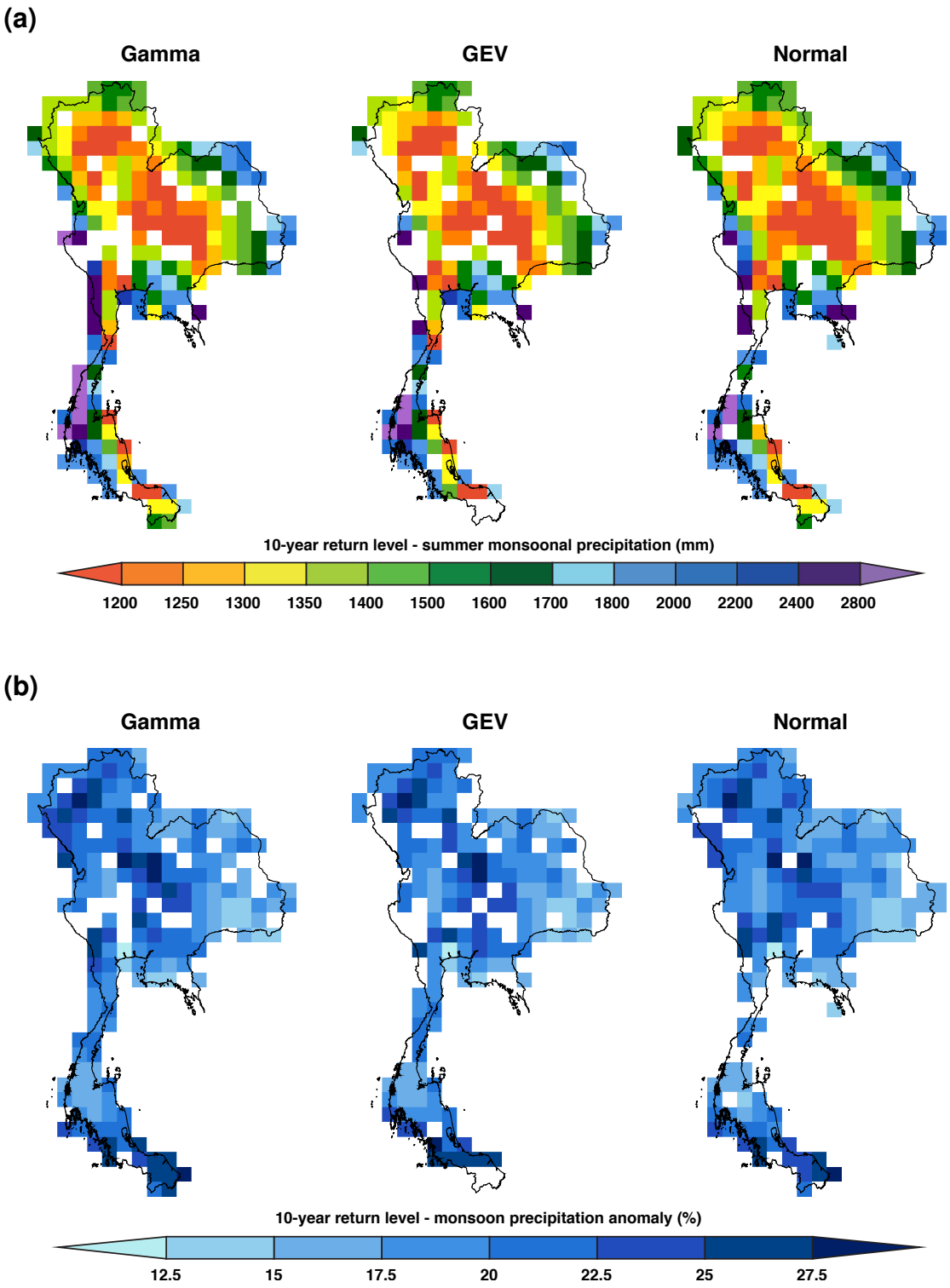

Figure 3.20: As Figure 3.18 but for the 10-year return period. Note the change in colour scale between Figures 3.18(b) and 3.20(b).

Seasonal & monthly precipitation

Figure 3.21 displays the 100-year return levels for (a) ASO and (b) September precipitation using the GEV distribution only. Here the return levels are displayed in terms of precipitation anomaly using the 1901–2012 climatology. Note the change in colour scale between the two sub-figures. On average, ASO return levels were +370 mm, +359 mm and +415 mm for the country, north and south respectively. Similarly, the September return levels were more anomalous in the south than the north (+247 mm and +223 mm respectively). These figures show return level variation is not solely caused by variation of the precipitation climatology.

Although these maps provide a country-wide view of the variation in return levels for any given return period, as with the return period maps, they do not convey the uncertainty in these estimates. As shown in the various examples in Section 3.3.2, return level estimates can vary by as much as 160 mm due to this

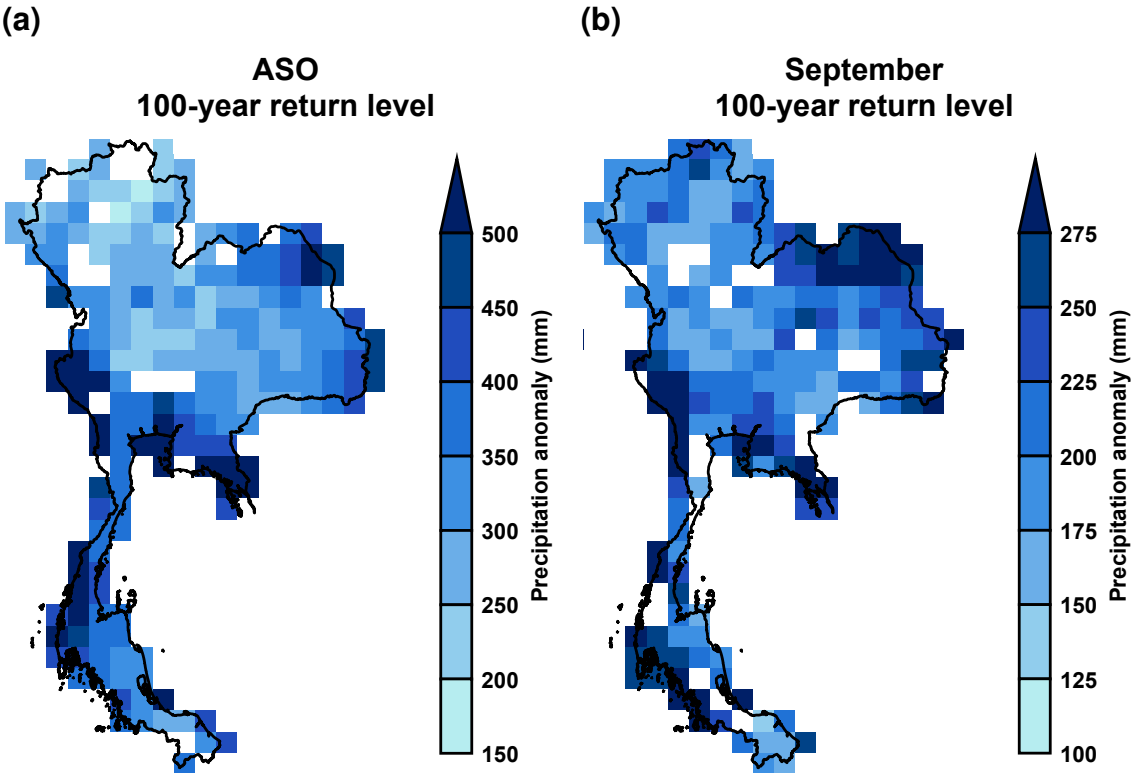

Figure 3.21: The (a) August–October (ASO) and (b) September precipitation return levels for the 100-year return period shown for the Generalized Extreme Value (GEV) distribution only. Here the return levels are given as precipitation anomalies using the 1901–2012 climatology. Note the change in colour scale between the sub-figures.

uncertainty.

3.4 Discussion

In this chapter I produced extreme rainfall return periods for all 0.5° grid squares in Thailand at multiple climatic timescales (annual, MJJASO, seasonal, monthly) using 112 years of data (1901–2012). I computed these using two methods: the basic method and the distribution method. The basic method is simple but is limited; it is not possible to estimate return periods longer than the length of the dataset, and it is not possible to estimate uncertainty. The distribution method is more complex and uses distribution fitting to estimate return periods longer than the dataset length. This second method also allows the estimation of uncertainty.

I implemented the Lilliefors goodness-of-fit test (an adapted version of the KS test) to identify the most suitable distribution (gamma, GEV or normal) for each grid square and timescale. The test was applied to all the data, but also to the upper 25 % and upper 5 % of the data only. This ensured the distributions successfully modelled the extreme climatic rainfall measurements (those with a return period of 10 years or over). The most suitable distribution varied depending on the timescale; the normal distribution tended to fit best for annual and summer monsoonal precipitation, whereas the gamma and GEV distributions were more suited to seasonal and monthly rainfall.

The method used in this work was designed so it can be applied easily to other countries around the world, although the distributions used will vary depending on the shape of the underlying precipitation distribution.

I produced three products from these return period calculations: return period curves for each grid square and timescale, return period maps showing return periods across the country for a given year and timescale, and return level maps showing the precipitation across the country associated with a given return period. The return period curves are particularly important as they also show the uncertainty associated with the return period estimates.

In some of the return period curves shown, the highest ten or so observations appeared to follow a different distribution to the one fitted to the entire data series. This could be examined further by applying EVT and distribution fitting to the

upper portion of the data only.

To conclude, this work produced extreme rainfall return periods for all 0.5° grid squares in Thailand at a variety of climatic timescales using 112 years of data (1901–2012). These return periods give the probability of occurrence of extreme climatic rainfall, information that can benefit a variety of industrial sectors (e.g. planning, insurance, public safety). This is the first study of its kind for extreme climatic rainfall in Thailand.

Chapter 4

Case study: the 2011 Thailand flood

4.1 Introduction

Thailand is one of the most developed and wealthiest countries in Southeast Asia. However, its tropical location, and the influence of summer monsoonal rains and local topography make it prone to floods. The Thailand floods in 2011 were especially severe causing estimated losses of US$30 billion (economic) and US$12 billion (insured; Swiss Re, 2012). This insured loss ranks easily as the highest ever worldwide from a freshwater flood disaster (Swiss Re, 2012). The primary factor behind the 2011 floods was record rainfall. Taking Thailand as a whole, annual rainfall in 2011 was the highest in the country's precipitation record (Thai Meteorological Department, 2011). In this chapter I first review the nature, impacts and historical ranking of the 2011 Thailand floods. Next I examine the 2011 rainfall totals and anomalies across Thailand and use these with other data to discuss the climate causes for the exceptional 2011 rainfall. I then estimate the return periods for the 2011 rains across Thailand and compare these to satellite-derived return periods for 2011 river flow. Finally I bring together the different estimated return periods to provide a firmer value for how likely it is that a flood of the magnitude of 2011 will reoccur.

4.2 Flood overview

4.2.1 Background and impacts

Thailand is a country prone to flooding. Its climate is monsoonal with over 80 % of annual rainfall occurring between May and October (Figure 4.1(a)) from the summer monsoon. During the wettest months of August and September rivers carry high runoffs and can overflow leading to flooding. In extreme rainfall years

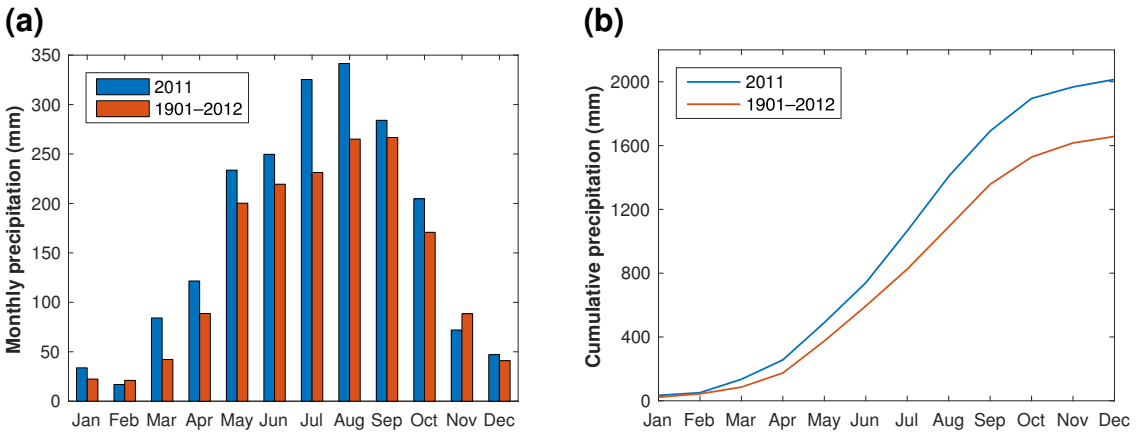

Figure 4.1: The (a) monthly and (b) cumulative monthly precipitation for 2011 (blue) averaged across Thailand. The 1901–2012 climatology for Thailand is shown for comparison (red). The data shown are from the Climatic Research Unit (CRU) TS3.21 gridded dataset (Section 2.2.2).

the flooding can spread along Thailand's main water artery, the CPRB (Figure 4.2), towards Bangkok, the country's capital, before emptying into the Gulf of Thailand. The CPRB is home to about 20 million people (30 % of the total population; DHI, 2011) and to much of Thailand's manufacturing industry (Swiss Re, 2012). The basin's relatively flat topography (a gradient of just 1.5 m per 100 km; DHI, 2011) means that flood waters drain away slowly and that floods have long durations. Due to its tropical location Thailand also experiences the remnants of Northwestern Pacific tropical storms. These storms bring additional heavy rainfall, which can initiate or exacerbate flooding during the summer monsoon season.

In 2011, the summer monsoon started early with Thailand experiencing record-high rainfall in March and April (Figure 4.1(a); Swiss Re, 2012). This led to unusually saturated soil moisture prior to the main summer monsoon season (Komori et al., 2012; Promchote et al., 2016). Above-average rainfall continued throughout the 6-month summer monsoon season, meaning accumulated rainfall was above average throughout 2011 (Figure 4.1(b)). This together with heavy rainfall from four tropical storm remnants crossing the north of the country led to rivers bursting their banks. Insufficient management of the main dams in Thailand (Komori et al., 2012; Koontanakulvong, 2012; Mateo et al., 2014) led to overtopping and to the release of yet more water, which further exacerbated

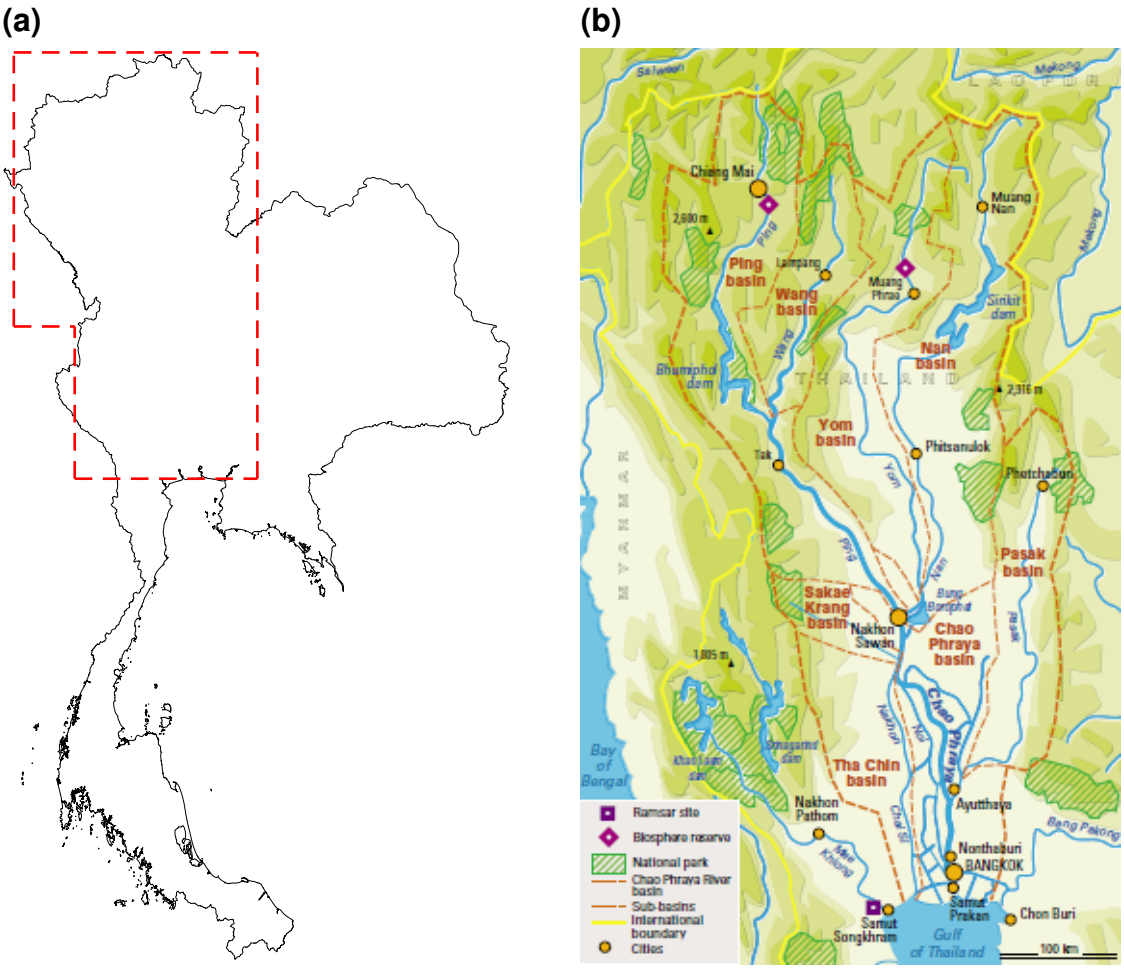

Figure 4.2: Maps showing the Chao Phraya River basin (CPRB). (a) shows the river basin area used in this work (based on the area used in Promchote et al. (2016)) and (b) shows a more detailed map of the basin (Office of Natural Water Resources Committee of Thailand, 2003).

the flooding. Abnormally high sea level in the Gulf of Thailand affected drainage from the lower CPRB, thereby exacerbating the flood (Rakwatin et al., 2013; Promchote et al., 2016). An area of about 30 000 km^2, roughly the size of Switzerland (as shown in Figure 4.3(b)), was inundated with flood water. In total, 65 out of 77 provinces in the country were affected by flooding to some extent (Aon Benfield, 2012a). The flooding caused extensive damage (as shown in Figure 4.3(a)) to homes, sites of historical interest, and industrial estates run by large multi-national companies (including Sony, Honda and Toyota; Aon Benfield, 2012a; Haraguchi and Lall, 2014).

Figure 4.3: Impacts and extent of the 2011 Thailand flood. (a) Bangkok, Thailand's capital, suffered extensive flooding as seen in this aerial survey on 24 October 2011. (b) Thailand map showing the extent of the 2011 flood (in blue) with Switzerland shown for area-comparison. Images courtesy of (a) Cpl. Robert J. Maurer, U.S. Marine Corps and (b) Swiss Re (2012).

4.2.2 Historical ranking

How does the 2011 flood rank in comparison to other historical Thailand floods? Table 4.1 shows the ten largest Thailand flood events for the period 1985–2012 as documented by the Dartmouth Flood Observatory (Brakenridge, 2012). In terms of ranking by flood magnitude, 2011 is only fifth. However, if ranked by duration, the 2011 flood (at 158 days) is first. The flood in 1995 (described in more detail in Chapter 5) ranks highest in terms of magnitude and area affected, and it led to changes in flood management in Thailand. The event was unusual as it affected a large proportion (approximately 87 %) of the country despite rainfall totals in 1995 being lower than in 2011 (as will be shown later in this chapter). The explanation for this difference appears to be the lack of flood mitigation schemes in 1995 compared to 2011. After 1995, measures were introduced—including the use of better drainage systems and improved reservoir operations—to reduce the risk of flooding (Hungspreug et al., 2000).

Table 4.1 may be used to estimate the return period of the 2011 flood. Since five events of equal or greater magnitude have occurred in the last 28 years,

Table 4.1: The top 10 Thailand flood events for the period 1985–2012. The data are taken from the Dartmouth Flood Observatory Global Active Archive of Large Flood Events (Brakenridge, 2012). Ranking is by flood magnitude.

Year	Dates	Magnitude	Duration (days)	Area affected (km^2)
1995	1 Aug–9 Nov	7.9	101	444 000
2002	18 Aug–26 Nov	7.9	101	372 000
2006	20 Aug–13 Dec	7.7	116	213 000
2004	6 Aug–3 Oct	7.6	59	378 000
2011/12	5 Aug–9 Jan	7.5	158	97 000
2007	5 Sep–10 Nov	7.3	67	300 000
1994	3 Sep–18 Dec	7.1	107	65 000
2005	13 Aug–26 Sep	7.1	45	134 000
1996	18 Jul–21 Aug	7.0	35	314 000
2003	12 Sep–12 Oct	7.0	31	315 000

Flood magnitude $=$ log(Duration $\times$ Severity $\times$ Area affected)

Severity depends on the estimated recurrence interval of floods in the region affected and is defined on a scale between 1 and 2.

one may deduce a return period for the 2011 flood of 5.6 years (calculated using the basic method given in Equation 3.3). However, this estimate is likely to be low due to the improvements in flood protection that have occurred since 1995. These improvements mean that the flood magnitudes in Table 4.1 are not normalised to current conditions.

4.3 Data

4.3.1 Precipitation data

Two sources of Thailand precipitation data are used in this chapter. The primary dataset is from the TMD, which comprises daily precipitation totals from 99 Thai weather stations for the 20-year period 1992–2011. Further details of this dataset are given in Section 2.2.1. Section 4.5 also uses the 0.5° gridded monthly precipitation dataset from the CRU (detailed in Section 2.2.2) to calculate accurate extended return periods. Although this dataset has a longer data period (112 years, 1901–2012), fewer stations are used to produce the gridded product (only 49 stations in total).

4.3.2 Summer monsoon data

I used various data sources to evaluate the contribution of the Southeast Asian summer monsoon to the 2011 flood in Thailand. The anomaly in MJJASO MSLP can be used as a proxy for the summer monsoon strength. I calculated this anomaly using reanalysis data from NCEP/NCAR (detailed in Section 2.5; Kalnay et al., 1996) for each year in the 20-year period of study (1992–2011) based on the climate normal. A link exists between summer monsoonal rainfall in Thailand and ENSO (e.g. Cook and Buckley, 2009; Räsänen and Kummu, 2013); this is examined in detail in Chapter 6. Singhrattna et al. (2005a) found a positive correlation between the ASO SOI and precipitation in the same period (correlation seen post-1980 as shown in Figure 1.9). I used SOI data from the Australian Bureau of Meteorology (2014) (described in Section 2.3.1) to examine whether ENSO enhanced the summer monsoon in 2011. A link also exists between the Indian Ocean Dipole (IOD) and summer monsoonal rainfall in Thailand (Singhrattna et al., 2005a; Bridhikitti, 2013). This correlation was examined for 2011 using DMI data from JAMSTEC (2012) (detailed in Section 2.3.3).

4.3.3 Tropical storm data

Best-track data for Western Pacific tropical storms affecting Thailand were extracted from the Unisys (2015) website, which uses data provided by the JTWC (Chu et al., 2002). Details of these storms, and the method used to identify them, are given in Section 2.4.

4.3.4 River discharge data

Satellite-derived river flows in the CPRB—the Thai region most heavily flooded in 2011—were obtained from the Dartmouth Flood Observatory online repository of global river discharge data (Brakenridge et al., 2012). Further details are given in Section 2.6.

4.4 Climate causes

Interannual variability in Thailand rainfall is caused by year-to-year changes in the strength of the Southeast Asian summer monsoon (Singhrattna et al., 2005b) and by year-to-year changes in the number of Thai tropical storms. Here I examine the contribution of these two causes to the record-breaking annual rainfall in 2011. I begin by first examining the 2011 annual precipitation totals and 2011 annual precipitation anomalies across Thailand.

4.4.1 Precipitation in 2011

Figure 4.4 displays the Thai 2011 annual precipitation and annual precipitation anomaly spatially across the country. Anomalies were calculated relative to the 1992–2011 climatology. The spatial interpolation of precipitation was achieved using the kriging geostatistical technique. The technique employs observed values of a field to interpolate points where there are no field observations (Webster and Oliver, 2007; ESRI, 2013). The influence of other variables (e.g. elevation; Goovaerts, 2000) can improve the accuracy of the interpolation process for rainfall, although this has not been examined here. The kriging output also has a sensitivity to internal settings such as the 'search radius'. Here I used Ordinary Kriging, which is the most common type of kriging employed in meteorology and climatology. Each interpolated point was estimated using the weighted average of the surrounding data within a radius of 1.5 degrees ($\sim$165 km). These weights primarily depend on the distance between the station and the interpolated point, although other factors, such as the interpolated grid resolution and the clustering of stations, also affect the size of the weights (Webster and Oliver, 2007). I chose this search radius as it kept the interpolation relatively local whilst allowing for a completed interpolated surface across the country. Reducing this radius led to areas with no interpolated surface due to sparse station coverage.

The highest rainfall totals in 2011 occurred in southern Thailand (over 3200 mm), while in northern Thailand precipitation was between 1200 mm and 2000 mm. Taking the country as a whole, rainfall was 23 % above normal in 2011; the largest positive rainfall anomalies (up to 1800 mm above normal) occurred in

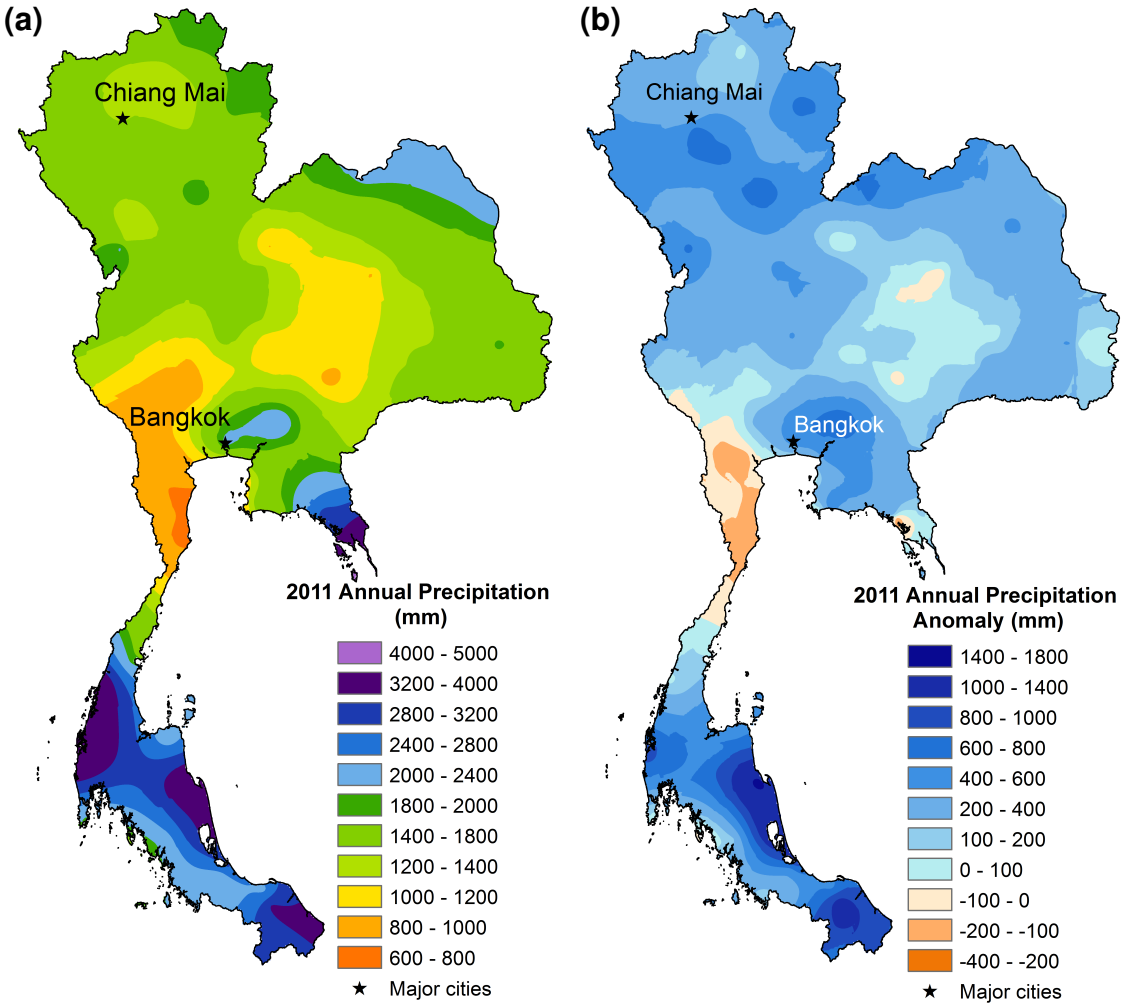

Figure 4.4: The nature and distribution of 2011 Thailand rainfall. Map (a) shows the 2011 annual precipitation and map (b) shows the 2011 annual precipitation anomaly using the Thai Meteorological Department (TMD) station data. A 20-year (1992–2011) climatology is used for the latter. The kriging technique (Webster and Oliver, 2007) is used for spatial interpolation with a grid size of 0.03° (the default in ArcGIS, the software used to produce these maps). Reproduced from Gale and Saunders (2013).

the south. Precipitation totalled 2073 mm (530 mm above normal) in Bangkok, and 1330 mm (255 mm above normal) in Chiang Mai.

4.4.2 Southeast Asian summer monsoon

Here I examine the contribution of the Southeast Asian summer monsoon to the record 2011 rainfall by considering time series (1992–2011) for the MJJASO MSLP anomaly (Figure 4.5(a)) and the MJJASO precipitation anomaly (Figure 4.5(b)). The MJJASO MSLP anomalies were calculated using NCEP/NCAR data (detailed in Section 2.5; Kalnay et al., 1996) averaged over the area 12.0–20.6°N,

97.2–105.8°E, which comprises most of Thailand (the Kra Isthmus in the south is excluded). The precipitation anomalies were computed for stations north of 12°N.

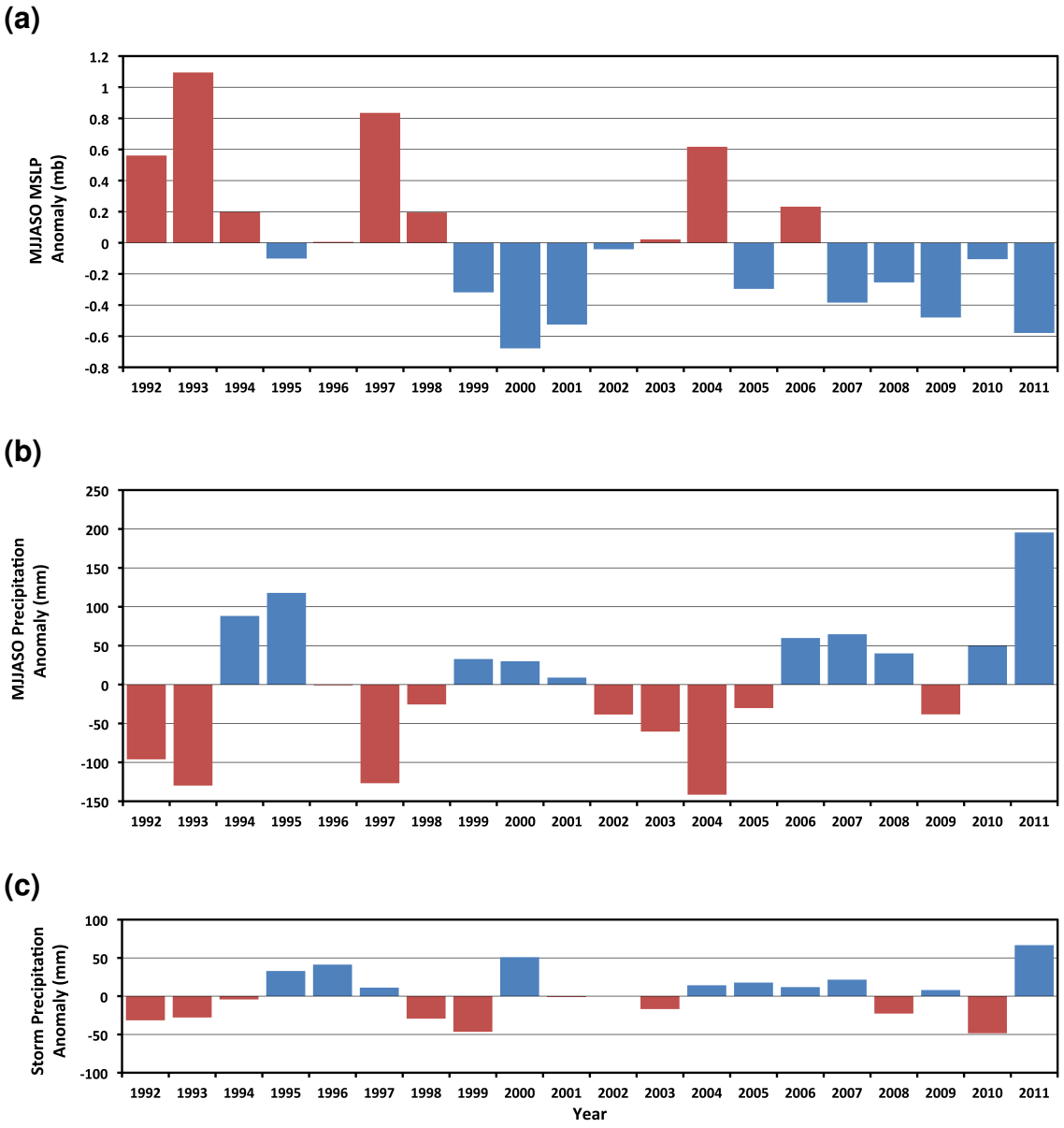

Figure 4.5: Examination of the climate causes for the record 2011 Thailand rainfall. The panels display climate time series (1992–2011) for the Thailand area north of the Kra Isthmus at 12°N. (a) Summer monsoon strength (proxy): anomaly in May–October (MJJASO) mean sea level pressure (MSLP) anomaly. (b) Summer monsoonal rainfall: anomaly in MJJASO precipitation. (c) Tropical storm rainfall only: anomaly in storm precipitation. Red and blue in (a) denote respectively high and low pressure anomalies. Red and blue in (b) and (c) denote respectively positive and negative precipitation anomalies. The Thai Meteorological Department (TMD) station data were used to compute the rainfall anomalies. Adapted from Gale and Saunders (2013).

The MSLP anomalies are a proxy for summer monsoon strength: positive anomalies indicate a weaker summer monsoon, negative anomalies a stronger one. As expected, a negative correlation exists between the MJJASO MSLP and the precipitation anomalies. Figure 4.5 shows that in 2011 the MJJASO precipitation anomaly (+246.1 mm) was by far the highest in the last 20 years, and that the MSLP anomaly was the second most negative (but comparable to that in three other years) for the same period. This suggests that the summer monsoon was a significant, but not the only, factor in the Thailand rainfall in 2011 being so high.

With regard to the cause of the strong summer monsoon over Thailand in 2011, Singhrattna et al. (2005a) examined the link between summer (ASO) Thai rainfall and large-scale climate indices. A statistically significant positive correlation between the contemporaneous SOI and Thai summer monsoonal rainfall was found after 1980 but not in earlier years. Interestingly, a significant link between the SOI and Indian summer monsoonal rainfall existed before 1980 but weakened after 1980. These changes were consistent with an SOI-related circulation change around 1980. The SOI was positive throughout 2011 and had a moderately high value of +7.1 for ASO (Australian Bureau of Meteorology, 2014), typical of La Niña conditions. This suggests that the sign and strength of the Southern Oscillation may have contributed to the Thai flooding in 2011. Additionally, I found multi-year La Niña events produce excess annual rainfall in Thailand (as described in detail in Chapter 6). The 2010–2011 multi-year La Niña was therefore another contributory cause of the 2011 flood.

Singhrattna et al. (2005a) also found a statistically significant negative correlation between Thailand ASO rainfall and the prior MAM DMI. The DMI, described in detail in Section 2.3.3, is a measure of the sign and strength of the Indian Ocean Dipole. The DMI value for MAM in 2011 was +0.19 °C (JAMSTEC, 2012); this weakly positive value suggests that the Indian Ocean Dipole did not contribute to the Thailand floods in 2011.

4.4.3 Tropical storms

The contribution of tropical storms to the Thailand 2011 record rainfall may be examined by comparing Figure 4.5(c), which displays the anomaly in annual Thai rainfall from tropical storms only, with Figure 4.5(b). As described in Section 2.4, the tropical storm remnants that cross Thailand originate from storms that form in the Northwestern Pacific basin—the most active basin for tropical storm formation worldwide (Xue and Neumann, 1984). They affect the country between May and December, with peak incidence in November. Using best-track data from the JTWC (Chu et al., 2002), I identified 54 tropical storms (or their remnants) that crossed Thailand between 1992 and 2011; an average of 2.7 storms per year. The number of storms affecting the country ranged from nil in 2002 to six in 1996. The rainfall from individual storms affects a smaller area than does summer monsoonal rainfall. The 'storm' rainfall for each of the 54 tropical storms was computed using daily rainfall data from the 99 Thai weather stations and the dates that each storm was over Thailand (given by the JTWC best-track data and the rainfall spikes seen, as described in Section 2.4).

In 2011, the remnants of four tropical storms caused significant Thailand rainfall; they primarily affected northern Thailand and occurred in late June, late July, late September and early November. The tracks of these storms are shown in Figure 4.6. Figure 4.5(c) shows the storm precipitation anomaly in 2011 was +66.7 mm, the highest storm precipitation anomaly in the 1992–2011 period. Figures 4.5(b) and (c) show that tropical storms contributed 27 % of the anomalous high MJJASO rainfall in 2011.

4.4.4 Summary

The 2011 Thailand floods were caused by a combination of a strong Southeast Asian summer monsoon that brought high rainfall across the country between May and October, and the remnants of four tropical storms that brought high rainfall primarily to northern Thailand between June and November. During the summer monsoon season the SOI was moderately positive and, as a result, is likely to have contributed to the high summer monsoonal rains. The

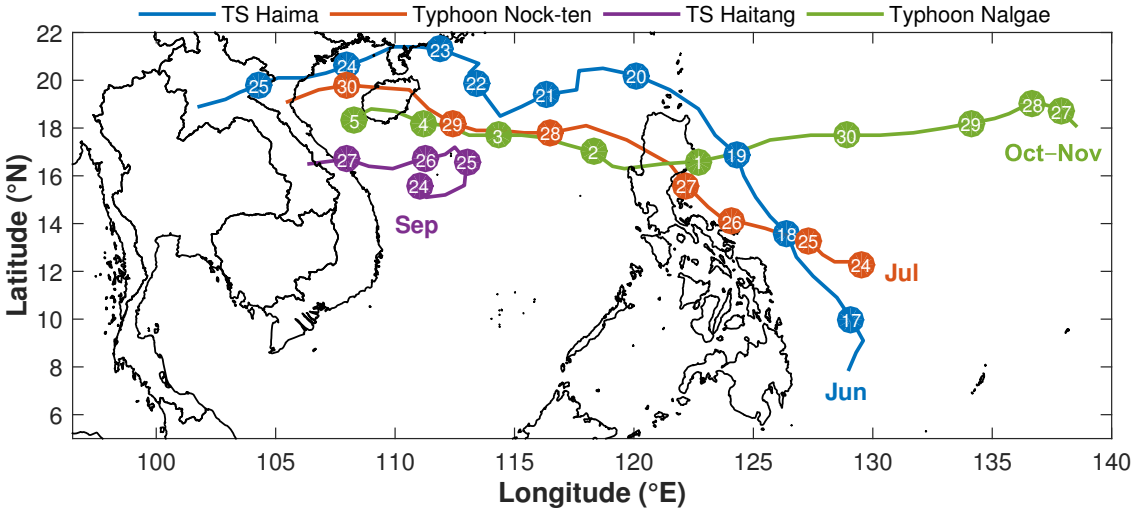

Figure 4.6: The tracks of the four tropical storms that affected Thailand in 2011 (based on best-track data from the Joint Typhoon Warning Center (JTWC) (Chu et al., 2002)). The numbered markers represent the date at 00 UTC of the month(s) in which the storm was active.

SOI enhancement of Thai summer monsoonal rains probably arises because the ascending branch of the Walker Circulation over the Pacific Ocean and Southeast Asia shifts westward towards Thailand during positive SOI conditions. Additionally, research detailed in Chapter 6 shows the 2010–2011 multi-year La Niña contributed towards the excess rainfall in 2011. In contrast the IOD was not a contributing factor.

4.5 Return periods

The 2011 Thailand flood return period may also be estimated from pan-Thailand historical rainfall data and from satellite-derived river flows in the CPRB. The computation of these return periods is described below.

4.5.1 Data and methodology for rainfall analysis

The rainfall return period analysis employs TMD station data for the 20-year period 1992–2011, and CRU gridded data for the 112-year period 1901–2012. The return periods for 2011 annual rainfall and annual tropical storm rainfall were computed for each of the 99 weather stations in the TMD dataset using the basic method described in Section 3.2.3 (Neumann, 1987). This method divides the number of years with complete rainfall data by the number of years

where the annual (or storm) rainfall total is greater than or equal to the observed total in 2011. For example, in Bangkok the annual total precipitation in 2011 was 2073 mm. As there were two occurrences of an annual total precipitation greater than or equal to 2073 mm in Bangkok between 1992 and 2011, the return period for 2011 rainfall in Bangkok is 10 years. In this basic method the return period is sensitive to the number of years of available rainfall data so, in this case, the longest return period that may be computed is 20 years. As a result, return periods may be underestimated.

As a comparison, I also computed precipitation return periods for multiple timescales using the extended CRU dataset and the distribution method described in Section 3.2.4. This method uses distribution fitting, which allows the estimation of return periods longer than the underlying dataset. These return periods are more accurate than those calculated using the basic method.

4.5.2 Rainfall return periods

Figure 4.7 displays the return periods for 2011 annual precipitation and 2011 tropical storm precipitation across Thailand, derived using the TMD station data and the kriging interpolation method. The Thailand hill country in the north and the Kra Isthmus in the south exhibit the longest rainfall return periods of between 8 and 20 years. Averaging across the country, the return period of annual precipitation in 2011 was 8.8 years.

A comparison of the two maps, combined with the map of storm tracks (Figure 4.6), shows that the long rainfall return periods in the north are linked to excess tropical storm precipitation, while those in the south are attributed to other causes. The area to the south-east of Bangkok exhibits long storm rainfall return periods, but this area was not hit by a tropical storm in 2011. This is a consequence of the method used to calculate storm precipitation return periods. If heavy rainfall attributed to another cause (e.g. the summer monsoon) occurs elsewhere on the same dates as a tropical storm, this may produce a long storm rainfall return period (as is the case here).

As explained previously, the basic method limits the return periods in Figure 4.7 to a maximum of 20 years. To assess this effect, Figure 4.8 shows the 2011

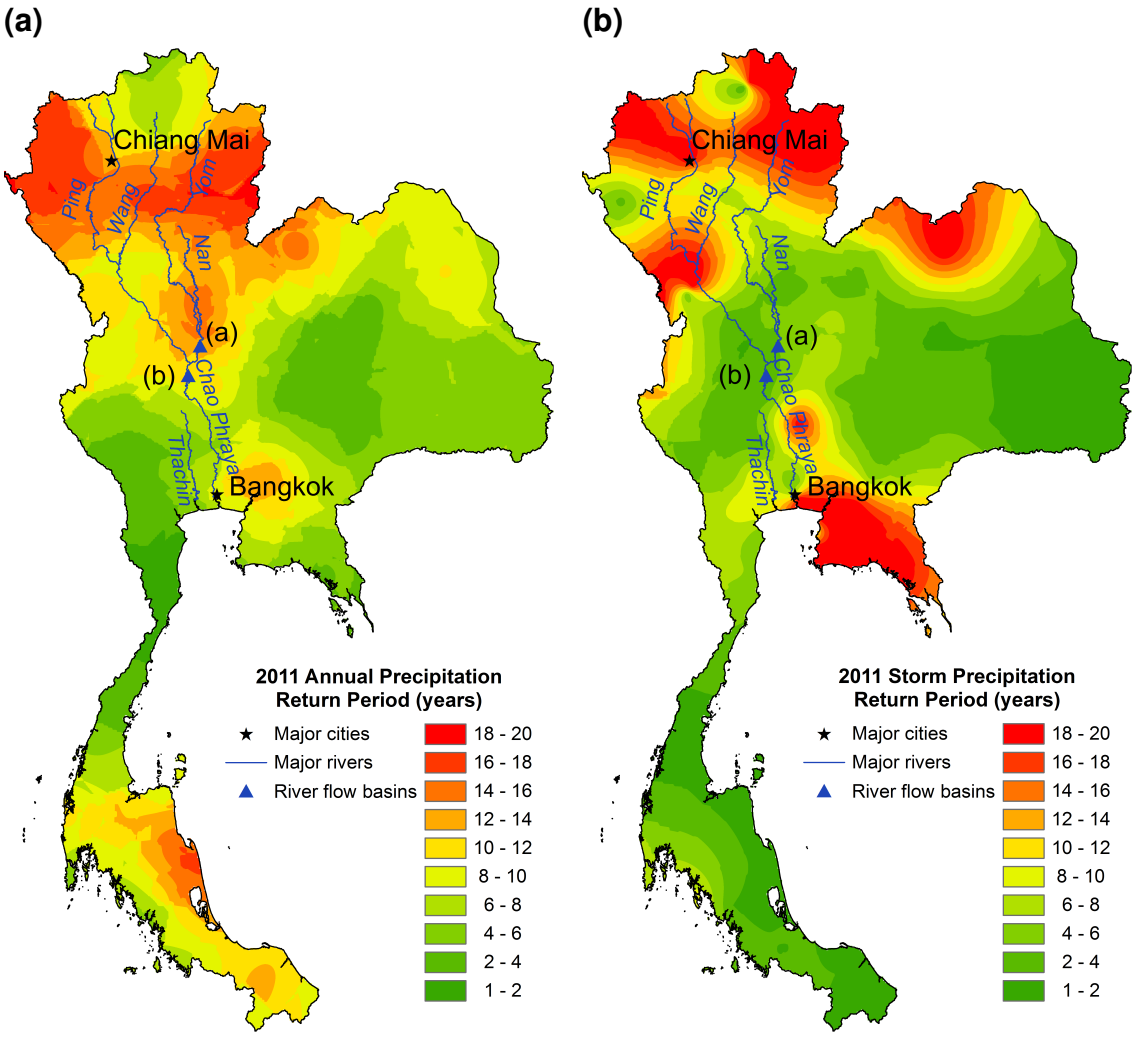

Figure 4.7: Return periods for 2011 Thailand annual rainfall displayed spatially across the country. These return periods are calculated using the Thai Meteorological Department (TMD) station data and the basic method (Section 3.2.3), and then interpolated using kriging (using a grid size of 0.03° as in Figure 4.7). (a) shows the return period in years for 2011 annual precipitation, and (b) displays the return period in years for 2011 tropical storm precipitation. The major rivers in the Chao Phraya River basin (CPRB) are included together with the two sites for which satellite-derived river discharge data are shown in Figure 4.13. Adapted from Gale and Saunders (2013).

annual precipitation return periods calculated using the 112 years of gridded CRU data (note the difference in the colour scale between Figures 4.7 and 4.8). The return periods in Figure 4.8(a) were calculated using the basic method, but here the maximum return period is 112 years due to the increased length of the CRU data. The return periods in Figures 4.8(b), (c) and (d) were calculated using the distribution method, so are not limited by the length of the dataset.

The pattern of long return periods is consistent across all four maps; the

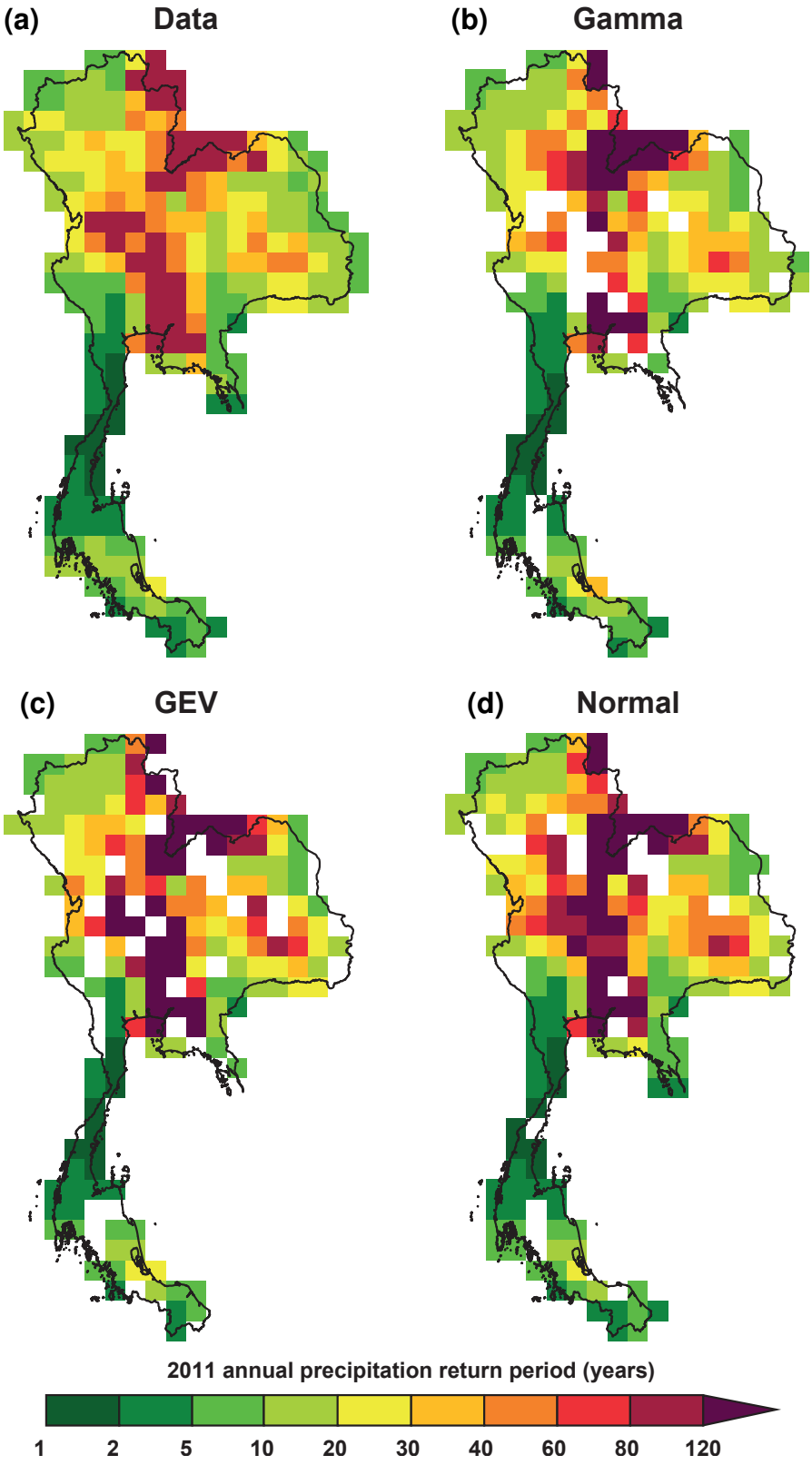

Figure 4.8: Maps showing the 2011 annual precipitation return period (years) using the raw data, gamma, Generalized Extreme Value (GEV) and normal distributions. These return periods are calculated using the Climatic Research Unit (CRU) gridded data, (a) the basic method and (b), (c) and (d) the distribution method (Section 3.2.4). The return period in (a) is limited to 112 years.

longest return periods occurred throughout the CPRB. As with the TMD data, the annual rainfall in the south of Thailand had a return period of approximately 10 to 20 years. Taking an average across the country (Table 4.2), the annual return period ranged from 31.9 years (using the basic method) to 90.1 years (normal distribution). Averaging across the CPRB (using the grid squares in the box shown in Figure 4.2), the annual return period was much longer (Table 4.3): from 47.1 years (basic method) to 164.0 years (normal distribution). The Lilliefors test (Table 3.2) shows the normal distribution was the most suitable for annual rainfall (shown using the shading in Table 4.2), hence the most accurate return period estimate was 164.0 years (as the majority of the flooding occurred in the CPRB). Therefore, the basic method underestimated the average annual return period by almost 117 years.

To extend the analysis of the 2011 rainfall, I also calculated CRU return periods for timescales of less than a year. Figure 4.9 shows the CRU return periods for the 2011 summer monsoon season. Here the longest return periods occurred predominantly in the north, coinciding with the area affected by tropical storms. The area surrounding Bangkok also experienced long return periods during this period, although tropical storms were not the cause here. On average, the summer monsoonal rainfall return periods were shorter than those for annual precipitation (country: 22.4 to 41.6 years; CPRB: 27.2 to 56.1 years). Again, the normal distribution was the most suitable for summer monsoonal rainfall; the return period for the 2011 summer monsoonal rainfall was therefore 56.1 years.

Tables 4.2 and 4.3 also show the average return periods for seasonal and monthly rainfall (for the country and the CPRB respectively). The country-average seasonal rainfall return periods varied between 3.1 years (NDJ; gamma distribution) and 53.0 years (JJA; GEV distribution) when considering the best distributions for each season. Figure 4.10 shows the seasonal return periods calculated using the basic method. The CPRB return periods were long from JFM through to JAS. Here the return periods varied between 1.4 years (NDJ; gamma distribution) and 108.2 years (MAM; GEV distribution).

The average monthly rainfall amounts were less extreme. July had the longest country-average monthly rainfall return period (27.4 years; GEV distribution) and

Table 4.2: The country-average return periods for annual, summer monsoonal, seasonal and monthly precipitation in 2011. The return periods are calculated using the gridded Climatic Research Unit (CRU) data and both the basic and distribution methods described in Chapter 3. The return periods given in the 'Data' column are limited to a maximum of 112 years. The country averages exclude the grid squares that did not pass the Lilliefors test (see Section 3.3.1). The shading marks the most successful distribution(s) in the Lilliefors test for each timescale.

		Country-average return period (years)			
Timescale		Data	Gamma	GEV	Normal
Annual		31.9	45.9	77.2	90.1
Summer monsoonal		22.4	25.9	36.7	41.6
Seasonal	NDJ	2.8	3.1	4.2	11.0
	DJF	4.3	4.5	5.6	6.7
	JFM	16.0	15.8	15.2	11.7
	FMA	19.5	8.2	35.1	85.8
	MAM	22.0	27.5	49.6	126.7
	AMJ	16.3	17.5	20.5	40.6
	MJJ	20.9	25.5	34.2	54.8
	JJA	21.0	40.7	53.0	168.7
	JAS	14.6	18.4	24.5	24.8
	ASO	13.2	13.1	17.0	19.1
	SON	7.7	10.3	9.6	9.4
	OND	7.7	5.8	8.2	15.5
Monthly	Jan	4.1	6.0	6.4	1.3
	Feb	2.9	2.1	3.1	2.5
	Mar	14.0	15.5	14.1	1.9
	Apr	9.4	10.5	9.8	16.6
	May	9.5	8.3	13.3	22.0
	Jun	8.2	9.0	10.2	90.0
	Jul	17.6	24.0	27.4	125.6
	Aug	9.0	9.2	10.2	13.7
	Sep	5.9	5.8	6.0	5.5
	Oct	8.8	8.3	9.0	12.6
	Nov	2.0	2.0	2.0	2.2
	Dec	2.1	3.4	3.9	4.2

Table 4.3: As Table 4.2 but here the return periods are averaged over the Chao Phraya River basin (CPRB) (using the area shown in Figure 4.2). Dashes are given where no grid squares in this area passed the Lilliefors test.

		Country-average return period (years)			
Timescale		Data	Gamma	GEV	Normal
Annual		47.1	72.9	127.6	164.0
Summer monsoonal		27.2	34.4	43.9	56.1
Seasonal	NDJ	1.5	1.4	1.4	2.4
	DJF	5.3	5.3	6.3	-
	JFM	32.6	30.9	33.5	64.4
	FMA	37.4	13.9	73.1	210.4
	MAM	47.7	57.2	108.2	317.2
	AMJ	33.0	34.2	40.5	98.3
	MJJ	37.6	43.4	62.8	131.6
	JJA	27.2	66.4	77.7	372.4
	JAS	13.3	19.1	31.0	25.8
	ASO	6.0	6.8	7.3	8.1
	SON	2.3	2.5	2.5	2.7
	OND	1.9	1.8	1.8	1.9
Monthly	Jan	4.7	1.9	-	-
	Feb	3.9	2.5	4.8	2.5
	Mar	24.8	32.5	24.2	-
	Apr	10.0	9.3	11.2	48.9
	May	18.9	16.8	26.3	40.4
	Jun	14.0	15.2	17.1	217.8
	Jul	14.2	15.0	16.6	24.5
	Aug	10.1	10.8	11.2	15.6
	Sep	2.8	3.0	2.7	2.6
	Oct	2.4	2.8	2.5	2.1
	Nov	1.7	1.4	1.4	-
	Dec	2.1	5.0	-	-

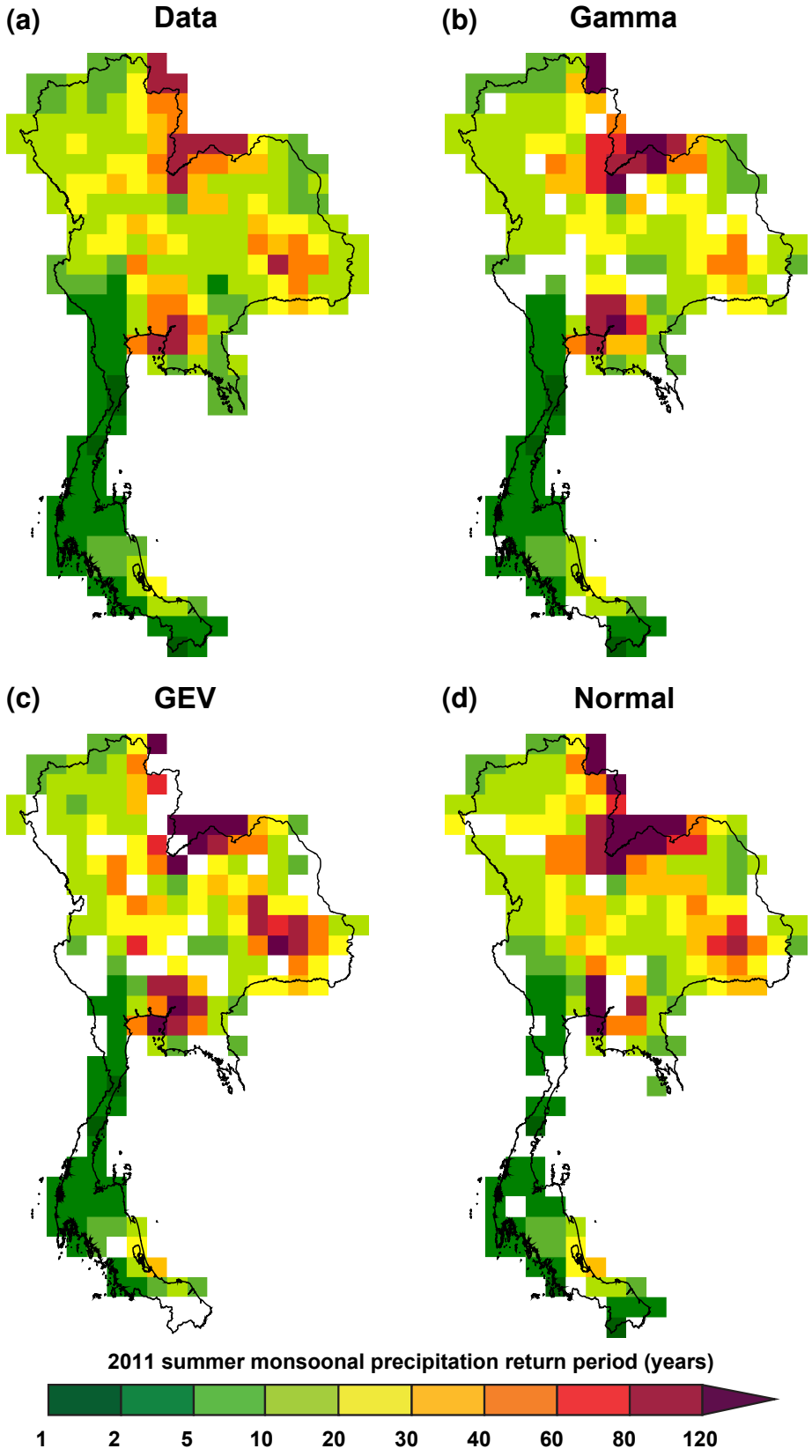

Figure 4.9: As Figure 4.8 but for summer monsoonal (MJJASO) precipitation.

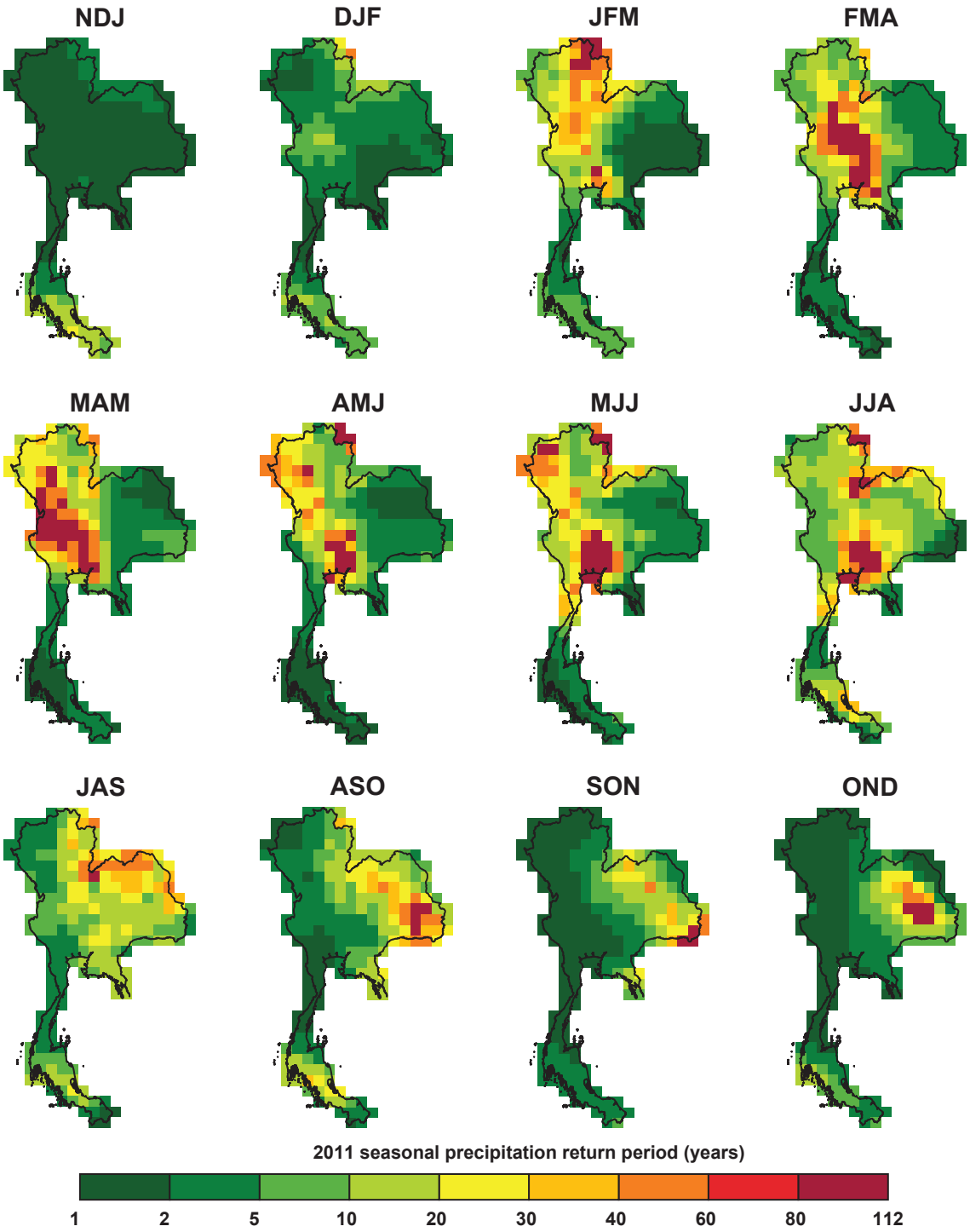

Figure 4.10: Return periods for 2011 Thailand seasonal rainfall displayed spatially across the country. These return periods are calculated using the Climatic Research Unit (CRU) gridded data and the basic method (Section 3.2.3). This method limits the return periods to a maximum of 112 years.

November the shortest (2.0 years; gamma distribution). November also had the shortest return period in the CPRB (1.4 years; gamma distribution), although here the longest monthly rainfall return period occurred in March (32.5 years;

gamma distribution). The longest monthly return periods (March and July) tended to correspond with the months with the highest rainfall anomaly (which can be deduced from Figure 4.1). Spatially, the heavy rainfall began in March with a swathe of rainfall across the CPRB with an average return period of 32.5 years (Figure 4.11 and Table 4.3). This was followed by heavy rainfall to the north-

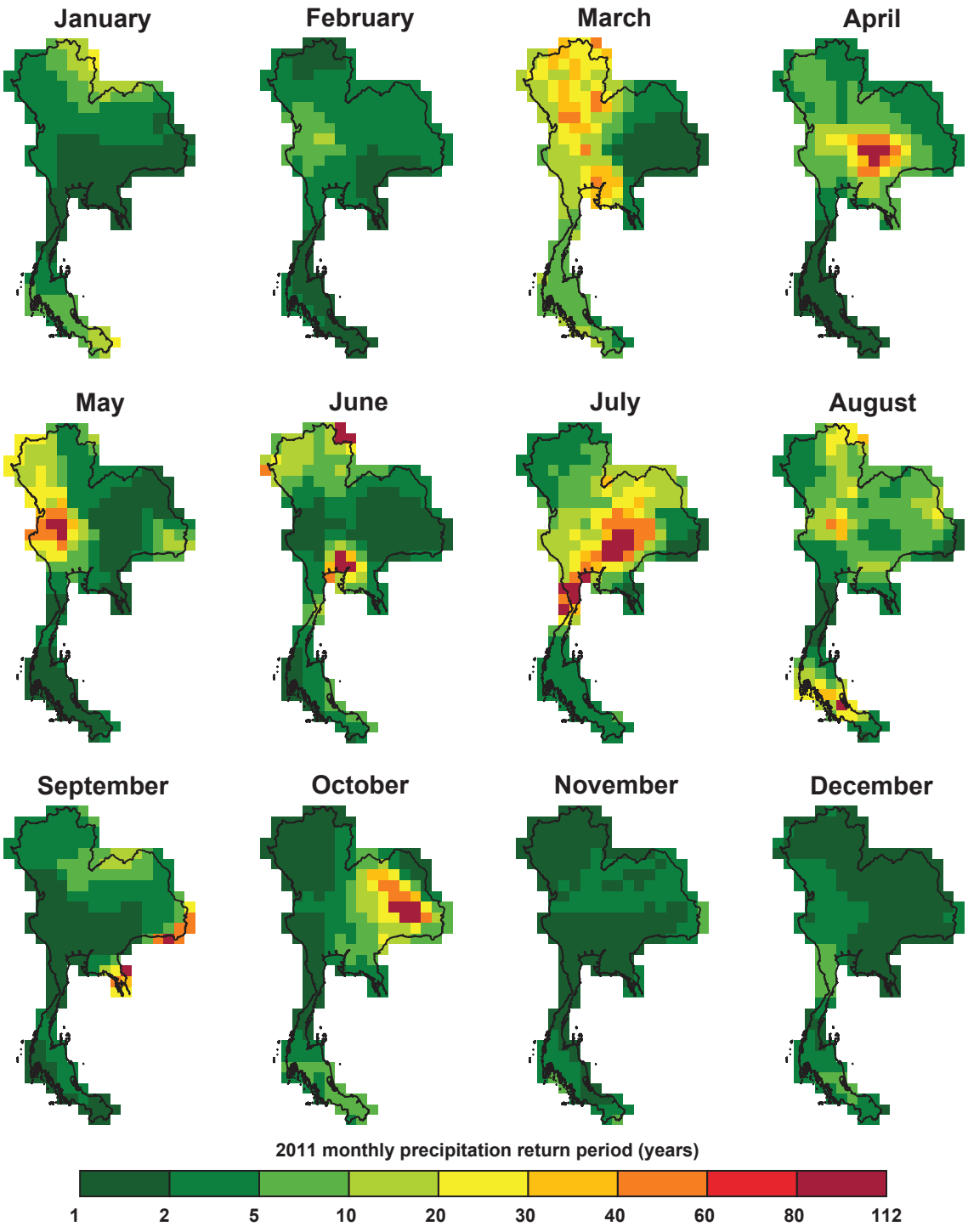

Figure 4.11: As Figure 4.10 but for monthly rainfall.

east of Bangkok in April, and to the north-west of Bangkok in May. June and July brought this heavy rainfall to Bangkok and the surrounding area, with a large area of long return periods (20–112 years) seen over much of the central region in the latter month. The rainfall in August and September was less extreme than previous months, but October brought an area of heavy rainfall to the eastern region.

Figure 4.11 also shows the impact of the 2011 tropical storms. Tropical Storm Haima brought heavy rainfall (return period of 112 years) to the north in June. This area was also hit by Typhoon Nock-ten in early August, although the return period was shorter on this occasion (20–30 years). In September Tropical Storm Haitang hit the south-east of continental Thailand, resulting in monthly rainfall with a return period of over 60 years. Typhoon Nalgae affected the north-east of the country in early November, however the return period in this month was short (2–5 years). As shown in Figure 4.1, the rainfall in November 2011 was below average despite the tropical storm; this suggests the rainfall throughout the remainder of the month was well below normal.

Although the distribution fitted return periods are more accurate than those using the basic method, the CRU dataset is comprised of only 14 underlying stations in 2011. Only 5 of these are in the CPRB. To assess the impact of this small number of stations on the return period estimates, I recomputed the 2011 annual precipitation return periods using the basic method and the gridded CRU data from 1992 to 2011 only (Figure 4.12). Overall, the return period pattern is similar between the two maps. The return periods were longest in the CPRB and the Kra Isthmus. However, the CRU data overestimated the rainfall return periods in the eastern region and the area around Bangkok. The return period in the east ranged from 2 to 8 years using the TMD data, but this increased to at least 10 years using the CRU data. In contrast, the return periods in the southern tip of the Kra Isthmus were underestimated by the CRU data.

A comparison of the three 2011 annual precipitation return period figures in this chapter (Figures 4.7, 4.8 and 4.12) shows the longest return periods occurred in the CPRB, predominantly in the north of the basin. The magnitude of these return periods varied depending on the method used to calculate them and the

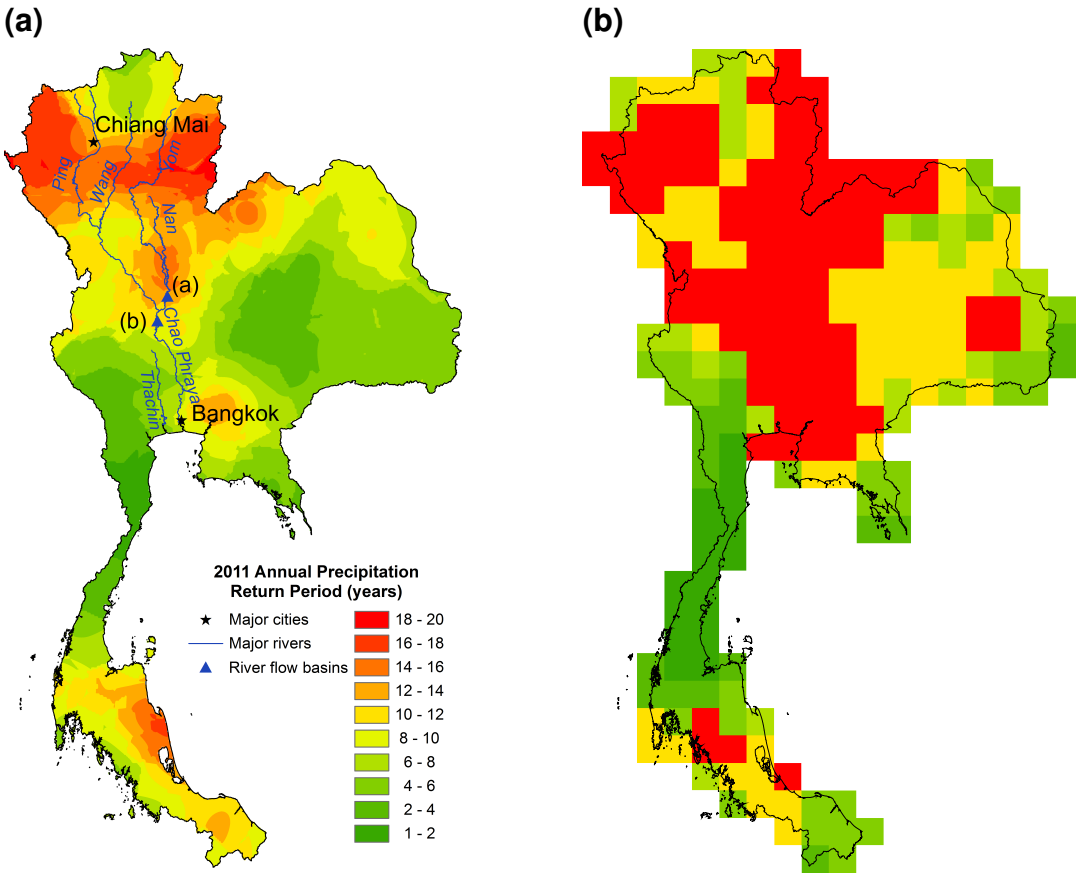

Figure 4.12: Comparison of the annual precipitation return periods for 2011 using the (a) Thai Meteorological Department (TMD) station data and (b) Climatic Research Unit (CRU) gridded data over the period 1992–2011. These return periods are calculated using the basic method (Section 3.2.3).

length of the underlying dataset. The return periods in the CPRB ranged from 8 to 20 years using the basic method and the TMD data. The basin average was 164 years using the distribution method and the longer CRU dataset. When using the basic method and the shortened CRU dataset (1992–2011), the basin return periods were longer than those using the TMD data over the same period; much of the rainfall in the basin had a return period of 20 years. It was only possible to calculate uncertainty for the distribution fitted return periods; even when considering the lower bound of the distribution return periods, the basic method underestimates the 2011 annual precipitation return period in much of the country. This suggests the 20-year length of the TMD dataset is too short to provide reliable return period estimates.

4.5.3 River flow return periods

Figure 4.13 displays time series, from January 2002 to mid-October 2012, of the 4-day mean river discharge for the two Chao Phraya River sites marked on Figure 4.7. The marked return periods were calculated by Brakenridge et al. (2012) using distribution fitting and data from 2002–2011. The seasonal variation in the river discharge is apparent with the main peak occurring in the latter part of each year. The peak discharge in 2011 was the highest since January 2002 at both sites. The northern site had a flood return period of 10 to 20 years and the southern site a flood return period of about 10 years. Due to the lack of data used in the return period calculation (only 10 years; 2002–2011), these estimates may not be very reliable (the confidence intervals are not provided by Brakenridge et al., 2012).

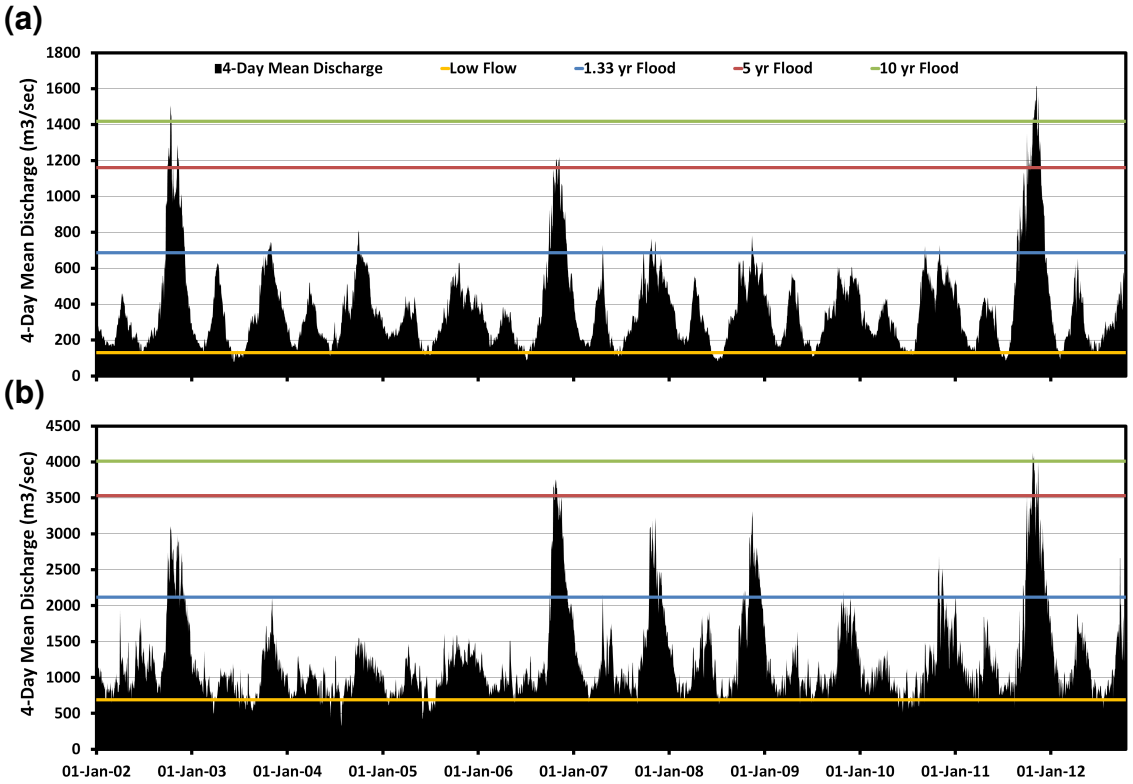

Figure 4.13: Satellite-derived discharge data for two locations on the Chao Phraya River 2002–2012. The 4-day mean river discharge records are displayed for the sites labelled (a) and (b) in Figure 4.7. Yellow, blue, red and green lines represent the low flow, 1.33-year, 5-year and 10-year flood amounts respectively. Location (b) has higher discharges as it is sited further downstream. (Adapted from Brakenridge et al., 2012).

4.5.4 Summary

I used four different methods to estimate the re-occurrence likelihood of a Thai flood of the magnitude of 2011. First, the Dartmouth Flood Observatory Global Active Archive of Large Flood Events ranks the event's magnitude fifth highest for the 1985–2012 period, suggesting a return period of 5 to 6 years. However, recent improvements to the Thai flood defences may bias this estimate short.

Secondly, satellite-derived river flows at two locations on the Chao Phraya River suggest a return period of 10–20 years, with the northerly site having the longer return period. However, this estimate may not be reliable due to the lack of data used in the return period calculation (only 10 years).

Thirdly, pan-Thailand historical weather station rainfall data from the TMD suggest a return period for annual precipitation that varies from 8–20 years in the north and south of the country to 1–8 years in the east and centre of the country. However, since the available precipitation records limit this technique to identifying return periods of up to 20 years, the 8–20 year values may be biased short.

Fourthly, extended gridded rainfall data from the CRU suggest a return period for annual precipitation ranging from 1–20 years in the south up to over 120 years in the CPRB. The basin-wide average return period for annual precipitation was 164.0 years. This method used distribution fitting to calculate return periods, which allows for estimation of return periods beyond the length of the dataset. Further analysis shows the return periods for summer monsoonal, seasonal and monthly rainfall were typically shorter than the estimate for annual rainfall, which suggests the 2011 flood was caused by accumulation of rainfall over much of the year rather than by a shorter period of extreme rainfall.

Bringing together these different return periods, it is difficult to estimate a 'consensus' return period for the 2011 Thai flood. The first three methods are likely to produce a value that is biased short due to the lack of available data. The fourth method may produce unreliable return periods due to a lack of underlying stations in some periods of the CRU dataset. Therefore, I estimate the return period of the 2011 flood to be between 20 and 164 years. Repeating this analysis

using version 7 of the GPCC gridded dataset could reduce the uncertainty of this estimate. GPCC return periods should be more reliable due to the increase in underlying station numbers.

4.6 Discussion

The 2011 Thailand flood ranks as the country's most damaging flood to date. The flooding was caused by an unusually strong summer monsoon (linked to a positive correlation with the SOI) and by four tropical storm remnants that crossed the north and east of the country, which both contributed to an accumulation of heavy rainfall throughout the year (10 out of 12 months were wetter than normal in 2011; Figure 4.1). The 2010–2011 multi-year La Niña also contributed to this excess rainfall (as discussed in Chapter 6). These factors combined to produce the highest annual rainfall in Thailand (in the period 1901–2012). Thailand's central water artery, the Chao Phraya River, could not cope with the volume of water runoff from the country's elevated north, and burst, inundating an area of about 30 000 km^2. Abnormally high sea level in the Gulf of Thailand affected drainage from the lower portion of the basin, thereby exacerbating the flood. As the CPRB is home to 30 % of the Thai population and to most of Thailand's manufacturing industry, economic and insured losses were severe.

A consensus of four different estimates suggests a return period for the 2011 Thailand flood of 20–164 years. However, three of these estimates may be biased short due to the limited 20–30 year extent of the historical data, and the fourth may be unreliable due to the low number of underlying stations used to compile the gridded dataset in some years.

A comparison of 2011 precipitation totals between values in this work and those in Promchote et al. (2016) revealed differences of over 15 % (this increased to almost 50 % in the lower CPRB). These differences were similar to those seen in Figure 2.3. Promchote et al. (2016) used rainfall data from APHRODITE combined with data from the Tropical Rainfall Measuring Mission (TRMM) (NASA Goddard Space Flight Center, 2016). The lower 2011 rainfall totals in the APHRODITE data led Promchote et al. (2016) to reduce the importance of excess precipitation on the Thai flooding in 2011. Further work needs to examine and

clarify why Thai precipitation totals vary with dataset and which totals are the most accurate. However, such a study is beyond the scope of my research.

Despite the uncertainty around the 2011 Thailand flood return period, one can reasonably expect that another Thailand flood as devastating as in 2011 will occur within the next 1–2 centuries unless flood defences and flood management practices are improved.

Chapter 5

Historical climatic flood events and their return periods

5.1 Introduction

As discussed in Chapter 4, the climatic flood in 2011 was one of the worst floods in Thailand's history; the insured loss of US$12 billion ranks as the highest ever worldwide from a freshwater flood disaster (Swiss Re, 2012). However, flooding is a frequent occurrence in Thailand due to it's tropical location and topography (e.g. Table 4.1). Tropical storms and the Southeast Asian summer monsoon regularly cause persistent climatic rainfall in Thailand, which often results in climatic flooding (flooding caused by climatic rainfall that persists for at least one month). Flooding is particularly common in urban areas where drainage is poor.

Despite this, previous studies have failed to closely examine the causes of historical Thai flood events, particularly the associated climatic rainfall and rainfall return periods. Therefore, the purposes of this chapter are to:

- apply the climatic rainfall return period analysis (described in Chapter 3 and used in Chapter 4) to determine the rainfall return periods for five other notable historical climatic flood events in Thailand;
- compare the climatic rainfall return periods for these other notable climatic floods with those for the 2011 Thailand flood to quantify their rarity (or not) in comparison to 2011;
- analyse the excess rainfall data for these five other historical floods to provide new insights as to the cause(s) of these additional climatic floods.

The selected historical climatic flood events occurred in 1942, 1983, 1995, 2002 and 2006 (Table 5.1). These large flood events all involved flooding in

Table 5.1: Table summarising the five notable historical climatic flood events in Thailand selected for analysis in this chapter.

Date	Flood Description	References
Sep–Nov 1942	Area affected = Bangkok Flood height = 5 m	DHI (2011); Meehan (2012)
Jul–Nov 1983	Area affected = Bangkok & CPRB Flood height = 2 m Damages = US$21 million	Engkagul (1993); Hungspreug et al. (2000); Sroikeeree and Bannatham (2006)
Aug–Nov 1995	Area affected = 86 % of Thailand Damages = US$2 billion	Hungspreug et al. (2000); Prajamwong and Suppataratarn (2009); DHI (2011); Brakenridge (2012)
Aug–Nov 2002	Area affected = 372 000 km^2 of Thailand and Cambodia Damages = US$32 million	Prajamwong and Suppataratarn (2009); Brakenridge (2012)
Aug–Dec 2006	Area affected = 40 provinces, primarily in the CPRB Damages = US$8 million 195 deaths and 2 million people displaced	UN Office for the Coordination of Humanitarian Affairs (2006); Suvanpimol (2007); Prajamwong and Suppataratarn (2009); DHI (2011); Brakenridge (2012)

the CPRB (Figure 5.1; Hungspreug et al., 2000; Prajamwong and Suppataratarn, 2009; Brakenridge, 2012; Meehan, 2012). The climatic floods in 1942, 1983 and 1995 also caused considerable flooding in Bangkok (Sroikeeree and Bannatham, 2006). Prior to the 2011 flood, the 1942 flood was considered to be Thailand's worst flood in modern times (Ziegler et al., 2012).

This chapter presents case studies for the five selected historical climatic floods in Thailand. For each event, I describe the underlying causes and impacts, analyse the climatic rainfall anomalies and calculate the climatic rainfall return period(s).

5.2 Bangkok, 1942

The 'Great Flood' of 1942 caused widespread flooding in Bangkok for three months (SON; Figure 5.2). The event is considered to be one of the most severe floods in Thailand; it was not surpassed until the severe flood of 1995 (Section 5.4). Exceptionally heavy rainfall in the CPRB upstream led to a peak flow of 6500 $m^3 s^{-1}$ at Nakhon Sawan (Meehan, 2012). The lack of flood protection in the city resulted in widespread flooding up to 5 m deep in places.

In 1942, precipitation in the CPRB was above normal for much of the year, particularly during April–September (AMJJAS) (+220 mm (+20 %); Figure 5.3(a)). The rainfall peaked in August; precipitation was 76 mm (31 %) higher than normal in this month. Spatially, AMJJAS rainfall was above normal across much of northern and central continental Thailand (Figure 5.3(b)). The far north-west and north-central areas of continental Thailand were particularly wet. The anomaly pattern was similar during August, although the wettest region shifted slightly; the peak anomalies were highest in the north-west and west of the CPRB in this period (Figure 5.3(c)). Rainfall in Bangkok itself was slightly below normal in both periods.

Averaging across the CPRB, the return period for AMJJAS rainfall ranged from 39 years (basic method) to 507 years (normal distribution; Figures 5.4 (a–d)). The basic method underestimated the return period in the wettest areas of the country. In the CPRB, the gamma distribution performed best in the Lilliefors test for this time period (this distribution had the smallest number of discarded grid squares),

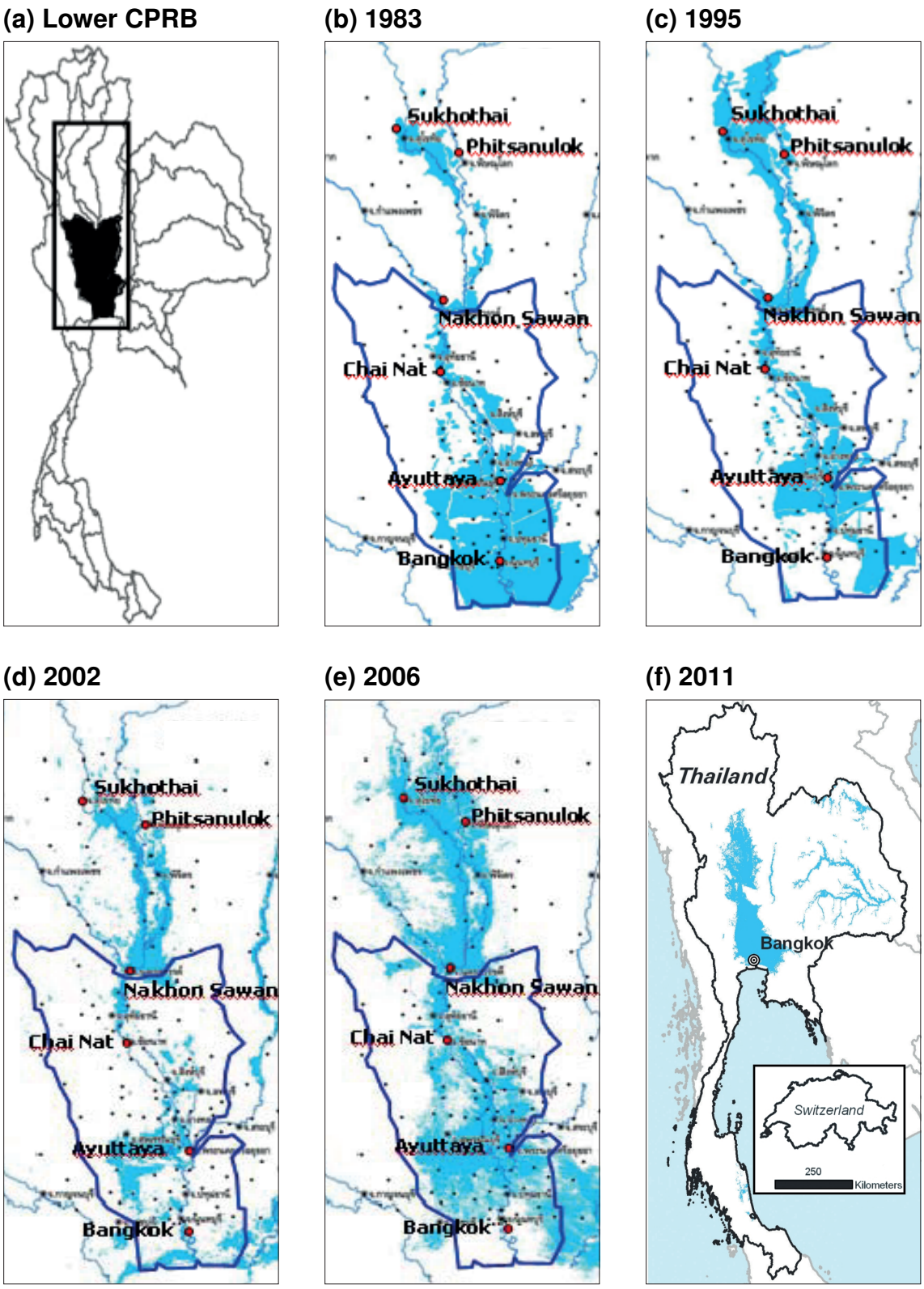

Figure 5.1: Maps showing the extent of the flooding in the lower Chao Phraya River basin (CPRB) (the shaded area in (a)) in (b) 1983, (c) 1995, (d) 2002 and (e) 2006. (f) The extent of the 2011 flood shown for comparison. Images courtesy of (a–e) Prajamwong and Suppataratarn (2009) and (f) Swiss Re (2012).

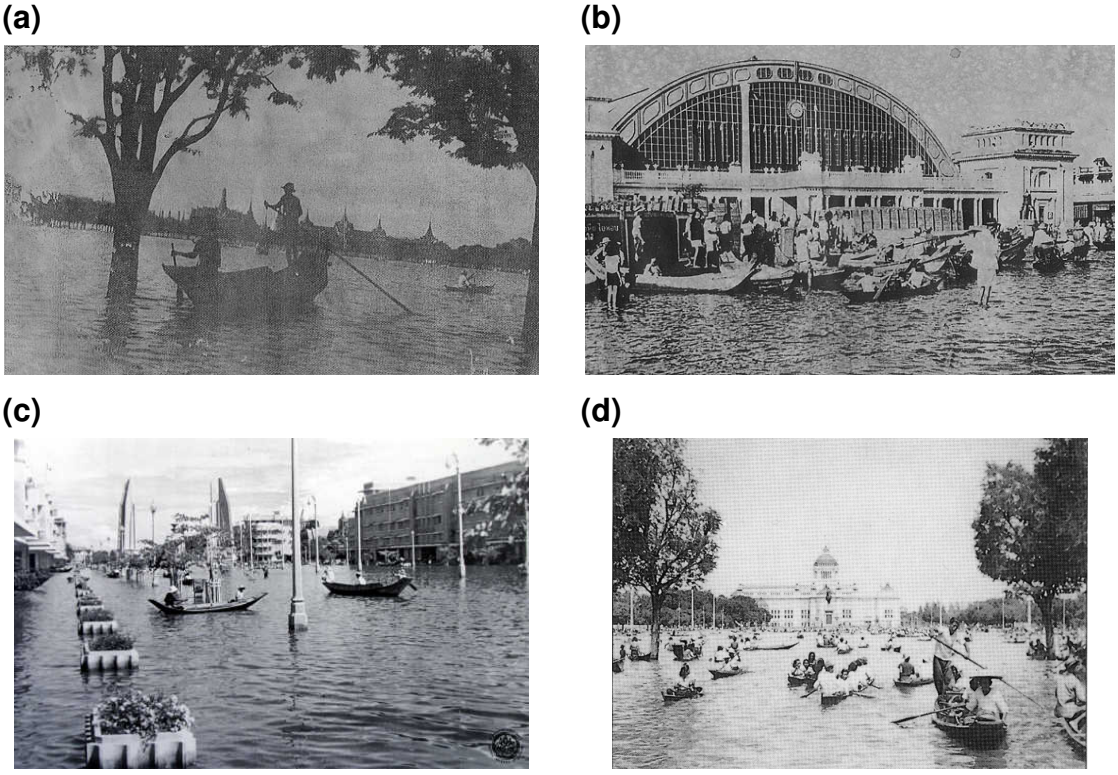

Figure 5.2: Photographs showing the 'Great Flood' of 1942 in Bangkok (2bangkok.com, 2016; Rural Surin, 2016).

so the best CPRB-average return period estimate for AMJJAS rainfall in 1942 was 117 years.

The range of basin-average return periods for August rainfall was larger than the AMJJAS range: from 30 years (basic method) to 1013 years (normal distribution; Figures 5.4 (e–h)). Although the GEV distribution provided the best fit for August precipitation country-wide (see Chapter 3 for more details), the gamma distribution performed best for August rainfall in the CPRB. Therefore, the best CPRB-average return period estimate for August rainfall in 1942 was 79 years.

These two climatic rainfall return period estimates (AMJJAS: 117 years; August: 79 years) were similar to the estimated flood return period of 100 years, which was calculated using annual maximum water levels at Ayutthaya (located on the Chao Phraya River north of Bangkok (Figure 5.1); DHI, 2011). Although this flood return period was calculated using a long data record, no information was provided regarding the method of calculation. Therefore, a like-for-like comparison of the two return period estimates is not appropriate.

To quantify the rarity of this event compared to 2011, I calculated the CPRB-

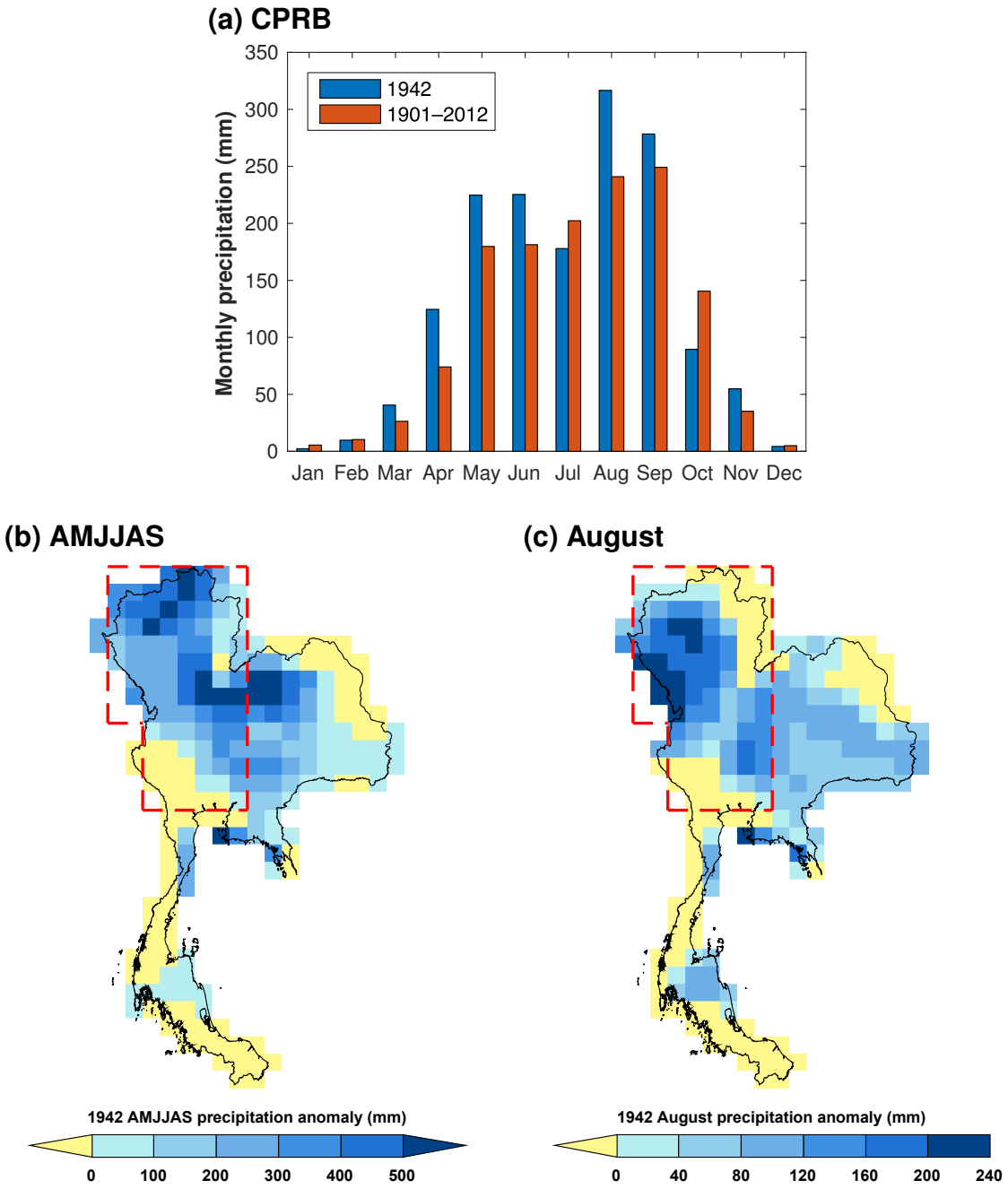

Figure 5.3: (a) The monthly precipitation for 1942 (blue) in the Chao Phraya River basin (CPRB) (averaged over the area shown in (b) and (c)). The 1901–2012 climatology for this area is shown for comparison (red). The data shown are from the Climatic Research Unit (CRU) TS3.21 gridded dataset (Section 2.2.2). The (b) April–September (AMJJAS) and (c) August 1942 precipitation anomaly (1901–2012 climatology; using data from the CRU; note the differing colour scales). The red dotted line represents the CPRB.

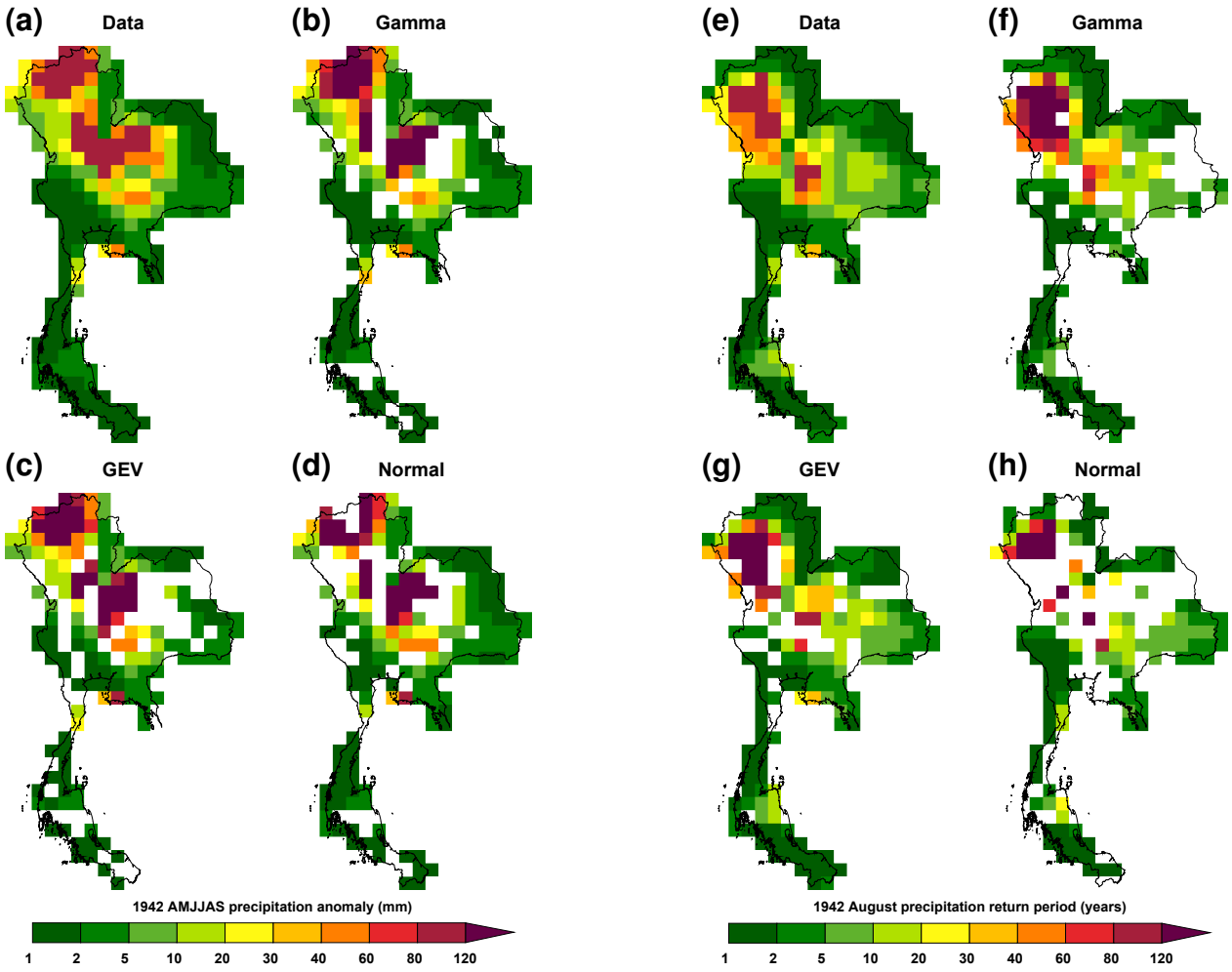

Figure 5.4: Maps showing the (a–d) April–September (AMJJAS) and (e–h) August 1942 precipitation return periods (years) using the raw data, gamma, Generalized Extreme Value (GEV) and normal distributions. The return periods in (a) and (e) are limited to 112 years.

average rainfall return period for AMJJAS and August 2011 (70 years and 11 years respectively). Although the 1942 and 2011 floods were both primarily caused by prolonged excess rainfall in the CPRB throughout much of the year, the rainfall return periods for AMJJAS and August were longer in 1942.

5.3 Bangkok, 1983

In 1983, unusually heavy rainfall in Bangkok and the lower CPRB led to 3–5 months of flooding in Bangkok (Sroikeeree and Bannatham, 2006). This rainfall was partly caused by Tropical Storm Kim, which passed over southern continental Thailand on 18 October (JTWC, 2016). The water level peaked on 24 November at a depth of almost 2 m (Engkagul, 1993). Damages in the CPRB were estimated to be US$21 million (Hungspreug et al., 2000).

Rainfall in Bangkok was above normal in five of the last six months of 1983. July–November (JASON) rainfall was 739 mm (67 %) above normal in Bangkok. Rainfall was particularly high during August: +428 mm (+162 %; Figure 5.5(a)). A similar pattern occurred in the lower CPRB (5.5(b)), although here rainfall was above normal throughout the last six months of the year. JASON and August rainfall in the lower CPRB was, on average, 529 mm (49 %) and 211 mm (74 %) above normal respectively. Spatially, the highest rainfall anomalies occurred in the south and south-west of the lower CPRB (Figures 5.5(c) and (d)).

Following the pattern of rainfall anomalies in JASON and August 1983, the return periods were longest in the lower CPRB (Figure 5.6). The lower CPRB-average JASON rainfall return period ranged from 45 years (basic method) to 1174 years (normal distribution; Figures 5.6(a–d)). The normal distribution performed best for this time period and region, so the best lower CPRB-average JASON rainfall return period estimate was 1174 years. The four Bangkok-average return periods were all longer than the lower CPRB averages (98 years (basic method) to 8314 years (normal distribution); Figures 5.6(e–h)), but the best estimate for this region was shorter (939 years; gamma distribution) than the best estimate for the lower CPRB.

The August return periods were shorter than those for JASON in both Bangkok and the lower CPRB, despite the higher percentage rainfall anomalies. The best

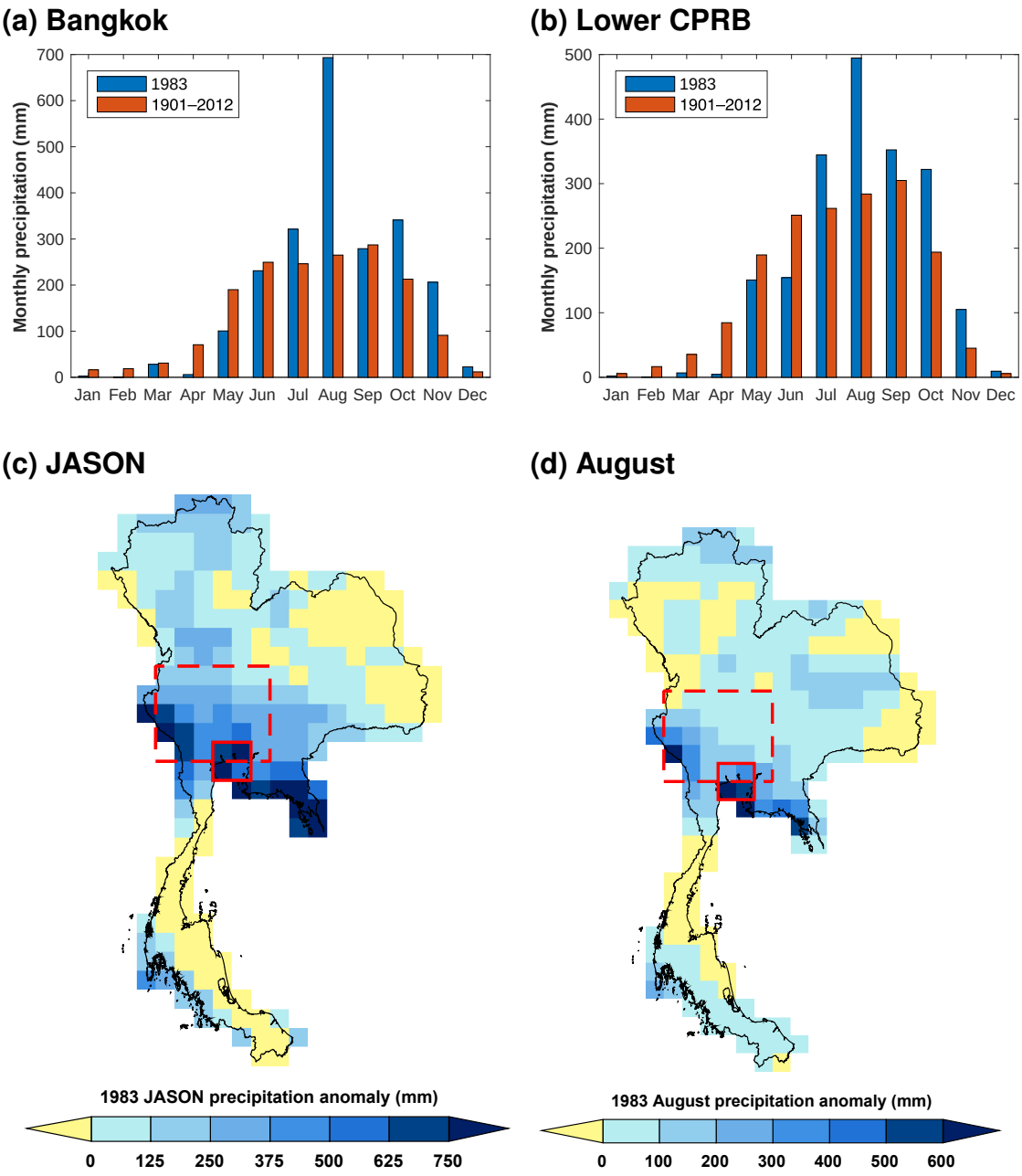

Figure 5.5: As Figure 5.3(a) but for 1983 precipitation in (a) Bangkok and (b) the lower Chao Phraya River basin (CPRB). As Figures 5.3(b) and 5.3(c) but for (c) July–November (JASON) and (d) August 1983. The red dashed and solid lines represent the lower CPRB and Bangkok respectively.

estimates were 331 years (GEV distribution) and 77–121 years (GEV and gamma distributions) for Bangkok and the lower CPRB respectively.

As the location of the heaviest rainfall in 1983 was further south than the rainfall in 2011, the rainfall return periods for Bangkok (JASON: 939 years; August: 331 years) and the lower CPRB (JASON: 1174 years; August: 77–

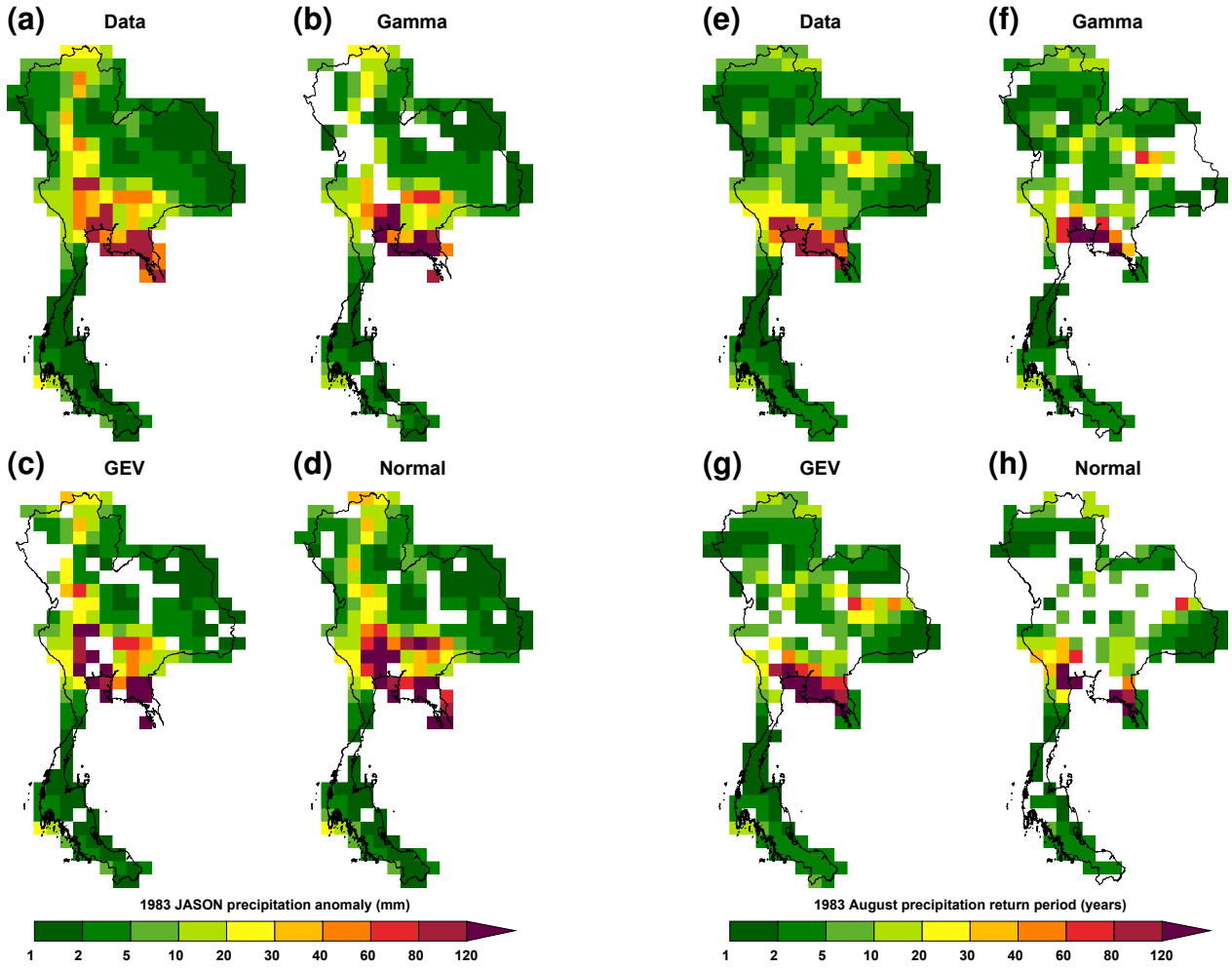

Figure 5.6: As Figure 5.4 but for (a–d) July–November (JASON) and (e–h) August 1983.

121 years) were much longer than the equivalent for 2011 (JASON: 5 years (Bangkok), 7 years (lower CPRB); August: 7 years (Bangkok), 6 years (lower CPRB)).

5.4 Chao Phraya River basin, 1995

According to the Dartmouth Flood Observatory's Global Active Archive of Large Flood Events (Brakenridge, 2012), the Thai flood of 1995 was the worst to hit the country during the 1985–2012 period (when ranked by magnitude; Table 4.1). Between 1 August and 9 November, 444 000 km^2 of the country experienced flooding at some stage (approximately 86 % of the total land area of Thailand).

The flooding was caused by a series of 6 tropical storms crossing continental Thailand (Figure 5.7). The first storm hit on 29 August (Typhoon Lois), with successive storms (TD 16W, TD 23W and Typhoon Yvette) passing regularly until the final storm passed on 2 November (Typhoon Zack). Precipitation was anomalously high in the CPRB throughout JAS 1995 (CPRB average of +197 mm (+28 %); Figures 5.8(a) and (b)). The rainfall peaked in August (CPRB average of +138 mm (+57 %); Figure 5.8(c)).

The CPRB experienced the worst of the flooding during 1995. Typhoon Lois caused heavy rainfall in the north of Thailand, resulting in spillage of the Sirikit

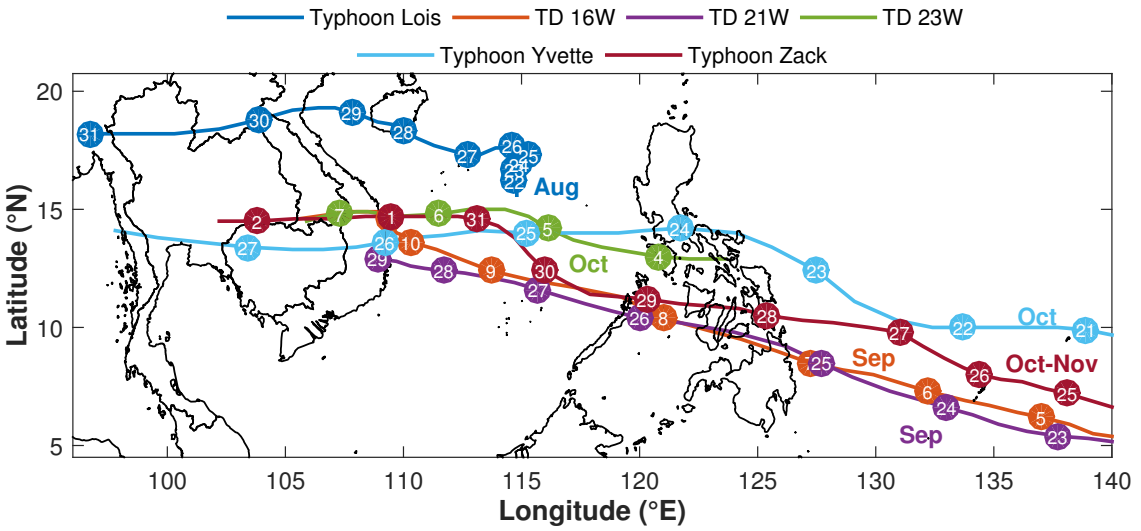

Figure 5.7: The tracks of the four tropical storms that affected Thailand in 1995 (based on best-track data from the Joint Typhoon Warning Center (JTWC) (Chu et al., 2002)). The numbered markers represent the date at 00 UTC of the month(s) in which the storm was active.

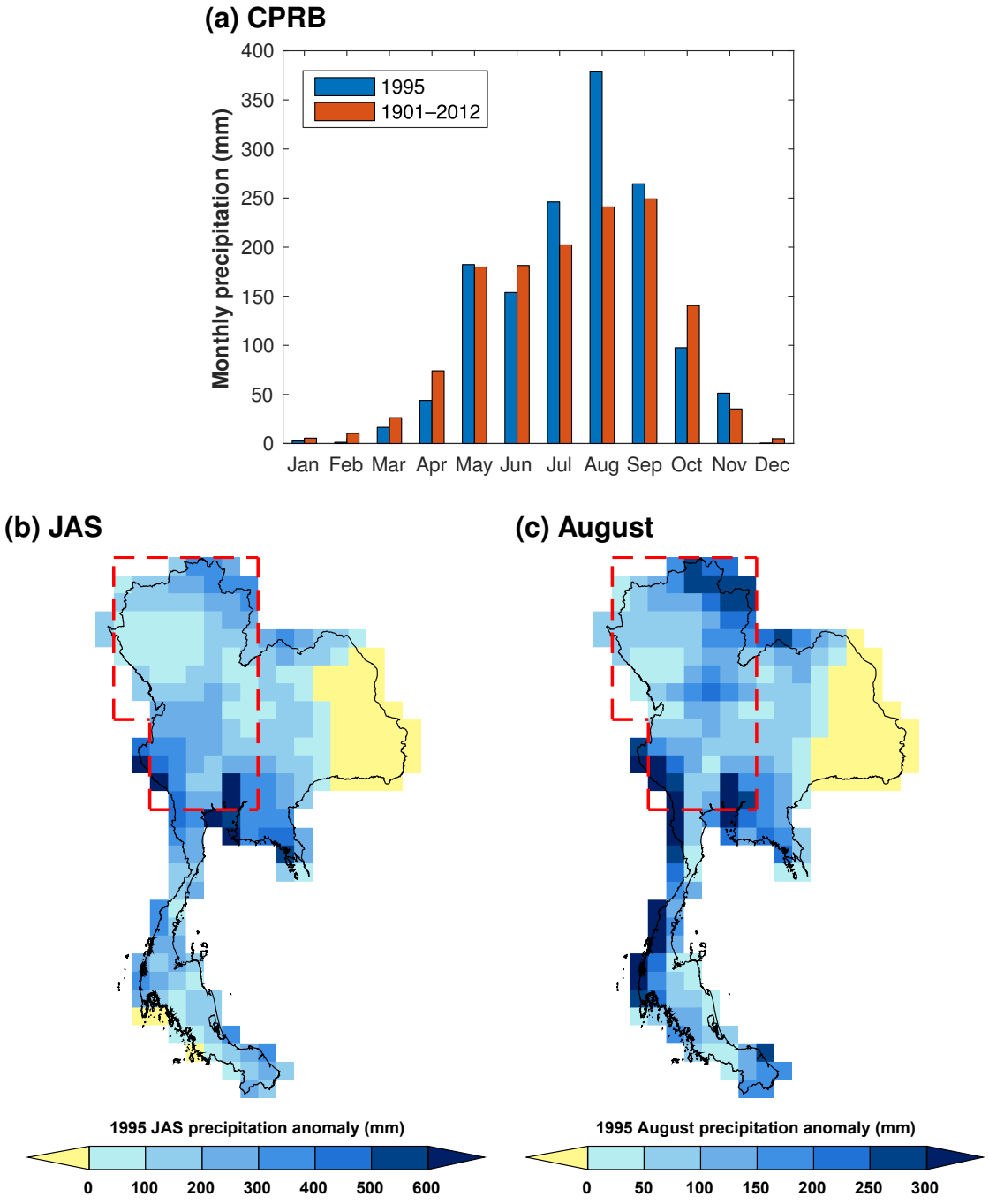

Figure 5.8: (a) As Figure 5.3(a) but for 1995 precipitation in the Chao Phraya River basin (CPRB) (averaged over the area shown in (b) and (c)). As Figure 5.3(b) but for (b) JAS and (c) August 1995. The red dotted line represents the CPRB.

Dam and high discharges in the Chao Phraya River system (Hungspreug et al., 2000). This inundated many provinces in the CPRB, both in the north and further downstream into Bangkok. Flooding in the capital and its vicinity lasted for more than two months. Overall damages were extensive: approximately US$2 billion

in total (Hungspreug et al., 2000), with the worst damages occurring in upstream areas.

The CPRB-average JAS precipitation return period ranged from 23 years (basic method) to 385 years (normal distribution; Figures 5.9 (a–d)). The normal distribution provided the best fit for the CPRB in this season, so the best return period estimate for 1995 JAS precipitation in the CPRB was 385 years. Although the August anomaly was higher, the best estimate return period for the CPRB was shorter: 64 years (gamma distribution; Figures 5.9 (e–h)).

These rainfall return periods were both longer than the flood return period estimates of 30 years and 50 years from Prajamwong and Suppataratarn (2009) and DHI (2011) respectively. They were also longer than the 2011 CPRB-average JAS and August rainfall return periods (26 years (normal distribution) and 11 years (gamma distribution) respectively).

The causes of the 1995 flooding were not solely natural. Poor land use in flood risk areas, development of areas upstream, and poor operation and coordination of flow control facilities all exacerbated the flood risk. Due to this, measures were introduced after the 1995 flood to reduce the risk of flooding in the CPRB. These included the use of better drainage systems, improved reservoir operations and heightening of existing insufficient flood barriers (Hungspreug et al., 2000).

5.5 Mekong and Chao Phraya River basins, 2002

Ranked second in terms of magnitude (1985–2012; Brakenridge, 2012), the flood of 2002 affected approximately 372 000 km^2 of Thailand and Cambodia between 18 August and 26 November. The flooding primarily occurred in the MRB, which covers much of eastern Thailand, although some provinces in the CPRB were also affected. The flood caused 65 deaths in Thailand, displacement of 40 000 people and US$32 million of damage (Brakenridge, 2012).

The flood was caused by a combination of heavy rainfall in upstream areas of the MRB and CPRB, which resulted in high discharge downstream, and locally heavy rainfall in the two basins (Prajamwong and Suppataratarn, 2009). In the MRB, rainfall was higher than normal in 7 of the last 8 months of the year (only July was drier than normal; Figure 5.10(a)). Rainfall was particularly

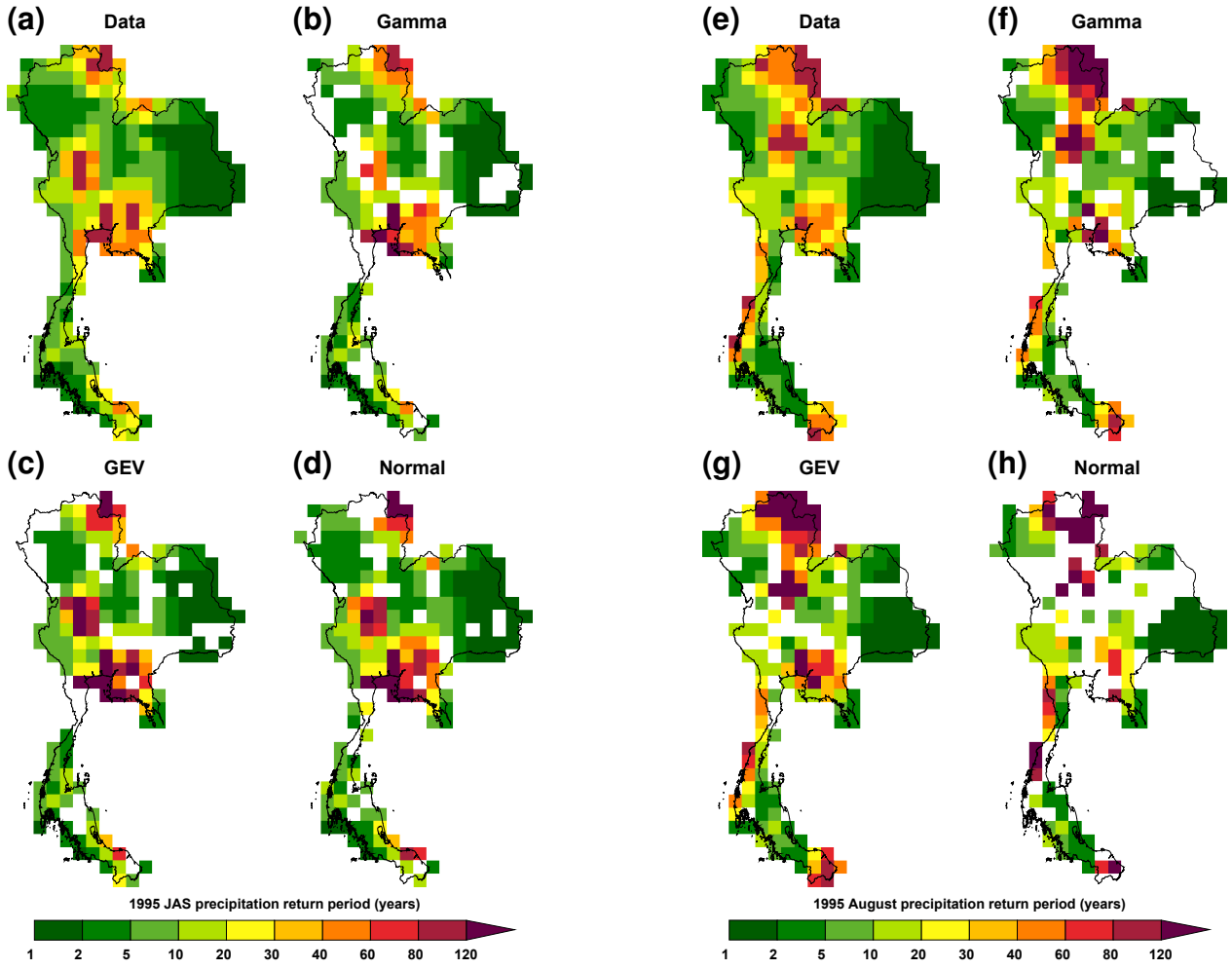

Figure 5.9: As Figure 5.4 but for (a–d) July–September (JAS) and (e–h) August 1995.

high in ASO: +254 mm (+39 %). The CPRB rainfall pattern was similar (Figure 5.10(b)), although the CPRB-average ASO anomaly was smaller: +146 mm (+23 %). Spatially, ASO rainfall was high across much of the country, but the peak anomalies occurred in the north-east of the MRB (Figure 5.10(c)).

Figure 5.11 shows the rainfall return periods for ASO 2002. The region of long return periods corresponded with the wettest area in Figure 5.10(c). Averaging across the MRB, the ASO rainfall return period ranged from 42 years (gamma distribution) to 111 years (normal distribution). The best estimate for the MRB-average ASO return period was 89 years (GEV distribution). The CPRB average ASO return periods were shorter: ranging from 12 years (gamma distribution) to 18 years (normal distribution). Here the normal distribution performed best, so

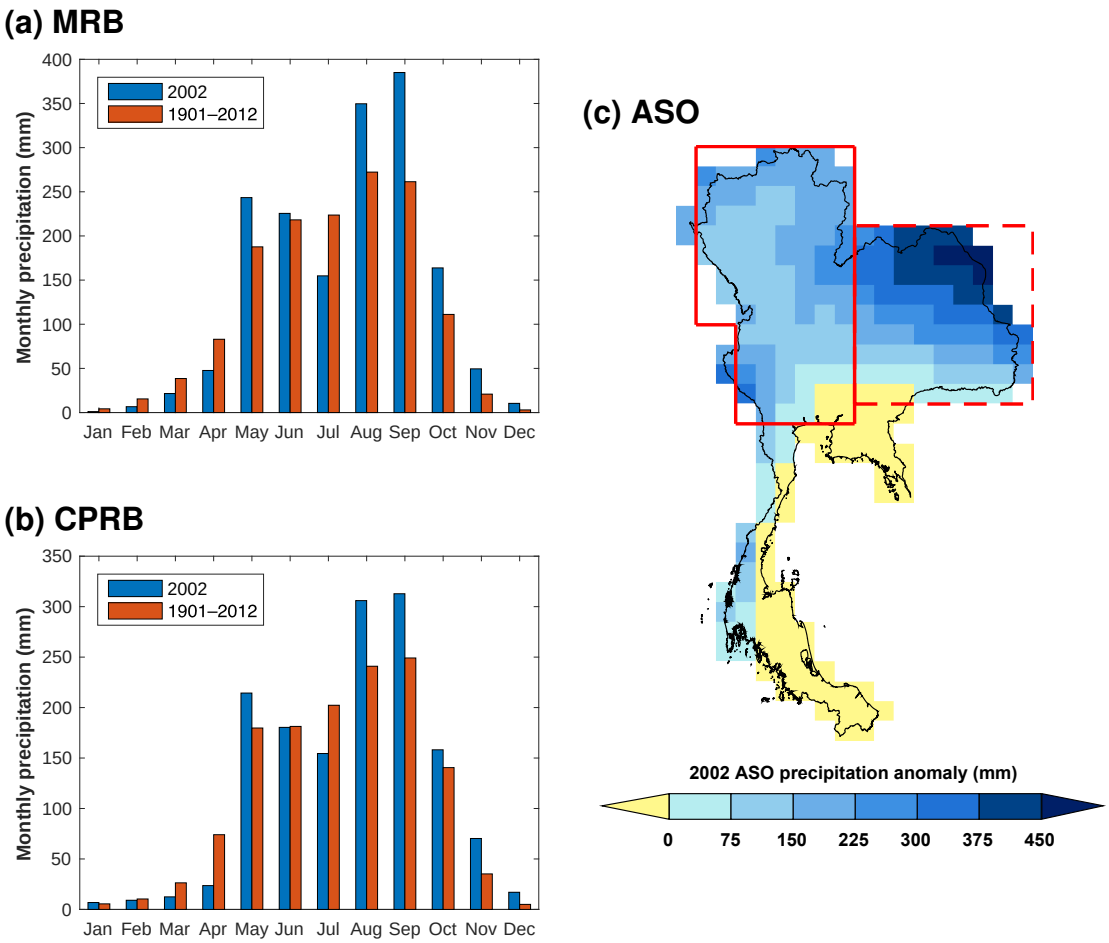

Figure 5.10: As Figure 5.3(a) but for 2002 precipitation in (a) the Mekong River basin (MRB) and (b) Chao Phraya River basin (CPRB). (c) As Figure 5.3(b) but for August–October (ASO) 2002. The red dashed and solid lines represent the MRB and CPRB respectively.

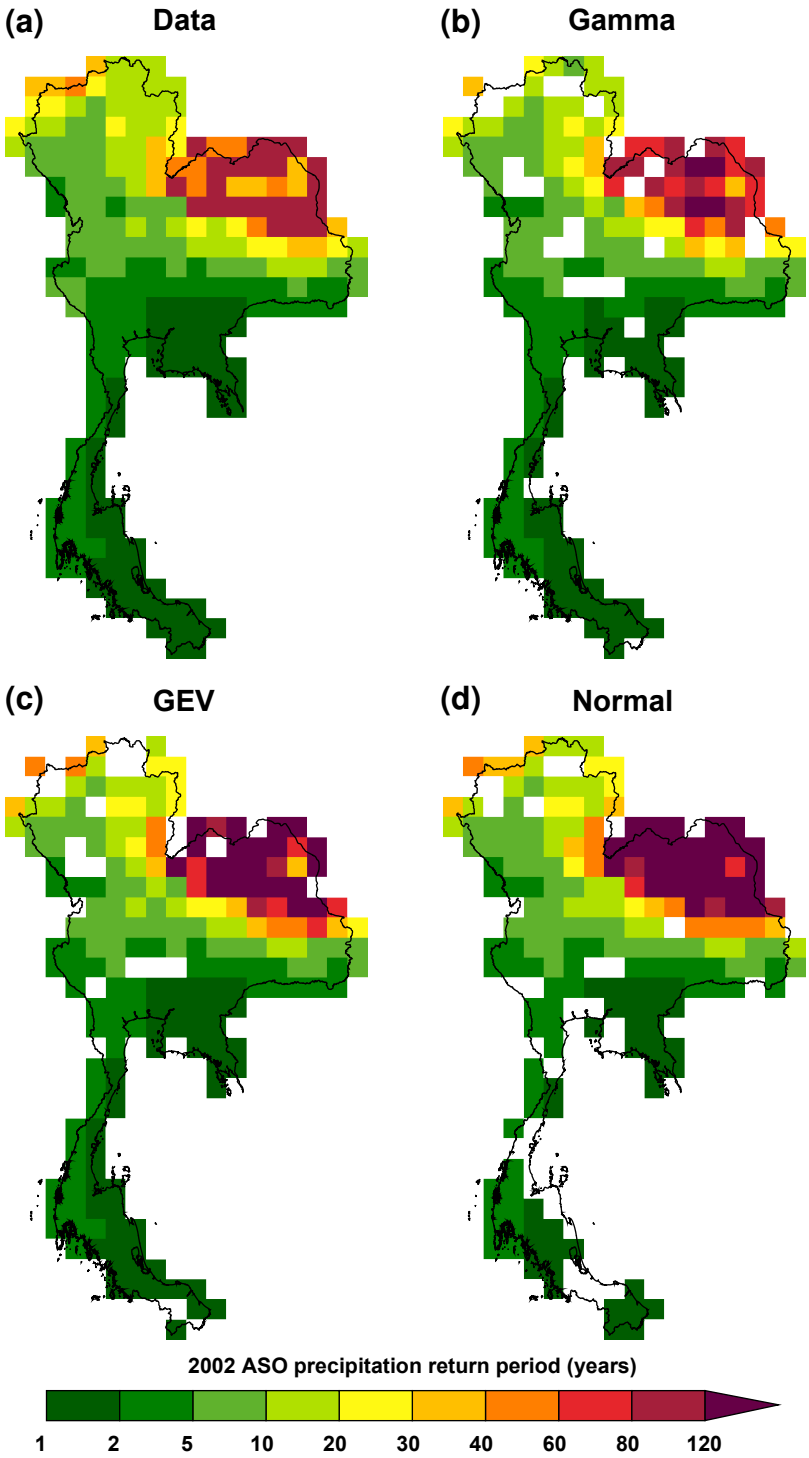

Figure 5.11: As Figure 5.4 but for August–October (ASO) 2002.

the CPRB-average ASO rainfall return period was 18 years. This was slightly longer than the flood return period estimate of 15 years from Prajamwong and Suppataratarn (2009). The 2002 ASO rainfall return periods averaged over the MRB and CPRB were both longer than the corresponding return periods for 2011 (35 years and 8 years for the MRB and CPRB respectively).

5.6 Chao Phraya River basin, 2006

Prolonged flooding from 20 August to 13 December 2006 affected more than 40 provinces in Thailand (Brakenridge, 2012), primarily throughout the CPRB. The event caused 195 deaths and displaced 2 million people. Damages were estimated to be over US$8 million.

This flood was primarily caused by above average rainfall in the CPRB throughout much of the year (Figure 5.12(a)) resulting in increased runoff in the basin (Suvanpimol, 2007). The event began in late May with flash flooding in northern Thailand following days of heavy rain locally (UN Office for the Coordination of Humanitarian Affairs, 2006). Rainfall in the basin was particularly high during April–August (AMJJA): +199 mm (+23 %). Spatially, rainfall in AMJJA was wetter than normal across a large proportion of the country (Figure 5.12(b)); the highest rainfall occurred in the south-west of the CPRB. Heavy rain in October from Typhoon Xangsan (Figure 5.13) added to the existing flooding, as shown in the satellite images of the lower CPRB (Figure 5.14).

Although this flood ranked third in magnitude in the Global Active Archive of Large Flood Events in Thailand (Brakenridge, 2012), the associated rainfall return period was not as long as other events (Figure 5.15). Averaging across the

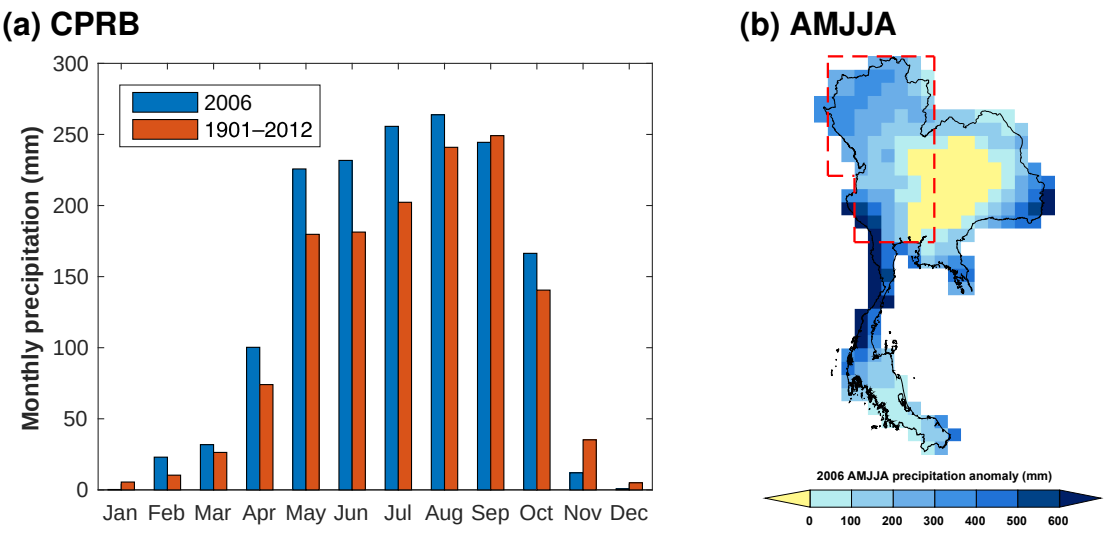

Figure 5.12: (a) As Figure 5.3(a) but for 2006 precipitation in the Chao Phraya River basin (CPRB) (averaged over the area shown in (b)). (b) As Figure 5.3(b) but for April–August (AMJJA) 2006. The red dotted line represents the CPRB.

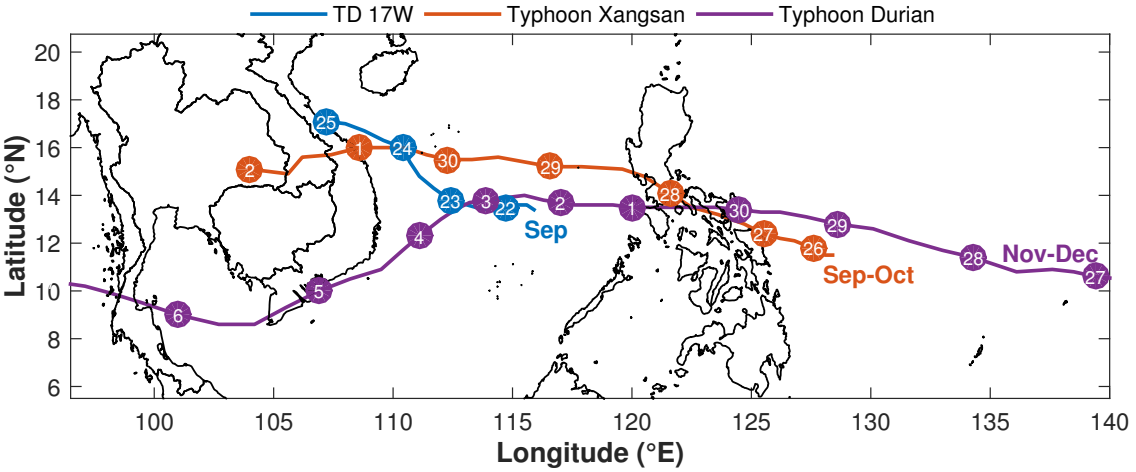

Figure 5.13: The tracks of the four tropical storms that affected Thailand in 2006 (based on best-track data from the Joint Typhoon Warning Center (JTWC) (Chu et al., 2002)). The numbered markers represent the date at 00 UTC of the month(s) in which the storm was active.

CPRB, the AMJJA rainfall return period ranged from 13 years (basic method) to 18 years (gamma distribution). The gamma distribution provided the best fit for this season and region. This was similar to the flood return period estimates of 10 years and 20 years from DHI (2011) and Prajamwong and Suppataratarn (2009) respectively. Unlike the other flood events in this chapter, the corresponding rainfall return period for 2011 was longer than the value for this flood; the 2011 CPRB-average AMJJA rainfall return period was 162 years.

5.7 Discussion

In this chapter I presented five case studies of climatic Thai flooding events over the period 1942–2006. Table 5.2 summarises these flood events; included are the date, causes, location and period of the main rainfall excess, and the rainfall return period(s). I also include the corresponding rainfall return period(s) from 2011, and the flood return periods obtained from other sources.

Like the 2011 flood, the five historical flood events were primarily caused by unusually heavy rainfall over multiple months (from 3 to 6 months). Additionally, tropical storms contributed to the excess rainfall in three of the events (1983, 1995 and 2006). Poor flood protection was an important contributing factor in exacerbating the 1942 and 1995 flood events. Indeed, the 1995 flood prompted the introduction of measures (e.g. better drainage systems, improved reservoir

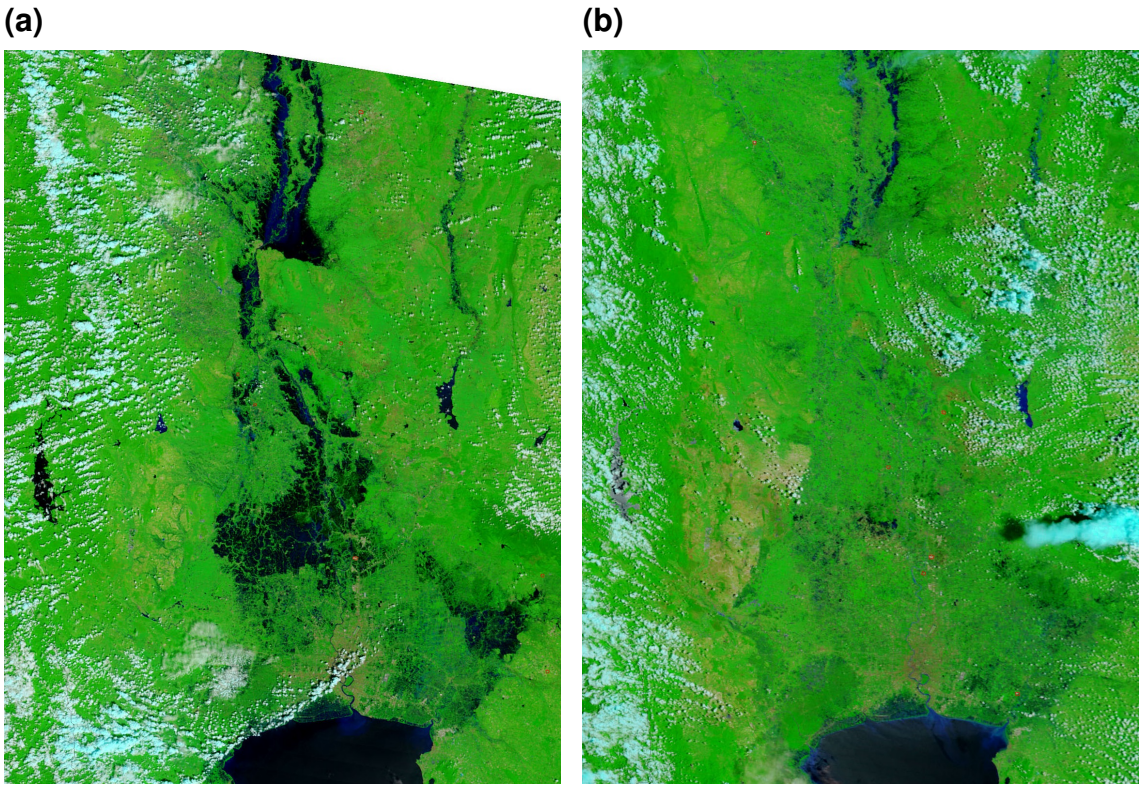

Figure 5.14: Satellite images of the 2006 flooding taken by the Moderate Resolution Imaging Spectroradiometer (MODIS) on NASA's Terra satellite (NASA Earth Observatory, 2006). (a) shows the exceptional flooding in the Chao Phraya River basin (CPRB) on 26 October 2006. (b) shows the same area on 5 September 2006, prior to the flood. These images focus on the southern portion of the CPRB; the Gulf of Thailand is visible in the south (dark blue) and the urban areas of Bangkok are visible to the north and northwest of the Gulf of Thailand (brown). The Chao Phraya River flows from north to south down the centre of each image. The remainder of the dark blue areas show the extent of the CPRB flooding. The white areas in these images are portions of cloud above the country.

operations) to reduce the risk of flooding in the CPRB.

The most recent of the five events, the 2006 CPRB flood, had the shortest rainfall return period of those examined (18 years, AMJJA). The most severe event in terms of rainfall return period was the 1983 flood, which primarily affected Bangkok and the lower CPRB. This event had a return period ranging from 77 years (August rainfall in the lower CPRB) to 1174 years (JASON rainfall in the lower CPRB). Although the rainfall return periods varied vastly across the different events, they were all associated with extreme climatic rainfall on monthly timescales or longer.

For all the events bar the 2006 flood, the rainfall return periods were longer than the same rainfall return period in 2011. This is due to the heavy rainfall in

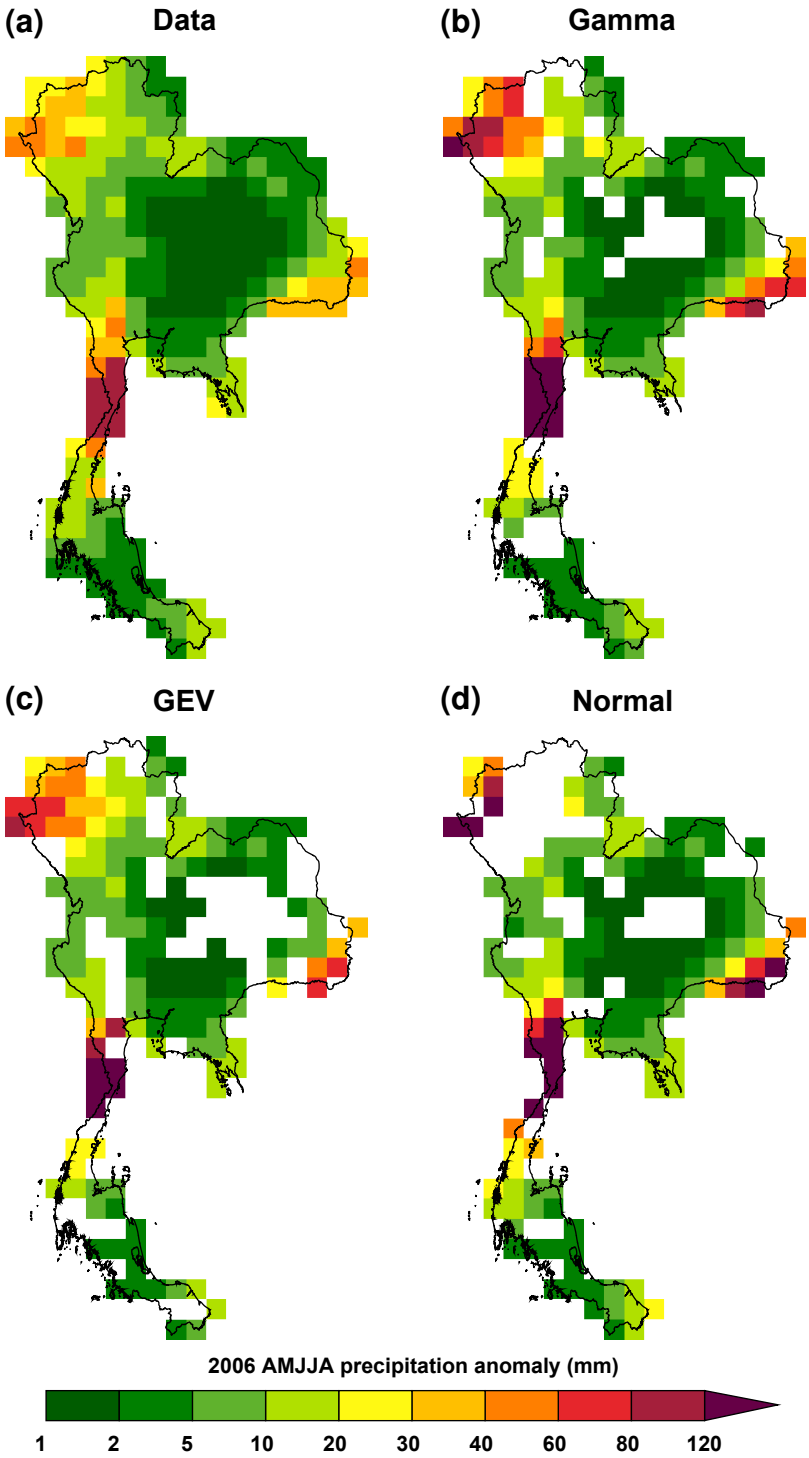

Figure 5.15: As Figure 5.4 but for April–August (AMJJA) 2006.

these events occurring over different months to that in 2011. The heavy rainfall in 2006 occurred over a similar time period to the heavy rainfall in 2011.

The CPRB rainfall return periods for 1942, 2002, and 2006 were similar to the flood return periods obtained from other sources. However a like-for-like comparison of the two types of return period was not wholly appropriate due

Table 5.2: Table summarising the five case studies presented in this chapter. Given are the date, causes and location of each flood, the rainfall return period for the given time period(s) and the corresponding rainfall return period for 2011. Flood return periods from other sources are also shown (where available; †estimated using annual maximum water levels at Ayutthaya (DHI, 2011), ‡calculation method unknown (Prajamwong and Suppataratarn, 2009)).

			Rainfall return periods (years)			
Date	Causes	Location	Period	Event	2011	Flood return periods (years)
Sep–Nov 1942	Exceptionally heavy rainfall in the CPRB	CPRB	AMJJAS	117	70	100†
	Lack of flood protection in Bangkok		August	79	11	
Jul–Nov 1983	Unusually heavy rainfall in Bangkok	Lower CPRB	JASON	1174	7	
	and the lower CPRB		August	77–121	6	
	Tropical Storm Kim	Bangkok	JASON	939	5	
			August	331	7	
Aug–Nov 1995	Series of 6 tropical storms	CPRB	JAS	385	26	50†, 30‡
	Spillage of Sirikit Dam		August	64	11	
	Poor land use					
Aug–Nov 2002	Heavy rainfall in upstream areas of the	MRB	ASO	89	35	15‡
	MRB and CPRB	CPRB	ASO	18	8	
Aug–Dec 2006	Persistent above average rainfall in the CPRB	CPRB	AMJJA	18	162	10†, 20‡
	Typhoon Xangsan					

to possible differences in the calculation method. The flood return periods for the 1995 event were much shorter than the rainfall return period. My research of previous studies did not find a flood return period estimate for the 1983 event.

Although the rainfall return period is a good indicator of the severity of rainfall, it does not necessarily correlate with the severity of the associated flood. Many other factors (e.g. flood protection, topography, land use) play a role in determining the severity of a flood event. The rainfall in 2006 was not particularly severe, but prolonged above average rainfall in 7 of the first 8 months of the year and the impact of Typhoon Xangsan in October resulted in flood damages of approximately US$8 million. Although the rainfall in 1995 did have a long return period, the flooding was exacerbated by poor land use and poor operation of flow control facilities. It is important to examine flood events as a whole, not just examine one contributing factor (such as rainfall).

The events presented in this work all affected the CPRB, although the rainfall and associated flooding in 2002 was more severe in the MRB. The geography of the CPRB lends itself to devastating flooding after extreme climatic rainfall. Therefore decision makers in Thailand must continuously improve flood mitigation in the basin to prevent future devastation.

Chapter 6

The observational relationship between ENSO and climatic rainfall in Thailand

6.1 Introduction

ENSO is a major driver of seasonal and annual climate variability in and around the Pacific Ocean. ENSO also influences climate variability in many areas worldwide. An established link exists between ENSO and precipitation; teleconnections are observed across the globe, either due to the alteration of the tropical Walker circulation or through Rossby wave propagation to mid and high latitudes (e.g. Kenyon and Hegerl, 2010; Smith et al., 2012; Davey et al., 2014). This change in the Walker circulation impacts precipitation in the areas surrounding the equatorial Pacific, particularly Southeast Asia, Indonesia and Australia.

Thailand—located on the Indochina Peninsula—has a rainfall climate that is somewhat influenced by ENSO. However, there is no current consensus as to the strength, significance and seasonality of this link. Previous studies focussed primarily on the seasonal link between ENSO and Thailand rainfall (e.g. Singhrattna et al., 2005a,b; Smith et al., 2012; Bridhikitti, 2013). Although Räsänen and Kummu (2013) investigated the ENSO link to annual rainfall in the MRB, which incorporates parts of eastern and northern Thailand, the work in this chapter is the first to examine the ENSO link to annual and summer monsoonal rainfall across Thailand as a whole.

Typically, El Niño (La Niña) events are associated with below (above) average seasonal rainfall in Thailand, although the strength of this relationship varies depending on the season. Singhrattna et al. (2005a) found statistically significant correlations between ASO rainfall and the SOI in the prior and concurrent

seasons (ranging from +0.44 in MJJ to +0.59 in ASO). In north-eastern Thailand, ENSO signals in JFM affected rainfall in the pre-summer monsoon months (MAM), whereas in the central region, ENSO signals in the pre-summer monsoon impacted the post-summer monsoonal rainfall (SON; Bridhikitti, 2013). Räsänen and Kummu (2013) saw a significant correlation (–0.58; using the Meyers Index (Meyers et al., 2007), where a positive (negative) index represents El Niño (La Niña)) between ENSO signals in DJF and annual rainfall in the south of the MRB (the area that includes parts of Thailand).

Previous studies were limited by their relatively short data period: from only 24 years (1981–2005; Räsänen and Kummu, 2013) to 67 years (1950–2007) of data (Singhrattna et al., 2012). Most of the previous work in this area relied on station data for analysis, which was limited to post-1950 due to poor data availability. As a result, only one study (Bridhikitti, 2013) examined the relationship between Thai precipitation and ENSO across the whole country, although spatial data coverage was poor (only 17 stations). Other studies focused on a small region of the country only: central Thailand (Singhrattna et al., 2005a,b), the Ping River basin in north-western Thailand (Singhrattna et al., 2012) and the Mekong River basin, which encompasses parts of northern and eastern Thailand (Räsänen and Kummu, 2013). Importantly, the established relationship between rainfall and ENSO was insignificant in much of the previous work (Smith et al., 2012; Bridhikitti, 2013), although Singhrattna et al. (2005a,b) found significance, but only from 1980 onwards. Interestingly, this change coincided with a decrease in correlation between ENSO and Indian summer monsoonal rainfall.

The aims of this chapter are to quantify the influence of ENSO on annual and summer monsoonal (MJJASO) rainfall in Thailand, and to do this by improving upon the methods used in previous studies. Using gridded monthly precipitation data over a 111-year period and long-term monthly records of multiple ENSO indices (Section 6.2.1), I developed a new and physically sound method of identifying ENSO events that can easily be applied to other regions and indices (Sections 6.2.2 and 6.2.3). I then examined the strength, significance and stationarity of the link between Thai rainfall and ENSO (Section 6.3.1), quantified the risk of drought and excessive wet periods due to ENSO using a highly

recommended probabilistic approach (Section 6.3.2; Rougier et al., 2010), and examined the possibility of a lag-effect (Section 6.3.3). Lastly, I examined the physical mechanism behind the Thai rainfall-ENSO relationship (Section 6.3.4).

6.2 Methodology

6.2.1 Data

Gridded 0.5° monthly precipitation data for 1901–2011 were taken from the Climatic Research Unit (CRU) TS3.21 dataset (Harris et al., 2014). More details on this dataset are given in Section 2.2.2. I used two ENSO indices: the SOI (Section 2.3.1), based on the MSLP difference between Tahiti and Darwin (Troup, 1965); and the ONI (Section 2.3.2), based on the SST anomaly in the Niño 3.4 region (5°N–5°S, 120°–170°W). The SOI data, available for the full 111-year period used in this chapter, were obtained from the Australian Bureau of Meteorology (2014) and recalculated using the 1901–2011 base climatology. The ONI data, available from 1950 only, were obtained from the NOAA Climate Prediction Center (2014). Here I used ONI data from 1951–2011.

To examine the stationarity of the rainfall-ENSO relationship, I focussed on three time periods: full (1901–2011), early (1901–1950) and late (1951–2011). This latter period was used to examine the effects of using different ENSO indices on the results; due to the limited availability of the ONI data, this was not possible in the full and early periods.

6.2.2 Calculating weighted ENSO indices

I calculated robust weighted time series for both ENSO indices using normalized country-averaged monthly rainfall totals for Thailand over each time period:

$$i_w = \sum_{m=1}^{12} i_m p_m, \tag{6.1}$$

where i_w is the annual weighted ENSO index, i_m is the ENSO index for month m, and p_m is the normalized country-averaged monthly rainfall (or weighting) for month m. Figure 6.1 shows these weightings for each month and time period.

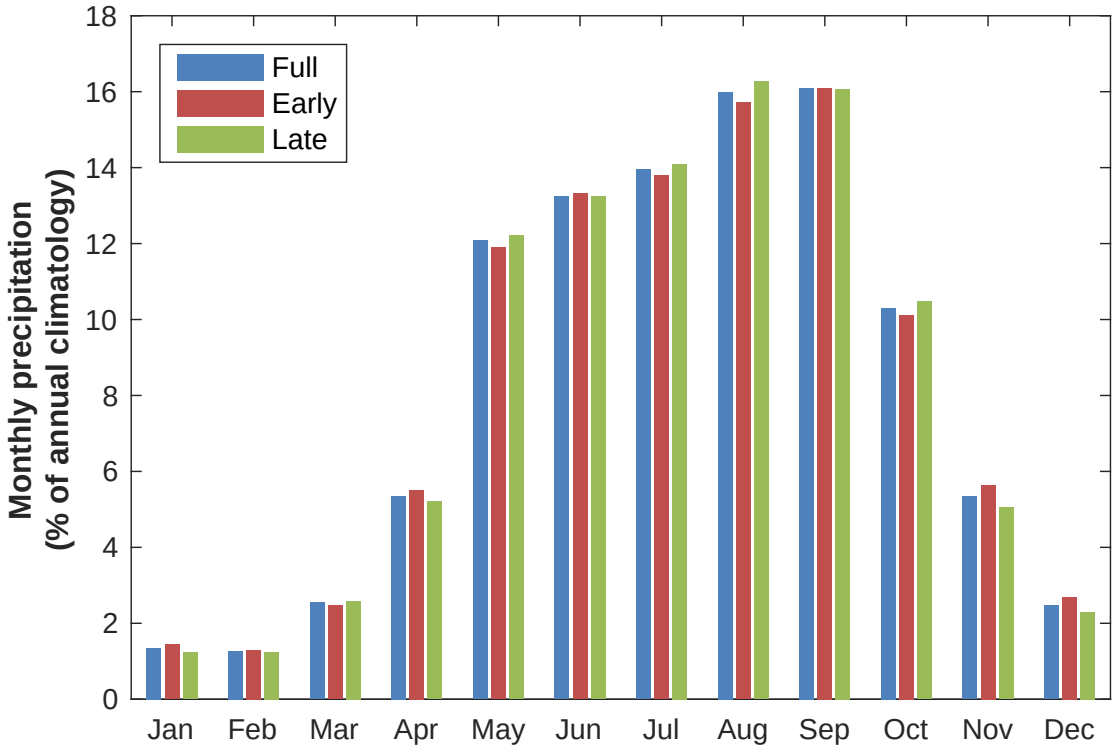

Figure 6.1: The country-averaged monthly rainfall totals for Thailand, given as a percentage of the annual rainfall climatology, for the full (1901–2011; blue), early (1901–1950; red) and late (1951–2011; green) periods. The data used are 0.5° gridded monthly rainfall totals taken from the Climatic Research Unit (CRU) TS3.21 dataset (Harris et al., 2014).

This is a new and physically sound method for examining the contemporaneous links between ENSO and climatic rainfall in Thailand. The method gives increased weighting to ENSO events that occur during Thailand's wet months (MJJASO) and decreased weighting to those that occur during the dry months (November–April). For example, during the 2010 La Niña (un-weighted annual SOI of +9.2) the SOI was high throughout the summer monsoon season. After weighting, the 2010 annual SOI increased to +14.5. In comparison, 1983 showed El Niño signals between January and April (un-weighted annual SOI of –8.0). After weighting, the annual SOI reduced to –0.9 because of the predominantly neutral ENSO conditions during the wettest months of the year. Figure 6.2 shows timeseries of the un-weighted and weighted ENSO indices used in this work.

To examine a possible lag in the Thai rainfall-ENSO relationship (Singhrattna et al., 2005a; Bridhikitti, 2013), I adapted Equation 6.1 by shifting the monthly weights backwards by 1, 2 and 3 months (e.g. the July precipitation weighting

(a) SOI

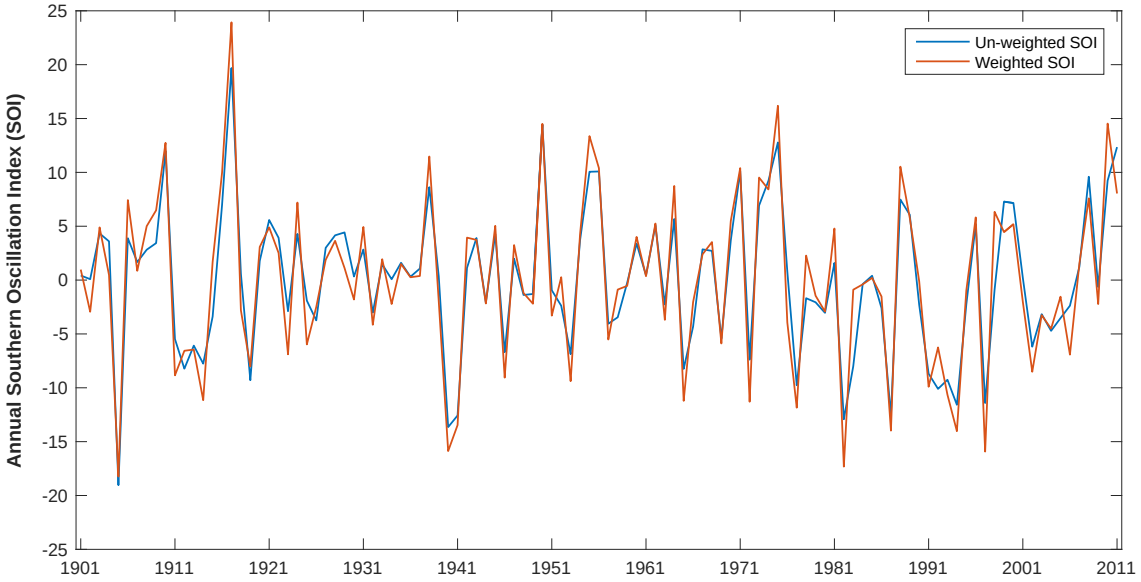

(b) ONI

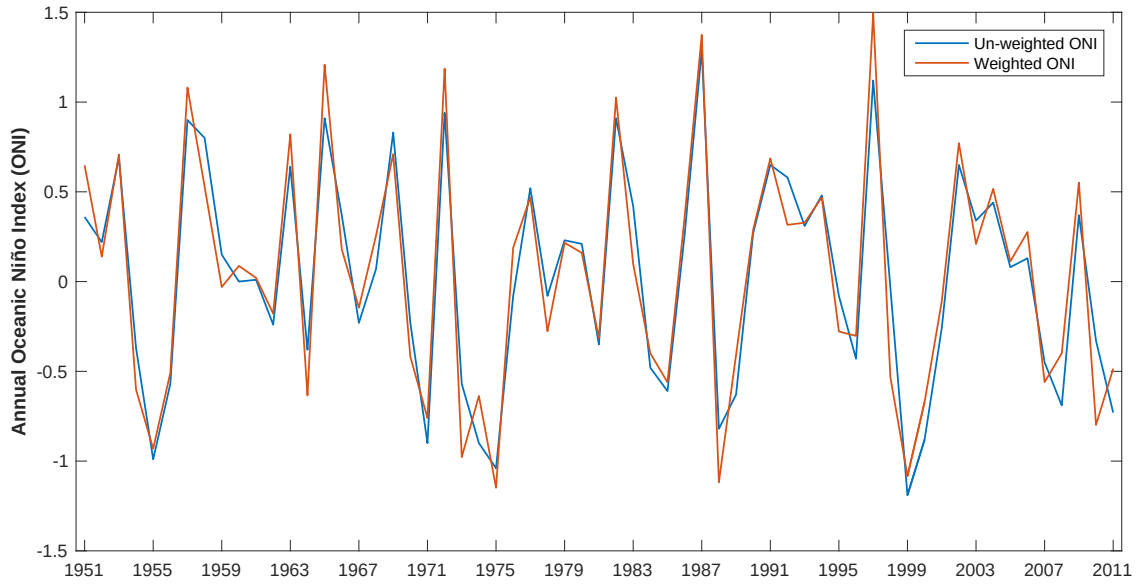

Figure 6.2: Time series showing the annual un-weighted (blue) and weighted (red) (a) Southern Oscillation Index (SOI) (1901–2012) and (b) Oceanic Niño Index (ONI) (1951–2012).

was applied to the June ENSO index for lag l_1, to the May ENSO index for l_2, and to the April ENSO index for l_3).

6.2.3 Classifying ENSO events

There is no consensus on the classification of ENSO events, so the selection of classification method may greatly affect the results (Kiem and Franks, 2001). There are two main methods of identifying ENSO events. The most common of these uses a threshold, often ± 0.5 standard deviations (Phillips et al., 1998) or a given index value threshold (e.g $\pm 0.5^{\circ}$C for SST based indices; Japan Meteorological Agency, 2014), which must be exceeded for a prolonged period of time (typically at least 5 months Ropelewski and Halpert, 1996; Lim et al., 2012). Kiem and Franks (2001) used a variation of this method where an ENSO event occurred if the October–March average index exceeded ± 0.5 standard deviations. This study focused on the effects of ENSO on rainfall in the Williams River basin, New South Wales, Australia; the October–March period was chosen as it coincides with the main period of rainfall in the river basin. The less common method of identifying ENSO events simply uses the strongest *n* events in a given time series. There is no definite method of choosing *n*; Mason and Goddard (2001) selected the 5, 8 and 11 strongest events during each season to test the robustness of their results. In their study, selecting the 8 strongest events ensured the index exceeded one standard deviation in most cases.

Using a quartile threshold, where I defined La Niña and El Niño events using the upper and lower quartile of the annual weighted ENSO time series respectively, resulted in ENSO years similar to those used in previous studies (e.g. Räsänen and Kummu, 2013). This method was repeated for the three time periods used in this study. Therefore in each period the number of La Niña and El Niño events were equal, although this quantity differed from period to period as the period length varied (28, 13, and 15 events of each ENSO type for the full, early and late periods respectively).

I divided these ENSO events further into single- and multi-year events based on their duration. A multi-year event occurs when the ENSO index persists with the same sign above (below) the upper (lower) quartile threshold for multiple consecutive years (Figure 6.3). Table 6.1 shows the ENSO events selected using the SOI for the full period. Appendix C shows the events for the early (SOI) and

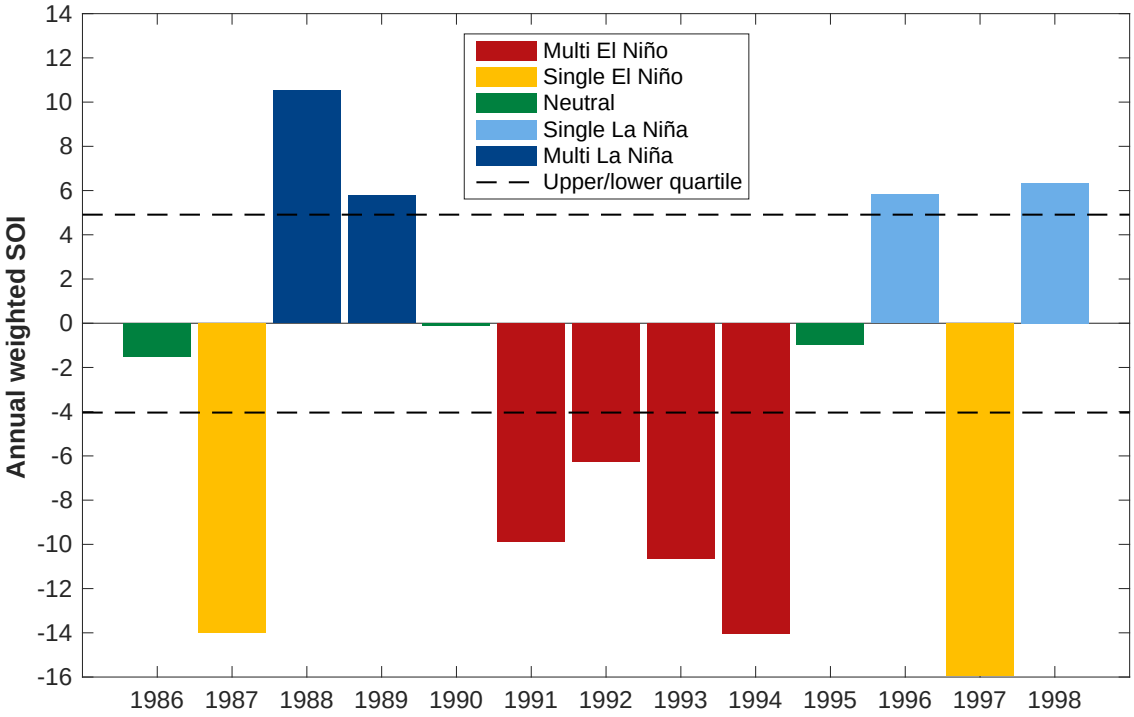

Figure 6.3: Time series of annual weighted Southern Oscillation Index (SOI) (1986–1998) depicting the method I used to define single- and multi-year El Niño Southern Oscillation (ENSO) events. The dotted lines represent the upper and lower quartile threshold calculated over the full period (1901–2011). El Niño events are shown in yellow (single-year) and red (multi-year). La Niña events are shown in light (single-year) and dark blue (multi-year). Neutral events are shown in green.

late periods (SOI and ONI).

6.2.4 Calculating the Standardised Precipitation Index (SPI)

I used the SPI, developed by McKee et al. (1993), to quantify precipitation excess and deficit by transforming the annual and summer monsoonal rainfall distributions into standard-normal distributions (Lloyd-Hughes and Saunders, 2002). Standardisation ensures that the frequency of extreme events at any location and on any timescale remains consistent (Table 6.2): 'extremely wet' events (SPI greater than or equal to 2) occur with a probability of 2.3 %, whereas 'mildly wet' events (SPI between 0 and 0.99) will occur more frequently (34.1 % occurrence probability).

I used Easyfit (Mathwave, 2014) to fit 49 distributions to the country-averaged annual and summer monsoonal precipitation anomaly data. I chose the Wakeby and Error distributions for annual and summer monsoonal rainfall anomaly data

Table 6.1: The El Niño Southern Oscillation (ENSO) events identified during the full period (1901–2011) using the Southern Oscillation Index (SOI). El Niño and La Niña events are the lower and upper quartile years of the SOI time series respectively. A multi-year event occurs when the SOI persists with the same sign above (below) the upper (lower) quartile threshold for multiple consecutive years.

La Niña		El Niño	
Single-year	Multi-year	Single-year	Multi-year
1906	1908–1910	1905	1911–1914
1924	1916–1917	1919	1940–1941
1931	1955–1956	1923	1991–1994
1938	1970–1971	1925	
1945	1973–1975	1932	
1950	1988–1989	1946	
1962	2010–2011	1953	
1964		1957	
1996		1965	
1998		1969	
2000		1972	
2008		1977	
		1982	
		1987	
		1997	
		2002	
		2004	
		2006	

Table 6.2: Classification of precipitation excess or deficit using the Standardised Precipitation Index (SPI). The category and event probabilities are given for each range of Standardised Precipitation Index (SPI) values.

SPI Value	Category	Probability (%)
$\geq$ 2.00	Extremely wet	2.3
1.50 to 1.99	Severely wet	4.4
1.00 to 1.49	Moderately wet	9.2
0 to 0.99	Mildly wet	34.1
–0.99 to 0	Mild drought	34.1
–1.49 to –1.00	Moderate drought	9.2
–1.99 to –1.50	Severe drought	4.4
$\leq$ –2.00	Extreme drought	2.3

respectively; these distributions gave the best average test result across the three goodness-of-fit tests used in Easyfit. Figure 6.4 shows the transformation of the Thailand-average annual precipitation anomaly to SPI. Using the Wakeby distribution, an annual precipitation of 8.5 % above normal is equivalent to an SPI of 1 (the summer monsoonal precipitation-to-SPI transformation is not shown). Comparatively, using the Error distribution a summer monsoonal precipitation of 8.4 % above normal is equivalent to an SPI of 1. An extremely wet event occurs if the annual precipitation anomaly is greater than or equal to +17.6 % or if the summer monsoonal precipitation anomaly is greater than or equal to +16.0 %.

6.3 Results

6.3.1 Thailand precipitation anomalies by ENSO type

I calculated annual and summer monsoonal precipitation anomalies by ENSO type (single- and multi-year La Niña and El Niño events) for each grid square in Thailand and each temporal split (full, early and late periods). I also computed

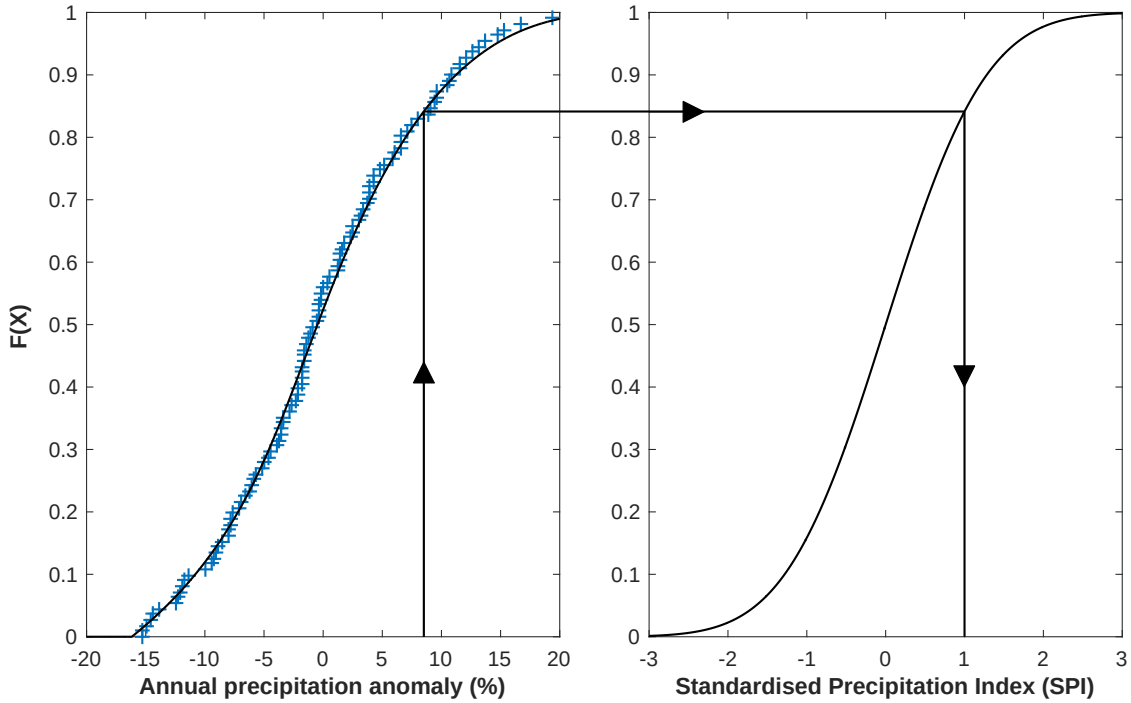

Figure 6.4: An example of the transformation from a fitted Wakeby distribution (left) to the standard normal distribution (right). The blue crosses represent the country-averaged annual precipitation anomaly for each year in the full period (1901–2011).

the statistical significance of these rainfall anomalies, using a method similar to Saunders and Lea (2005) as follows:

1. I randomly selected n years per ENSO type, where n is the number of years in each set (given in brackets in Table 6.4),
2. repeated this 10 000 times, and
3. calculated rainfall anomalies for each grid square using these 10 000 random samples of ENSO events.

The following constraints were applied to the first step:

- Single-year events of the same ENSO phase could not be consecutive.
- Multi-year events could not immediately precede or follow a single-year event of the same sign.

The observed rainfall anomalies were classed as significant if 500 or less samples (p-value ≤ 0.05) had a rainfall anomaly greater than or less than the observed anomaly for La Niña and El Niño events respectively. To calculate the significance of the country-average rainfall anomalies (Tables 6.3 and 6.4), I averaged the 10 000 random samples over the country before calculating the p-value.

Averaging across the country, annual rainfall during a La Niña phase was 8.7 % higher than during an El Niño phase (full period). This difference was similar for summer monsoonal rainfall (8.8 %). Across all three time periods, the observed annual and summer monsoonal rainfall anomalies were positive during La Niña phases and negative during El Niño phases (Table 6.3). These anomalies were all statistically significant when using the SOI to identify ENSO events, but were not significant when using the ONI. The strongest annual rainfall anomalies occurred in the full period for La Niña (+5.0 %) and in the early period for El Niño (–4.4 %). For summer monsoonal rainfall, the strongest anomalies occurred in the early period for both ENSO phases (+6.9 % and –4.1 % for La Niña and El Niño respectively).

After splitting the ENSO events into single- and multi-year durations, the observed rainfall anomalies were positive during La Niña and negative during

Table 6.3: The strength and significance of Thailand precipitation anomalies linked to the El Niño Southern Oscillation (ENSO). Values are shown by ENSO sign. Precipitation anomalies were averaged over the country and are given as the average percentage departure from the climatology over all ENSO events in each time period. The analysis was done separately for annual and summer monsoonal periods. The ENSO events were identified using both the Southern Oscillation Index (SOI) and the Oceanic Niño Index (ONI). The shaded cells represent the statistically significant average precipitation anomalies (p-value ≤ 0.05). The values in brackets show the number of ENSO events in the set followed by the p-value.

ENSO Index	Time Period	La Niña		El Niño	
Annual data					
SOI	1901–2011	5.0	(28; 0.00)	–3.5	(28; 0.00)
SOI	1901–1950	4.5	(13; 0.01)	–4.4	(13; 0.00)
SOI	1951–2011	3.8	(15; 0.02)	–3.1	(15; 0.04)
ONI	1951–2011	2.6	(15; 0.08)	–1.2	(15; 0.26)
Summer monsoonal data					
SOI	1901–2011	5.4	(28; 0.00)	–3.5	(28; 0.00)
SOI	1901–1950	6.9	(13; 0.00)	–4.1	(13; 0.02)
SOI	1951–2011	3.1	(15; 0.03)	–3.7	(15; 0.01)
ONI	1951–2011	2.0	(15; 0.11)	–1.6	(15; 0.16)

El Niño in all cases bar single-year La Niña events during the early period (Table 6.4). In all cases, the multi-year annual rainfall anomalies were stronger than single-year anomalies. The anomalies were particularly significant when using the SOI to select ENSO events.

When using the ONI, although the multi-year annual rainfall anomalies were stronger than the single-year anomalies, they were not statistically significant. The results were similar for summer monsoonal rainfall although the single-year rainfall anomaly exceeded the multi-year anomaly in two cases (early period El Niño and late period La Niña).

Focussing on the full period, on average annual precipitation was 4.5 % higher for multi-year La Niña and 4.9 % lower for multi-year El Niño than during single-year events of the same phase. Similarly, on average summer monsoonal precipitation was 4.7 % higher during multi-year La Niña events and 3.1 % lower during multi-year El Niño events than during single-year events of the same phase. Annual and summer monsoonal rainfall anomalies over the full period

Table 6.4: As Table 6.3 but here the El Niño Southern Oscillation (ENSO) events are divided into single- and multi-year events.

ENSO	Time	La Niña				El Niño			
Index	Period	Single-year		Multi-year		Single-year		Multi-year	
Annual data									
SOI	1901–2011	2.3	(12; 0.15)	7.1	(16; 0.00)	–1.6	(18; 0.17)	–7.0	(10; 0.01)
SOI	1901–1950	–0.2	(8; 0.52)	11.9	(5; 0.00)	–3.9	(7; 0.07)	–5.1	(6; 0.09)
SOI	1951–2011	2.5	(4; 0.26)	4.2	(11; 0.02)	–1.1	(11; 0.31)	–8.7	(4; 0.04)
ONI	1951–2011	2.1	(6; 0.24)	2.9	(9; 0.10)	–0.4	(13; 0.42)	–6.9	(2; 0.17)
Summer monsoonal data									
SOI	1901–2011	2.6	(12; 0.12)	7.5	(16; 0.00)	–2.3	(18; 0.07)	–5.6	(10; 0.03)
SOI	1901–1950	2.9	(8; 0.13)	13.2	(5; 0.00)	–4.3	(7; 0.06)	–3.8	(6; 0.18)
SOI	1951–2011	0.4	(4; 0.47)	4.0	(11; 0.01)	–2.7	(11; 0.08)	–6.6	(4; 0.05)
ONI	1951–2011	3.1	(6; 0.14)	1.2	(9; 0.23)	–1.1	(13; 0.26)	–4.9	(2; 0.18)

were 2.4 to 4.4 times greater in magnitude during multi-year ENSO events than during single-year ENSO events. Table 6.4 also shows that annual (summer monsoonal) rainfall during multi-year La Niña events was on average 14.4 % (13.2 %) higher than during multi-year El Niño events.

Figure 6.5 shows the spatial variation of the ENSO-related precipitation anomalies across Thailand using the SOI to identify ENSO events. During La Niña events, large areas of the country were wetter than normal, particularly during the late and full periods. During single-year La Niña events in these two periods, the central region was the wettest area of the country (up to 17 % wetter in some cases); this region corresponds with the 11 % (late period) and 14 % (full period) of the country that had significantly more rainfall than usual. In comparison, the single-year La Niña rainfall anomalies in the early period were insignificant throughout the country. During multi-year La Niña events, precipitation was much higher across most of the country (on average 50 % of the country had statistically significant rainfall across the three temporal splits), particularly during the early period, where the annual rainfall in the area to the west of Bangkok was up to 29 % higher than usual. The highest rainfall anomalies were predominantly in the CPRB.

Much of Thailand was drier than normal during El Niño events. The north of Thailand was the driest region during single-year El Niño events in the early period; 21 % of the country had significantly less rainfall than usual in this period. The single-year El Niño rainfall deficits were weaker in the late and full periods. The strongest and most significant rainfall deficits occurred during the multi-year El Niño events in the late period; annual rainfall was as much as 24 % drier than usual in some parts of the CPRB. Across the three time periods, approximately 31 % of the country was significantly drier than usual when El Niño events persisted over multiple years.

Interestingly, an area in the east of the country was anomalously wet during single-year El Niño events across all three time periods, particularly so during the early and full periods. However, rainfall anomalies in this region switched sign when the El Niño events persisted; annual rainfall was significantly less than normal in much of the east during multi-year El Niño events. A similar pattern was

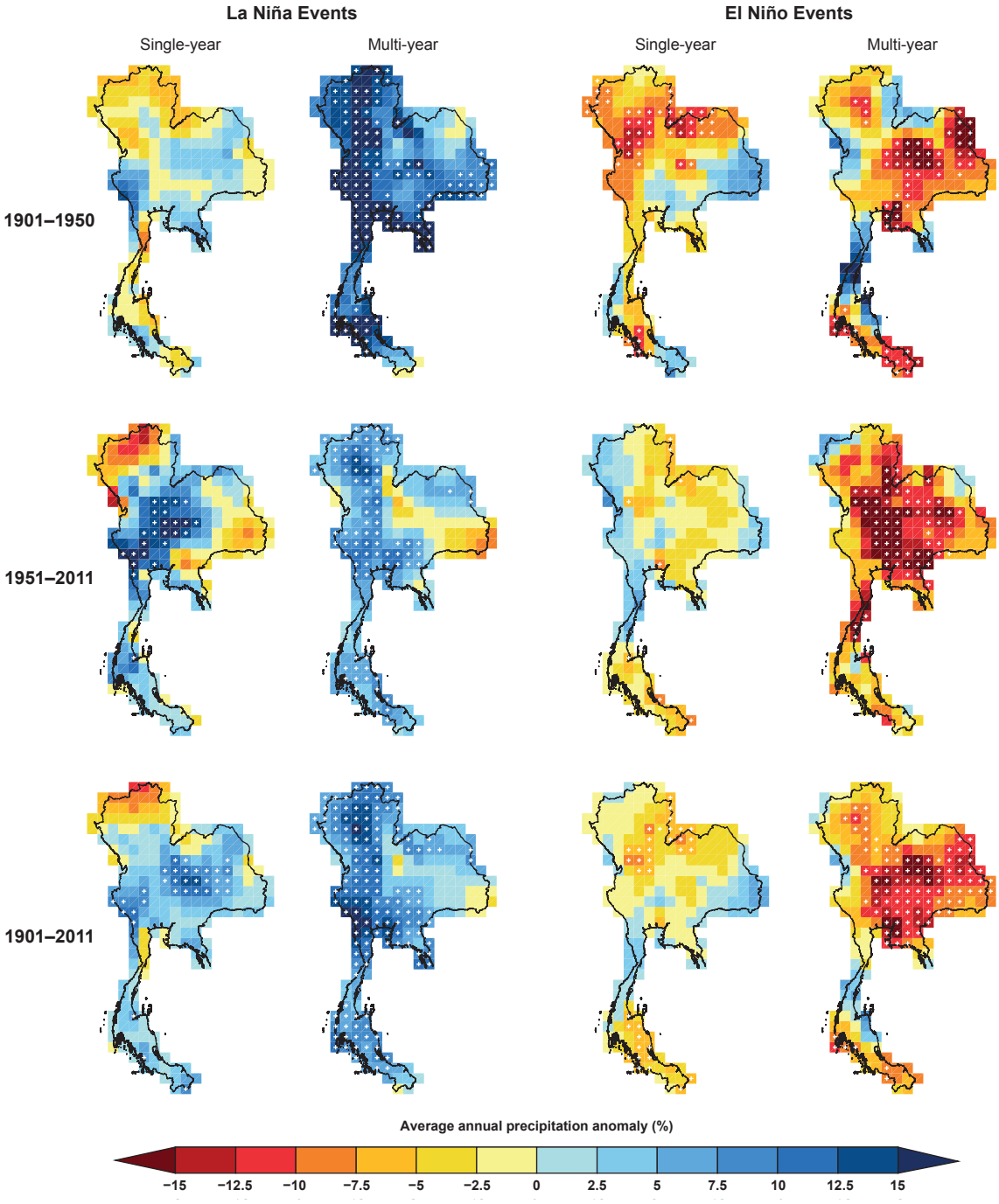

Figure 6.5: Average annual Thailand precipitation anomalies by El Niño Southern Oscillation (ENSO) type, given as the average percentage departure from the climatology over the given period. The Southern Oscillation Index (SOI) was used to identify ENSO years. Wetter than usual conditions are shown in blue and drier conditions are shown in red. Statistically significant anomalies (p-value ≤ 0.05) are shown using a white cross. Left to right: single-year La Niña, multi-year La Niña, single-year El Niño, multi-year El Niño. Top to bottom: early (1901–1950), late (1951–2011) and full (1901–2011) periods.

seen during single-year La Niña events (although the region was anomalously dry), but the switch in sign when the La Niña events persisted only occurred during the early period. Examination of a wider area of Southeast Asia would show whether this pattern extends or whether it is an abnormality restricted to this small region of Thailand. However, this is beyond the scope of this work.

As discussed previously (Chapter 2), the quality of the CRU data may be poor prior to 1911 and post 2000 (as the number of stations was reduced in these periods). To assess the impact of this possibly poor data I recalculated the weighted SOI, reselected ENSO events (shown in Appendix E), and recalculated the precipitation anomalies due to ENSO over two shorter periods: 1911–2000 (90 years) and 1911–2011 (101 years). As shown in Table 6.5, excluding these possibly poor data does affect the annual and summer monsoonal rainfall anomalies (predominantly the anomaly for multi-year La Niña events) but the changes from the main conclusions evident in Table 6.4 were small.

Five single-year El Niño events were removed when using the 90-year period (1905, 1932, 2002, 2004 and 2006); this caused a slight strengthening of the annual anomaly (from –1.6 % to –2.0 % for the 111-year and 90-year periods respectively), and a greater strengthening of the summer monsoonal anomaly (from –2.3 % to –3.7 % for the 111-year and 90-year periods respectively). The latter anomaly became statistically significant. For the 101-year period, only 3 single-year El Niño events were removed (1905, 1932 and 2004). Here the annual anomaly weakened (from –1.6 % to –1.0 % for the 111-year and 101-year periods respectively) and the summer monsoonal anomaly strengthened (from –2.3 % to –2.5 % for the 111-year and 101-year periods respectively). There was no change to the multi-year El Niño events selected, so the changes in the anomalies were purely caused by the slight change to the underlying climatology.

The number of single-year La Niña events remained the same for each period, although the years included were different. In the 90-year period, 1906 and 2008 were replaced with 1921 and 1981. In the longer 101-year period, 2008 was included but again, 1906 was replaced with 1921. Despite these changes, the impact on the rainfall anomalies was negligible. The three-year La Niña event from 1908 to 1910 was removed from both shorter periods, and

Table 6.5: As Table 6.4 but for two shorter periods (1911–2000 and 1911–2011). The anomalies for the full period (1901–2011) are also shown for comparison. All El Niño Southern Oscillation (ENSO) events are selected using the Southern Oscillation Index (SOI).

Time	La Niña				El Niño			
Period	Single-year		Multi-year		Single-year		Multi-year	
Annual data								
1911–2000	2.4	(12; 0.11)	5.3	(11; 0.01)	–2.0	(13; 0.16)	–6.0	(10; 0.01)
1911–2011	2.5	(12; 0.09)	5.6	(13; 0.00)	–1.0	(15; 0.37)	–6.8	(10; 0.01)
1901–2011	2.3	(12; 0.15)	7.1	(16; 0.00)	–1.6	(18; 0.17)	–7.0	(10; 0.01)
Summer monsoonal data								
1911–2000	2.5	(12; 0.10)	6.2	(11; 0.00)	–3.7	(13; 0.02)	–4.4	(10; 0.05)
1911–2011	2.5	(12; 0.08)	6.4	(13; 0.00)	–2.5	(15; 0.12)	–5.3	(10; 0.05)
1901–2011	2.6	(12; 0.12)	7.5	(16; 0.00)	–2.3	(18; 0.07)	–5.6	(10; 0.03)

the 2010–2011 event was removed from the 90-year period. These changes led to a reduction in both the annual and summer monsoonal multi-year La Niña anomalies (annual: from 7.1 % (111-year) to 5.3 % (90-year) and 5.6 % (101-year); summer monsoonal: from 7.5 % (111-year) to 6.2 % (90-year) and 6.4 % (101-year)). Despite this reduction, the multi-year La Niña anomalies were still statistically significant, and still higher than those in single-year La Niña events.

These results show that the strengthening of Thailand rainfall anomalies in multi-year ENSO events was not controlled by possibly erroneous data prior to 1911 and post 2000.

To analyse the effect of weighting the ENSO indices, I reselected the ENSO events without weighting the indices beforehand (shown in Appendix D) and recalculated the country-average annual rainfall anomalies (Table 6.6).

In all cases, annual rainfall was higher during single-year La Niña events than during La Niña events persisting for multiple years, and in three cases more significant (annual rainfall during multi-year La Niña events in the late period (SOI) was lower than in single-year events but more significant). The 'unweighted' single-year La Niña anomalies were higher than the 'weighted' equivalent for all time periods and indices. Conversely, the 'unweighted' multi-year La Niña anomalies were lower than the 'weighted' equivalents in all cases bar during the late period, where the rainfall anomaly was 0.5 percentage points higher using the unweighted SOI.

For El Niño events, annual rainfall remained lower in multi-year events than during single-year events. The use of weighting had less effect on the single-year El Niño anomalies than on the single-year La Niña anomalies; the biggest impact occurred in the early period, where the 'unweighted' El Niño anomaly was 1.6 percentage points weaker than the 'weighted' anomaly (–2.3 % and –3.9 % respectively). As with the 'weighted' anomalies, all four 'unweighted' single-year El Niño anomalies were insignificant. There was a greater effect on the multi-year anomalies; the 'unweighted' anomalies in the full and early period were much weaker than the 'weighted' equivalent (full period: –3.8 % and –7.0 % respectively; early period: –3.5 % and –5.1 % respectively). There was no change to the SOI anomaly in the late period, but the 'unweighted' ONI anomaly was

Table 6.6: As Table 6.4 but here the El Niño Southern Oscillation (ENSO) events are selected without applying any weighting to the ENSO indices. The anomalies are shown for annual rainfall only. For comparison, the annual rainfall anomalies from Table 6.4 are also included.

ENSO	Time	La Niña				El Niño			
Index	Period	Single-year		Multi-year		Single-year		Multi-year	
Unweighted ENSO indices									
SOI	1901–2011	5.1	(11; 0.02)	1.9	(17; 0.15)	–1.8	(12; 0.21)	–3.8	(16; 0.04)
SOI	1901–1950	6.2	(7; 0.02)	–4.4	(6; 0.88)	–2.3	(6; 0.22)	–3.5	(7; 0.18)
SOI	1951–2011	5.0	(4; 0.10)	4.7	(11; 0.01)	–2.0	(9; 0.20)	–8.7	(6; 0.02)
ONI	1951–2011	11.5	(2; 0.02)	3.1	(13; 0.04)	–0.9	(11; 0.34)	–10.0	(4; 0.01)
Weighted ENSO indices									
SOI	1901–2011	2.3	(12; 0.15)	7.1	(16; 0.00)	–1.6	(18; 0.17)	–7.0	(10; 0.01)
SOI	1901–1950	–0.2	(8; 0.52)	11.9	(5; 0.00)	–3.9	(7; 0.07)	–5.1	(6; 0.09)
SOI	1951–2011	2.5	(4; 0.26)	4.2	(11; 0.02)	–1.1	(11; 0.31)	–8.7	(4; 0.04)
ONI	1951–2011	2.1	(6; 0.24)	2.9	(9; 0.10)	–0.4	(13; 0.42)	–6.9	(2; 0.17)

stronger and more significant than the 'weighted' anomaly (–10.0 % and –6.9 % respectively).

This analysis shows the importance of weighting to examine the contemporaneous links between ENSO and Thailand climatic rainfall. Many of the 'unweighted' ENSO events were strongest during Thailand's drier months, which resulted in more variability in the ENSO-related annual rainfall anomalies.

6.3.2 Probability of exceedance

Formal methods and recommendations for assessing and quantifying uncertainty in climate hazard impacts sadly do not exist. However, a recent advisory study for the UK Natural Environment Research Council (NERC) (Rougier et al., 2010) recommended the use of a probabilistic description and probability of exceedance curves as a primary tool for quantifying the uncertainty associated with hazard processes and impacts. I followed and applied the Rougier et al. (2010) recommendation to quantify the uncertainty in Thailand rainfall due to ENSO. This application was considered appropriate and useful because:

1. there is variability in the strength of annual and summer monsoonal rainfall impacts in Thailand due to ENSO,

2. the presence of this uncertainty requires the use of probability to quantify the likelihood of different rainfall totals due to ENSO, and

3. probability of exceedance is the most useful probabilistic tool for quantifying the likelihood of different rainfall outcomes predicated by ENSO.

I believe this approach for quantifying uncertainty will aid scientific progress, and benefit risk management, decision-making and policy development.

I calculated probability of exceedance curves for both annual and summer monsoonal precipitation anomalies in Thailand (full period only; Figure 6.6). Curves are shown for single- and multi-year ENSO events (defined using the SOI), ENSO neutral years and all 111 years combined ('all years'). The secondary x-axis shows the corresponding SPI for both annual and summer monsoonal rainfall.

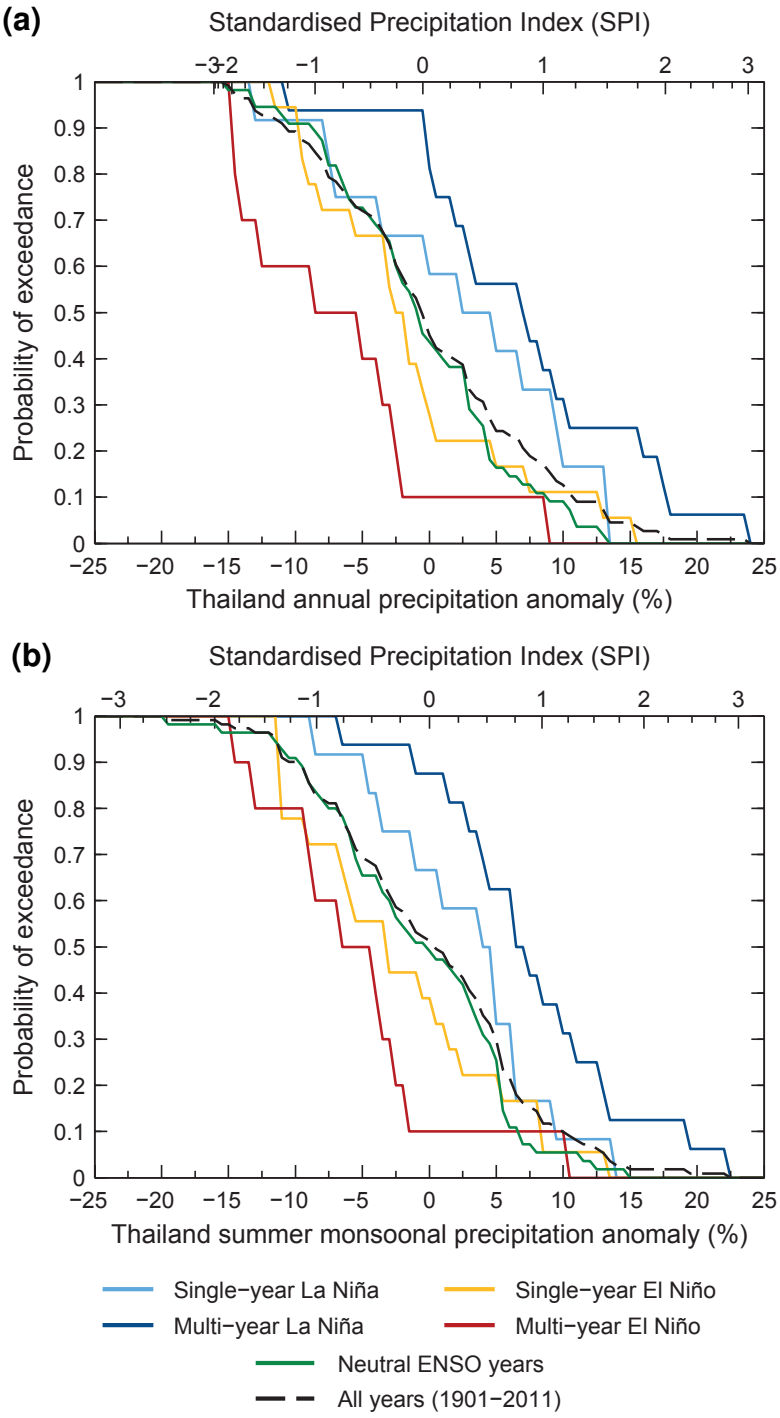

Figure 6.6: Probability of exceedance curves for (a) annual and (b) summer monsoonal (May–October (MJJASO)) Thailand precipitation anomalies by El Niño Southern Oscillation (ENSO) type during the full period (1901–2011). The Southern Oscillation Index (SOI) was used to identify ENSO years. La Niña events are shown in blue, El Niño in yellow/red, and neutral in green. The dashed black line represents the probability of exceedance curve for all years in the period. The primary x-axes show the precipitation anomalies, given as the average percentage departure from the climatology. The corresponding Standardised Precipitation Index (SPI) is given on the secondary x-axes. The Wakeby and Error distributions were used to transform the annual and summer monsoonal precipitation into the SPI respectively.

For the most part, the probability of exceedance curve for annual rainfall in neutral years follows the 'all years' curve; the curves deviate when the rainfall anomaly exceeds +3.5 %, which suggests the probability of more extreme positive annual rainfall anomalies in ENSO neutral years is lower than the average for all years. During La Niña events, there is a 58 % chance that annual Thailand rainfall will be greater than usual during single-year events, rising to over 81 % for multi-year events. In comparison, during El Niño events the probability of less rainfall than normal is 72 % for single-year events, rising to 90 % during multi-year events. Thus, above-average annual rainfall was 8 times more likely in a multi-year La Niña event than in an multi-year El Niño event. The spread between the multi-year La Niña and El Niño curves is approximately 1.5 standard deviations.

As discussed in Section 3.2.3, the probability of exceedance for an annual rainfall value and the return period are inversely related (Equation 3.1). Therefore a return period of 10 years, for example, is equivalent to a probability of exceedance of 0.1. As there is an increased probability of anomalously high rainfall during La Niña events, the return period of this increased rainfall is shorter than during El Niño events (where increased rainfall is abnormal). Thailand annual rainfall 10 % above normal during a multi-year El Niño event would be considered extreme (return period of 10 years), whereas if this rainfall were to occur during a multi-year La Niña event, the return period would be only 3 years.

With respect to the SPI, the extremely wet events (SPI $\geq$ 2.0) occurred solely during multi-year La Niña events (1908 and 2011). The more common severely wet (1.50 $\leq$ SPI $\leq$ 1.99) and moderately wet (1.00 $\leq$ SPI $\leq$ 1.49) events occurred during all ENSO phases, but were more prevalent during La Niña years (47 % compared with 18 % and 35 % for El Niño and neutral phases respectively). Two extremely dry events occurred in the 111 year period: 1979 (ENSO neutral) and 1993 (multi-year El Niño). The less extreme droughts occurred predominantly during El Niño events (53 %), although neutral conditions were also favourable (33 %). Severe droughts were more common during multi-year El Niño events (50 % of all severe droughts) whereas single-year El Niño conditions were more favourable for moderate droughts (44 % of all moderate droughts).

During both single- and multi-year La Niña, the probability of excess summer

monsoonal rainfall was higher than for annual rainfall: 67 % and 88 % for single- and multi-year events respectively. The probability of drought during single-year El Niño events decreased to 61 % for summer monsoonal rainfall. However, the chance of drought during multi-year El Niño events remained at 90 %. During the 111-year period, 1908 and 2011 were the only extremely wet summer monsoon seasons. Fifty-five percent of severely and moderately wet summer monsoon seasons occurred during the La Niña phase—predominantly during multi-year events (33 % and 40 % of all severe and moderate events respectively). Neutral and El Niño conditions were favourable for the three worst drought classifications. The only extreme summer monsoon season drought occurred in 1928 (ENSO neutral). Half of all severe and moderate summer monsoon season droughts occurred during El Niño conditions; two-thirds of the severe droughts were during multi-year El Niño events, whereas moderate droughts were more prevalent during single-year El Niño events than multi-year (33 % and 13 % of all moderate droughts respectively). The majority of moderately dry summer monsoon seasons occurred during ENSO neutral conditions (47 %).

6.3.3 Examination of a lag-effect

Appendix F shows the ENSO events selected using lags of 1, 2 and 3 months. For La Niña, the number of single- and multi-year events remained similar: the number of single-year events increased from 12 (l_0) to 14 (l_3), and the number of multi-year events decreased from 16 (l_0) to 14 (l_3). There was a greater change in the number of single- and multi-year El Niño events: a decrease from 18 (l_0) to 10 (l_3) single-year events, and an increase from 10 (l_0) to 18 (l_3) multi-year events.

Although in some cases the number of events didn't vary greatly, the actual years selected changed considerably. For all lag lengths, some events switched from being a single- to a multi-year event (or vice versa). For example, 2002 and 2004 were single-year El Niño events when using no lag, but became multi-year El Niño events when using 2 months of lag as 2003 and 2005 were now classified as El Niño events.

Table 6.7 shows the rainfall anomalies calculated using the lagged ENSO events (using the SOI over the full period). For La Niña, the anomalies followed

Table 6.7: As Table 6.4 but here the El Niño Southern Oscillation (ENSO) events were selected by shifting the monthly weights backwards by 1, 2 and 3 months (as described in Section 6.2.2). These ENSO events were selected using the Southern Oscillation Index (SOI) over the full period (1901–2011). The anomalies for the full period with no lag applied are shown for comparison.

	La Niña				El Niño			
Lag	Single-year		Multi-year		Single-year		Multi-year	
Annual data								
-	2.3	(12; 0.15)	7.1	(16; 0.00)	–1.6	(18; 0.17)	–7.0	(10; 0.01)
1 month	1.3	(12; 0.28)	7.4	(16; 0.00)	–0.8	(16; 0.33)	–6.1	(12; 0.01)
2 months	1.0	(13; 0.31)	6.7	(15; 0.00)	–2.6	(10; 0.13)	–3.2	(18; 0.06)
3 months	0.9	(14; 0.32)	6.3	(14; 0.00)	–1.1	(10; 0.33)	–3.8	(18; 0.02)
Summer monsoonal data								
-	2.6	(12; 0.12)	7.5	(16; 0.00)	–2.3	(18; 0.07)	–5.6	(10; 0.03)
1 month	2.1	(12; 0.16)	6.9	(16; 0.00)	–1.6	(16; 0.18)	–4.5	(12; 0.05)
2 months	1.7	(13; 0.20)	6.1	(15; 0.00)	–4.2	(10; 0.04)	–1.6	(18; 0.22)
3 months	1.4	(14; 0.23)	5.5	(14; 0.01)	–2.8	(10; 0.12)	–2.4	(18; 0.11)

the same pattern as those where no lag was applied; the rainfall was higher in multi-year La Niña events than those lasting only one year. As the lag increased, the single-year La Niña anomaly decreased. This also occurred for multi-year events, although the annual anomaly for l_1 was slightly higher than for l_0 (7.4 % and 7.1 % respectively). Despite this decrease, the rainfall anomalies for multi-year La Niña events were still statistically significant.

The pattern for El Niño anomalies was less consistent. For all lag lengths, annual rainfall in multi-year El Niño events was drier than during single-year events, but for summer monsoonal rainfall this only applies for l_1. For l_2 and l_3, summer monsoonal rainfall in single-year El Niño events was drier than in multi-year events. For both annual and summer monsoonal rainfall, the multi-year El Niño anomalies were weaker for all lag lengths than the anomaly with no lag applied. This is not the case for single-year El Niño anomalies.

Importantly, these results show that an increase in lag leads to a decrease in the average percentage departures from the climatology and their significances. Thus stronger and more significant ENSO links were found using contemporaneous (i.e. non-lagged) ENSO indices.

6.3.4 Prediction of multi-year ENSO events

This study focused primarily on the observational relationship between Thailand rainfall and ENSO. This raised an important question: can one anticipate, after one year, whether an ENSO event will persist for further year(s), and hence cause stronger rainfall anomalies in Thailand?

Figure 6.7 shows the relationship between the ENSO indices and annual rainfall anomalies in the three periods used throughout this chapter. Here the ENSO years were grouped into two sets: those that persisted for an additional year (all years in multi-year events bar the last), and those that did not (single years and the last year of each multi-year event).

As expected, in all four cases rainfall was predominantly wetter than normal in La Niña years and drier than normal in El Niño years. However, the correlation between ENSO strength (i.e. the SOI or ONI) and ENSO annual rainfall anomalies was only moderately strong (Spearman rank correlation coefficient,

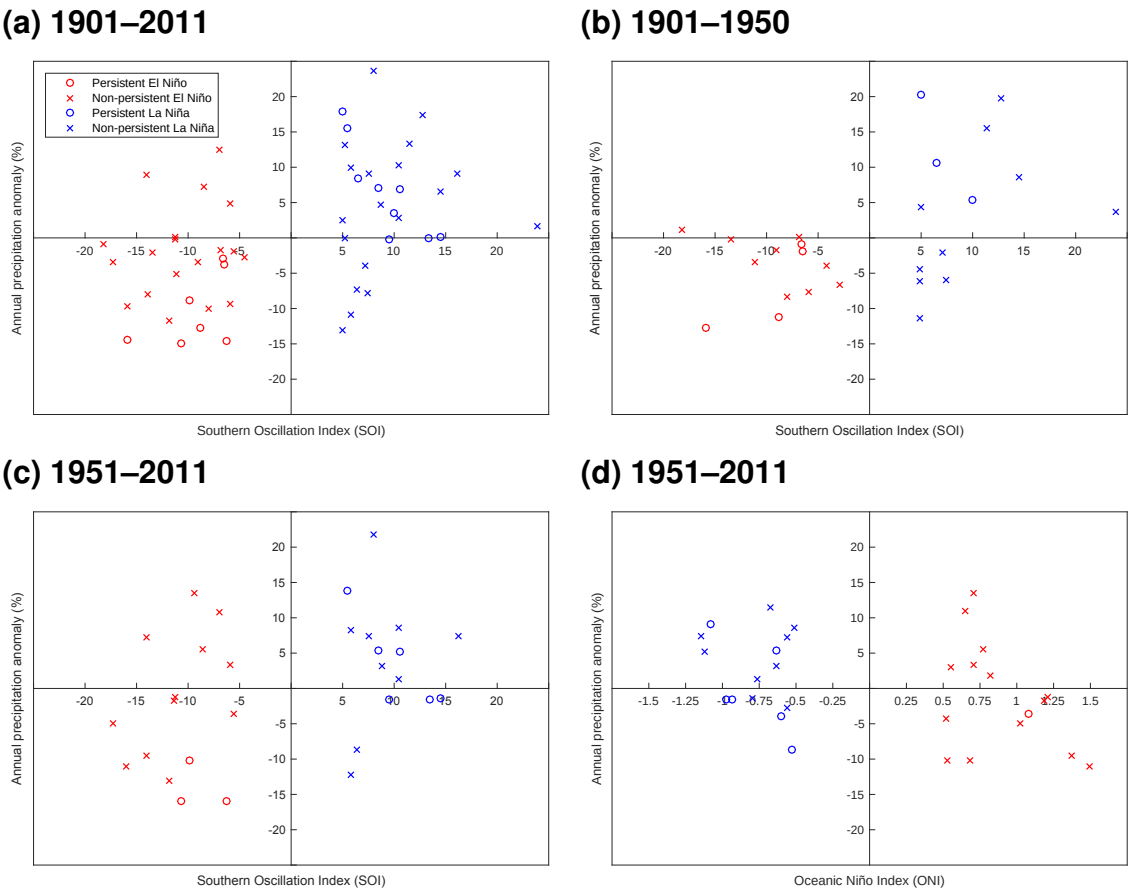

Figure 6.7: Scatter plots showing the relationship between the El Niño Southern Oscillation (ENSO) indices (a–c: Southern Oscillation Index (SOI), d: Oceanic Niño Index (ONI)) (x-axis) and annual precipitation anomaly (y-axis) in the (a) full (1901-2011), (b) early (1901–1950) and (c), (d) late (1951–2011) periods. The La Niña and El Niño events are shown in blue and red respectively. Circles and crosses represent persistent and non-persistent events respectively.

r_{rank}, of +0.47, +0.49, +0.37 and –0.37 for Figures 6.7(a), (b), (c) and (d) respectively). The relationship was strongest during the early and full periods. Interestingly, the correlations in the late period were the same strength for both the SOI and ONI, despite the differences in the underlying ENSO events.

The average strength of ENSO events varied depending on the time period, ENSO index and ENSO type (Table 6.8). On average, persisting La Niña events were stronger than non-persisting events in the late period (both indices; 16 % and 6 % stronger for SOI and ONI respectively). However, the averages for non-persisting La Niña events in the full and early periods were skewed by the anomalously high (and possibly erroneous) SOI of +23.9 in 1917. If this year was removed, the average strength for non-persisting events in these two periods

Table 6.8: The average strength of persisting and non-persisting El Niño Southern Oscillation (ENSO) events. The results are shown for each time period and ENSO index used throughout this study.

ENSO	Time	La Niña		El Niño	
Index	Period	Persisting	Non-persisting	Persisting	Non-persisting
SOI	1901–2011	+9.26	+9.31	−9.22	−10.16
SOI	1901–1950	+7.11	+9.68	−9.42	−8.86
SOI	1951–2011	+10.32	+8.82	−8.94	−11.02
ONI	1951–2011	−0.79	−0.75	+1.08	+0.87

reduced to +8.5 and +8.1 respectively, which meant persisting La Niña events in the full period were now stronger than those that did not persist.

Persisting El Niño events were stronger than non-persisting events in the early and late (ONI) periods only (6 % and 25 % stronger respectively). However it would be unwise to conclude that persistent El Niño events in the late period selected using the ONI were stronger than non-persistent events due to such a small population size (only 1 persistent event).

I computed, for each time period and ENSO index, the probability of an ENSO event persisting for an additional year as the ENSO indices increased in strength (Figure 6.8). The persistence probability varied greatly depending on ENSO strength, time period and ENSO index. On average, the probability of persistence was higher for La Niña than El Niño in all cases bar the early period. In all cases, the strongest ENSO event(s) did not persist ($p = 0$ as the ENSO index strengthened). There were only two occasions where the probability of persistence exceeded 0.5 (i.e. a higher chance of persisting than not), both of which occurred in the late period (La Niña only; both ENSO indices; SOI between +8 and +14; ONI between −0.80 and −0.95). Despite some increase in persistence probability with ENSO strength in some cases (before reducing to zero; e.g. El Niño in the early (SOI) and late (ONI) periods, La Niña in the late period (SOI)), there was no clear evidence that stronger ENSO events were more likely to persist.

Examination of the ENSO index data showed that strong El Niño events in particular did not tend to persist. In the full period, the Thailand-weighted SOI

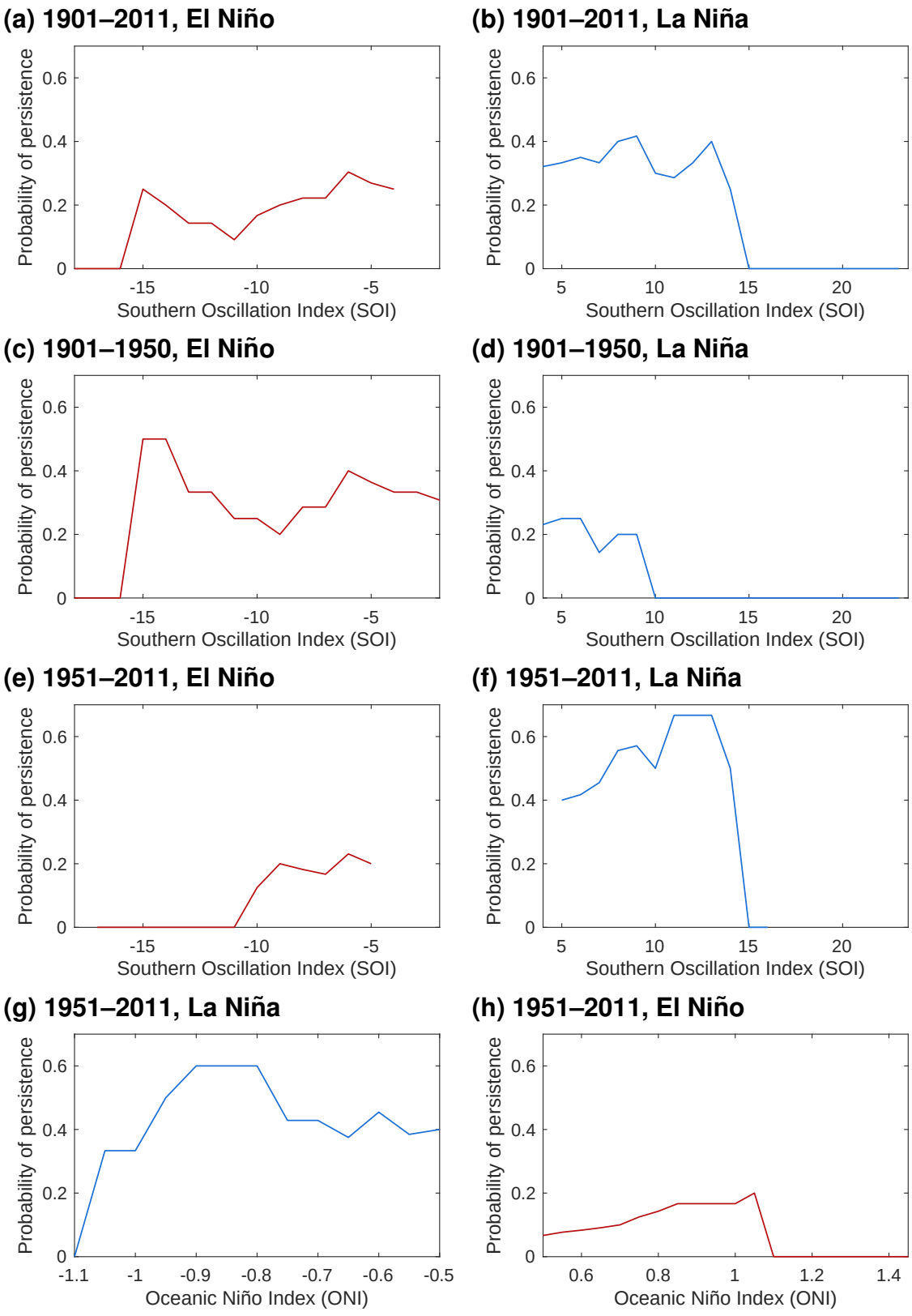

Figure 6.8: The probability of an El Niño Southern Oscillation (ENSO) event persisting for an additional year for (a–f) an Southern Oscillation Index (SOI) less (greater) than or equal to x for El Niño (La Niña), and (g–h) an Oceanic Niño Index (ONI) greater (less) than or equal to x for El Niño (La Niña). The results are shown for each time period and ENSO index used throughout this study.

ranked the well-known 'super' El Niño events of 1982 and 1997 second and third in terms of strength (SOI of −17.3 and −15.9 respectively). These, alongside the El Niño in 1905 (SOI of −18.2), were all non-persisting single-year events. In fact, only 20 % of El Niño events with an SOI less than −10 persisted for an additional year: 1940 and 1993 (SOI of −15.9 and −10.7 respectively). In comparison, 43 % of La Niña events in the full period with an SOI greater than +10 persisted: 1955, 1988 and 2010 (SOI of +13.4, +10.5 and +14.5 respectively). This suggests that strong El Niño conditions were harder to maintain than strong La Niña conditions, and that slightly weaker conditions (SOI between −6 and −10) were more favourable for El Niño persistence.

Although this analysis showed some evidence that stronger ENSO events were more likely to persist in some time periods, it is clear that strength is not the only controlling factor in the persistence of ENSO events. Further work must be done to address this question, but this is beyond the scope of this work.

6.4 Discussion

Extending on limited previous studies (e.g. Singhrattna et al., 2005a,b; Bridhikitti, 2013), I confirmed that ENSO is a substantial driver of interannual variability in Thailand annual and summer monsoonal rainfall. Using 111 years of gridded precipitation data, I saw anomalously high rainfall during La Niña events and drier conditions during El Niño events. This correlation remained consistent throughout the time period examined. On average, annual Thailand rainfall during a La Niña phase was 8.7 % higher than during an El Niño phase (an SPI difference of 1.0).

Multi-year ENSO events (those that persist in the same phase for more than one year) were associated with larger and more significant annual and summer monsoonal rainfall anomalies across much of Thailand. This effect was apparent in each temporal split, but appeared strongest for La Niña, where summer monsoonal rainfall during multi-year La Niña events was as much as 13 % higher than usual (early period; compared to an insignificant rainfall anomaly of 3 % during single-year La Niña events in the same period). Averaging across the country, Thailand annual rainfall totals were 4.5 % greater during multi-year La Niña events than during those persisting over only one year. Annual rainfall

during multi-year La Niña events was 14.4 % higher than during multi-year El Niño events (an SPI difference of 1.7). These results were not affected by the possibly erroneous data at the beginning and end of the data period.

In this data record, extremely wet periods (during both annual and summer monsoonal periods) occurred solely during multi-year La Niña events; severely and moderately wet events were also more common during La Niña periods. Droughts tended to occur during the El Niño phase of ENSO, although neutral conditions were also favourable. Probability of exceedance analysis showed that Thailand annual rainfall was 8 times more likely to be above normal in a multi-year La Niña event than in a multi-year El Niño event.

I examined a possible lag in the Thai rainfall-ENSO relationship by shifting the weights applied to the ENSO indices backwards by 1, 2 and 3 months. Although the rainfall anomalies seen in multi-year La Niña events were still higher and more significant than those seen in single-year events of the same phase, these anomalies were lower than those seen where no lag was applied. The pattern was less consistent during the El Niño phase. Overall, this analysis showed that the ENSO influence on Thailand climatic rainfall was stronger and more significant when ENSO was contemporaneous with the Thailand wet season than when ENSO was lagged.

This study focused primarily on the observational relationship between Thailand rainfall and ENSO, but this raised an important question: can one anticipate, after one year, whether an ENSO event will persist for further year(s), and hence cause stronger rainfall anomalies in Thailand? Across all time periods, there was a moderate correlation between Thai annual rainfall anomalies and both ENSO indices. On average, persistent ENSO events were stronger than non-persistent events in some time periods but not in others. The probability of persistence varied greatly depending on ENSO strength, time period and ENSO index. Overall, there was no clear evidence that suggested stronger events were more likely to persist. In fact, the ENSO index data suggested that strong El Niño events in particular did not tend to persist. Further work is required to address this question.

To conclude, I established a new and physically sound method for examining

the contemporaneous link between ENSO and climatic rainfall in Thailand; a technique that could be readily applied to other countries. I found a significant and stationary relationship between ENSO and rainfall in Thailand. Annual rainfall was on average 14.4 % higher during multi-year La Niña events than during multi-year El Niño events (an SPI difference of 1.7). Furthermore, Thailand annual rainfall was 8 times more likely to be above normal during a multi-year La Niña event than during a multi-year El Niño event. With 2011 being the second year of a multi-year La Niña event, it would appear likely that this effect contributed to the excessive rainfall totals and flooding.

Chapter 7

Conclusions and Future Work

Extreme climatic rainfall—defined in this thesis as extreme rainfall over monthly, seasonal or annual timescales with a return period of 10 years or more—is common in Thailand due to its tropical location and monsoonal climate. Flooding caused by persistent heavy rainfall occurs regularly in the country and often results in considerable damage to homes, businesses and sites of historical interest. Despite the substantial impacts from extreme climatic rainfall events in Thailand, there is little detailed historical information regarding the incidence of such events. The aim of this thesis was to quantify the incidence of extreme climatic rainfall in Thailand, and to clarify the causes and impacts of this rainfall.

I produced extreme rainfall return periods for all 0.5° grid squares in Thailand at multiple climatic timescales (monthly to annual) using 112 years of data (1901–2012; Chapter 3). These were computed using two methods: the basic method (Section 3.2.3) and the distribution method (Section 3.2.4). The basic method is simple but limited; it is not possible to estimate return periods longer than the length of the dataset, and it is not possible to estimate uncertainty. The distribution method is more complex and uses distribution fitting to estimate return periods longer than the dataset length. This second method also allows the estimation of uncertainty. These return periods give the probability of occurrence of extreme climatic rainfall, information that can benefit a variety of industrial sectors (e.g. planning, insurance, public safety).

I applied this return period analysis to examine the climatic rainfall associated with the 2011 Thailand flood—the country's most damaging flood to date—and to assess the causes and impacts of this extreme rainfall (Chapter 4). The flooding was caused by an unusually strong summer monsoon (Section 4.4.2) and by four tropical storm remnants that crossed the north and east of the country (Section 4.4.3), which both contributed to an accumulation of heavy rainfall throughout

the year. The 2010–2011 multi-year La Niña also contributed to this excess rainfall. These factors combined to produce the highest recorded annual rainfall in Thailand (Section 4.4.1).

I used four different methods to estimate the re-occurrence likelihood of a Thai flood of the magnitude of 2011. First, the Dartmouth Flood Observatory Global Active Archive of Large Flood Events ranks the event's magnitude fifth highest (1985–2012), suggesting a return period of 5 to 6 years (Section 4.2.2). However, recent improvements to the Thai flood defences may bias this estimate short. Secondly, satellite-derived river flows at two locations on the Chao Phraya River suggest a return period of 10–20 years (Section 4.5.3). However, this estimate may not be reliable due to the lack of data used in the return period calculation (only 10 years). Thirdly, pan-Thailand station rainfall data from the Thai Meteorological Department (TMD) (1992–2011) suggest a return period for annual precipitation that varies from 8–20 years in the Chao Phraya River (Section 4.5.2). However, since the available precipitation records limit this technique to identifying return periods of up to 20 years, these values may be biased short. Fourthly, extended gridded rainfall data from the Climatic Research Unit (CRU) suggest a return period for annual precipitation in the Chao Phraya River of 164 years (Section 4.5.2). This method used distribution fitting to calculate return periods, which allows for estimation of return periods beyond the length of the dataset.

Bringing together these different return periods, it is difficult to estimate a 'consensus' return period for the 2011 Thai flood. I estimate the return period of the 2011 flood to be between 20 and 164 years. The flood primarily affected the Chao Phraya River, so this 'consensus' estimate reflects the range of return period estimates for the basin. Despite the uncertainty around the 2011 Thailand flood return period, one can reasonably expect that another Thailand flood as devastating as in 2011 will occur within the next 1–2 centuries unless flood defences and management practices are improved.

I also examined five further case studies of climatic Thai flooding events; these occurred in 1942, 1983, 1995, 2002 and 2006 (Chapter 5). Like the 2011 flood, these five historical flood events were all associated with extreme climatic rainfall

on monthly timescales or longer, although the rainfall return periods varied vastly across the different events (from 18 years to 1174 years). Although the rainfall return period is a good indicator of the severity of rainfall, analysis of these events showed that it does not necessarily correlate with the severity of the associated flood. Many other factors (e.g. flood protection, topography, land use) play a role in determining the severity of a flood event.

Chapters 4 and 5, alongside limited previous studies, suggest a link between El Niño Southern Oscillation (ENSO) and climatic rainfall in Thailand. Using observational data, I established a new and physically sound method for examining the contemporaneous link between these two variables (Chapter 6). I found a significant and stationary relationship between ENSO and rainfall in Thailand; on average, annual Thailand rainfall during a La Niña phase was 8.7 % higher than during an El Niño phase (Section 6.3.1). Furthermore, multi-year ENSO events (those that persist in the same phase for more than one year; Section 6.2.3) were associated with larger and more significant annual and summer monsoonal rainfall anomalies across much of Thailand. Annual rainfall during multi-year La Niña events was 14.4 % higher than during multi-year El Niño events. This analysis raised an important question: can one anticipate, after one year, whether an ENSO event will persist for further year(s), and hence cause stronger rainfall anomalies in Thailand? Overall, there was no clear evidence that suggested stronger events were more likely to persist, but other potential causes were not examined (Section 6.3.4).

During the preparation of this thesis, one of the strongest El Niño events on record occurred—the El Niño from November 2014 to May 2016. I briefly examined this ENSO event to assess whether the Thailand rainfall associated with this event followed the pattern seen in Chapter 6. As this event primarily occurred in 2015, I focussed my examination on this year. I calculated the annual-weighted Southern Oscillation Index (SOI) for 2015 using the method described in Section 2.3.1; the SOI was strongly negative (−14.1; ranked 5th in terms of El Niño strength). According to the TMD Annual Weather Summary for 2015 (Thai Meteorological Department, 2015), annual rainfall was below the 1981–2010 normal (−11 %). On a monthly timescale, rainfall was below normal during

9 months of 2015. Spatially, the below-average rainfall anomalies affected much of the country. Therefore, the Thailand rainfall pattern observed in this thesis was also observed during the most recent ENSO event.

As with all scientific research, this work is not without its weaknesses and limitations. The primary issue underlying all work contained within this thesis is that of precipitation data accuracy. Chapter 2, and the comparison with Promchote et al. (2016) in Chapter 4, showed much variation in Thailand rainfall between different datasets. Variation between gridded datasets is understandable due to the differences in gridding methods, but why is there so much variation in station data when the measurements reported are from the exact same location and rain gauge? And how are we to know which data are correct? All results reported in this thesis rely on the underlying precipitation data, so it is important that these are as accurate as possible. It would be useful to perform return period analysis using a variety of different underlying datasets to assess the effect this has on results. In particular, I would like to use version 7 of the Global Precipitation Climatology Center (GPCC) dataset (1901–2013) as there are more underlying stations in Thailand than in the current CRU dataset, and the length also allows analysis of the 2011 flood (unlike the previous GPCC version).

I developed the method used to estimate return periods in Chapter 3 to be easily applicable to other countries worldwide. However, it requires some modifications before this can be done. I only used four grid squares to select the three most suitable distributions (gamma, Generalized Extreme Value (GEV), normal) for the entire country. The process I used was too labour-intensive to apply to each of Thailands 233 grid squares. Before applying this method to other countries, the distribution selection process must be automated and applied to the climatic rainfall distributions at each timescale in each individual grid square. Implementing this automation would ensure the fitted distributions are the most accurate models of climatic rainfall in each individual grid square, and hence ensure the climatic rainfall return periods are as accurate as possible given the underlying dataset used. Additionally, in some of the return period curves shown, the highest ten or so observations appeared to follow a different distribution to the

one fitted to the entire data series. This could be examined further by applying the Peak-Over-Threshold method of extreme value theory (EVT) (e.g. Palutikof et al., 1999). This could provide better distributions fits to the upper portion of the data, and hence more accurate extreme climatic rainfall return periods.

The case studies in Chapters 4 and 5 present a good initial analysis of the climate causes and rainfall return periods of each historical Thailand flood event, particularly the 2011 flood, which I examined in more detail than the other events. However, I feel that a more in-depth analysis of these events is needed to glean as much information as possible regarding extreme climatic flood events in Thailand. At a minimum, it would be useful to examine the strength of the monsoon and the possible effect of ENSO on the rainfall during each of the Chapter 5 events. For all six events discussed in this work, it would be beneficial to use detailed river flow data to link the extreme climatic rainfall with the subsequent river flooding. This would provide a greater understanding of the impact of extreme climatic rainfall. Extensive Thailand river flow data are available from the Royal Irrigation Department (e.g. Aon Benfield, 2012a; Kure and Tebakari, 2012; Lim et al., 2012), but I was, unfortunately, unable to establish contact with them during my research period.

Although the results in Chapter 6 greatly extended our knowledge of the observational relationship between ENSO and climatic rainfall in Thailand, I was unable to establish the cause(s) of ENSO event persistence, and hence the cause(s) of stronger rainfall anomalies in the country. This information is vital as prediction of these multi-year ENSO events would be greatly beneficial to a variety of sectors (e.g. planning, insurance, public safety). I believe that examination of the atmospheric conditions related to these ENSO events may assist the identification of the cause(s) of ENSO event persistence.

To conclude, this thesis has quantified the incidence of extreme climatic rainfall in Thailand using return period analysis, and clarified the causes and impacts of such rainfall. I believe this is the first study of its kind for extreme climatic rainfall in Thailand. Extreme climatic rainfall not only affects Thailand, but many other countries worldwide. I envisage that, following some improvements, the techniques developed within this work will be applied elsewhere.

Appendix A

Station data

Table A.1: Details of the Thai precipitation stations contained in the Met Office Integrated Data Archive System (MIDAS), Thai Meteorological Department (TMD), National Climatic Data Center (NCDC) and Climatic Research Unit (CRU) datasets. For each station the location, time period covered and the percentage of missing data within that time period is given. All TMD stations have a time period of 1992–2011.

			CRU		MIDAS		NCDC		TMD
Station name	Lat. (°N)	Lon. (°E)	Time Period	Missing Data (%)	Time Period	Missing Data (%)	Time Period	Missing Data (%)	Missing Data (%)
Aranyaprathet	13.7	102.5	1932–2012	3.9	1985–2011	10.0	1954–2011	40.1	0.2
Bang Na Agromet	13.7	100.6			2008–2011	10.2	2008–2011	46.6	0.0
Bangkok	13.7	100.6	1882–2012	9.9	1989–2011	3.0	1954–2011	37.3	0.4
Bangkok Pilot	13.4	100.6							0.4
Bhumibol Dam	17.2	99.1	1960–2000	4.7	1989–2011	10.1	1973–2011	30.0	0.4
Bua Chum	15.3	101.2			1985–2011	8.9	1974–2011	59.1	0.4
Chachoengsao Agromet	13.6	101.5							0.4
Chai Nat Agromet	15.2	100.2							0.0
Chaiyaphum	15.8	102.0	1911–2000	10.2	1989–2011	7.3	1960–2011	41.3	0.0
Chanthaburi	12.6	102.1	1911–2012	1.3	1985–2011	7.5	1954–2011	37.6	0.0
Chiang Mai	18.8	99.0	1911–2012	3.8	1985–2011	4.0	1943–2011	43.7	0.4
Chiang Rai	20.0	99.9	1911–2012	8.9	1989–1993	22.4	1956–2011	43.0	0.5
Chiang Rai Agromet	19.9	99.8							0.0
Chok Chai	14.7	102.2							0.8
Chon Buri	13.4	101.0	1911–2000	0.6	1985–2011	9.3	1954–2011	46.3	0.0

Continued on next page

Table A.1: (Continued)

			CRU		MIDAS		NCDC		TMD
Station name	Lat. (°N)	Lon. (°E)	Time Period	Missing Data (%)	Time Period	Missing Data (%)	Time Period	Missing Data (%)	Missing Data (%)
Chumphon	10.5	99.2	1911–2012	1.5	1989–2011	7.9	1954–2011	37.1	7.3
Doi Musor Agromet	16.8	98.9							1.0
Don Muang	13.9	100.6	1951–1990	0.0	1985–2011	11.0	1943–2011	45.8	0.0
Hat Yai	6.9	100.4			1989–2011	8.9	1973–2011	17.5	0.0
Hua Hin	12.6	100.0	1942–2000	10.7	1993–2011	4.7	1954–2011	42.2	0.4
Huai Pong Agromet	12.7	101.1							0.0
Kabin Buri	14.0	101.7							0.0
Kamphaeng Phet	16.5	99.5			1989–2011	8.3	1979–2011	62.4	0.4
Kamphaeng Saen	14.0	100.0							0.0
Kanchanaburi	14.0	99.5	1913–2000	6.8	1989–1993	28.3	1954–2011	46.4	0.4
Khlong Yai	11.8	102.9	1932–2000	5.6	1985–2011	4.2	1956–2011	45.8	0.4
Kho Hong Agromet	7.0	100.5							0.1
Khon Kaen	16.4	102.8	1914–2000	2.1	1989–2011	8.3	1954–2011	42.1	0.0
Ko Lanta	7.5	99.1			1989–2011	7.8	1954–2011	58.8	0.0
Ko Samui	9.5	100.1			1989–1993	19.7	1973–2011	26.0	0.4
Ko Sichang	13.2	100.8	1959–2000	0.6	1989–2011	8.4	1962–2011	47.6	0.4
Kosum Phisai	16.2	103.1							0.0

Continued on next page

Table A.1: (Continued)

			CRU		MIDAS		NCDC		TMD
Station name	Lat. (°N)	Lon. (°E)	Time Period	Missing Data (%)	Time Period	Missing Data (%)	Time Period	Missing Data (%)	Missing Data (%)
Lampang	18.3	99.5	1911–2000	1.3	1989–2011	7.0	1954–2011	43.5	7.5
Lampang Agromet	18.3	99.3							0.4
Lamphun	18.6	99.0			1985–2011	7.0	1985–2011	37.0	0.0
Loei	17.5	101.7	1911–2000	4.2	1989–2011	9.3	1954–2011	43.1	0.4
Loei Agromet	17.4	101.7							0.4
Lom Sak	16.8	101.2	1911–2000	1.0					0.1
Lopburi	14.8	100.6	1911–2000	1.0	1985–2011	6.7	1954–2011	46.2	0.1
Mae Hong Son	19.3	97.8	1911–2000	6.5	1989–2011	8.2	1959–2011	38.8	0.0
Mae Sariang	18.2	97.9	1932–2000	4.6	1985–2011	7.7	1960–2011	40.6	0.1
Mae Sot	16.7	98.6	1941–2000	5.0	1989–2011	8.2	1954–2011	44.6	0.0
Mukdahan	16.5	104.7	1934–2000	3.7	1989–2011	8.1	1954–2011	44.4	0.0
Nakhon Phanom	17.4	104.8	1912–2000	4.5	1985–2011	8.5	1954–2011	45.8	0.0
Nakhon Phanom Agromet	17.3	104.8							0.0
Nakhon Ratchasima	15.0	102.1	1911–2012	2.0	1985–2011	8.9	1954–2011	39.8	0.4
Nakhon Sawan	15.7	100.1	1911–2012	7.0	1989–2011	8.2	1954–2011	42.7	0.0
Nakhon Si Thammarat	8.4	100.0	1912–2000	3.0	1985–2011	7.6	1954–2011	41.1	0.5
Nakhon Si Thammarat Agromet	8.3	100.1							0.0

Continued on next page

Table A.1: (Continued)

			CRU		MIDAS		NCDC		TMD
Station name	Lat. (°N)	Lon. (°E)	Time Period	Missing Data (%)	Time Period	Missing Data (%)	Time Period	Missing Data (%)	Missing Data (%)
Nan	18.8	100.8	1911–2000	1.9	1985–2011	9.3	1954–2011	42.1	0.8
Nan Agromet	18.9	100.8							0.4
Nang Rong	14.6	102.7							0.1
Narathiwat	6.4	101.8	1914–2000	4.8	1989–2011	8.0	1955–2011	40.5	0.0
Nong Khai	17.9	102.7	1965–2000	1.6	1989–1993	21.9	1973–2011	26.6	0.4
Nong Phlap	12.6	99.7							0.7
Pak Chong	14.6	101.3							0.4
Phatthalung Agromet	7.6	100.2							0.4
Pattani	6.8	101.2			1989–2011	7.0	1973–2011	32.0	0.4
Pattaya	12.9	100.9							0.1
Phetchaburi	13.2	100.1			1989–2011	9.3	1978–2011	55.2	0.0
Phayao	19.2	99.9			1993–2011	5.5	1987–2011	29.7	0.0
Phetchabun	16.4	101.2	1912–2000	5.5	1985–2011	7.6	1954–2011	43.3	0.0
Phitsanulok	16.8	100.3	1911–2012	1.6	1989–2011	8.2	1954–2011	41.2	0.4
Phlew Agromet	12.5	102.2							0.0
Phrae	18.2	100.2	1912–2000	4.6	1989–1993	19.5	1954–2011	45.0	0.4
Phuket	7.9	98.4	1951–2000	0.5	1989–2011	7.3	1954–2011	50.0	0.1

Continued on next page

Table A.1: (Continued)

			CRU		MIDAS		NCDC		TMD
Station name	Lat. (°N)	Lon. (°E)	Time Period	Missing Data (%)	Time Period	Missing Data (%)	Time Period	Missing Data (%)	Missing Data (%)
Phuket Airport	8.1	98.3	1911–2012	9.3			1957–2011	38.4	
Phichit	16.4	100.3							0.4
Prachinburi	14.0	101.4	1911–2000	1.0	1985–2011	7.4	1954–2011	43.8	0.0
Prachuap Khiri Khan	11.8	99.8	1932–2012	4.4	1989–2011	9.1	1954–2011	41.2	0.1
Ranong	10.0	98.6			1989–2011	7.2	1959–2011	33.4	0.0
Ratchaburi Agromet	13.5	99.8							0.4
Rayong	12.6	101.3							0.4
Roi Et	16.1	103.7	1911–2000	0.6	1985–2011	7.9	1954–2011	46.3	0.0
Roi Et Agromet	16.1	103.6							0.4
Sakon Nakhon 2	17.1	104.1							0.0
Sakon Nakhon	17.2	104.1	1911–2000	1.9	1989–2011	10.2	1954–2011	43.2	1.0
Sattahip	12.7	101.0	1938–2000	0.5	1989–2011	11.5	1955–2011	46.9	2.3
Satun	6.7	100.1							0.4
Sawi Agromet	10.3	99.1							0.8
Songkhla	7.2	100.6	1911–2012	2.2	1985–2011	4.7	1943–2011	39.4	0.1
Sisaket Agromet	15.1	104.3							0.5
Sukhothai	17.1	99.8					2008–2011	55.9	

Continued on next page

Table A.1: (Continued)

			CRU		MIDAS		NCDC		TMD
Station name	Lat. (°N)	Lon. (°E)	Time Period	Missing Data (%)	Time Period	Missing Data (%)	Time Period	Missing Data (%)	Missing Data (%)
Suphan Buri	14.5	100.1	1911–2000	1.3	1989–2011	8.3	1954–2011	52.2	0.0
Surat Thani	9.1	99.4	1914–1998	2.9	1985–2011	9.0	1954–2011	38.5	
Surat Thani Agromet	9.1	99.7							0.8
Surin	14.9	103.5	1911–2002	3.0	1985–2011	9.9	1954–2011	45.7	0.0
Surin Agromet	14.9	103.4							0.4
Tak	16.9	99.0	1911–2000	4.1	1989–2011	9.8	1955–2011	46.5	0.0
Tak Fa Agromet	15.3	100.5							0.4
Taphra Agromet	16.3	102.8							0.4
Tha Tum	15.3	103.7			1989–1993	19.8	1974–2011	58.1	0.4
Tha Wang Pha	19.1	100.8			1989–1993	22.8	1974–2011	62.6	0.4
Thong Pha Phum	14.8	98.6					1974–2011	52.0	
Trang	7.5	99.6	1911–2000	0.5	1985–2011	10.1	1962–2011	32.0	0.0
U Thong Agromet	14.3	99.9							0.0
Ubon Ratchathani	15.2	104.9	1911–2012	8.8	1985–2011	8.1	1954–2011	42.8	0.4
Ubon Ratchathani Agromet	15.2	105.0							0.0
Udon Thani	17.4	102.8	1911–2012	1.8	1989–2011	8.4	1943–2011	43.4	0.4
Umphang	16.0	98.9							0.4

Continued on next page

Table A.1: (Continued)

			CRU		MIDAS		NCDC		TMD
Station name	Lat. (°N)	Lon. (°E)	Time Period	Missing Data (%)	Time Period	Missing Data (%)	Time Period	Missing Data (%)	Missing Data (%)
Uttaradit	17.6	100.1	1915–2000	0.9	1989–2011	9.1	1954–2011	43.0	0.0
Wichian Buri	15.6	101.1			1989–1993	20.2	1974–2011	62.6	5.3
Yala Agromet	6.5	101.3							0.4

Appendix B

Lilliefors test

Table B.1: Table showing the percentage of grid squares that failed the Lilliefors test when applied to all 112 years of data. The results are shown for each distribution and timescale. The shading marks the most successful distribution(s) for each timescale.

		Failed grid squares (%)		
Timescale		Gamma	GEV	Normal
Annual		3.4	4.3	5.2
Summer monsoonal		4.3	7.7	7.7
Seasonal	NDJ	29.2	36.1	83.3
	DJF	29.6	39.1	86.3
	JFM	15.0	15.9	78.1
	FMA	25.8	1.7	35.6
	MAM	14.6	9.0	25.3
	AMJ	7.7	5.2	24.0
	MJJ	3.0	7.3	17.2
	JJA	9.0	7.3	16.3
	JAS	7.7	7.7	9.0
	ASO	3.9	3.4	10.3
	SON	6.0	5.2	25.8
	OND	18.0	6.0	31.8
Monthly	Jan	79.0	76.4	45.1
	Feb	69.1	59.7	80.7
	Mar	34.3	33.0	91.8
	Apr	24.9	9.4	64.8
	May	11.6	4.3	28.8
	Jun	3.4	6.0	38.6
	Jul	9.0	6.9	40.8
	Aug	8.2	8.2	30.5
	Sep	5.2	3.0	26.2
	Oct	19.3	9.0	57.5
	Nov	45.9	50.6	85.4
	Dec	75.5	76.8	45.9

Table B.2: As Table B.1 but for the upper 25 % of the data only.

		Failed grid squares (%)		
Timescale		Gamma	GEV	Normal
Annual		3.9	8.6	7.7
Summer monsoonal		4.7	12.0	7.7
Seasonal	NDJ	8.2	12.9	58.4
	DJF	2.6	19.7	49.8
	JFM	3.4	3.0	32.2
	FMA	4.7	0.0	15.9
	MAM	10.3	14.6	28.3
	AMJ	7.3	7.7	15.9
	MJJ	8.2	11.2	18.5
	JJA	4.3	9.9	14.2
	JAS	4.3	11.2	7.7
	ASO	3.0	6.9	7.3
	SON	4.7	9.0	12.0
	OND	7.7	5.6	20.2
Monthly	Jan	9.4	78.5	94.8
	Feb	6.4	58.8	67.4
	Mar	3.0	21.9	53.2
	Apr	3.4	2.1	30.5
	May	11.6	12.9	27.0
	Jun	6.0	6.4	22.3
	Jul	10.7	6.9	36.9
	Aug	5.6	7.3	22.7
	Sep	7.7	7.3	23.6
	Oct	8.2	7.3	30.0
	Nov	6.4	32.6	69.5
	Dec	10.3	75.5	85.0

Table B.3: As Table B.1 but for the upper 5 % of the data only.

		Failed grid squares (%)		
Timescale		Gamma	GEV	Normal
Annual		14.2	15.0	3.9
Summer monsoonal		15.5	7.7	2.6
Seasonal	NDJ	6.9	33.0	3.4
	DJF	4.7	47.6	10.7
	JFM	15.5	18.5	2.6
	FMA	36.1	3.0	2.1
	MAM	17.2	6.4	1.3
	AMJ	10.7	6.4	0.4
	MJJ	5.2	7.3	0.0
	JJA	9.9	9.9	1.3
	JAS	16.3	15.5	3.9
	ASO	7.7	6.0	1.3
	SON	8.2	7.7	0.9
	OND	25.8	6.4	0.4
Monthly	Jan	5.2	82.8	40.3
	Feb	0.9	93.1	23.2
	Mar	6.4	45.9	8.2
	Apr	27.5	6.0	0.4
	May	19.3	12.4	1.7
	Jun	11.2	9.0	0.0
	Jul	8.2	4.3	0.0
	Aug	17.2	9.0	1.7
	Sep	8.2	4.7	0.4
	Oct	31.3	6.9	0.9
	Nov	2.1	60.1	7.3
	Dec	12.9	83.7	29.2

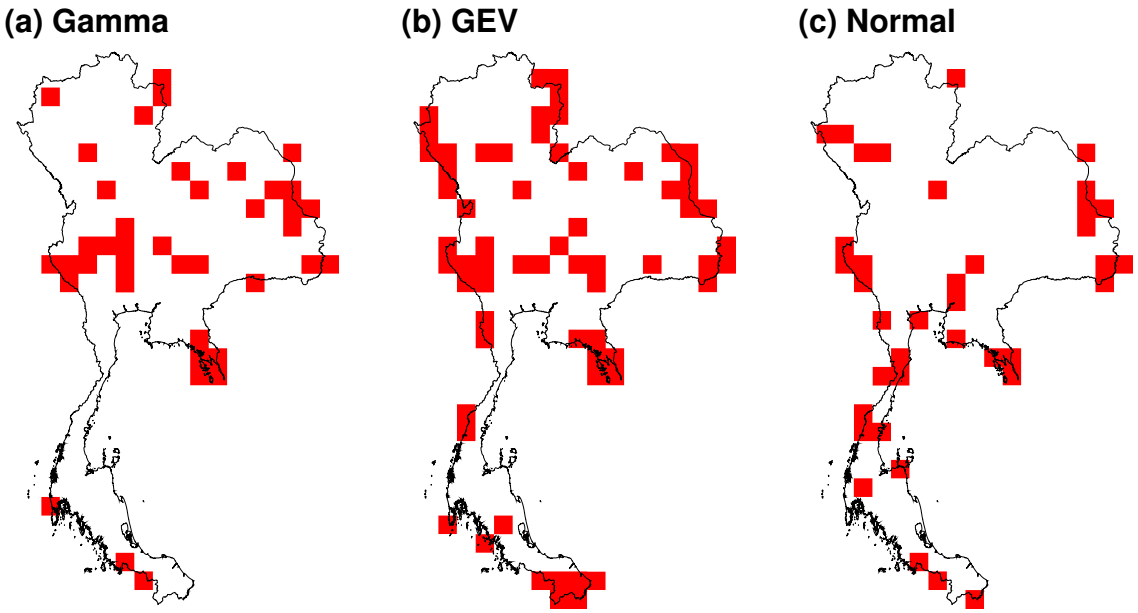

Figure B.1: As Figure 3.9 but for May–October (MJJASO) precipitation.

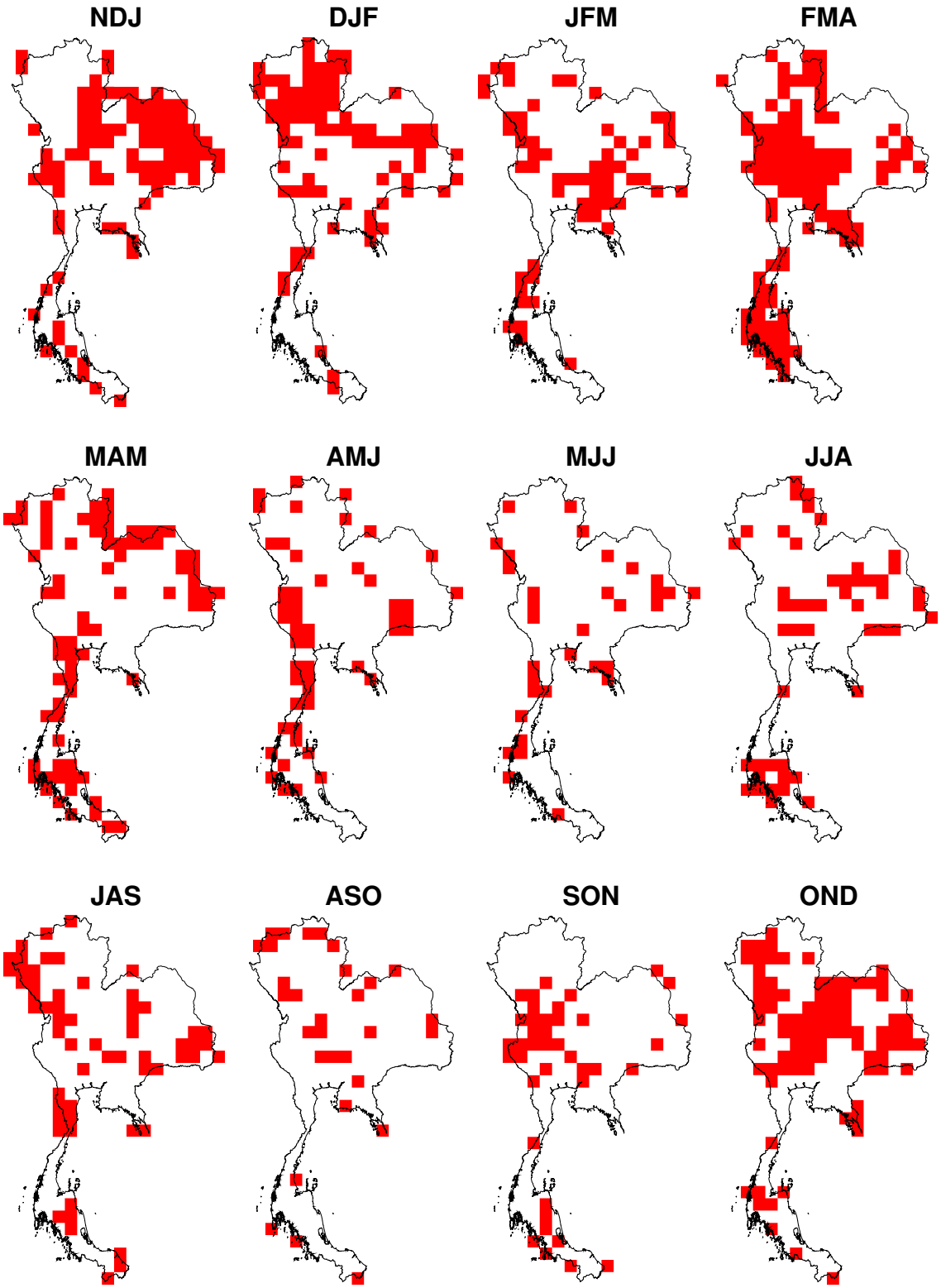

Figure B.2: As Figure 3.9 but for seasonal precipitation using the gamma distribution only.

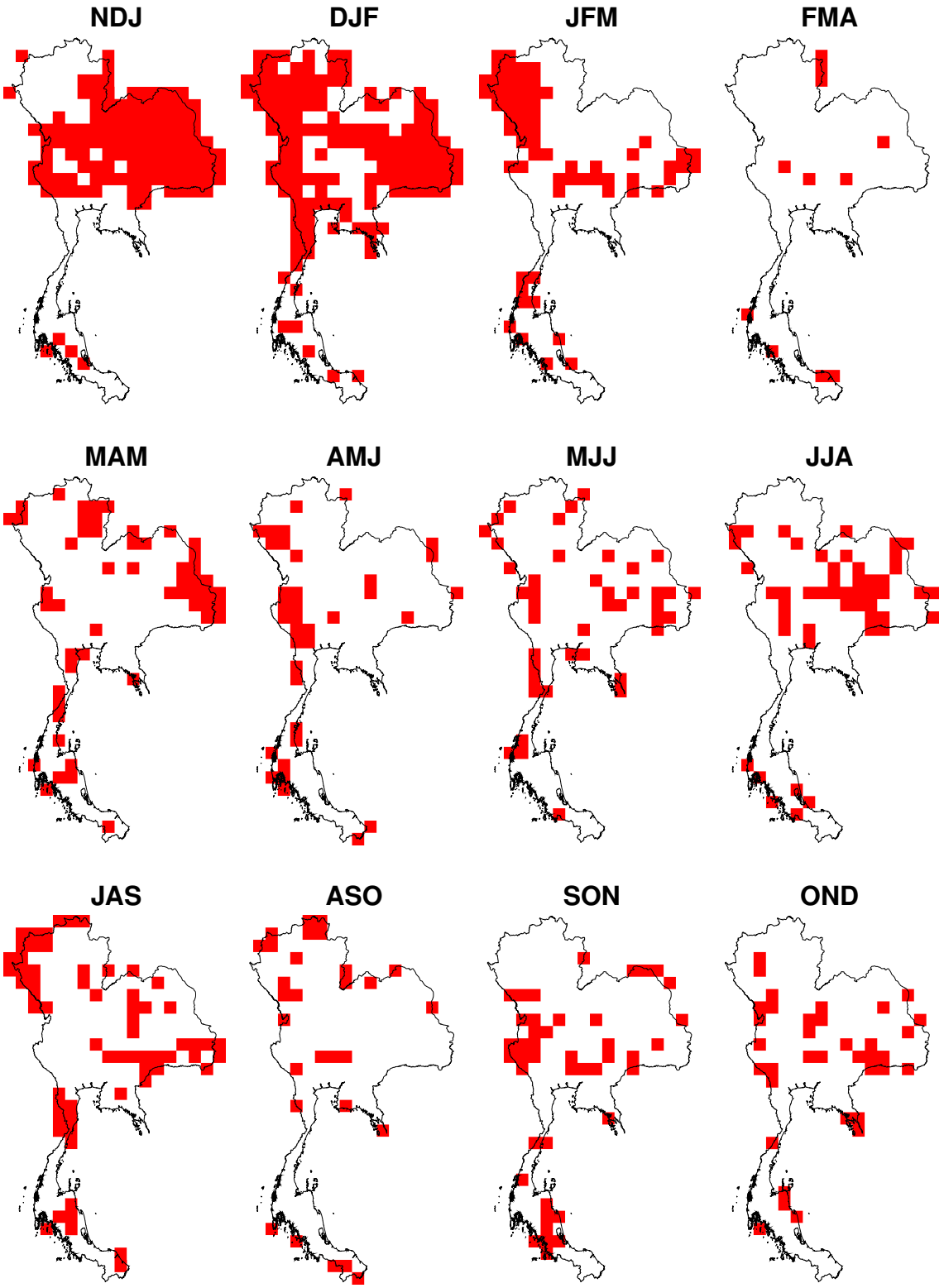

Figure B.3: As Figure 3.9 but for seasonal precipitation using the Generalized Extreme Value (GEV) distribution only.

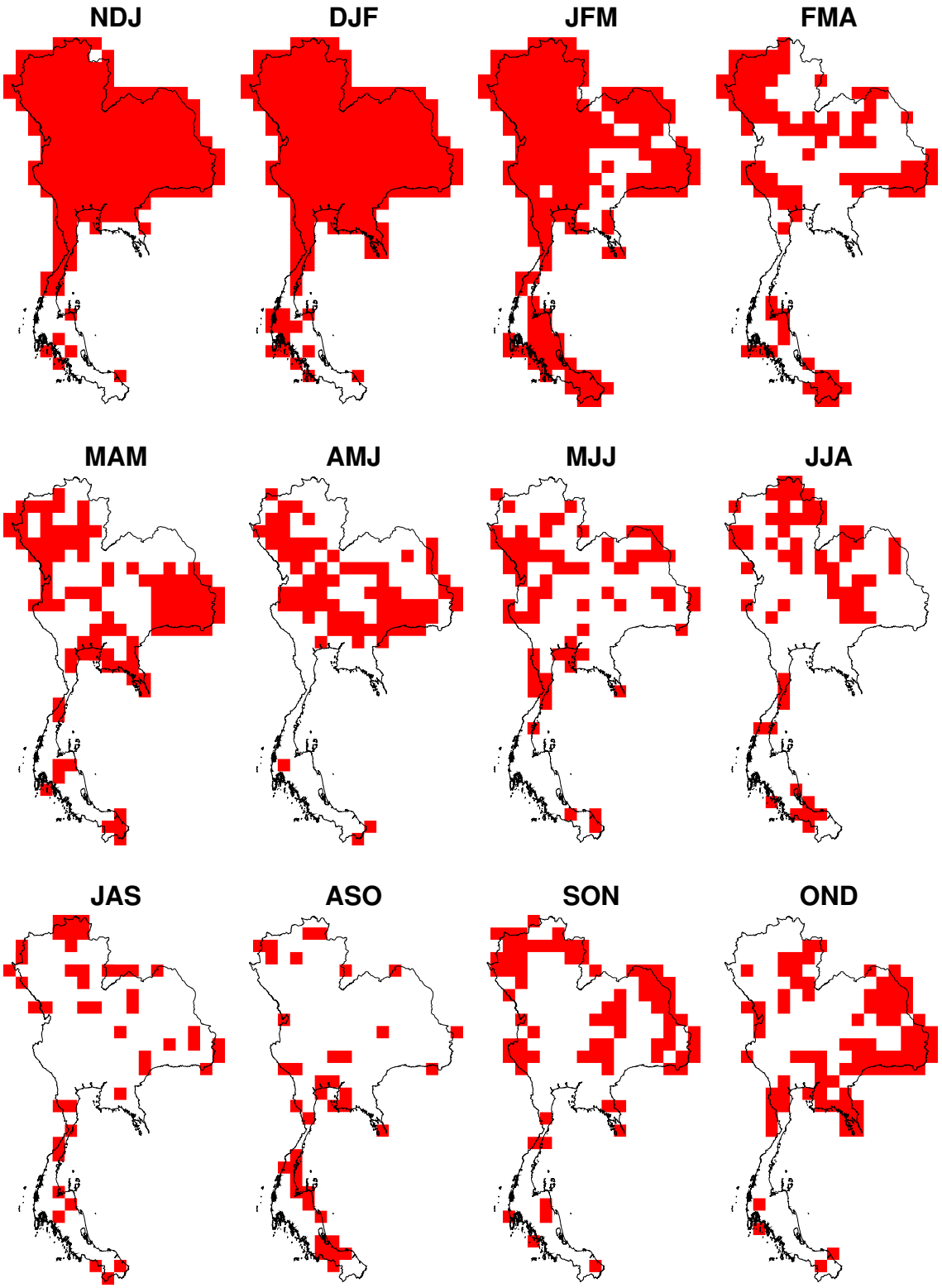

Figure B.4: As Figure 3.9 but for seasonal precipitation using the normal distribution only.

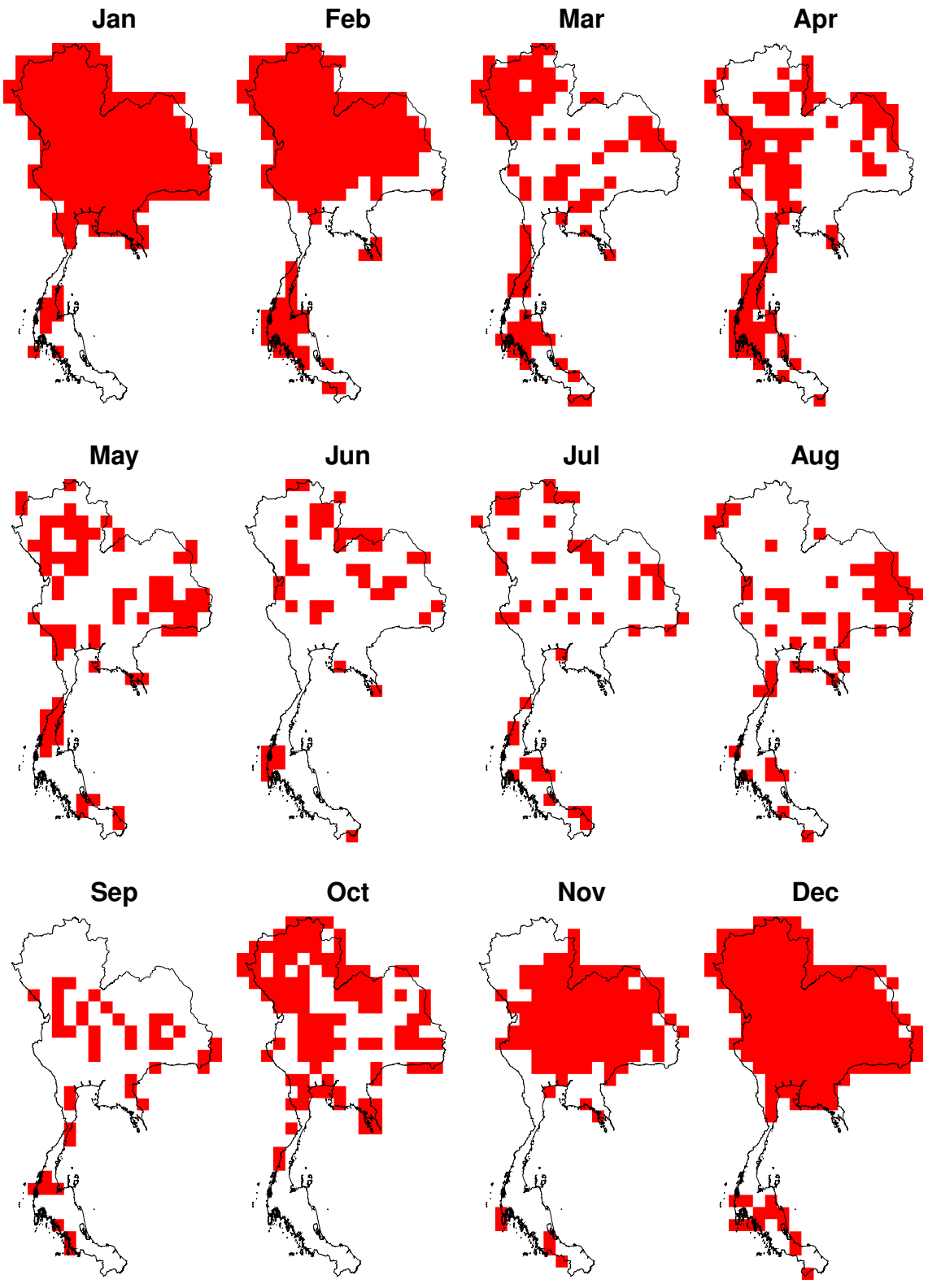

Figure B.5: As Figure 3.9 but for monthly precipitation using the gamma distribution only.

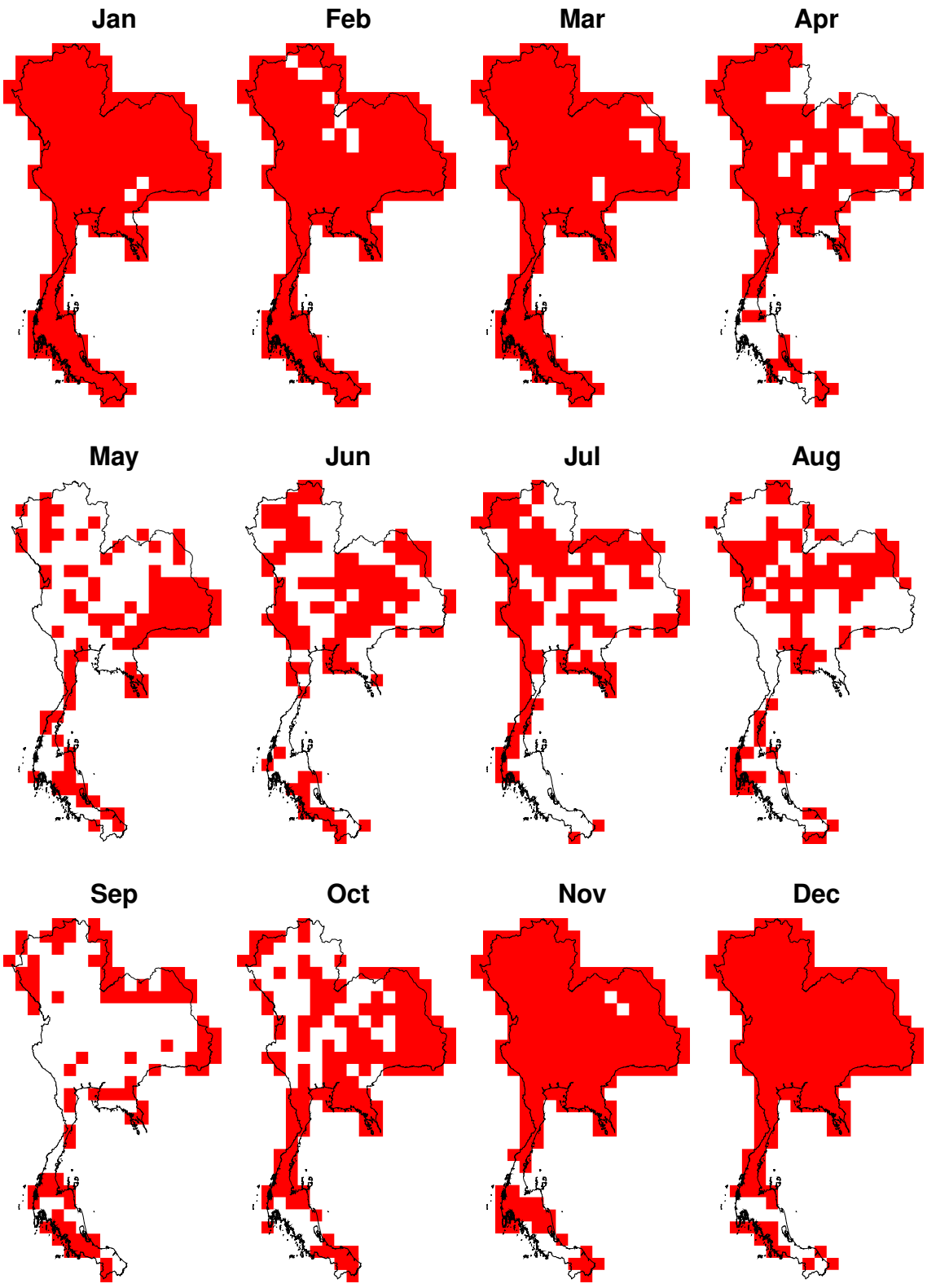

Figure B.6: As Figure 3.9 but for monthly precipitation using the normal distribution only.

Appendix C

ENSO events

Table C.1: As Table 6.1 but for the early period (1901–1950).

La Niña		El Niño	
Single-year	Multi-year	Single-year	Multi-year
1903	1908–1910	1902	1911–1914
1906	1916–1917	1905	1940–1941
1921		1919	
1924		1923	
1931		1925	
1938		1932	
1945		1946	
1950			

Table C.2: As Table 6.1 but for the late period (1951–2011).

La Niña		El Niño	
Single-year	Multi-year	Single-year	Multi-year
1964	1955–1956	1953	1991–1994
1996	1970–1971	1957	
1998	1973–1975	1965	
2008	1988–1989	1969	
	2010–2011	1972	
		1977	
		1982	
		1987	
		1997	
		2002	
		2006	

Table C.3: As Table C.2 but using the Oceanic Niño Index (ONI).

La Niña		El Niño	
Single-year	Multi-year	Single-year	Multi-year
1964	1954–1956	1951	1957–1958
1971	1973–1975	1953	
1985	1998–2000	1963	
1988		1965	
2007		1969	
2010		1972	
		1982	
		1987	
		1991	
		1997	
		2002	
		2004	
		2009	

Appendix D

ENSO events: unweighted

Table D.1: As Table 6.1 but for the full period (1901–2011) using the unweighted Southern Oscillation Index (SOI).

La Niña		El Niño	
Single-year	Multi-year	Single-year	Multi-year
1903	1916–1917	1905	1911–1914
1910	1921–1922	1919	1940–1941
1924	1928–1929	1926	1965–1966
1938	1955–1956	1946	1982–1983
1945	1973–1975	1953	1991–1994
1950	1988–1989	1957	2004–2005
1962	1999–2000	1969	
1964	2010–2011	1972	
1971		1977	
1996		1987	
2008		1997	
		2002	

Table D.2: As Table 6.1 but for the early period (1901–1950) using the unweighted Southern Oscillation Index (SOI).

La Niña		El Niño	
Single-year	Multi-year	Single-year	Multi-year
1903	1916–1917	1905	1911–1915
1910	1921–1922	1919	1940–1941
1924	1928–1929	1923	
1938		1926	
1943		1932	
1945		1946	
1950			

Table D.3: As Table 6.1 but for the late period (1951–2011) using the unweighted Southern Oscillation Index (SOI).

La Niña		El Niño	
Single-year	Multi-year	Single-year	Multi-year
1964	1955–1956	1953	1982–1983
1971	1973–1975	1965	1991–1994
1996	1988–1989	1969	
2008	1999–2000	1972	
	2010–2011	1977	
		1987	
		1997	
		2002	
		2004	

Table D.4: As Table 6.1 but for the full period (1901–2011) using the unweighted Oceanic Niño Index (ONI).

La Niña		El Niño	
Single-year	Multi-year	Single-year	Multi-year
1971	1955–1956	1953	1957–1958
2011	1973–1975	1963	1991–1992
	1984–1985	1965	
	1988–1989	1969	
	1999–2000	1972	
	2007–2008	1977	
		1982	
		1987	
		1994	
		1997	
		2002	

Appendix E

ENSO events: shorter periods

Table E.1: As Table 6.1 but using the 90-year period 1911–2000.

La Niña		El Niño	
Single-year	Multi-year	Single-year	Multi-year
1921	1916–1917	1919	1911–1914
1924	1955–1956	1923	1940–1941
1931	1970–1971	1925	1991–1994
1938	1973–1975	1946	
1945	1988–1989	1953	
1950		1957	
1962		1965	
1964		1969	
1981		1972	
1996		1977	
1998		1982	
2000		1987	
		1997	

Table E.2: As Table 6.1 but using the 101-year period 1911–2011.

La Niña		El Niño	
Single-year	Multi-year	Single-year	Multi-year
1921	1916–1917	1919	1911–1914
1924	1955–1956	1923	1940–1941
1931	1970–1971	1925	1991–1994
1938	1973–1975	1946	
1945	1988–1989	1953	
1950	2010–2011	1957	
1962		1965	
1964		1969	
1996		1972	
1998		1977	
2000		1982	
2008		1987	
		1997	
		2002	
		2006	

Appendix F

ENSO events: lag-effect

Table F.1: As Table 6.1 but events were selected by shifting the monthly weights backwards by 1 month.

La Niña		El Niño	
Single-year	Multi-year	Single-year	Multi-year
1902	1908–1910	1905	1911–1914
1906	1916–1917	1919	1940–1941
1924	1955–1956	1923	1982–1983
1931	1973–1975	1926	1991–1994
1938	1988–1989	1946	
1945	1999–2000	1953	
1950	2010–2011	1957	
1962		1965	
1964		1969	
1971		1972	
1996		1977	
2008		1987	
		1997	
		2002	
		2004	
		2006	

Table F.2: As Table F.1 but for a lag of 2 months.

La Niña		El Niño	
Single-year	Multi-year	Single-year	Multi-year
1901	1909–1910	1905	1911–1914
1903	1916–1917	1919	1940–1941
1921	1955–1956	1926	1965–1966
1927	1973–1975	1946	1982–1983
1931	1988–1989	1953	1991–1994
1938	1999–2000	1969	2002–2005
1945	2010–2011	1972	
1950		1977	
1964		1987	
1968		1997	
1971			
1996			
2008			

Table F.3: As Table F.1 but for a lag of 3 months.

La Niña		El Niño	
Single-year	Multi-year	Single-year	Multi-year
1901	1903–1904	1905	1911–1912
1910	1916–1917	1919	1914–1915
1921	1938–1939	1926	1940–1941
1927	1955–1956	1946	1965–1966
1931	1974–1975	1953	1982–1983
1945	1999–2000	1969	1991–1994
1950	2010–2011	1972	1997–1998
1962		1977	2002–2003
1964		1987	
1968		2005	
1971			
1989			
1996			
2008			

Acknowledgements

First and foremost, I'd like to thank my wonderful parents and my long-suffering partner, James, for your unwavering support throughout my PhD. It's been tough, but you've always encouraged me to persevere. I genuinely wouldn't have got to this stage without you. To my best friend, Kay: thank you so much for always being there to cheer me on when I needed it, and for letting me be a part of the lives of your gorgeous children. Their little faces always bring joy to my life. I'd also like to thank all of my Girlguiding family, particularly all of 'my' Brownies. I'm so glad I continued to be your Fluffy Owl throughout my PhD; I've thoroughly enjoyed the fun and laughter of our adventures together. Long may it continue!

On a professional note, I'd like to thank Mark Saunders, my supervisor, and Zsuzsanna Vizi and Adam Lea, my MSSL officemates. Thank you for your guidance, critique and expertise provided throughout the course of my PhD. You've helped develop my skills as a scientist, which is something I will never lose. I wish to thank all the staff at MSSL for making me feel welcome as a Climate Scientist in a sea of Space Scientists; my knowledge of space has increased tremendously thanks to the wonderful talks I have attended throughout my time at the lab.

Finally, I would like to express my gratitude to my financial supporters. Thanks to NERC for funding my PhD studentship, and to Aon Benfield for providing CASE sponsorship during my first year. Also to the UCL Doctoral School and the Royal Meteorological Society for their financial contributions that allowed me to attend multiple conferences throughout my PhD studies.

Bibliography

2bangkok.com, 2016: The Great Flood of 1942. Available online at: http://2bangkok.com/2bangkok-masstransit-flood.html.

Ahrens, C., 2008: *Meteorology Today: An Introduction to Weather, Climate, and the Environment*. 9th ed., Cengage Learning, 624 pp.

Anderson, T. W., and D. A. Darling, 1952: Asymptotic Theory of Certain 'Goodness of Fit' Criteria Based on Stochastic Processes. *The Annals of Mathematical Statistics*, **23**, 193–212, doi:10.1214/aoms/1177729437.

Aon Benfield, 2012a: 2011 Thailand Floods Event Recap Report. Tech. rep., 40 pp.

Aon Benfield, 2012b: Thailand Flood Model. Tech. rep., 2 pp.

APHRODITE, 2013: APHRODITE's Water Resources. Available online at: http://www.chikyu.ac.jp/precip/.

Artlert, K., C. Chaleeraktrakoon, and V. Nguyen, 2013: Modeling and analysis of rainfall processes in the context of climate change for Mekong, Chi, and Mun River Basins (Thailand). *Journal of Hydro-environment Research*, **7**, 2–17, doi:10.1016/j.jher.2013.01.001.

Australian Bureau of Meteorology, 2014: Southern Oscillation Index (SOI) Archives. Available online at: http://www.bom.gov.au/climate/current/soihtm1.shtml.

Australian Bureau of Meteorology, 2015: Climate Glossary - Southern Oscillation Index (SOI). Available online at: http://www.bom.gov.au/climate/glossary/soi.shtml.

Becker, A., P. Finger, A. Meyer-Christoffer, B. Rudolf, K. Schamm, U. Schneider, and M. Ziese, 2013: A description of the global land-surface precipitation

data products of the Global Precipitation Climatology Centre with sample applications including centennial (trend) analysis from 1901–present. *Earth System Science Data*, **5**, 71–99, doi:10.5194/essd-5-71-2013.

Ben-Gai, T., A. Bitan, A. Manes, P. Alpert, and S. Rubin, 1998: Spatial and temporal changes in rainfall frequency distribution patterns in Israel. *Theoretical and Applied Climatology*, **61**, 177–190, doi:10.1007/s007040050062.

Berolo, W., 2013: Assessment of 10 year and 100 year return period monthly rainfall. Available online at: http://gravitaire.oca.eu/spip.php?article185.

Box, G., G. Jenkins, and G. Reinsel, 2008: *Time Series Analysis: Forecasting and Control*. 4th ed., John Wiley & Sons, Ltd, 746 pp.

Brakenridge, G., 2012: Global Active Archive of Large Flood Events. Available online at: http://floodobservatory.colorado.edu/Archives/index.html.

Brakenridge, G., S. Cohen, and A. J. Kettner, 2012: Satellite River Discharge Measurements. Available online at: http://floodobservatory.colorado.edu/IndexMapweb.htm.

Bricquet, J. P., A. Boonsaner, T. Phommassack, and T. D. Toan, 2003: Statistical analysis of long series rainfall data: a regional study in Southeast Asia. *Integrated watershed management for land and water conservation and sustainable agricultural production in Asia*, Hanoi, Vietnam, 158–162.

Bridhikitti, A., 2013: Connections of ENSO/IOD and aerosols with Thai rainfall anomalies and associated implications for local rainfall forecasts. *International Journal of Climatology*, **33**, 2836–2845, doi:10.1002/joc.3630.

Chansaengkrachang, K., N. Aschariyaphotha, U. Humphries, A. Wangwongchai, and P. Wongwises, 2011: Empirical orthogonal function analysis of rainfall over Thailand and its relationship with Indian Ocean Dipole. *Chiang Mai University International Conference*, Chiang Mai, Thailand, 47–58.

Chen, C.-T., and T. Knutson, 2008: On the Verification and Comparison of

Extreme Rainfall Indices from Climate Models. *Journal of Climate*, **21**, 1605–1621, doi:10.1175/2007JCLI1494.1.

Chen, M., P. Xie, J. E. Janowiak, and P. A. Arkin, 2002: Global Land Precipitation: A 50-yr Monthly Analysis Based on Gauge Observations. *Journal of Hydrometeorology*, **3**, 249–266, doi:10.1175/1525-7541(2002)003⟨0249:GLPAYM⟩2.0.CO;2.

Chu, J., C. Sampson, L. AS, and F. E, 2002: The Joint Typhoon Warning Center tropical cyclone best-tracks, 1945-2000. Tech. rep., 22 pp.

Chu, P.-S., X. Zhao, Y. Ruan, and M. Grubbs, 2009: Extreme Rainfall Events in the Hawaiian Islands. *Journal of Applied Meteorology and Climatology*, **48**, 502–516, doi:10.1175/2008jamc1829.1.

Clarke, J., A. McConkey, C. Samuel, and J. Wicks, 2015: Delivering benefits through evidence: Quantifying the benefits of flood risk management actions and advice. Tech. rep., 127 pp.

Climatic Research Unit, 2013a: CRU TS3.20: Climatic Research Unit (CRU) Time-Series (TS) Version 3.20 of High Resolution Gridded Data of Month-by-month Variation in Climate (Jan. 1901–Dec. 2011). Available online at: http://catalogue.ceda.ac.uk/uuid/2949a8a25b375c9e323c53f6b6cb2a3a.

Climatic Research Unit, 2013b: CRU TS3.21: Climatic Research Unit (CRU) Time-Series (TS) Version 3.21 of High Resolution Gridded Data of Month-by-month Variation in Climate (Jan. 1901—Dec. 2012). doi:10.5285/D0E1585D-3417-485F-87AE-4FCECF10A992.

Coles, S., 2001: *An Introduction to Statistical Modeling of Extreme Values*. Springer London, 209 pp.

Cook, B. I., and B. M. Buckley, 2009: Objective determination of monsoon season onset, withdrawal, and length. *Journal of Geophysical Research*, **114**, 1–12, doi:10.1029/2009JD012795.

Cowpertwait, P. S. P., C. G. Kilsby, and P. E. O'Connell, 2002: A space-time Neyman-Scott model of rainfall: Empirical analysis of extremes. *Water Resources Research*, **38**, 1–14, doi:10.1029/2001WR000709.

Crutcher, H. L., 1975: A Note on the Possible Misuse of the Kolmogorov-Smirnov Test. *Journal of Applied Meteorology*, **14**, 1600–1603, doi:10.1175/1520-0450(1975)014⟨1600:ANOTPM⟩2.0.CO;2.

Davey, M. K., A. Brookshaw, and S. Ineson, 2014: The probability of the impact of ENSO on precipitation and near-surface temperature. *Climate Risk Management*, **1**, 5–24, doi:10.1016/j.crm.2013.12.002.

DHI, 2011: Thailand Floods 2011 - The need for holistic flood risk management. Tech. rep., 8 pp.

Encyclopedia Britannica, 2016: Thailand. Available online at: https://www.britannica.com/place/Thailand.

Engkagul, S., 1993: Flooding features in Bangkok and vicinity: Geographical approach. *GeoJournal*, **31**, 335–338, doi:10.1007/BF00812783.

ESRI, 2013: Kriging - GIS Dictionary. Available online at: http://support.esri.com/en/knowledgebase/GISDictionary/term/kriging.

Everitt, B., 2013: *The Cambridge Dictionary of Statistics*, Vol. 53. 1689–1699 pp., doi:10.1017/CBO9781107415324.004, arXiv:1011.1669v3.

Feng, S., S. Nadarajah, and Q. Hu, 2007: Modeling Annual Extreme Precipitation in China Using the Generalized Extreme Value Distribution. *Journal of the Meteorological Society of Japan*, **85**, 599–613, doi:10.2151/jmsj.85.599.

Few, R., 2003: Flooding, vulnerability and coping strategies: local responses to a global threat. *Progress in Development Studies*, **3**, 43–58, doi:10.1191/1464993403ps049ra.

Fisher, R. A., 1925a: *Statistical Methods for Research Workers*. Oliver & Boyd, Edinburgh, UK.

Fisher, R. A., 1925b: Theory of Statistical Estimation. *Mathematical Proceedings of the Cambridge Philosophical Society*, **22**, 700–725, doi:10.1017/S0305004100009580.

Gale, E. L., and M. A. Saunders, 2013: The 2011 Thailand flood: climate causes and return periods. *Weather*, **68**, 233–237, doi:10.1002/wea.2133.

Gleason, K. L., J. H. Lawrimore, D. H. Levinson, T. R. Karl, and D. J. Karoly, 2008: A Revised U.S. Climate Extremes Index. *Journal of Climate*, **21**, 2124–2137, doi:10.1175/2007jcli1883.1.

Goovaerts, P., 2000: Geostatistical approaches for incorporating elevation into the spatial interpolation of rainfall. *Journal of Hydrology*, **228**, 113–129, doi:10.1016/S0022-1694(00)00144-X.

Guha-Sapir, D., R. Below, and P. Hoyois, 2016: EM-DAT: The CRED/OFDA International Disaster Database. Available online at: http://www.emdat.be.

Haraguchi, M., and U. Lall, 2014: Flood risks and impacts: A case study of Thailand's floods in 2011 and research questions for supply chain decision making. *International Journal of Disaster Risk Reduction*, **14**, 1–17, doi:10.1016/j.ijdrr.2014.09.005.

Harris, I., P. Jones, T. Osborn, and D. Lister, 2014: Updated high-resolution grids of monthly climatic observations - the CRU TS3.10 Dataset. *International Journal of Climatology*, **34**, 623–642, doi:10.1002/joc.3711.

Hijmans, R. J., S. E. Cameron, J. L. Parra, P. G. Jones, and A. Jarvis, 2005: Very high resolution interpolated climate surfaces for global land areas. *International Journal of Climatology*, **25**, 1965–1978, doi:10.1002/joc.1276.

Hungspreug, S., W. Khao-uppatum, and S. Thanopanuwat, 2000: Flood management in Chao Phraya River basin. *The Chao Phraya Delta Conference*, Bangkok, Thailand, 1–20.

Husak, G. J., J. Michaelsen, and C. Funk, 2007: Use of the gamma distribution

to represent monthly rainfall in Africa for drought monitoring applications. *International Journal of Climatology*, **27**, 935–944, doi:10.1002/joc.1441.

IPCC, 2012: *Managing the Risks of Extreme Events and Disasters To Advance Climate Change Adaptation*. Cambridge University Press, 582 pp.

JAMSTEC, 2012: Indian Ocean Dipole. Available online at: http://www.jamstec.go.jp/frsgc/research/d1/iod/e/iod/dipole_mode_index.html.

Japan Meteorological Agency, 2014: Historical El Niño and La Niña Events. Available online at: http://ds.data.jma.go.jp/tcc/tcc/products/elnino/ensoevents.html.

JBA Consulting, 2014: JBA Risk Management releases probabilistic flood model for Thailand. Available online at: http://www.jbaconsulting.com/news/jba-risk-management-releases-probabilistic-flood-model-thailand.

JTWC, 2016: Western North Pacific Best Track Data. Available online at: http://www.usno.navy.mil/NOOC/nmfc-ph/RSS/jtwc/best_tracks/wpindex.php.

Kalnay, E., and Coauthors, 1996: The NCEP/NCAR 40-year reanalysis project. *Bulletin of the American Meteorological Society*, **77**, 437–471, doi:10.1175/1520-0477(1996)077⟨0437:TNYRP⟩2.0.CO;2.

Karl, T. R., R. W. Knight, D. R. Easterling, and R. G. Quayle, 1996: Indices of Climate Change for the United States. *Bulletin of the American Meteorological Society*, **77**, 279–292, doi:10.1175/1520-0477(1996)077⟨0279:IOCCFT⟩2.0.CO;2.

Kenyon, J., and G. C. Hegerl, 2010: Influence of Modes of Climate Variability on Global Precipitation Extremes. *Journal of Climate*, **23**, 6248–6262, doi:10.1175/2010jcli3617.1.

Kidson, R., K. S. Richards, and P. a. Carling, 2005: Reconstructing the ca. 100-year flood in Northern Thailand. *Geomorphology*, **70**, 279–295, doi:10.1016/j.geomorph.2005.02.009.

Kiem, A. S., and S. W. Franks, 2001: On the identification of ENSO-induced rainfall and runoff variability: a comparison of methods and indices. *Hydrological Sciences Journal*, **46**, 715–727, doi:10.1080/02626660109492866.

Komori, D., and Coauthors, 2012: Characteristics of the 2011 Chao Phraya River flood in Central Thailand. *Hydrological Research Letters*, **6**, 41–46, doi:10.3178/hrl.6.41.

Koontanakulvong, S., 2012: Thailand Floods 2011: Causes and Future Management System. *The 8th International Symposium on Social Management Systems SSMS2012 Disaster Prevention and Reconstruction Management*, Kaohsiung, Taiwan.

Kure, S., and T. Tebakari, 2012: Hydrological impact of regional climate change in the Chao Phraya River Basin, Thailand. *Hydrological Research Letters*, **6**, 53–58, doi:10.3178/hrl.6.53.

Legates, D. R., and C. J. Willmott, 1990: Mean seasonal and spatial variability in gauge-corrected, global precipitation. *International Journal of Climatology*, **10**, 111–127, doi:10.1002/joc.3370100202.

Lilliefors, H. W., 1967: On the Kolmogorov-Smirnov Test for Normality with Mean and Variance Unknown. *Journal of the American Statistical Association*, **62**, 399–402, doi:10.2307/2283970.

Lilliefors, H. W., 1973: The Kolmogorov-Smirnov and other distance tests for the Gamma distribution and for the extreme-value distribution when parameters must be estimated. Tech. rep.

Lim, H. S., and K. Boochabun, 2012: Flood generation during the SW monsoon season in northern Thailand. *Natural Hazards in the AsiaPacific Region*, **361**, 7–20, doi:10.1144/SP361.3.

Lim, H. S., K. Boochabun, and A. D. Ziegler, 2012: Modifiers and Amplifiers of High and low Flows on the Ping River in Northern Thailand (1921–2009):

The Roles of Climatic Events and Anthropogenic Activity. *Water Resources Management*, **26 (1)**, 4203–4224, doi:10.1007/s11269-012-0140-z.

Lindsey, R., 2013: In Watching for El Niño and La Niña, NOAA Adapts to Global Warming. *ClimateWatch*, Available online at: https://www.climate.gov/news-features/understanding-climate/watching-el-nino-and-la-nina-noaa-adapts-global-warming.

Lloyd-Hughes, B., and M. A. Saunders, 2002: A drought climatology for Europe. *International Journal of Climatology*, **22**, 1571–1592, doi:10.1002/joc.846.

Longobardi, A., and P. Villani, 2009: Trend analysis of annual and seasonal rainfall time series in the Mediterranean area. *International Journal of Climatology*, n/a–n/a, doi:10.1002/joc.2001.

Mason, S. J., and L. Goddard, 2001: Probabilistic Precipitation Anomalies Associated with ENSO. *Bulletin of the American Meteorological Society*, **82**, 619–638, doi:10.1175/1520-0477(2001)082⟨0619:PPAAWE⟩2.3.CO;2.

Massey Jr., F. J., 1951: The Kolmogorov-Smirnov Test for Goodness of Fit. *Journal of the American Statistical Association*, **46**, 68–78, doi:10.1080/01621459.1951.10500769.

Mateo, C. M., and Coauthors, 2014: Assessing the impacts of reservoir operation to floodplain inundation by combining hydrological, reservoir management, and hydrodynamic models. *Water Resources Research*, **50**, 7245–7266, doi:10.1002/2013WR014845.

Mathwave, 2014: EasyFit - Distribution Fitting Made Easy. Available online at: http://www.mathwave.com/.

MATLAB, 2015a: Gamma parameter estimates - MATLAB gamfit. Available online at: http://uk.mathworks.com/help/stats/gamfit.html.

MATLAB, 2015b: Generalized extreme value parameter estimates - MATLAB gevfit. Available online at: http://uk.mathworks.com/help/stats/gevfit.html.

MATLAB, 2015c: Sample autocorrelation - MATLAB autocorr. Available online at: http://uk.mathworks.com/help/econ/autocorr.html#btzi9yc-1.

Matsuura, K., and C. J. Willmott, 2009: Terrestrial Precipitation: 1900–2008 Gridded Monthly Time Series. Available online at: http://climate.geog.udel.edu/~climate/html_pages/Global2_Ts_2009/README.global_p_ts_2009.html.

McKee, T. B., N. J. Doesken, and J. Kleist, 1993: The relationship of drought frequency and duration to time scales. *8th Conference on Applied Climatology*, Anaheim, California, 179–184.

Meehan, R., 2012: Thailand floods 2011: causes and prospects from an insurance perspective. Tech. rep., 33 pp.

Merz, B., H. Kreibich, R. Schwarze, and A. Thieken, 2010: Review article 'Assessment of economic flood damage'. *Natural Hazards and Earth System Science*, **10**, 1697–1724, doi:10.5194/nhess-10-1697-2010.

Met Office, 2012: *Met Office Integrated Data Archive System (MIDAS) Land and Marine Surface Stations Data (1853–current)*. Available online at: http://catalogue.ceda.ac.uk/uuid/220a65615218d5c9cc9e4785a3234bd0.

Met Office, 2015a: Tropical cyclone facts. Available online at: http://www.metoffice.gov.uk/weather/tropicalcyclone/facts.

Met Office, 2015b: UK Climate Averages. Available online at: http://www.metoffice.gov.uk/public/weather/climate.

Metropolis, N., and S. Ulam, 1949: The Monte Carlo Method. *Journal of the American Statistical Association*, **44**, 335–341, doi:10.1080/01621459.1949.10483310.

Meyers, G., P. McIntosh, L. Pigot, and M. Pook, 2007: The Years of El Niño, La Niña, and Interactions with the Tropical Indian Ocean. *Journal of Climate*, **20**, 2872–2880, doi:10.1175/JCLI4152.1.

Mitchell, T. D., and P. D. Jones, 2005: An improved method of constructing a database of monthly climate observations and associated high-resolution grids. *International Journal of Climatology*, **25**, 693–712, doi:10.1002/joc.1181.

Mooley, D. A., 1973: Gamma Distribution Probability Model for Asian Summer Monsoon Monthly Rainfall. *Monthly Weather Review*, **101**, 160–176, doi:10.1175/1520-0493(1973)101⟨0160:GDPMFA⟩2.3.CO;2.

NASA Earth Observatory, 2006: Floods in Thailand - 2006. Available online at: http://earthobservatory.nasa.gov/NaturalHazards/view.php?id=17314.

NASA Goddard Space Flight Center, 2016: Tropical Rainfall Measurement Mission. Available online at: http://trmm.gsfc.nasa.gov/.

NCDC, 2012: *Global Surface Summary of the Day*. Available online at: https://data.noaa.gov/dataset/global-surface-summary-of-the-day-gsod.

Neumann, C. J., 1987: The National Hurricane Center Risk Analysis Program (HURISK). Tech. rep., 59 pp.

New, M., M. Hulme, and P. Jones, 1999: Representing twentieth-century space-time climate variability. Part I: Development of a 1961–90 mean monthly terrestrial climatology. *Journal of Climate*, **12**, 829–856, doi:10.1175/1520-0442(1999)012⟨0829:RTCSTC⟩2.0.CO;2.

New, M., M. Hulme, and P. Jones, 2000: Representing twentieth-century space-time climate variability. Part II: Development of 1901–96 monthly grids of terrestrial surface climate. *Journal of Climate*, **13**, 2217–2238, doi:10.1175/1520-0442(2000)013⟨2217:RTCSTC⟩2.0.CO;2.

New, M., M. Todd, M. Hulme, and P. Jones, 2001: Precipitation measurements and trends in the twentieth century. *International Journal of Climatology*, **21**, 1889–1922, doi:10.1002/joc.680.

NOAA Climate Prediction Center, 2014: Cold & Warm Episodes by Season. Available online at: http://www.cpc.ncep.noaa.gov/products/analysis_monitoring/ensostuff/ensoyears.shtml.

NOAA Hurricane Research Division, 2013: Record number of storms by basin. Available online at: http://www.aoml.noaa.gov/hrd/tcfaq/E10.html.

NOAA Tropical Atmosphere Ocean Project, 2016: TAO Diagrams. Available online at: http://www.pmel.noaa.gov/tao/proj_over/diagrams/index.html.

Office of Natural Water Resources Committee of Thailand, 2003: Chao Phraya River Basin, Thailand. *The 1st UN World Water Development Report: Water for People, Water for Life*, World Water Assessment Programme, Ed., Berghahn Books, 390–400.

Ono, K., and S. Kazama, 2011: Analysis of extreme daily rainfall in southeast Asia with a gridded daily rainfall data set. *Hydro-Climatology: Variability and Change*, Melbourne, Australia, 169–175.

Palutikof, J., B. Brabson, D. Lister, and S. Adcock, 1999: A review of methods to calculate extreme wind speeds. *Meteorological Applications*, **6**, 119–132, doi:10.1017/S1350482799001103.

Pearson, K., 1900: X. On the criterion that a given system of deviations from the probable in the case of a correlated system of variables is such that it can be reasonably supposed to have arisen from random sampling. *Philosophical Magazine Series 5*, **50**, 157–175, doi:10.1080/14786440009463897.

Peterson, T. C., T. R. Karl, P. F. Jamason, R. Knight, and D. R. Easterling, 1998a: First difference method: Maximizing station density for the calculation of long-term global temperature change. *Journal of Geophysical Research*, **103**, 25 967–25 974, doi:10.1029/98JD01168.

Peterson, T. C., and Coauthors, 1998b: Homogeneity adjustments of in situ atmospheric climate data: a review. *International Journal of Climatology*, **18**, 1493–1517, doi:10.1002/(SICI)1097-0088(19981115)18:13⟨1493::AID-JOC329⟩3.0.CO;2-T.

Phien, H. N., A. Arbhabhirama, and A. Sunchindah, 1980: Distribution of Monthly Rainfall in Northeast Thailand. *Southeast Asian Studies*, **18**, 110–123.

Phillips, J., M. Cane, and C. Rosenzweig, 1998: ENSO, seasonal rainfall patterns and simulated maize yield variability in Zimbabwe. *Agricultural and Forest Meteorology*, **90**, 39–50, doi:10.1016/S0168-1923(97)00095-6.

Pinkayad, S., and C. Ertuna, 1970: Frequency distributions of maximum annual rainfall of short durations in Thailand. Tech. rep., 13 pp.

Prajamwong, S., and P. Suppataratarn, 2009: Integrated Flood Mitigation Management in the Lower Chao Phraya River Basin. *Expert Group Meeting on Innovative Strategies Towards Flood Resilient Cities in Asia-Pacific*, 1–13.

Promchote, P., S.-Y. Simon Wang, and P. G. Johnson, 2016: The 2011 Great Flood in Thailand: Climate Diagnostics and Implications from Climate Change. *Journal of Climate*, **29**, 367–379, doi:10.1175/JCLI-D-15-0310.1.

Rakwatin, P., T. Sansena, N. Marjang, and A. Rungsipanich, 2013: Using multi-temporal remote-sensing data to estimate 2011 flood area and volume over Chao Phraya River basin, Thailand. *Remote Sensing Letters*, **4**, 243–250, doi:10.1080/2150704X.2012.723833.

Räsänen, T. A., and M. Kummu, 2013: Spatiotemporal influences of ENSO on precipitation and flood pulse in the Mekong River Basin. *Journal of Hydrology*, **476**, 154–168, doi:10.1016/j.jhydrol.2012.10.028.

Rayner, N. A., 2003: Global analyses of sea surface temperature, sea ice, and night marine air temperature since the late nineteenth century. *Journal of Geophysical Research*, **108**, 1–37, doi:10.1029/2002JD002670.

Robert Brakenridge, G., S. Cohen, A. J. Kettner, T. De Groeve, S. V. Nghiem, J. P. Syvitski, and B. M. Fekete, 2012: Calibration of satellite measurements of river discharge using a global hydrology model. *Journal of Hydrology*, **475**, 123–136, doi:10.1016/j.jhydrol.2012.09.035.

Ropelewski, C. F., and M. S. Halpert, 1996: Quantifying Southern Oscillation-Precipitation Relationships. *Journal of Climate*, **9**, 1043–1059, doi:10.1175/1520-0442(1996)009⟨1043:QSOPR⟩2.0.CO;2.

Rougier, J., and Coauthors, 2010: SAPPUR: NERC Scoping Study on Uncertainty and Risk in Natural Hazards. Tech. rep., 64 pp.

Rural Surin, 2016: Siam, Thailand & Bangkok Old Photo Thread - Page 61 - TeakDoor.com - The Thailand Forum. Available online at: http://teakdoor.com/famous-threads/39970-siam-thailand-bangkok-old-photo-thread-61.html.

Saffir, H. S., 1973: Hurricane Wind and Storm Surge. *The Military Engineer*, **423**, 4–5.

Saji, N., and T. Yamagata, 2003: Possible impacts of Indian Ocean Dipole mode events on global climate. *Climate Research*, **25**, 151–169, doi:10.3354/cr025151.

Saji, N. H., B. N. Goswami, P. N. Vinayachandran, and T. Yamagata, 1999: A dipole mode in the tropical Indian Ocean. *Nature*, **401**, 360–363.

Saunders, M. A., and A. S. Lea, 2005: Seasonal prediction of hurricane activity reaching the coast of the United States. *Nature*, **434**, 1005–1008, doi:10.1038/nature03454.

Schaake, J., A. Henkel, and S. Cong, 2004: Application of PRISM climatologies for hydrologic modeling and forecasting in the western US. *18th Conference on Hydrology*, Seattle, WA, 1–7.

Schneider, U., A. Becker, P. Finger, A. Meyer-Christoffer, B. Rudolf, and M. Ziese, 2011a: GPCC Full Data Reanalysis Version 6.0 at 0.5: Monthly Land-Surface Precipitation from Rain-Gauges built on GTS-based and Historic Data. doi: 10.5676/DWD_GPCC/FD_M_V6_050.

Schneider, U., A. Becker, P. Finger, A. Meyer-Christoffer, B. Rudolf, and M. Ziese, 2011b: GPCC Full Data Reanalysis Version 6.0 at 1.0: Monthly Land-Surface Precipitation from Rain-Gauges built on GTS-based and Historic Data. doi: 10.5676/DWD_GPCC/FD_M_V6_100.

Schneider, U., A. Becker, P. Finger, A. Meyer-Christoffer, B. Rudolf, and M. Ziese, 2011c: GPCC Full Data Reanalysis Version 6.0 at 2.5: Monthly Land-Surface

Precipitation from Rain-Gauges built on GTS-based and Historic Data. doi: 10.5676/DWD_GPCC/FD_M_V6_250.

Schneider, U., A. Becker, P. Finger, A. Meyer-Christoffer, B. Rudolf, and M. Ziese, 2015a: GPCC Full Data Reanalysis Version 7.0 at 0.5: Monthly Land-Surface Precipitation from Rain-Gauges built on GTS-based and Historic Data. doi: 10.5676/DWD_GPCC/FD_M_V7_050.

Schneider, U., A. Becker, P. Finger, A. Meyer-Christoffer, B. Rudolf, and M. Ziese, 2015b: GPCC Full Data Reanalysis Version 7.0 at 1.0: Monthly Land-Surface Precipitation from Rain-Gauges built on GTS-based and Historic Data. doi: 10.5676/DWD_GPCC/FD_M_V7_100.

Schneider, U., A. Becker, P. Finger, A. Meyer-Christoffer, B. Rudolf, and M. Ziese, 2015c: GPCC Full Data Reanalysis Version 7.0 at 2.5: Monthly Land-Surface Precipitation from Rain-Gauges built on GTS-based and Historic Data. doi: 10.5676/DWD_GPCC/FD_M_V7_250.

Schneider, U., A. Becker, P. Finger, A. Meyer-Christoffer, M. Ziese, and B. Rudolf, 2014: GPCC's new land surface precipitation climatology based on quality-controlled in situ data and its role in quantifying the global water cycle. *Theoretical and Applied Climatology*, **115**, 15–40, doi:10.1007/s00704-013-0860-x.

Shepard, D., 1968: A two-dimensional interpolation function for irregularly-spaced data. *23rd ACM national conference*, New York, NY, 517–524.

Simpson, R. H., 1974: The Hurricane DisasterPotential Scale. *Weatherwise*, **27**, 169–186, doi:10.1080/00431672.1974.9931702.

Singhrattna, N., M. S. Babel, and S. R. Perret, 2012: Hydroclimate variability and long-lead forecasting of rainfall over Thailand by large-scale atmospheric variables. *Hydrological Sciences Journal*, **57**, 26–41, doi:10.1080/02626667.2011.633916.

Singhrattna, N., B. Rajagopalan, M. Clark, and K. Krishna Kumar, 2005a: Seasonal forecasting of Thailand summer monsoon rainfall. *International Journal of Climatology*, **25**, 649–664, doi:10.1002/joc.1144.

Singhrattna, N., B. Rajagopalan, K. K. Kumar, and M. Clark, 2005b: Interannual and Interdecadal Variability of Thailand Summer Monsoon Season. *Journal of Climate*, **18**, 1697–1708, doi:10.1175/JCLI3364.1.

Smith, D. M., A. A. Scaife, and B. P. Kirtman, 2012: What is the current state of scientific knowledge with regard to seasonal and decadal forecasting? *Environmental Research Letters*, **7**, 1–11, doi:10.1088/1748-9326/7/1/015602.

Smith, T. M., R. W. Reynolds, T. C. Peterson, and J. Lawrimore, 2008: Improvements to NOAA's Historical Merged LandOcean Surface Temperature Analysis (18802006). *Journal of Climate*, **21**, 2283–2296, doi:10.1175/2007JCLI2100.1.

Sroikeeree, K., and R. Bannatham, 2006: Historical Floods, Flood Management, Vulnerabilities, and Risk Assessment in Bangkok. Tech. rep.

Stephenson, D. B., 2008: Definition, diagnosis, and origin of extreme weather and climate events. *Climate Extremes and Society*, H. F. Diaz, and R. J. Murnane, Eds., Cambridge University Press, Cambridge, 11–23.

Supharatid, S., 2006: The Hat Yai 2000 flood: the worst flood in Thai history. *Hydrological Processes*, **20**, 307–318, doi:10.1002/hyp.5912.

Suvanpimol, P., 2007: Hydrology and Damage of Chao Phraya Flood 2006. *International Symposium on 2006 flood of Chao Phraya River*, Bangkok, Thailand.

Svensson, C., and D. Jones, 2010: Review of rainfall frequency estimation methods. *Journal of Flood Risk Management*, **3**, 296–313, doi:10.1111/j.1753-318X.2010.01079.x.

Swiss Re, 2012: Natural catastrophes and man-made disasters in 2011. Tech. rep., 44 pp.

Thai Meteorological Department, 2011: Annual Weather Summary of Thailand in 2011. Tech. rep., 13 pp.

Thai Meteorological Department, 2014: Annual Weather Summary over Thailand in 2014. Tech. rep., 7 pp.

Thai Meteorological Department, 2015: Annual Weather Summary over Thailand in 2015. Tech. rep., 18 pp.

The World Bank, 2016: Poverty headcount ratio at $3.10 a day (2011 PPP) (% of population). Available online at: http://data.worldbank.org/indicator/SI.POV.2DAY/countries?display=default.

Thom, H. C. S., 1958: A note on the Gamma distribution. *Monthly Weather Review*, **86**, 117–122, doi:10.1175/1520-0493(1958)086⟨0117:ANOTGD⟩2.0.CO;2.

Tingsanchali, T., and F. Karim, 2010: Flood-hazard assessment and risk-based zoning of a tropical flood plain: case study of the Yom River, Thailand. *Hydrological Sciences Journal*, **55**, 145–161, doi:10.1080/02626660903545987.

Troup, A. J., 1965: The 'southern oscillation'. *Quarterly Journal of the Royal Meteorological Society*, **91**, 490–506, doi:10.1002/qj.49709139009.

Tunstall, S., C. L. Johnson, and E. C. P. Rowsell, 2004: Flood hazard management in England and Wales: from land drainage to flood risk management. *World Congress on Natural Disaster Mitigation*, New Delhi, India, 1–8.

Ummenhofer, C. C., R. D. D'Arrigo, K. J. Anchukaitis, B. M. Buckley, and E. R. Cook, 2013: Links between Indo-Pacific climate variability and drought in the Monsoon Asia Drought Atlas. *Climate Dynamics*, **40**, 1319–1334, doi:10.1007/s00382-012-1458-1.

UN Office for the Coordination of Humanitarian Affairs, 2006: Thailand: Floods OCHA Situation Report No. 1 - Thailand. Tech. rep.

Unisys, 2015: West Pacific Tropical Storm Tracking by Year. Available online at: http://weather.unisys.com/hurricane/w_pacific/index.php.

van Oldenborgh, G. J., A. van Urk, and M. Allen, 2012: The absence of a role of climate change in the 2011 Thailand floods. *Bulletin of the American Meteorological Society*, **93**, 1047–1049.

Wang, B., 2006: *The Asian Monsoon*. Springer Praxis, 787 pp.

Ward, P. J., H. De Moel, and J. C. J. H. Aerts, 2011: How are flood risk estimates affected by the choice of return-periods? *Natural Hazards and Earth System Science*, **11**, 3181–3195, doi:10.5194/nhess-11-3181-2011.

Webster, P. J., A. M. Moore, J. P. Loschnigg, and R. R. Leben, 1999: Coupled ocean-atmosphere dynamics in the Indian Ocean during 1997-98. *Nature*, **401**, 356–360.

Webster, R., and M. A. Oliver, 2007: *Geostatistics for Environmental Scientists*. 2nd ed., John Wiley & Sons, Ltd, 332 pp.

Weinkle, J., R. Maue, and R. Pielke, 2012: Historical Global Tropical Cyclone Landfalls. *Journal of Climate*, **25**, 4729–4735, doi:10.1175/JCLI-D-11-00719.1.

Wikimedia, 2016: Thailand Topography. Available online at: https://commons.wikimedia.org/wiki/File:Thailand{_}Topography.png.

Wilks, D. S., 2011: *Statistical Methods in the Atmospheric Sciences*. 3rd ed., Academic Press, 676 pp.

Willmott, C. J., C. M. Rowe, and W. D. Philpot, 1985: Small-Scale Climate Maps: A Sensitivity Analysis of Some Common Assumptions Associated with Grid-Point Interpolation and Contouring. *Cartography and Geographic Information Science*, **12**, 5–16, doi:10.1559/152304085783914686.

Wolter, K., and M. S. Timlin, 1998: Measuring the strength of ENSO events: How does 1997/98 rank? *Weather*, **53**, 315–324, doi:10.1002/j.1477-8696.1998.tb06408.x.

World Climate Research Programme, 2011: The Global Monsoon System. Tech. rep., 4 pp.

World Meteorological Organization, 2015: World Weather Records. Available online at: http://www.wmo.int/pages/prog/wcp/wcdmp/GCDS_2.php.

Xue, Z., and C. J. Neumann, 1984: Frequency and motion of western North Pacific tropical cyclones. Tech. rep., 91 pp.

Yatagai, A., O. Arakawa, K. Kamiguchi, H. Kawamoto, M. I. Nodzu, and A. Hamada, 2009: A 44-Year Daily Gridded Precipitation Dataset for Asia Based on a Dense Network of Rain Gauges. *SOLA*, **5**, 137–140, doi:10.2151/sola.2009-035.

Yatagai, A., K. Kamiguchi, O. Arakawa, A. Hamada, N. Yasutomi, and A. Kitoh, 2012: APHRODITE: Constructing a Long-Term Daily Gridded Precipitation Dataset for Asia Based on a Dense Network of Rain Gauges. *Bulletin of the American Meteorological Society*, **93**, 1401–1415, doi:10.1175/BAMS-D-11-00122.1.

Ziegler, A. D., L. H. She, C. Tantasarin, N. R. Jachowski, and R. Wasson, 2012: Floods, false hope, and the future. *Hydrological Processes*, **26**, 1748–1750, doi:10.1002/hyp.9260.